A Fast Forward Electromagnetic Solver for Microwave Imaging

Chaber, Bartosz; Mohr, Johan Jacob

Published in:
XVIII International Symposium on Theoretical Electrical Engineering ISTET'15 & Symposium on Electromagnetic Evaluation of Materials SEEM'15

Publication date:
2015

Document Version
Publisher's PDF, also known as Version of record

XVIII International Symposium on Theoretical Electrical Engineering
ISTET'15

&

Symposium on Electromagnetic Evaluation of Materials SEEM'15

ISBN 978 - 83 - 7663 - 196 - 7

XVIII International Symposium on Theoretical Electrical Engineering ISTET'15

&

Symposium on Electromagnetic Evaluation of Materials SEEM'15

Kołobrzeg, Poland June 7th–10th, 2015

The ISTET symposium series is devoted to research and education in theory and applications of electromagnetic fields, electrical and electronic circuits, signal processing and control of electromagnetic systems. Detailed information can be found on website www.istet.zut.edu.pl.

Additionally, for the first time the Szczecin Section of Polish Society for Nondestructive Testing and Technical Diagnostic (PTBNiDT) will organize a specialized session SEEM'15 on the selected topics of electromagnetic nondestructive testing and evaluation of materials.

www.istet.zut.edu.pl
e-mail: istet@zut.edu.pl
phone: (+48) 91 449 49 67

Organized by

West Pomeranian University of Technology, Szczecin
Faculty of Electrical Engineering

Under auspices of

Electrical Engineering Committee of Polish Academy of Sciences

Association of Polish Electrical Engineers SEP

Rector of West Pomeranian University of Technology Szczecin

with support of

Szczecin Section of Polish Society for Nondestructive Testing and Technical Diagnostic (PTBNiDT)
Szczecin Section of Polish Society for Theoretical and Applied Electrical Engineering (PTETiS)

Sponsors

www.ndt-system.com.pl

www.comsol.com

www.pse.pl

www.medcom.com.pl

ISTET'15 International Scientific Committee

Local Organizing Committee

Editorial Board

WELCOME TO ISTET'15 & SEEM'15 KOŁOBRZEG, POLAND

The Local Organizing Committee of ISTET'15 and SEEM'15 Kołobrzeg, Poland has a pleasure to welcome you to attend the XVIII International Symposium on Theoretical Electrical Engineering (ISTET) and Symposium on Electromagnetic Evaluation of Materials (SEEM) held on Kołobrzeg, Poland between 7th and 10th of June, 2015.

ISTET Symposium was founded by a group of experts in theoretical electrical engineering. The first of the symposiums took place in 1981 in Bratislava, and has been followed by conferences held in various parts of the world: Bratislava, Slovakia (1981); Ilmenau, Germany (1983); Moscow, Russia (1985); Ilmenau, Germany (1987); Budapest, Hungary (1989); Cottbus, Germany (1991); Szczecin, Poland (1993); Thessaloniki, Greece (1995); Palermo, Italy (1997); Magdeburg, Germany (1999); Linz, Austria (2001); Warsaw, Poland (2003); Lviv, Ukraine (2005); Szczecin, Poland (2007); Lubeck, Germany (2009); Klagenfurt, Austria (2011); Pilsen, Czech Republic (2013).

The Technical Programme of the Conferences includes 88 contributed papers, subdivided into 6 oral and 3 poster sessions. There are 4 invited lectures, namely:

1. Masato Enokizono, *"How to Decrease Loss and Upgrade Efficiency of Electrical Machines by Vector Magnetic Characteristic Technology";*
2. Ludger Klinkenbusch, Hendrik Brüns, *"Multipole Analysis and Complex-Source Beams in Scalar and Electromagnetic Fields";*
3. João Marcos Rebello, Cesar Camerini, Gabriela Pereira, *"Materials Characterization Using Electromagnetic Nondestructive Techniques";*
4. Tomasz Krupicz, Ad Van Der Linden, *"COMSOL Multiphysics® for Electromagnetic Simulations"*.

Authors of accepted contributions are invited to submit a full paper, that will be considered for publication in:

1. The International Journal for Computation and Mathematics in Electrical and Electronic Engineering (COMPEL);
2. Przeglad Elektrotechniczny (Review on Electrical Engineering – the oldest magazine of Polish electricians; it appears since 1919 and is edited by SEP – Society of Polish Electrical and Electronics Engineers);
3. Archives of Electrical Engineering (AEE) – the journal of Polish Academy of Sciences.

The Issue 35/4 of COMPEL in 2016 will be a Special Issue containing selected extended and enhanced papers originally presented at the Joined International Symposium on Theoretical Electrical Engineering ISTET 2015 and Symposium on Electromagnetic Evaluation of Materials SEEM 2015. The special issue will have a title: "Special issue on advances in theoretical electrical engineering".

The organizers wish to express their belief that all participants will find interesting presentations, discussions and informal meetings during the Conferences.

Local Organizing Committee

XVIII International Symposium on Theoretical Electrical Engineering ISTET'2015

&

Symposium on Electromagnetic Evaluation of Materials SEEM'15

Kołobrzeg, Poland
June 7th–10th, 2015

(*preliminary program*)

Sunday 7.06.2015		
15:00	**20:00**	**Registration**
19:00	**21:00**	**Welcome reception**
Monday 8.06.2015		
08:00	**08:40**	**Registration**
08:40	**09:05**	**Opening ceremony**
09:05	**09:10**	Break
09:10	**09:50**	**Keynote lecture**
09:50	**10:50**	**Oral Session 1 (part I)**
10:50	**11:10**	Coffee break
11:10	**12:30**	**Oral Session 1 (part II)**
12:30	**14:50**	**Lunch**
14:50	**16:20**	**Poster Session 1**
16:20	**16:40**	Coffee break
16:40	**18:00**	**Oral Session 2**
16:40	17:40	**Invited Lectures**
18:30	**21:00**	**Barbecue**
Tuesday 9.06.2015		
08:40	**10:30**	**Oral Session 3**
08:40	09:10	**Invited Lecture**
10:30	**11:00**	Coffee break
11:00	**12:20**	**Oral Session 4**
12:30	**14:50**	**Lunch**
14:00	**14:50**	**Meeting of the ISTET International Scientific Committee**
14:50	**16:40**	**Poster Session 2**
16:40	**17:00**	Coffee break
17:00	**18:00**	**Oral Session 5**
18:30	**21:00**	**Banquet**
Wednesday 10.06.2015		
08:40	**10:10**	**Poster Session 3**
10:10	**11:30**	**Oral Session 6**
11:30	**11:50**	**Closing ceremony**
12:30	**14:20**	**Lunch**

ORAL SESSION 1 (Monday 8.06.2015, 9:10 – 12:30)			
Chairman: Ludger Klinkenbusch lbk@tf.uni-kiel.de Chairman: Ryszard Sikora ryszard.sikora@zut.edu.pl			
	Time	**Authors**	**Title**
Keynote lecture	**9:10 – 9:50**	**Masato Enokizono**	**How to Decrease Loss and Upgrade Efficiency of Electrical Machines by Vector Magnetic Characteristic Technology**
1	9:50 – 10:10	Goga Cvetkovski, Lidija Petkovska	Multi-Objective Optimization of Permanent Magnet Disc Motor Using Genetic Algorithm
2	10:10 – 10:30	Jerzy Barglik	Mathematical Modeling of Surface Induction Heating Processes
3	10:30 – 10:50	Sreedhar Unnikrishnakurup, C.V. Krishnamurthy, Krishnan Balasubramaniam	Monitoring Tig Welding Using Infrared Thermography – Simulations and Experiments
4	11:10 – 11:30	Václav Kotlan, Roman Hamar, David Panek, Ivo Dolezel	Combined Heat Treatment of Metal Materials
5	11:30 – 11:50	Antonios Lalas, Nikolaos Kantartzis, Theodoros Tsiboukis	Metamaterial-based Wireless Power Transfer Through Interdigitated SRRs
6	11:50 – 12:10	Dagmar Faktorová, Eva Luptáková	Numerical Evaluation of Advanced Microwave Sensor Tuned with Metamaterial
7	12:10 – 12:30	Bartosz Chaber, Johan Jacob Mohr	A Fast Forward Electromagnetic Solver for Microwave Imagining

Masato ENOKIZONO

Vector Magnetic Caracteristic Technical Laboratory

How to decrease Loss and upgrade Efficiency of Electrical Machines by Vector Magnetic Characteristic Technology

Abstract. *This manuscript is described the vector magnetic characteristic technology for upgrading the low loss and high efficiency on electrical machines. The most important technical point is vector magnetic characteristic technology which is the approach from new point of view. Especially, it is very useful that the effect of stress is very sensitive on vector magnetic property. However it is very complex and necessary the new treatment technology. The controlling method by the vector magnetic characteristic approach is necessary and indispensable for development of high efficiency machines.*

Keywords: vector magnetic characteristic, magnetic characteristic analysis, loss analysis, efficiency.

Introduction

When thinking about the decreasing magnetic power loss and upgrading highly effective, it is possible to see from the law of the electromagnetic theory in two aspects of the following expression.

(1) $$\mathbf{F} = \int_V rot\left(\frac{1}{\mu}\mathbf{B}\times\mathbf{B}\right)dV \text{ , [N]}$$

(2) $$W = \frac{1}{\rho T}\int_0^T (\mathbf{H}\bullet\frac{\partial\mathbf{B}}{\partial t})dt \text{ , [w/kg]}$$ 5ECu002V5K

Where **B** is magnetic flux density, μ magnetic permeability, ρ density, and **H** magnetic field strength. Magnetic forth **F** is introduced **B** only, but magnetic power loss W is used both **B** and **H**. Equation (1) can obtain the conventional numerical simulation technology such as FEM commercial package software program. However W cannot obtain the conventional one. It is necessary to obtain both the vector behavers of **H** and **B** to accomplish the loss analysis. We have proposed the vector magnetic characteristic technology that catches **H** and **B** as a vector relation. In the vector magnetic characteristics as shown in Fig.1, the phase angle θ_{BH} is most important parameter on vector magnetic characteristic analysis [1, 2].

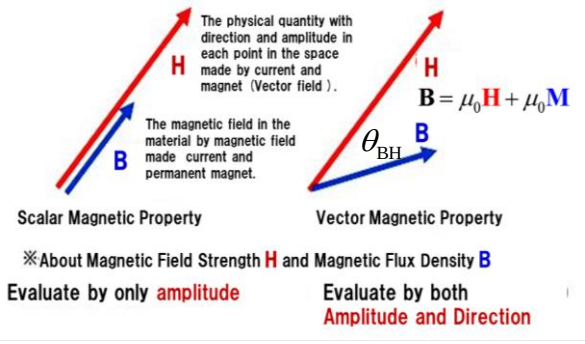

Fig.1. Vector magnetic property?

Outline of presentation

In this presentation the vector magnetic characteristic technology for development of high efficiency electrical machines will be introduced as following terms.

1. Effect of stress on vector magnetic characteristics.
2. The concept theory for decreasing magnetic power loss.
3. The introduction of adaptation example for decreasing loss of motor.

Parameter of Vector Magnetic Property for decreasing Loss

Fig. 2 shows the parameter of vector magnetic property for the methods of decreasing magnetic power loss and upgrading efficiency of electrical machines. In this figure θ_{BH} is spatial phase angle between the vector **B** and the vector **H** as shown in Fig. 1. The θ_B is the inclination angle of the vector **B** from rolling direction of the electrical steel sheet. The α is the axis ratio of the locus of the vector **B** under rotational flux condition. In order to decrease the magnetic power loss it is necessary to reduce the value of these parameter. This is called "Vector Magnetic Controlled Method" which is used the applied stress or dividing magnetic domain structure. Some results will be introduced in conference presentation by using vector magnetic characteristic technology.

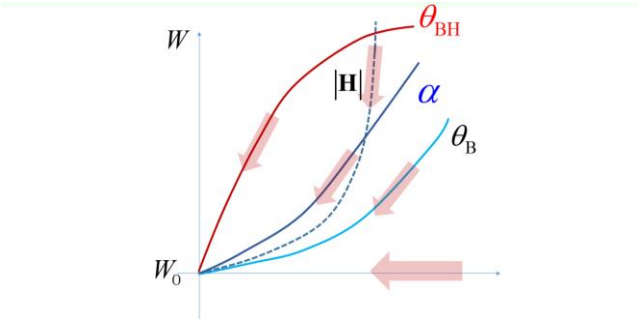

Fig. 2. Parameter of vector magnetic property for decreasing loss

REFERENCES

[1] Kai Y., Enokizono M., Kido M., "Influence of shear stress on vector magnetic properties of non-oriented electrical steel sheets", *International Journal of Applied Electromagnetics and Mechanics*, (in press 2014).

[2] Kai Y., Tsuchida Y., Enokizono M., Vector Magnetic Characteristic Analysis of a Permanent Magnet Motor by controlling Local Stress, *IEEE Trans. on Magn.,* CEFC 2014 (to be published 2015).

Authors*: Masato Enokizono, Vector Magnetic Characteristic Technical Laboratory,533 Joi, Usa 879-0442, Japan, e-mail: enoki@oita-u.ac.jp g*

Goga CVETKOVSKI, Lidija PETKOVSKA

Ss. Cyril and Methodius University, Faculty of Electrical Engineering & Information Technologies

Multi-Objective Optimization of Permanent Magnet Disc Motor Using Genetic Algorithm

***Abstract**. The analysed permanent magnet disc motor (PMDM) is used for direct wheel drive in electric vehicle. Therefore there are several objectives that could be tackled in the design procedure, such as an increased efficiency, reduced total weight of the motor or reduced weight of the permanent magnets (reduced rotor weight). In this paper an optimal design of a PMDM using multi-objective genetic algorithm optimization procedure is performed. Comparative analysis of the optimal motor solution and its parameters in relation to the prototype is presented.*

Keywords: Design optimization, electric vehicle, genetic algorithm, permanent magnet disc motor.

Introduction

When optimizing an electric motor, there are varieties of choices for defining the objective function. In fact the objective function is a specific feature of the machine to be optimized, for example efficiency, torque, volume or cost. Sometimes it is important to tackle several objective functions at once. In this paper the authors present an optimal design of a PMDM using a genetic algorithm as an optimisation tool and as multi-objective function, which combines the efficiency, the weight of the iron, the permanent magnet weight, and the weight of the copper, as separate objective functions.

The optimized motor is a brushless three phase synchronous permanent magnet axial field motor, with rated torque 54 Nm at 750 rpm@50 Hz, fed by a pulse width modulated (PWM) inverter. The PMDM is a double sided disc motor with two laminated stators having 36 slots and a centred rotor with 8 skewed neodymium-iron-boron permanent magnets (B_r = 1.17 T and H_c = – 883 kA/m).

Consequently, the investigation is focused on the design improvement of the PMDM by using a genetic algorithm as an optimization tool to increase the efficiency of the motor and to reduce the total weight of the motor, as well as the weight of the rotor including the PM. In order to tackle all these objectives a multi-objective genetic algorithm optimization was performed [1].

The optimal design program GA-ODEM (Genetic Algorithm for Optimal Design of Electrical Machines) uses the Genetic Algorithm as an optimization tool. The design variables are presented as vectors of floating-point numbers. The main genetic operators of the GA-ODEM implemented in the GA optimization procedure are reproduction, crossover and mutation.

Multi-Objective Optimization of PMDM

In this design optimisation the following parameters are chosen to be variable: inside radius of the stator cores and PM R_i, outside radius of the stator cores and PM R_o, permanent magnet fraction α_m, permanent magnet axial length l_m, air-gap g, single wire diameter d_w, and stator sloth width b_s. In this research the optimal design of the PMDM will be analysed as a multi-objective function which is a sum of the individual values the efficiency, iron weight, PM total weight and copper weight. Each term of the objective function is multiplied by its own weight factor to represent how much is attached to this individual term. Since the GA optimisation in general is a maximisation problem some of the multi-objective terms have to be defined properly. Therefore the efficiency has to be defined as a maximisation term and the weight of the iron, the weight of the PM and the cooper weight as minimisation term. The multi-objective function for the PMDM optimisation can be presented with the following equation:

$$F_{m-o} = eff + \left(\frac{1}{c_1 \cdot W_{totFe}}\right) + \left(\frac{1}{c_2 \cdot W_{totPM}}\right) + \left(\frac{1}{c_3 \cdot W_{Cu}}\right) \quad (1)$$

where: *eff*-motor efficiency, W_{totFe}-total weight of the stator and rotor iron, W_{totPM}-total weight of the PMs and W_{Cu}-total weight of cooper. The comparative optimization parameters data of the initial and optimized model are presented in Table 1.

Table 1. Genetic algorithm optimization results

Parameter	Prototype	GA solution
R_i (m)	0.072	0.070286
α_m (/)	0.6646	0.70448
l_i (m)	0.01	0.009002
g (m)	0.002	0.0018
R_o (m)	0.133	0.134665
d_w (m)	0.001	0.0011
b_s (m)	0.008	0.009
Objective function	1.144	1.487
Efficiency	0.8325	0.8412

In the full version of the paper a more detailed description of the GA procedure will be presented. The comparison analysis of the optimised solution and the prototype is going to be based on the values of the optimised objective function, on the values of the optimisation parameters, and on a set of electric and magnetic parameters of the motor, some of them shown in Table 1. The change of the value of the objective function and the optimisation parameters through the optimisation procedure will be also presented. Finally the optimised model and the initial model, using the results of the 2D FEM magnetic field calculation, are going to be analysed and compared. Performance characteristics, as magnetic field and air gap flux density distribution will be presented and analysed for both models.

REFERENCES

[1] Liuzzi G., Lucidi S., Parasiliti F., Villani M., Multi-objective Optimization Techniques for the Design of Induction Motors, *IEEE Trans. on Mag.*, 39(2003), No. 3, 1261–1264.

***Authors**: Goga Cvetkovski, Ss. Cyril & Methodius University, Faculty of Electrical Engineering & Information Technologies, Rugjer Boskovic 18, P. O. Box 574, 1000, Skopje, Macedonia, e-mail: gogacvet@feit.ukim.edu.mk, Lidija Petkovska, Ss. Cyril and Methodius University, Faculty of Electrical Engineering and Information Technologies, Rugjer Boskovic 18, P. O. Box 574, 1000, Skopje, Macedonia, E-mail: lidijap@feit.ukim.edu.mk.*

Jerzy BARGLIK

Silesian University of Technology

Mathematical Modeling of Surface Induction Hardening Processes

***Abstract**. A short overview in mathematical modeling of selected surface induction hardening processes was presented. Some specific features of the processes and their technical background were discussed. A set of simplifications was discussed and accepted. Based upon that some suitable numerical models were elaborated. Two selected illustrative examples were described. The computations done by means of professional software and single owned procedures were compared with measurement results. A reasonable accordance between calculations and measurements was achieved. Final conclusions were formulated.*

Keywords: surface induction hardening, coupled problems, electromagnetic field, upper critical temperature.

Idea of Induction Surface Hardening

Induction surface hardening is a kind of heat treatment consisting of three consecutive stages: induction heating, holding and intensive cooling. As a result an expected surface hardness and a martensitic structure in a thin surface zone are obtained. It means keeping the soft core of the treated material. The thickness of hardened layer could be controlled by changing of basic process parameters like for instance the field current frequency, time and power of induction heating [1]. For induction heating often a very high heating rate could be achieved. As a result of that a distinct increase of the upper critical temperature Ac_3 is noticed and consequently the hardening temperature T_h could be even of about 200°C bigger than in the conventional heat treatment process [2]. In order to apply surface induction hardening technologies to industry, an improvement of mathematical modeling methods is required. Some simplifications were introduced. However the modeling have been still a big challenge. The reason was connected with coupling of several physical fields and taking into account non-linear phenomena of heat transfer and metallurgical transformations during the whole process. The paper presents a short overview of mathematical modeling of surface induction hardening processes. Then some illustrative examples were presented.

Features of Mathematical Models

Models of induction hardening were given by a set of differential equations describing time-variable distribution of the electromagnetic, temperature and heat stresses fields. For the first stage of induction heating the fields must be analyzed as hard coupled. For a short second stage of holding the body in order to achieve austenite equilibrium state only temperature field is analysed. For the third stage hard coupled temperature, heat stresses and hardness fields were calculated. In many practical cases especially for axi-symmetrical bodies the electromagnetic field could be formulated as 2D task and described by the tangent component of the magnetic vector potential A_t only. But even for such a simplified approach the solution is not easy because of a huge disproportion between the field current frequency f and the time of heating t_h. A big number of time steps for temperature field calculations was required. The model was simplified by the assumption that magnetic field was considered as harmonic and described by the Helmholtz equation for the phasor of the magnetic vector potential $\underline{\boldsymbol{A}}$. However it means the assumption that the magnetic permeability of ferromagnetic parts of the system was considered as constant. For induction hardening of elements with more complicated shapes like gear wheels the 3D approach should be used. The correct formulation of the third kind of the boundary condition for temperature field was important in order to take into consideration not only convection but also the radiation. And finally dependence of hardness distribution within the surface layer should be calculated based upon measurements.

Illustrative examples and results

As illustrative examples two kinds of induction surface hardening technologies were analyzed:

- induction hardening of steel sections used for plastic working (see Fig.1 left),
- contour induction hardening of gear wheel by means of one cylindrical inductor (see Fig.1 right)

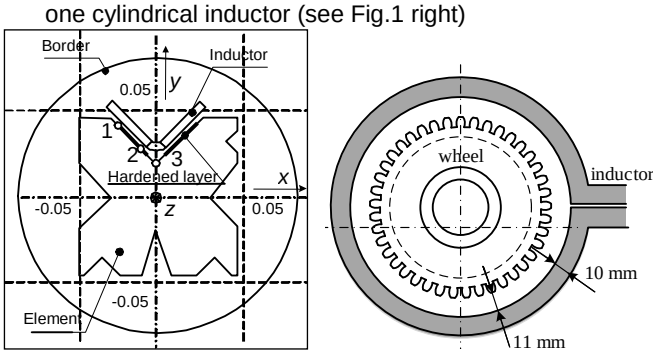

Fig.1. Cross section of induction heating systems for steel section (left) and for gear wheel (right)

The first heat treatment process was realized as continual induction hardening. The moving inductor-sprayer system was applied. The zone with the expected hardness distribution was depicted in Fig.1 (the segment between points 1 and 2). The internal part of the element and the segment between points 2 and 3 (see Fig.1) remained soft. The second process was realized in several consecutive steps including technological breaks between them. At first induction heating was realized as dual frequency heating approach: longer medium frequency and shorter high frequency heating. After that intensive cooling by spraying was provided. Detailed description of computation and measurement results, their comparison as well as conclusions will be presented during the conference.

REFERENCES

[1] Lupi S., Forzan M., Alifierov A., Induction and Direct Resistance Heating. Theory and Numerical Modelling. *Springer International Publishing* 2015.

[2] Barglik J., Ducki K., Mathematical Modelling of Continual Induction Surface Hardening of Axi-symmetric Bodies, *Archives of Electrical Engineering,* (2005), No. 4, 479–487

***Author**: Jerzy Barglik, Silesian University of Technology, 40-019 Katowice, ul. Krasińskiego 8, e-mail, jerzy.barglik@polsl.pl*

Sreedhar UNNIKRISHNAKURUP[1], C.V. Krishnamurthy[2], Krishnan BALASUBRAMANIAM[1]

CNDE, Mechanical Engineering Department, Indian Institute of Technology Madras, Chennai 600036.
Department of Physics, Indian Institute of Technology Madras, Chennai 600036.

Monitoring TIG Welding Using Infrared Thermography – Simulations and Experiments

Abstract. *Knowledge of temperature distribution patterns is useful in any welding process to predict the micro structure and distortion. In the current work a 3D model has been developed to predict the thermal cycles during the Tungsten Inert Gas welding of Aluminum 2219. This paper describes the step by step procedure adopted to get the actual cooling rate during the TIG welding process. The model was developed in the COMSOL Finite Element Package and considered a Gaussian heat distribution. Temperature measurements were performed using Infrared Camera. Results show a good comparison between model and experiment.*

Keywords: Infrared Thermography, Online Monitoring, Finite Element Method, Image Analysis.

Introduction

Arc welding is inherently a thermal processing method. To this end, infrared sensing is a natural choice for weld process monitoring. Infrared sensing is the non contact measurement of emissions in the infrared portion of the electromagnetic spectrum. Many investigators have used thermographic system for the measurement of temperature distribution and control of welding online [1]. Modeling of this complex physical phenomena is more challenging due to the interaction of different physics. Simulation tools based on finite element method are very useful in the prediction of temperature fields in welding [2].

Experimental Study

A circumferential welding was carried out between shell and dome structure of a propellant tank. IR Camera was tied on the arm of the weld torch as shown in fig (1). The welding was carried out in two passes. The IR camera was focused to an area 150 mm away from the weld torch to avoid the saturation of detector due to the higher temperature near the weld pool region. The thermal image obtained during the experiment is shown in Fig. 2.

Fig. 1. Experimental set up

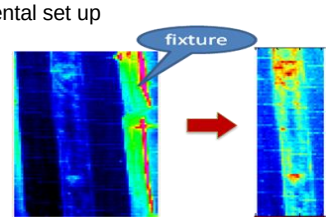

Fig. 2. Raw thermal image and processed thermal image

We developed an algorithm for thermal images to find out the temperature decay on the weld bead. The comparison of experimental and calculated temperature distribution of a point on the top of the weld bead is shown in Fig. 3.

Modeling and Simulations

The Heat transfer module in COMSOL was used to create a model that combined conduction, convection and radiation. The thermal problem is setup by specification of the domain, material parameters, initial condition and boundary condition. There are some assumptions made when studying the problem, which are regarded as reasonable.

Results

Several trials were carried out with variants of the basic source model, the specimen length and the specimen support structure. The results shown in Fig. 3 correspond to the finalized model for the spatio-temporal source distribution, for the specimen length and for the associated support structure. The trend seen in the 3D simulation appears to agree reasonably well with the trends seen in the experiments on the actual specimen. Although the thermograms contain “noise”, the trends can be clearly discerned.

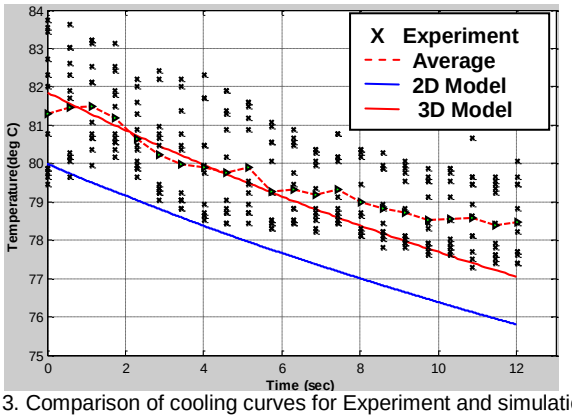

Fig. 3. Comparison of cooling curves for Experiment and simulation

Acknowledgment: This work was financially supported by Indian Space Research Organization, India, under the project entitled Development of an Online Weld Defect Characterization using Thermal Imaging Techniques.

REFERENCES

[1] Nagarajan S., Banerjee P, W Chen and B A Chin, Control of the welding process using infrared sensors, *IEEE Transactions on Robotics and automation*, 8 (1992), 86–93

[2] Lu F., Yao S., Lou S., Li Y. Modeling and finite element analysis on GTAW arc and weld pool, Computational Material Science, 29 (2004), Issue 3, 371–378.

Authors: *Sreedhar U, IITM, sreedhar.aie@gmail.com, C.V. Krishnamurthy, IITM, cvkm@iitm.ac.in, K. Balasubramaniam, IITM, balas@iitm.ac.in*

Václav KOTLAN[1], Roman HAMAR[1], David PANEK[1], Ivo DOLEZEL[2]

University of West Bohemia, Pilsen, Czech Republic (1), Czech Technical University, Prague, Czech Republic (2)

Combined Heat Treatment of Metal Materials

***Abstract**. A combined heat treatment of metal materials is proposed and analyzed, consisting in classic induction pre-heating and/or post-heating and full heating by laser beam. This technology is prospective for some kinds of surface hardening and welding because its application leads to lower temperature gradients at the heated spots, which substantially reduces local residual mechanical strains and stresses. The paper presents fully 3D nonlinear and nonstationary mathematical model of the task, its numerical solution and a typical example whose results are verified by experiment.*

Keywords: induction heating, laser heating, numerical analysis, combined heat treatment.

Introduction

A specific heat treatment of steel bodies is modeled, where the high-temperature heating is realized by a laser beam [1]. The process is supplemented with pre-heating and/or post-heating of the heated strip by a classic inductor to avoid high temperature gradients and subsequent mechanical stresses in the processed material. Its continuous mathematical model is solved numerically in 3D.

Formulation of the technical problem

The task is to model laser heating (for the purpose of welding) of a massive steel plate accompanied by its induction post-heating, see Fig. 1. The plate moves at a given velocity below the system laser head-inductor.

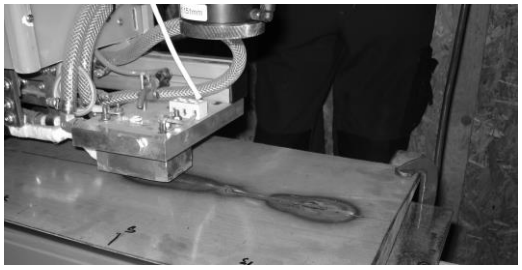

Fig. 2. Production of weld on a massive steel plate

Mathematical model and its numerical solution

From the physical viewpoint, the process of combined heating represents a coupled non-linear problem characterized by a hard interaction of the magnetic and temperature fields mutually influencing one another.

Magnetic field produced by the inductor is described in terms of magnetic vector potential [2]. Its distribution satisfies a modified Helmholtz equation supplemented with the term quantifying the component of eddy currents due to the movement of the plate.

The temperature field is described by the heat transfer equation [3], taking into account the influence of motion. Heating by the laser beam is considered in the form of delivery a specified heat power at a given spot of the plate.

The numerical solution of the mathematical model was carried out by professional code COMSOL Multiphysics 5.

Illustrative example

The heated plate is made of steel S355. The temperature-dependent physical properties of this material, its saturation curve and other important quantities are known. The inductor is wound by one hollow massive copper turn cooled by water, placed in a ferrite shell. The power of the laser beam of diameter 1 mm is 500 W. The distance between the laser head and inductor is 40 mm. The velocity of the plate is 3.4 mm/s.

Figure 2 shows the distribution of the measuring thermocouples used for experiment. For illustration, Fig. 3 shows the calculated and measured time evolutions of temperature at probe 2 (3 mm from the axis of the weld).

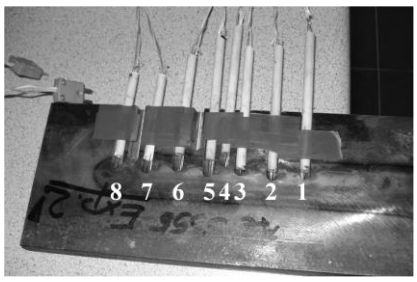

Fig. 2. Distribution of thermocouples along the weld

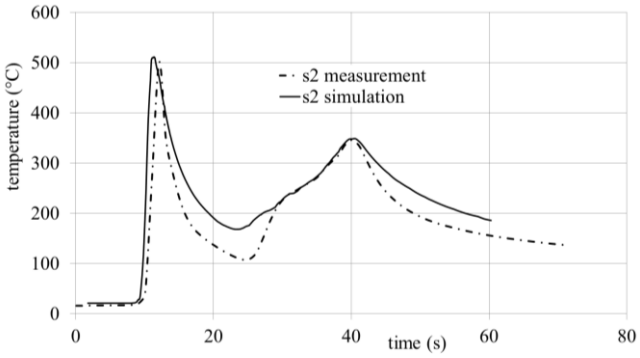

Fig. 3. Calculated and measured temperatures at thermocouple 2

The accordance of both curves may be considered very good and next work in the field will be aimed at further reduction of the differences (both calculations and measurements were burdened by specific errors).

Financial support of the Grant project TACR TA03010354 is gratefully acknowledged.

REFERENCES

[1] Mackwood A.P., Crafer R.C., Thermal modelling of laser welding and related processes: a literature review. *Optics & Laser Technology*, Vol. 37 (2005), No. 2, pp. 99–115.

[2] Kuczmann M., Iványi A., The finite element method in magnetics. *Akadémiai Kiadó*, Budapest, 2008.

[3] Holman J.P., Heat transfer. *McGraw-Hill*, New York, 2002.

***Authors**: Vaclav Kotlan, Roman Hamar and David Panek, University of West Bohemia, FEL, Univerzitni 26, 306 14 Plzen, Czech Republic, e-mail {vkotlan, hamar, panek50}@kte.zcu.cz*

Ivo Dolezel, Czech Technical University, FEL, Technicka 2, 166 27 Praha 6, Czech Republic, e-mail: dolezel@fel.cvut.cz

Antonios LALAS, Nikolaos KANTARTZIS, Theodoros TSIBOUKIS

Aristotle University of Thessaloniki

Metamaterial-based Wireless Power Transfer through Interdigitated SRRs

Abstract. *A systematic investigation concerning the efficiency of a novel wireless power transfer (WPT) system, which utilizes interdigitated split-ring resonators (SRRs) as its elementary blocks, is comprehensively conducted in this paper. The proposed arrangement reveals a noteworthy enhancement of the power delivered to the load as well as a promising tuning of the operational frequency via the interdigitated topology.*

Keywords: Metamaterials, resonators, wireless energy, wireless power transfer.

Introduction

Wireless power transfer (WPT) is considered as a rapidly evolving technology with several stimulating applications, such as wireless charging devices, biomedical implants, and electric vehicles. A non-radiant mid-range technique has been recently introduced [1], displaying prominent efficiency at longer distances. Furthermore, various contemporary RF applications are associated with metamaterials, exhibiting unique electromagnetic features, not available in nature. Hence, the incorporation of metamaterials in WPT can be proven beneficial for establishing high-end devices with adaptable traits [2]. Since, resonators constitute every WPT system that involves coupled magnetic resonances, split-ring resonators (SRRs) have been proposed to create a WPT link [3]. In this paper, a new interdigitated split-ring resonator (I-SRR) is introduced as the basic part of a WPT system, exhibiting enhanced levels of efficiency. A thorough parametric study via the finite element method (FEM) unveils the advantages of the featured configuration.

Development and evaluation of the WPT system

The topology of the WPT system, along with the source loop and the I-SRR, are depicted in Fig. 1. The design parameters of the associated copper parts are selected as: r_s = 45 mm, w_s = 10 mm, g_s = 5 mm, r = 45 mm, w_1 = 10 mm, w_2 = 9 mm, w_3 = 5 mm, g_1 = 0.75 mm, and g_2 = 1.5 mm. Also, the thickness of the Taconic^{TM} TLY5 substrate is 1.5748 mm, while a = 160 m. In this context, the distance between the source loop and the transmitting (Tx) resonator as well as between the load loop and the receiving (Rx) resonator are d_s = d_l = 20 mm. It must be noted that all system components are aligned along a straight line, whereas the distance between the Tx and Rx resonators is denoted as d.

The properties of the WPT system are assessed via an adequate number of numerical investigations through the FEM, as illustrated in Fig. 2. The real parts of the I-SRR constitutive parameters denote the existence of a promising magnetic resonance in the range of 257.5 MHz to 283.5 MHz, whereas the maximum values of the electric field are observed in the vicinity of the interdigitated geometry. In addition, a performance evaluation, when distance d between the Tx and Rx parts varies from 60 mm to 120 mm, is pursued. It is discerned that there are two discrete frequencies of maximum efficiency, when the resonators are close enough, while transfer efficiency levels are decreased when d augments. Specifically, the frequency of maximum efficiency is modified from 283.5 MHz to 276.5 MHz, whereas the efficiency of the device reduces from 98.74% to 75.95%.

Acknowledgements

This research has been financed by the National Scholarships Foundation of Greece (IKY) through IKY Fellowships of Excellence for Postgraduate Studies in Greece – Siemens Program, under Grant No. SR 22103/13.

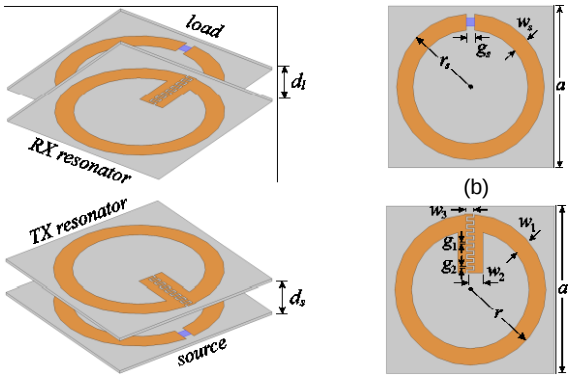

Fig.1. Geometry and design parameters of the (a) metamaterial-based WPT system, (b) source loop, and (c) I-SRR

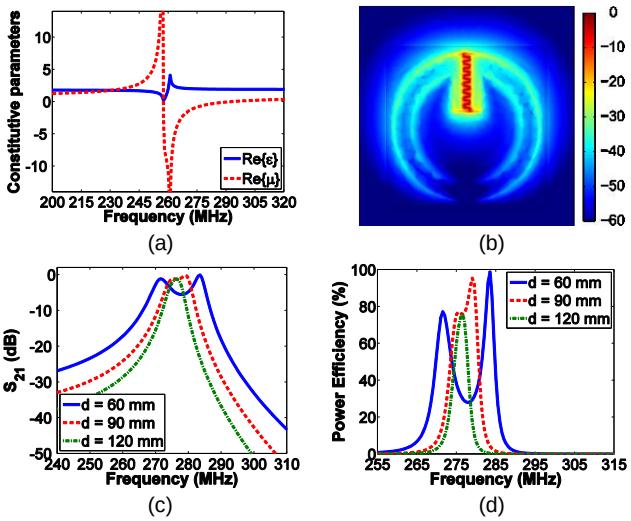

Fig.2. Performance assessment of the proposed WPT system in terms of (a) the I-SRR effective constitutive parameters and (b) electric field intensity at the surface of the I-SRR. (c) Magnitude of S_{21}-parameters and (d) power efficiency for various Tx-Rx distances d

REFERENCES

[1] Karalis A., Joannopoulos J.D., Soljacic M., Efficient wireless non-radiative mid-range energy transfer, *Annals Phys.*, 323 (2008), 34–48

[2] Kim H., Seo C., Highly efficient wireless power transfer using metamaterial slab with zero refractive property, *Electron. Lett.*, 50 (2014), No. 16, 1158–1160

[3] Hu H., Georgakopoulos S.V., Wireless powering based on strongly coupled magnetic resonance with SRR elements, in *Proc. IEEE Antennas Propag. Soc. Int. Symp.*, (2012), 1–2

Authors: *Antonios Lalas, lant@faraday.ee.auth.gr*
Nikolaos Kantartzis, kant@auth.gr
Theodoros Tsiboukis, tsibukis@auth.gr
Department of Electrical and Computer Engineering, Aristotle University of Thessaloniki, GR-54124, Thessaloniki, Greece

Dagmar FAKTOROVÁ, Eva LUPTÁKOVÁ

University of Žilna

Numerical Evaluation of Advanced Microwave Sensor Tuned with Metamaterial

Abstract. *The paper is devoted to the numerical simulation of possibility to the design the microwave sensor tuned with metamaterial for dielectric properties of solid sample changing detection. The sensor was designed with the classical waveguide sensor with added the metamaterial structure consisting of the split ring resonators (SRR) and disrupted wire structure. The most interesting application of SRR and wire structure is due to its resonant nature and strong response on applied electromagnetic field and in our case this not in nature find properties are used for finding the response of metamaterial to the dielectric properties changing.*

Keywords: metamaterial, microwave sensor, numerical simulation, dielectric properties.

Introduction

Metamaterials are artificial structures that can be designed to exhibit specific electromagnetic properties not commonly found in nature. Metamaterials with simultaneously negative permittivity ε and permeability μ have received substantial attention in the scientific and engineering communities, because their unique properties have allowed novel applications, concepts and devices to be developed [1]. In this paper we describe the approach with implementation of metamaterial structure over open waveguide sensor for permittivity of dielectric sample measurement in order to achieve the effective noninvasive method in microwave frequency region for finding the changes in dielectric properties of investigated sample.

Theory of Metamaterials

Split ring resonators are structures having strong response on electromagnetic field. The overall SRR can be represented by the equivalent circuit of a LC oscillator [2]. The band gap in the SRR transmission spectrum is produced by either magnetic or electrical resonances caused by the charge distribution of the incident field. The magnetic resonance is obtained mainly because of its capacitive components. The gap with width *d* represents a main component of overall capacitance of the SRR. By changing the dimensions of the gap and ring or by introducing additional gaps or rings inside, the magnetic resonance can be influenced [2].

The resonant behavior and band-stop properties of MMS were numerically simulated and experimentally observed by measuring the transmission through the waveguide with inserted MMS. The proposed metamaterial unit (Fig. 1a) interaction with electromagnetic field can be study through frequency dependence of scattering parameters S_{11} a S_{21}.

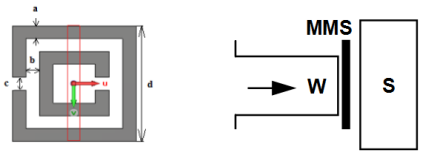

Fig. 1. a) The SRR and wire on the substrate – conventional metamaterial unit, b) arrangement of numerical simulation – W – open waveguide sensor, MMS – metamaterial structure, S – dielectric sample

Numerical Simulations Results

The numerical simulatons were performed by using 7x7 metamataerial units. This arrangement created 2D structure, which was placed over open waveguide sensor.

There was in the near electromagnetic filed area of waveguide sensor tuned with 2D metamaterial structure placed dielectric sample, Fig. 1b. Our idea was to find the shift of resonant frequency due to changing of sample dilectric properties. The proposed metamaterial structure exhibits four resonance frequencies in the range of the microwave spectra, Fig. 2. The metamaterial structure also exhibits double-negative properties at four frequencies. Electromagnetic simulations were done in commercially available software CST Microwave Studio. The scattering S_{21} parameter which responds to transmission of electromagnetic wave through the volume of investigated sample was calculated in frequency range from 2 to 5 GHz.

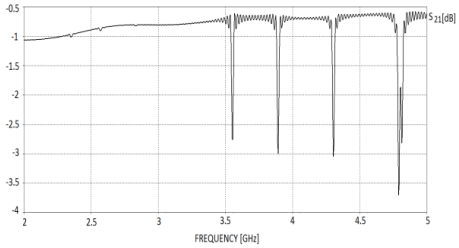

Fig. 2. Four resonant frequencies for 2D double negative metamaterial structure

The resonant frequencies of MMS can be adjusted for investigated dielectric sample by changing of metamaterial unit dimensions and also their distance. The dielectric properties are in some cases changed. The shift of resonant frequency due to the change of relative permittivity can be observed. The numerical results showed that the change of dielectric properties causes the change of amplitude one of resonant frequencies. It can be in this way predicted dangerous situation not only in technical practice, but also can be useful in finding of pathological processes in biological tissues, which can lead to the diseases like cancer.

REFERENCES

[1] Pendry J., Holden A., Robbins D., Steward W., Magnetism from Conductors and Enhanced Nonlinear Phenomena, *IEEE Trans. on Microwave Theory and Tech.*, 50 (1999), No. 2, 2075–2084.

[2] Puentes M., Stelling B., Schüssler M., Penirschke A., Jacoby R., Planar Sensor for Permittivity and Velocity Detection Based on Metamaterial Transmission Line Resonator, *37th European Microwave Conference*, *EuMC 2009*, 2009, 57–60.

Acknowledgment

This work was supported by the Slovak Scientific Agency VEGA under the grant No. 1/0846/13.

***Authors**: Dagmar Faktorová, dagmar.faktorova@fel.uniza.sk, Eva Luptáková, eva.luptakova@fel.uniza.sk, University of Žilina, Univerzitná 8215/1, 010 26 Žilina, Slovak Republic*

Bartosz CHABER[1], Johan Jacob MOHR[2]

Warsaw University of Technology (1), Technical University of Denmark (2)

A Fast Forward Electromagnetic Solver for Microwave Imaging

Abstract*. This paper describes an efficient model of an antenna system for microwave imaging. The authors present techniques employed in the process of preparation of this model, as well as an accuracy comparison with the working prototype system.*

Keywords: microwave imaging, nonlinear inverse problems, radio frequency, computational methods, meshing.

Background and the need of fast full-wave solver

Microwave imaging is a technique that allows for noninvasive tomography with the use of antennas. During data acquisition, one antenna acts as transmitter while the rest are receiving. The process is repeated for each antenna and as the result we get off-diagonal elements of the S-matrix. Based on the measurements one can solve a nonlinear inverse problem and obtain the unknown distribution χ in the region surrounded by the antennas (known as the imaging domain). The unknown distribution χ can describe the electrical permittivity and/or conductivity in the region. In this paper, the authors present the technique in the context of breast cancer detection.

In order to solve the nonlinear inverse problem often a linearization method is employed (e.g. distorted wave Born approximation) followed by a linear optimization solver. The forward electromagnetic solver is then used to evaluate the "guess" of the unknown distribution and calculate the same quantities as the ones measured by the system.

Right now, an in-house Method of Moments solver [1] is used in the post-processing part of the microwave imaging system. It is fast, accurate and tested. However it has some limitations which pushed authors' focus towards commercial software. The most significant flaws of the solver are: steep learning curve, tedious process of building a model and lack of portability. Most of commercial software for solving scientific problems provides user with advanced tools for model building and meshing. It is especially important in development phase, where building an efficient digital prototype is crucial. Commercial software tends to be more general and have better post-processing capabilities which make model inspection easier and faster. The portability and documentation is often far better than in an in-house software. This leads to much easier knowledge transfer.

Prototype system

The current prototype system [2] consists of a large tank filled with a coupling liquid. Inside the tank there are 8 layers of 4 monopole antennas made out of a coaxial cable with 3.5 cm of the outer conductor stripped. The antennas are placed in a circular layout with the imaging domain in their center. The operating frequency range is from 0.5 to 2 GHz. The coupling liquid is a 90**–**10% glycerin-water solution with ε_r = 9.45 and σ = 0.843 S/m at 1.5 GHz at 22°C. The wavelength in the liquid is about 6 cm.

Numerical model

To simplify the model the wave equation is solved only in the liquid, imaging domain and the antennas dielectrics. There has been a great deal of attention paid to meshing the model. After preparation of an initial model, the elements of the worst quality had been plotted. They appeared at the boundaries between domains. Making the mesh denser at the boundaries increased the overall mesh quality, which in turn improved the convergence of the solution. To improve the speed of computations a frequency-dependent mesh had been used.

Communication with the rest of environment

There are different ways of connecting COMSOL simulations with the rest of a processing toolchain. One of them is using the MATLAB LiveLink connection to define the model with MATLAB scripts. In this paper a simpler (file-based) approach is presented. The "guess" of χ distribution is read as an interpolating function and used to prescribe the material parameters of the imaging domain.

Choosing the most efficient solving method

The biggest improvement in terms of speed was made by switching to a direct solver (i.e. MUMPS). Changing from BiCGStab to MUMPS decreased the calculation time almost 3 times while increasing memory usage almost 5 times.

Validation with measurements

In order to assess usefulness of the solver, its results were compared to measurements. In the experiment a ball filled with water was placed in the imaging domain to be recognized by the system and the same was modelled using the COMSOL forward solver. The results agreed except for offsets attributed to uncertainties in liquid parameters and antenna positioning.

Conclusions

This paper shows that COMSOL Multiphysics allows building an efficient full-wave solver that can be used in the process of solving the tomography problem. Such a simulation allows faster prototyping, analysis of different configurations and deepens the understanding of the model. Using commercial software reduces the software effort, which allows focusing more on the scientific part of research rather than on software engineering.

REFERENCES

[1] Oleksiy S. Kim, Peter Meincke, Adaptive Integral Method for Higher Order Method of Moments, *IEEE Transactions on Antennas and Propagation*, 56 (2008), No. 8

[2] V. Zhurbenko, T. Rubæk, V. Krozer, P. Meincke, Design and realisation of a microwave three-dimensional imaging system with application to breast-cancer detection, *IET Microwaves, Antennas & Propagation*, 2010

Authors*: Bartosz Chaber, Warsaw University of Technology, Koszykowa 75, 00-662 Warsaw, Poland, chaberb@iem.pw.edu.pl*
Johan Mohr, Technical University of Denmark, Ørsteds Plads, 2800 Kgs. Lyngby, Denmark, jm@elektro.dtu.dk

This work has been supported by the European Union in the framework of European Social Fund through the project: Supporting Educational Initiatives of the Warsaw University of Technology in Teaching and Skill Improvement Training in the Area of Teleinformatics

POSTER SESSION 1 & YOUNG RESEARCHER POSTER COMPETITION
(Monday 08.06.2015, 14:50 – 16:20)

Chairman: Georgi Tsenov gogotzenov@tu-sofia.bg
Chairman: Barbara Szymanik barbara.szymanik@zut.edu.pl
Chairman: Grzegorz Psuj grzegorz.psuj@zut.edu.pl

	Authors	Title
1	Sai Pavan Kumar Veeranki, Jean Chamberlain Chedjou, Kyandoghere Kyamakya, Nkiediel Alain Akwir, Baraka Olivier Mushage	On the Analysis of Discrete Problems Using Continuous Models
2	Hanwu Luo, Peng Cheng, Haibo Liu, Kai Kang, Fan Yang, Qi Yang	Research on the UHF Microstrip Antenna for Partial Discharge Detection in High Voltage Switchgear
3	Hanwu Luo, Peng Cheng, Haibo Liu, Kai Kang, Fan Yang, Qi Yang	Investigation of the Needle-plate Discharge Characteristics in Atmospheric Air Based on Coupling Fields
4	Hanwu Luo, Peng Cheng, Haibo Liu, Kai Kang, Fan Yang, Qi Yang	Investigation of Propagation Characteristics of UHF Electromagnetic Wave Due to PD in Switchgear
5	Eugenio Costamagna	Some Quantitative Evaluations on Finite Difference Local and Global Results
6	Xiaokuo Kou, Jiajia Hu, Degui Yao, Manling Dong, Fan Yang	Research on the Grounding Grid Fault Diagnosis Based on Regularization Method
7	Piotr Jankowski	About The Lack of Convergence in An Environment with Limited Representation of the Number
8	Meinolf Klocke	Simultaneous Current Density and Temperature Calculation
9	Lubomir Kolev	A New Approach to Hull Consistency
10	Mikołaj Książkiewicz	Self-Adjusting Genetic Algorithm for Optimization of Magnetic Field Value in Close Proximity of a Power Line
11	Hua Li, Wolfgang M. Rucker	A Hybrid Method for the Calculation of the Inductances of Coils with and without Deformed Turns
12	Stanisław Gratkowski, Krzysztof Stawicki, Marcin Ziolkowski	General Closed-Form Asymptotic Boundary Conditions for Finite Element Analysis of Exterior Electrical Field Problems
13	Daniel Marcsa, Miklós Kuczmann	Closed Loop Voltage Control of a Solenoid Using Parallel Finite Element Method
14	Michael Popp, Patrick Laza, Wolfgang Mathis	Modelling and Simulation Aspects of Electrical AC Machines
15	Marco Reit, Michael Berens, Wolfgang Mathis	Ambiguities in Input-Output Behavior of Driven Nonlinear Systems Close to Bifurcation
16	Thomas Vennemann, Florian Mehringer, Victor Vu, Esther Dietrich, Wolfgang Mathis	Self-Adjusting Feed Forward Path to Compensate the Switching Noise in a ZePoC AC Voltage Standard
17	Daniel Stahl, Wolfgang Mathis	Energy Transitions in Electrical Oscillators Studied by the Generalized Liouville Equation
18	Mirosław Wołoszyn, Kazimierz Jakubiuk, Mateusz Flis	Analysis of Resistive and Inductive Heating of Railway Turnouts
19	Zuzanna Krawczyk, Jacek Starzyński	Bone Structure Segmentation with Bio-inspired Methods
20	Paweł Karol Frankowski, Tomasz Chady	Massive Multi-Frequency Eddy Current Method for Clad Material Inspection
21	Diana Olejnik, Tomasz Chady, Paweł Karol Frankowski	Climbing Quadruped Robot for Non-Destructive Testing

Sai Pavan Kumar VEERANKI, Jean Chamberlain CHEDJOU, Kyandoghere KYAMAKYA, Nkiediel Alain AKWIR, Baraka Olivier MUSHAGE

Alpen Adria Universität, Klagenfurt (AAU)

On the Analysis of Discrete Problems Using Continuous Models

Abstract. *This paper develops a general, robust and efficient concept for analyzing discrete problems. The concept is based on ordinary differential equations (ODEs), which are continuous time model. To demonstrate the effectiveness of the concept, we address the minimum cost path detection problem amongst many other discrete problems such as travelling salesman problem, etc. As proof of concepts, several application examples are considered (directed and undirected graphs) and the efficiency of the concept is demonstrated.*

Keywords: Discrete problems, Ordinary differential equations, Optimization.

Introduction

We have considered combinatorial optimization problems, which are discrete problems to demonstrate the concept of ODEs. Some interesting application examples are: in-vehicle route guidance systems (RGS) automated vehicle dispatching systems (AVDS), real-time traffic information sensing, fleet management, etc. [1]. An interesting problem amongst discrete problems is the traditional minimum cost path detection problem. The minimum cost path corresponds to the shortest path, which corresponds to the walk from a source to destination with the minimum cost. Our analysis is restricted to the case of additive costs.

The general optimization problem is defined by an objective function and a set of constraints. The objective function and constraints are combined to obtain the Lagrange function [2]. Then, applying the Basic Differential Multiplier Method (BDMM [2] to the Lagrange function leads to the derivation of a set of coupled nonlinear ODEs.

Methodology

The steps involved in the derivation of the couple nonlinear ODEs are expressed as follows:

Step 1: *Formulation of the objective function:*

(1) $\min f(x)$

$f(x)$ = is the total cost of the graph and x is the state of all the edges of the graph.

Step 2: *Formulation of constraints:*

(2 a) $g(\vec{x}) = 0$

The constraints are formulated according to some specific requirements.

For the minimum cost path, $g(x)$ is expressed in (2 b.)

(2 b.) $$\sum_{i=1, i\neq k}^{M} x_{i\to k} - \sum_{i=1, i\neq l}^{M} x_{l\to i} = \delta_i$$

δ_i = 1 if i is source, δ_i = 0 if i is intermediate and δ_i = –1 if i is destination node.

Step 3:*Formulation of Lagrange function:*

(3) $$\tilde{L}(\vec{x},\vec{\lambda}) = f(x) + \sum_{j=1}^{M} \lambda_j [g_j(\vec{x})]$$

M is the number of nodes in the graph, $g(x)=0$ are Constraints to assign one of the attributes (source, intermediate and destination) to each node of the graph and λ is the vector of multiplier neurons. This vector insures that each node is assigned a unique attributes.

Step 4: *Application of the Basic differential multiplier method (BDMM):*

(4 a.) $$\frac{d\vec{x}}{dt} = -\frac{d\tilde{L}}{dx}$$ (4 b.) $$\frac{\partial\vec{\lambda}}{\partial t} = +\frac{\partial\tilde{L}}{\partial\lambda}$$

Equations (4) is used to derive the set of coupled nonlinear ODEs, which are expressed into the compact form in (5) [3].

(5) $$\frac{dx_i}{dt} = -x_i + \sum_{j=1} A_{ij}x_j + \sum_{j=1} B_{ij}x_i x_j + \sum_{j=1} C_{ij}x_j^2 + I$$

A, B, C and I are the parameter settings of the (5). The binary solutions $x_i \in \{0,1\}$ are used to depict the state of edges connectivity. x_i = 1 for edges belonging to the shortest path and x_i = 0 otherwise.

Simulation results

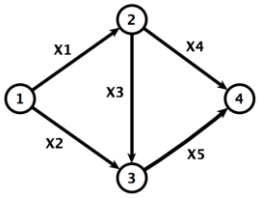

Fig. 1. A directed graph of magnitude 4 and size 5 for costs (C_1 = 2, C_2 = –1; C_3 = –4; C_4 = 3; C_5 = –6)

Table 1. Paths for corresponding source-destination pair

Source---->destination	Convergence	Path
1---->4	Yes	X_1-----> X_3----> X_5
1---->3	Yes	X_1-----> X_3

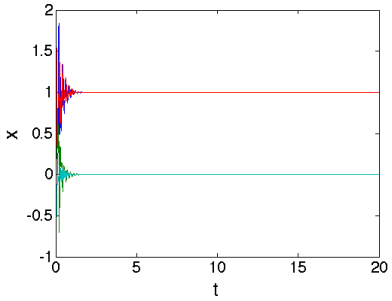

Fig. 2: Convergence behavior of (5)

Conclusion

From Table 1 and Fig. 2, we can conclude that the continuous model (based on ODEs) proposed in this paper can successfully solve discrete problem. This model has been applied on the minimum cost path detection problem.

REFERENCES

[1] L. Fu, An Adaptive routing algorithm for in-vehicle route guidance systems with real time information, Transportation research part B, vol. 35, pp. 749–765, 2001.

[2] C. Platt John, H. Barr Alan, Constrained differential optimization for neural networks, Caltech.

[3] O, Chua L, "Cellular neural networks: applications, IEEE transactions on circuits and systems, Vol. 35, pp. 1273–1290, 1988.

Authors: *S.P.K. Veeranki, AAU, Klagenfurt, Austria, sai.veeranki@edu.aau.at, J.C. Chedjou, AAU, Klagenfurt, Austria, jean.chedjou@aau.at, K. Kyamakya, AAU, Klagenfurt, Austria, kyandoghere.kyamakya@aau.at, N.A. Akwir, AAU, Klagenfurt, Austria, nkawir@edu.aau.at, B.O. Mushage, AAU, Klagenfurt, Austria, bamushage@edu.aau.at*

Hanwu LUO[1], Peng CHENG[2], Haibo LIU[1], Kai KANG[1], Fan YANG[2], Qi YANG[2]

East Inner Mongolia Electric Power Company Limited (1), Chongqing University (2)

Research on the UHF Microstrip Antenna for Partial Discharge Detection in High Voltage Switchgear

Abstract. *In order to detect the ultra-high-frequency (UHF) signals generated from partial discharges (PDs) in high voltage switchgear, a microstrip antenna sensor is designed. Influences of geometric parameters on the capability of the proposed antenna sensor are researched by numerical simulation. Measured characteristic results show that this antenna sensor is very suitable for partial discharge detection.*

Keywords: ultra-high-frequency (UHF), partial discharge, microstrip antenna sensor.

Introduction

High voltage switchgear are widely used as important fundamental equipment in electric power system, which are directly relative to the power supply reliability and quality. Partial discharge (PD) as a potential threat directly affects the insulation safety in high voltage switchgears and power system.

In previous studies [1-2], many scholars focus on the application of UHF sensors for PD detection in transformers and gas-insulation switches, but the study on the application of an ultra-wideband (UWB) antenna is not enough.

In this paper, an UWB planar monopole microstrip antenna is proposed and it is developed based on the optimal design procedure.

Design Criteria of the Antenna Sensor

According to the structure and PD characteristics of the high voltage switchgears, the design criteria of an UHF antenna sensor for PD detection are: ① work frequency band of 500MHz to 1500MHz, ② built-in installation, ③ higher gain, ④ omnidirectional radiation patterns, ⑤ reasonable size and shape.

Optimization of the Antenna Sensor

After the simulation optimization of HFSS software, the schematic configuration of the proposed UWB planar monopole microstrip antenna is shown in Fig.1.

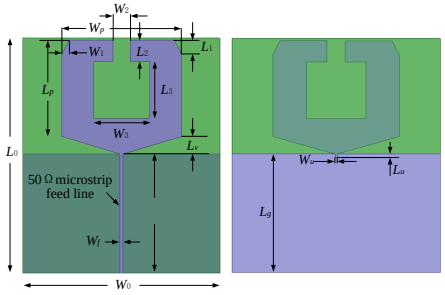

(a) (b)

Fig. 1. Schematic configuration of the proposed UWB antenna sensor. (a) Top view; (b) Back view

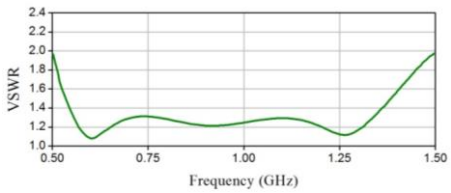

Fig. 2. Simulated VSWR of the proposed UWB antenna sensor

The voltage standing wave ratio (VSWR) of the proposed antenna is shown in Fig. 2.

Fabrication and Measurement Results

The VSWR parameter, 2D normalized radiation patterns and peak gain of the fabricated antenna sensor have been measured and the results are shown in Fig. 3–5, respectively.

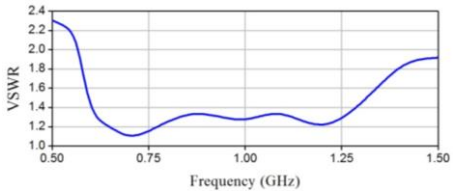

Fig. 3. Measured VSWR of the fabricated UWB antenna sensor

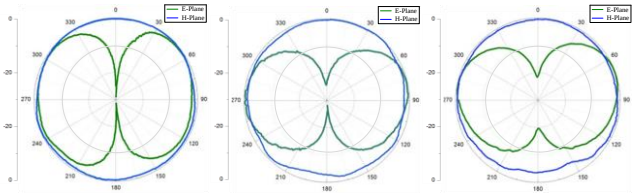

(a) (b) (c)

Fig. 4. Measured 2D normalized radiation patterns of the fabricated UWB antenna sensor. (a) 500MHz, (b) 1000MHz, (c) 1500MHz

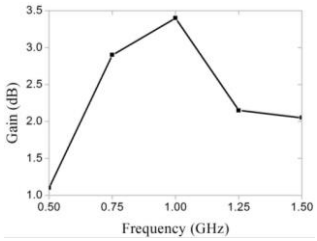

Fig. 5. Measured peak gain of the fabricated UWB antenna sensor

Conclusion

An UWB planar monopole microstrip antenna sensor for PD UHF detection in high voltage switchgears was presented. The design of the antenna is optimized through simulation studies. Measurement results show the performance are very suitable.

REFERENCES

[1] G. Robles, et al, Shielding effect of power transformers tanks in the ultra-high-frequency detection of partial discharges, IEEE Trans. Dielectr. Electr. Insul., Vol. 20, no. 2, pp. 678–684, 2013.

[2] T. Li, et al, Development simulation and experiment study on UHF partial discharge sensor in GIS, IEEE Trans. Dielectr. Electr. Insul., Vol. 19, no. 4, pp. 1421–1430, 2012.

***Authors**: Cheng Peng, the State Key Laboratory of Power Transmission Equipment & System Security and New Technology, School of Electrical Engineering, Chongqing University, Chongqing 400044 China, e-mail: chengpeng19870825@163.com*

Hanwu LUO[1], Peng CHENG[2], Haibo LIU[1], Kai KANG[1], Fan YANG[2], Qi YANG[2]

East Inner Mongolia Electric Power Company Limited (1), Chongqing University (2)

Investigation of the Needle-plate Discharge Characteristics in Atmospheric Air Based on Coupling Fields

Abstract. *In order to investigate the partial discharge characteristics, a needle-plate discharge model, which is built based on magneto-hydrodynamic (MHD) theory, is taken as an example. Based on this model, the distributions of coupling fields can be calculated. The simulation results are helpful for us to understand the fundamental characteristics in the process of partial discharge.*

Keywords: partial discharge, needle-plate discharge, magneto-hydrodynamic (MHD), coupling fields.

Introduction

Partial discharge (PD) process is a complicated phenomenon, which includes a mutual coupling between flow field, electromagnetic field and thermal field. In previous studies, many scholars focus on the arc investigation through experimental method. Due to the development of computer technology, it is possible for us to investigate the arc by using simulation method [1–2].

In this paper, a needle-plate discharge model is built based on magneto-hydrodynamic (MHD) theory. Through the calculation, the distributions of the electric, temperature and flow fields are investigated.

Methodology

The process of discharge can be described by the following equations.

(1) $$\frac{\partial \rho}{\partial \mathrm{t}}+\mathrm{div}(\rho \mathbf{v})=0$$

(2) $$\frac{(\partial \rho v_i)}{\partial \mathrm{t}}+\mathrm{div}(\rho \mathbf{v} v_i)=-\frac{\partial p}{\partial x_i}+\mathrm{div}(\eta \mathrm{grad} v_i)+(\mathbf{J}\times\mathbf{B})$$

(3) $$\frac{(\partial \rho H)}{\partial \mathrm{t}}+\mathrm{div}(\rho \mathbf{v} H)-\mathrm{div}(\lambda \mathrm{grad} T)=\frac{\partial p}{\partial t}-S_R+\frac{1}{\sigma}\mathbf{J}^2$$

where: t – time, v_i – the components of velocity in rectangular coordinates, P – pressure, T – temperature, H – enthalpy, $\mathbf{J}$ – current density, $\mathbf{B}$ – magnetic induction intensity, S_R – radiation loss, ρ – density, η – viscosity, λ – thermal conductivity, σ – electrical conductivity.

The electric field and current density are determined by the Maxwell equations.

(4) $$\mathrm{div}(\sigma \mathrm{grad}\phi)=0$$

(5) $$\mathbf{J}=-\sigma \mathrm{grad}\phi$$

where: ϕ – electric potential.

Example Simulation and Analysis

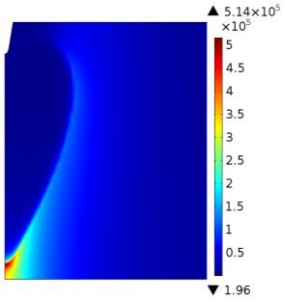

(a)

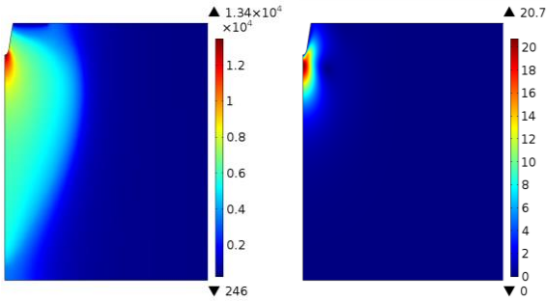

(b) (c)

Fig. 1. Coupling fields distributions in needle-plate discharge process. (a) electric field; (b) temperature field; (c) velocity field

When the distance between needle and plate is 10 mm and electric potential ϕ is 2000 · sin(2π · 50 · t) V, the electric field, temperature field and velocity field of t = 0.78 ms are shown in Fig. 1. Temperature distributions along the symmetric axis at different time are shown in Fig. 2.

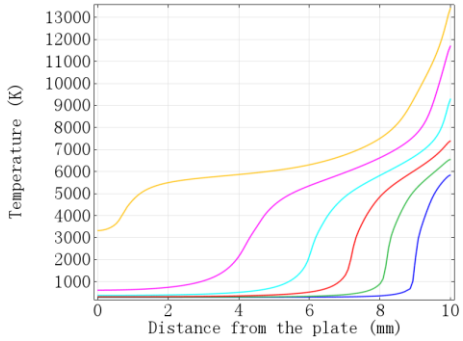

Fig. 2. Temperature distribution curves with different time

Conclusion

A needle-plate discharge model in atmospheric air based on MHD theory is built. Based on this method, the distributions of the electric, temperature and flow fields in the discharge process are investigated.

REFERENCES

[1] M. Iwata, et al, CFD calculation of pressure rise due to internal AC and DC arcing in a closed container, IEEE Trans. Power.Del., vol. 26, no. 3, pp. 1700-1709, Jul. 2011.

[2] B. H. Bang, et al, Prediction and improvement of dielectric breakdown between arc contacts in gas circuit breaker, 2nd International Conference on Electric Power Equipment, Matsue, Japan, 2013.

***Authors**: Cheng Peng, the State Key Laboratory of Power Transmission Equipment & System Security and New Technology, School of Electrical Engineering, Chongqing University, Chongqing 400044 China , e-mail: chengpeng19870825@163.com*

Hanwu LUO[1], Peng CHENG[2], Haibo LIU[1], Kai KANG[1], Fan YANG[2], Qi YANG[2]

East Inner Mongolia Electric Power Company Limited (1), Chongqing University (2)

Investigation of Propagation Characteristics of UHF Electromagnetic Wave Due to PD in Switchgear

Abstract. *In order to investigate the propagation characteristics of ultra-high-frequency (UHF) electromagnetic wave caused by partial discharge (PD) in high voltage switchgear, a simulation model was established by using the finite-difference-time-domain (FDTD) method. The simulation results have instructive meanings for the installation of UHF sensor to detect PDs in switchgear.*

Keywords: propagation characteristic, ultra-high-frequency (UHF), electromagnetic wave, partial discharge (PD).

Introduction

Switchgear is the key equipment in urban distribution power network, its operation reliability directly relates to the security and stability of power system. PDs are major causes leading to insulation faults in switchgear. The main methods used for PD detection in switchgear include ultrasonic method, radio frequency (RF) method, transient earth voltage (TEV) method and UHF method. Due to strong anti-interference ability and high sensitivity, the UHF method has a great application prospect.

In this paper, the switchgear model is established and the influences of the main components on the propagation characteristics of UHF electromagnetic wave are investigated by using XFDTD software. The simulation results provide theoretical references for the installation of UHF sensor to detect PDs in switchgear.

Modeling

The KYN28-12 high voltag switchgear is taken as an example and its physical model is shown in Fig.1. The dimension is 1500 mm × 800 mm × 2300 mm.

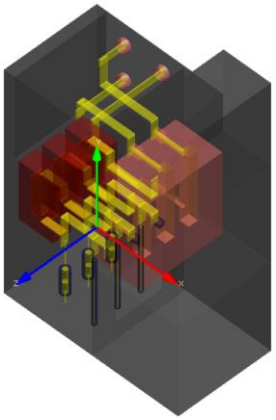

Fig. 1 Simulation model of the high voltage switchgear

The Gaussian current pulse is chosen as the PD source and its time-domain expression is shown as follows:

$$I(t) = I_0 \exp\left[-\frac{4\pi(t-t_0)}{\tau^2}\right] \quad (1)$$

where: τ – a constant value, which determines the width of the Gaussian pulse; I_0 – the amplitude of the Gaussian pulse; t – time of the pulse wave; t_0 – the time for the amplitude of the Gaussian pulse.

Discussion

After the parameter settings, mesh generation and PD source setting, the propagation characteristics of UHF electromagnetic wave in high switchgear can be investigated.

When the amplitude of the Gaussian pulse current is 1 A the width of the Gaussian pulse is 616 ps and the distance between PD source point and detection is given, the UHF waveform at detection point is shown in Fig. 2.

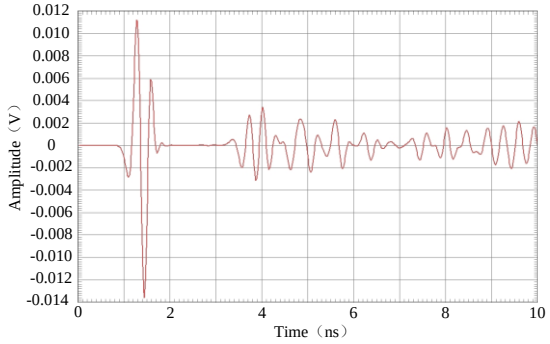

Fig. 2 UHF waveform at detection point

Based on this model, the influences of the amplitude of the Gaussian pulse current, the width of the Gaussian pulse, the distance between PD source point and detection and main components in switchgear on the UHF waveform can be investigated.

Conclusion

The simulation model of a KYN28-12 high voltage switchgear is established and the influences of the some factors on the propagation characteristics of UHF electromagnetic wave are investigated by using FDTD method. The simulation results can be used to optimize the location of inner UHF sensors inside switchgear.

REFERENCES

[1] Manabu Yoshimura, et al., Propagation properties of electromagnetic wave through T-branch in GIS, IEEE Trans. Dielectr. Electr. Insul., Vol. 14, no. 2, pp. 328–333, Apr. 2007.

[2] Tianhui Li, et al, Investigation on the placement effect of UHF sensor and propagation characteristics of PD-induced electromagnetic wave in GIS based on FDTD method, IEEE Trans. Dielectr. Electr. Insul., Vol. 21, no. 3, pp. 1015–1025, Jun. 2014.

Authors:
Luo Hanwu, Liu Haibo and Kang Kai are with East Inner Mongolia Electric Power Company Limited, Hohhot 010020, China.
Cheng Peng, Yang Fan and Yang Qi are with the State Key Laboratory of Power Transmission Equipment & System Security and New Technology, School of Electrical Engineering, Chongqing University, Chongqing 400044 China, e-mail: chengpeng19870825@163.com

Eugenio COSTAMAGNA

University of Pavia (Retired)

Some Quantitative Evaluations on Finite Difference Local and Global Results

Abstract. *Refined Schwarz-Christoffel (SC) conformal transformations allow us to perform reliable quantitative evaluation of the accuracy of local computation of electric and magnetic fields with limited effort, which can be useful to complement well known comparisons of global results. In this paper some example are presented for mesh point potentials in obtained by means of finite difference (FD) methods, but it is possible that similar considerations will be useful in case of finite methods (FEM) or meshless computations too.*

Keywords: Schwarz-Christoffel, finite difference, static fields.

Introduction

Availability of powerful methods for numerical computation an inversion of the Schwarz-Christoffel formula allows us to compare with limited computational effort not only global quantities, as capacitances in the following FD examples, but local results too, as mesh point potentials. Indeed, the examples concern classic case studies, but the author is not aware of studies related to the accuracies of single point potentials.

An L shaped domain

A capacitance is obtained by means of considering two equal side dihedral electrodes and sides magnetic walls, as in Fig. 1: the geometry was already considered as test problem when introducing a novel approach to the SC formula calculations [3].

A short side geometry was selected here to enhance the effects of the electrode shape on the field behavior. The domain was mapped into a rectangle via SC numerical inversion (SCNI), and a capacitance in air of about CSC = $2.2654 \cdot 10^{-11}$ F was found. In the figure a vertical line is traced, and in Fig. 2 both the rectangle and the transformed map of the quoted vertical line are shown.

For the same geometry, capacitances and mesh potentials have been obtained from a simple FD code for various numbers of points. With 1+8 and 1+4 points on the L sides (the mesh points lie in this case on the figure grid) the two capacitance values obtained for the “exterior” and for the “interior” electrodes were equal respectively to about CSC·1.026489 and CSC· 1.0180854.

Now, if the vertical line of Fig. 1 coincides with the a mesh vertical line, the true (i.e., the SC) potentials of the mesh points lying on it can be derived from the abscissas of the corresponding points on the map of Fig. 2.

Comparison with the potentials obtained from the FDs for the grid points adjacent to the boundary (used, of course, to evaluate the electrode dielectric fluxes) shows ratios to SC potential ranging from about 1.01 to about 1.036, the errors being of the same order as capacitance errors. Similar conclusions have been obtained with L side lengths of 256 and 128 points, with a capacitance ratio to CSC of about 1.005.

A stripline geometry

Similar computations have been performed for a strip line, with width proportional to 48, centered in a rectangular box having both the width and the height proportional to 64.

When the potentials on the mesh points adjacent to the box sides were considered, the ratios to the corresponding SC potentials were somewhat greater than the capacitance ratios. This was not true, of course, for the mesh points close to the strip end. For the point at distance proportional to 1 (abscissa proportional to 15) the ratio of potentials was about 1.06.

Conclusions

When the conditions are suitable (no singularity, or at least favorable way of lying of the boundary on the mesh, as in the L shaped domain) local and global accuracies are similar. Apparently, simple procedures to summing up the discrete contributions to the boundary flux are adequate in these cases.

This kind of analyses follows some observations on discretization problems sketched in [5, 6] and probably can contribute to explain good results obtained from FEMs

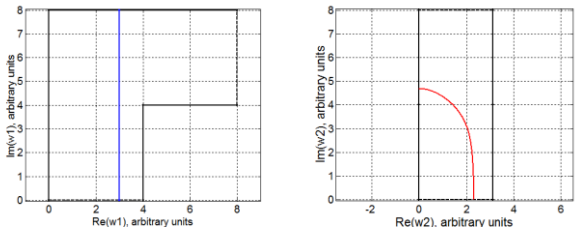

Fig.1. An example of L shaped domain (left) and the rectangle SC map of it.

REFERENCES

[1] T. A. Driscoll and L.N. Trefethen, Schwarz-Christoffel Mapping, Cambridge University Press, 2002, pp. 9–30 and 70–74.

[2] E. Costamagna, P. Di Barba, M.E. Mognaschi, A. Savini, Fast algorithms for the design of complex-shape devices in electromechanics, in Computational Methods for the Innovative Design of Electrical Devices, Springer 2010, pp. 61–65.

[3] E. Costamagna, A new approach to standard Schwarz-Christoffel formula calculations, Microwave Technol Opt Lett, 51 (2002), No. 3, 196–199.

[4] E. Costamagna, P. Di Barba, A. Savini, A kinematic approach to the optimal shape synthesis of electric fields, Electrical Review, ISSN 0033-2097, Vol. 88, no. 7b, pp. 90–93, 2012.

[5] E. Costamagna, A Simple Procedure to Optimize Small Radius Rounded Corners Obtained from Schwarz-Christoffel Conformal Transformations,” to appear in IEEE Trans. Magn., 51, (2015).

***Author**: Eugenio Costamagna, University of Pavia, Via Ferrata 1, Pavia, Italy, E-mail: eugenio.costamagna@unipv.it*

Xiaokuo KOU[1], Jiajia HU[2], Degui YAO[1], Manling DONG[1], Fan YANG[2]

State Grid Henan Electric Power Corporation Research Institute, China (1), Chongqing University (2)

Research on the Grounding Grid Fault Diagnosis Based on Regularization Method

Abstract: *This paper uses electric circuit theory to establish grounding grid fault diagnosis equations and proposes the regularization method to solve them, which can better solve the ill-posed issues of the equations. Finally, the laboratory test is performed to verify the feasibility and accuracy of the method.*

Keywords: electric circuit theory**,** regularization method, grounding grid, fault diagnosis.

Introduction

Grounding grid plays an important role in the normal operation of substation. A good grounding grid not only provides a common potential reference ground for various electric devices within the substation, but also can release fault current and reduce the rise of substation ground potential when suffering the shortcut in power system or attacked by lighting. The performance of grounding grid will be directly related to the personal safety and the normal operation of electric equipment[1, 2].

There are mainly two pivotal methods to diagnose the grounding grid. The first one is a method based on the electromagnetic field theory, while the other based on the electric circuit theory. However, it is difficult to solve the equations established by circuit theory because of its an ill-posed problem. Thus the regularization algorithm is proposed to solve the fault diagnosis equations in this paper and we can attain a better solution of the fault diagnosis for grounding grid.

The regularization method

Assume the grounding grid has N nodes and B branches, equations built by the electrical network theory are:

$$(1) \qquad \boldsymbol{Y}_n\boldsymbol{U}_n = \boldsymbol{I}_n,\ \ \boldsymbol{Y}_n = \boldsymbol{A}\boldsymbol{Y}_b\boldsymbol{A}^T,\ \ \boldsymbol{U}_b = \boldsymbol{A}^T\boldsymbol{U}_n,\ \ \boldsymbol{I}_b = \boldsymbol{Y}_b\boldsymbol{U}_b$$

where: $\boldsymbol{A}$ – network connection matrix, $\boldsymbol{Y}_b$ – branch admittance matrix, $\boldsymbol{Y}_n$ – node admittance matrix, $\boldsymbol{U}_b$ – branch voltage vector, $\boldsymbol{U}_n$ –node voltage vector, $\boldsymbol{I}_n$ – node current vector, $\boldsymbol{I}_b$ – branch current vector.

Through calculation, $f(\boldsymbol{R})$ could be obtained. By minimizing the $f(\boldsymbol{R})$ we can get the branch resistance and its variation in accordance with measured value.

$$(2) \qquad \min\ \ f(\boldsymbol{R}) = \frac{1}{2}\left\|\boldsymbol{U}_n(\boldsymbol{R}) - \boldsymbol{U}_{n0}\right\|^2,\ \boldsymbol{R} = [R_1, R_2, \cdots, R_B]^T$$

where: $\boldsymbol{U}_{n0}$ **–** node voltage measurements, $\boldsymbol{U}_n(\boldsymbol{R})$ – calculated node voltage value, $\boldsymbol{R}$ – unknown resistance vector.

By solving (2) we can get the optimal solution of each branch resistance, and then compared with resistance design value of each branch, we can judge the corrosion and fracture of branch conductor. Make a derivation for (2) at $\boldsymbol{R}^{(k)}$,we can finally obtain (3):

$$(3) \qquad \boldsymbol{R}^{(k+1)} = \boldsymbol{R}^{(k)} - \left(\boldsymbol{J}_k^T\boldsymbol{J}_k\right)^{-1}\boldsymbol{J}_k^T\left(\boldsymbol{U}_n(\boldsymbol{R}^{(k)}) - \boldsymbol{U}_{n0}\right)$$

where: $\boldsymbol{J}_k = \dfrac{\partial \boldsymbol{U}_n}{\partial \boldsymbol{R}}(\boldsymbol{R}^{(k)})$ – Jacobi matrix.

Equation (3) is the Newton-Raphson iterative format of grounding grid fault diagnosis.

The grounding grid fault diagnosis method based on regularization method

$\boldsymbol{J}_k^T\boldsymbol{J}_k$ has many condition numbers and its inverse matrix cannot be easily accurately calculated. We can get a new iteration formula (4) by adding penalty function based on N-R algorithm:

$$(4) \quad \boldsymbol{R}^{(k+1)} = \boldsymbol{R}^{(k)} - \left(\boldsymbol{J}_k^T\boldsymbol{J}_k + \alpha\boldsymbol{L}^T\boldsymbol{L}\right)^{-1}\left[\boldsymbol{J}_k^T\left(\boldsymbol{U}_n(\boldsymbol{R}^{(k)}) - \boldsymbol{U}_{n0}\right) - \alpha\boldsymbol{L}^T\boldsymbol{L}(\boldsymbol{R}^{(k)} - \boldsymbol{R}^{(0)})\right]$$

Thus the eigenvalues of the matrix $\boldsymbol{J}_k^T\boldsymbol{J}_k + \alpha\boldsymbol{L}^T\boldsymbol{L}$ can be adjusted by changing α constantly in the process of iteration, to improve the condition number of the matrix $\boldsymbol{J}_k^T\boldsymbol{J}_k + \alpha\boldsymbol{L}^T\boldsymbol{L}$ and to meet the requirements of matrix inversion, so it is able to make the process of iterative fast convergence, and the stability of the process of solving inverse problem is greatly improved.

Laboratory tests

To test the accuracy of this algorithm, a laboratory test was performed, and the fault diagnosis results obtained by using the regularization method matched the situation designed, which indicated the regularization algorithm was effective. The diagnosis result was shown in Figure 1.

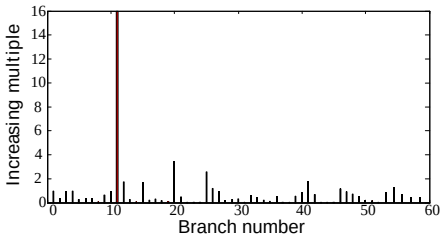

Fig. 1. The result of fault diagnosis

REFERENCES

[1] Jin Liang, Herong Zeng, The Grounding Technology of Power System, *BeiJing*: *Science press*, 2007.

[2] Chongwu Xu, Xuewen Hu, Research on Anticorrosive Metal Material Performance Test for Grounging Grid, *The Grid Technology*, 21 (2003), No. 8, 77–79.

Authors*: Xiaokuo Kou, State Grid Henan Electric Power Corporation Research Institute, Zhengzhou, Henan Province, China, E-mail: koukuo@163.com.*

Jiajia Hu, Chongqing University, Chongqing, China, E-mail: hujj_fish@qq.com

Piotr JANKOWSKI

Gdynia Maritime University

About The Lack of Convergence in An Environment with Limited Representation of The Number

Abstract. *The article presents cases of lack of convergence of transitional problems solutions both for the linear and non-linear problem. In a linear case, electric circuit solution using state variables was presented. As a non-linear case, ferroresonance system solved by various numerical procedures was shown. To solve the proposed problems, the 64-bit PTC Mathcad Prime 3.0 environment was used.*

Keywords: Mathcad, convergence, transitional matrix.

Introduction

Nowadays, to solve technical matters described by mathematical equations, ready applications such as Matlab Mathcad, or Mathematica are used. The programs contain numerous preset procedures allowing to change various parameters which also have influence on accuracy. It is obvious that the value of many of these parameters has its limitations. Such a limitation is the maximum number of digits representing the number in these environments (17digits). The solutions of the classical problems of electrotechnics theory such as transients for linear and non-linear circuit will be presented in the paper. On their example the problem of achieving convergence solutions in Mathcad environment was shown.

Examples of linear and nonlinear circuit analysis

To solve the linear circuit (Fig. 1) the equation of state variables was applied (1). In turn, to determine the transition matrix the Sylvester method, and further the method of Taylor series developing were used (2). Using of computer it should be emphasized that the method of Taylor is offered in references as effective for any non-singular matrix A, and for any time [1].

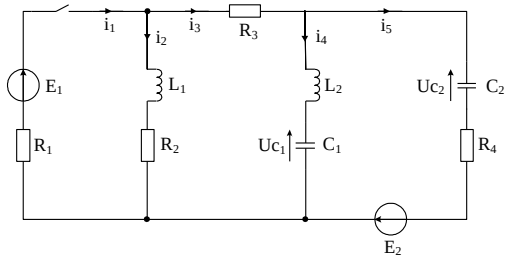

Fig.1. Tested linear circuit

(1) $$\dot{\boldsymbol{x}} = \boldsymbol{A}\cdot\boldsymbol{x} + \boldsymbol{Be(t)}$$

(2) $$e^{\mathbf{A}t} = \sum_{K} \frac{(\mathbf{A}\cdot t)^K}{K!}$$

In the Fig. 2 are examples of solutions of the homogeneous equation with the selected voltage of the circuit. Comparing these solutions, it was found that after a short time, the bifurcation of these solutions was started. It turns out that in environments such as Mathcad one cannot obtain satisfactory accuracy of transitional matrix determined on the basis of Taylor series development even using a large number of components. In this case, for K> 170 Mathcad generates a message: *Found a number with a magnitude greater than 10^307 while trying to evaluate this expression.*

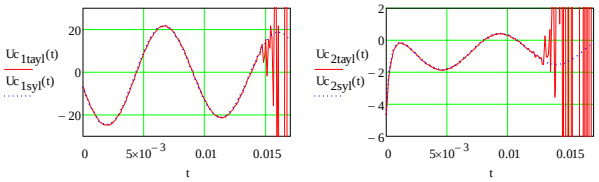

Fig. 2. The waveforms of the state variables for the solution of the homogeneous equation by Sylvester and Taylor method

The second considered example is a circuit with the highly non-linear coil (Fig. 3). The circuit was a simplified model of the system power transformer [2]. Characteristics *i(Ψ)* was approximated by a polynomial of 11-th degree. Using all family of procedures of Mathcad environment one did not get convergence for any desired time range (Fig. 4). What is worse, Mathcad should display a message: *not converging*, and in the consider case it does not appear.

$C = 1250\,\text{nF}\quad R = 10^{20}\,\Omega\quad E_m = 13.5\,\text{kV}$

$i = 2.8\times10^{-3}\Psi + 7.2\times10^{-3}\Psi^{11}$

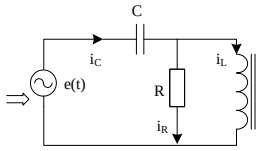

Fig. 3. Tested nonlinear circuit

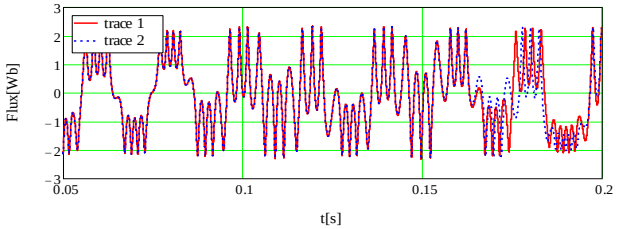

Fig. 4. Flux for rkfixed (for h step -trace 1, for 0.5h step -trace 2)

REFERENCES

[1] Bolkowski S. Teoria Obwodów Elektrycznych, Warszawa WNT 2005 p. 343

[2] Marti J. R., Soudack A. C., Ferrorezonans in power systems: Fundamental solutions. *IEEE proceedings-C* Vol. 138, No.4. pp. 321–329, July 1991

***Authors**: Piotr Jankowski Department of Marine Electrical Engineering, Gdynia Maritime University*
email: keopiotr@am.gdynia.pl

Meinolf KLOCKE

Siemens AG

Simultaneous Current Density and Temperature Calculation

Abstract. *A combined simultaneous calculation method for electrical contacts is presented based on a finite element analysis of both the current density distribution as well as the heat flow distribution. For an exact prediction of local hotspots special attention is put on the transition conditions at the joints where current and heat transfer with defined transfer coefficients takes place and temperature and electrical potential face a discontinuity. The conditions for the maximum temperature to be expected at a thermo-electrical contact are derived by an analytical consideration.*

Keywords: thermo-electrical coupling, FEM, contact temperature, temperature and potential discontinuity.

Introduction

Manufacturers of electrical machines are obliged to keep temperature limits for insulation materials as well as for electrical joints. The temperature at a screwed silver plated contact surface e.g. may not exceed 115°C [1].

Description of the arrangement

A special service modified type of an axial lead connection between exciter machine and turbine generator is investigated. The conductive path consists of three parts in electrical and thermal coupling. One is the axial lead itself. The other is an adapter threaded bushing, in which the third part – a cylindrical bolt – is inserted and electrically connected to the inner surface of the threaded bushing by three contact lamella belts. Owing to symmetry properties only a quarter of the arrangement has to be modelled including the central insulation wall between the positive and the negative lead.

Governing equations

GETDP [2] is used for the treatment of the problem. The electric potential φ in case of dc-current density distributions in bulks with conductivity γ is given in its weak formulation:

$$\iiint_V \gamma \operatorname{grad}\varphi \cdot \operatorname{grad}\phi \,\mathrm{d}V - \oint_{\partial V} \gamma \operatorname{grad}\varphi \cdot \phi \vec{n} \,\mathrm{d}a = 0 \tag{1}$$

with a resulting volumetric loss density of

$$p_\mathrm{V} = \gamma \cdot (\operatorname{grad}\varphi)^2 \ . \tag{2}$$

This is besides the temperature boundary conditions the excitation of the thermal problem which is analogous to the electrical one:

$$\iiint_V \lambda \operatorname{grad}\vartheta \cdot \operatorname{grad}\theta \,\mathrm{d}V - \oint_{\partial V} \lambda \operatorname{grad}\vartheta \cdot \theta \vec{n} \,\mathrm{d}a - \iiint_V p_\mathrm{V} \cdot \theta \,\mathrm{d}V = 0 \tag{3}$$

In the present case the problem is subdivided into three coupled domains for which six different function spaces are defined. By this definition the geometrically identical nodes on the surfaces in contact can take two different values of φ and ϑ like in [3]. The transfer conditions given by

$$J_{\mathrm{n},1} = J_{\mathrm{n},2} = -\gamma \operatorname{grad}\varphi \cdot \vec{n} = g_\mathrm{A}(\varphi_1 - \varphi_2) \tag{4}$$

$$\text{with} \quad p_\mathrm{A} = g_\mathrm{A}(\varphi_1 - \varphi_2)^2$$

for electrical joints and

$$\dot{q}_{\mathrm{n},1} = \dot{q}_{\mathrm{n},2} = -\lambda \operatorname{grad}\vartheta \cdot \vec{n} = \alpha(\vartheta_1 - \vartheta_2) \tag{5}$$

for heat transfer conditions are incorporated into the weak formulation by the surface integrals in (1) and (3). Here g_A is the surface transfer conductivity in S/m^2 and α the heat transfer coefficient in W/(m^{2}K). p_A is the surface loss density in the contact area. ϑ denotes the temperature and θ the respective test function.

A theoretical analysis of a simplified three layer model with a vanishing intermediate layer between two bulks shows that the maximum temperature can be taken within the intermediate layer, i.e. the contact surface, depending on the loss entry p_A in that very layer given by the contact resistance.

$$\vartheta_{1,2,\max} = \begin{cases} \dfrac{\alpha(\vartheta_1 - \vartheta_2)^2}{2g_\mathrm{A}(\varphi_1 - \varphi_2)^2} \cdot + \dfrac{g_\mathrm{A}}{8\alpha}(\varphi_1 - \varphi_2)^2 + \dfrac{1}{2}(\vartheta_1 + \vartheta_2), \\ \qquad\qquad \text{if } |\vartheta_1 - \vartheta_2| \le \dfrac{g_\mathrm{A}}{2\alpha}(\varphi_1 - \varphi_2)^2; \\ \max(\vartheta_1, \vartheta_2), \quad \text{if } |\vartheta_1 - \vartheta_2| > \dfrac{g_\mathrm{A}}{2\alpha}(\varphi_1 - \varphi_2)^2 \end{cases} \tag{6}$$

Result

An example for a resulting temperature distribution is given in Fig. 1 showing a hot spot on the outer thread close to the central insulation layer of the axial lead. However, allowable temperature limits are not exceeded.

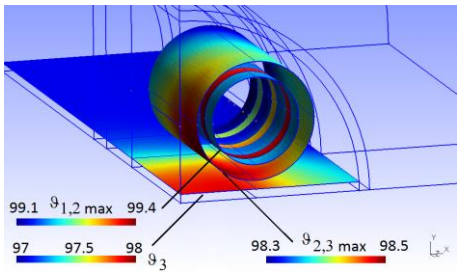

Fig. 1. Temperature distribution on contact surfaces and central insulation layer

REFERENCES

[1] IEC 60137, Ed. 7: Insulated bushings for alternating voltages above 1000 V.

[2] Dular, P.; Geuzaine, C.; Henrotte, F.; Legros, W., A General Environment for the Treatment of Discrete Problems and its Application to the Finite Element Method, *IEEE Trans. Mag.*, Vol. 34, No. 5, p. 3395–3398, May 1998.

[3] Runge, B., Dreidimensionale Berechnung der Stillstandserwärmung von Kurzschlußringen und Stäben explosionsgeschützter Asynchronmotoren mittels Finiter-Elemente und Zeitschrittverfahren, PhD thesis, University of Dortmund, 1995.

Author: *Meinolf Klocke, Siemens AG, D 45478 Mülheim a.d. Ruhr, Germany, meinolf.klocke@tu-dortmund.de*

Lubomir KOLEV

Technical University of Sofia

A New Approach to Hull Consistency

Abstract. *Hull consistency is a known technique to improve the efficiency of iterative interval methods for solving nonlinear systems describing steady-states in various circuits. Presently, hull consistency is imposed in a scalar manner, i.e. successively for each equation of the nonlinear system with respect to (wrt) a single variable. In the present poster, a new more general approach to implementing hull consistency is suggested which consists in treating simultaneously several equations wrt the same number of variables.*

Keywords: nonlinear circuits, interval methods, constraint satisfaction, hull consistency.

Introduction

As is well known, determining all steady-states (stable and instable operating points) in nonlinear circuits (or systems) is equated to globally solving the following nonlinear system of *n* equations in *n* variables

(1) $f(x)=0$,

(2) $x \in \boldsymbol{x}$,

where $\boldsymbol{x}$ is a given initial interval domain (a box). Interval methods [1] have proved to be a reliable tool for global solution of (1), (2). However, they suffer a serious draw-back: the computer time needed may become in some cases prohibitively long, especially for large circuits (large *n*).

One of the techniques used to improve the numerical efficiency of the interval methods is the so-called hull consistency [2]. Presently, it is applied in a scalar manner, i.e. successively to each ith equation of the system with respect to (wrt) a single jth variable; the remaining variables are allowed to take on their initial interval values. Thus, an attempt is made to contract the initial $\boldsymbol{x}_j$ of the jth variable to a narrower interval $\boldsymbol{x}_j'$. If this is the case, $\boldsymbol{x}_j$ is replaced with $\boldsymbol{x}_j'$. The same constraint satisfaction is applied to the next (i+1)th equation wrt a new variable x_{j+1} trying to reduce its interval $\boldsymbol{x}_{j+1}$ to a smaller $\boldsymbol{x}_{j+1}'$ interval.

A new more general approach is suggested here which consists in simultaneously treating several equations wrt the same number of variables. It is expected that the contraction effects of such a vector constraint satisfaction will be more pronounced than the known scalar hull consistency.

The new approach

Let $1<n'<n$ and partition x as follows: $x=(\xi, p)$ where ξ is an n'-dimensional auxiliary vector formed by choosing n' components x_i of x while p is an $n''=n-n'$ dimensional vector whose components are treated as parameters. To simplify the notations, it is assumed that ξ is made up of the first n' components of x so p regroups the next n'' elements of x; also the vector f is partitioned into (f', f'') where f' involves the first n' equations of f. Now we consider the reduced-size nonlinear system

(3) $f'(\xi, p)=0, \quad \xi \in \boldsymbol{\xi}=\boldsymbol{x}', \quad p \in \boldsymbol{p}=\boldsymbol{x}''$,

where $\boldsymbol{\xi}$ and $\boldsymbol{p}$ correspond to the partition of $\boldsymbol{x}$ into $\boldsymbol{x}=(\boldsymbol{x}', \boldsymbol{x}'')$. Following [3], we now introduce the so-called hull solution $\boldsymbol{\xi}^h$ of the nonlinear parameter system (3) (the narrowest interval vector containing all possible solution vectors ξ when p varies within $\boldsymbol{p}$). If any component $\boldsymbol{\xi}_j^h$ is smaller than the corresponding $\boldsymbol{x}_j$, then $\boldsymbol{x}_j$ is replaced by ξ_j^h. Since $n'>1$, system (3) imposes more stringent constraints than a single equation $f_i(x)=0$ wrt a single variable x_j so it is expected that $\boldsymbol{\xi}^h$ will, in general, provide a better contraction than the scalar contraction.

The reduced intervals $\boldsymbol{\xi}_j^h$ are now substituted for the corresponding initial intervals $\boldsymbol{x}_j$ in (1), (2) and a new system (3) is formed where ξ and p regroup the next n' components of x and f, respectively.

Implementation

As the determination of the exact hull solution $\boldsymbol{\xi}^h$ is presently impossible, two approximate hull solutions will be suggested here.

The first possibility is to transform the original nonlinear system (3) into an equivalent linear interval parametric system; the latter system can be solved by the method of [3].

Another possibility is to determine an outer solution $\boldsymbol{\xi}^{\text{out}}$ to (3) rather than $\boldsymbol{\xi}^h$ since $\boldsymbol{\xi}^h \subset \boldsymbol{\xi}^{\text{out}}$. A method for finding $\boldsymbol{\xi}^{\text{out}}$ is proposed.

The choice of n' is also discussed.

REFERENCES

[1] Kolev L., Interval methods for circuit analysis, World Scientific 1993.

[2] Hansen E., Walster G., Global optimization using interval analysis, Marcel Dekker 2004.

[3] Kolev L., Componentwise determination of the interval hull solution for linear interval parameter systems, *Reliable Computing*, 20 (2014), 1–24.

***Author**: Lubomir Kolev, Technical University of Sofia, 1000 Sofia, Bulgaria, E-mail: lkolev@tu-sofia.bg*

Mikołaj KSIĄŻKIEWICZ

Poznan University of Technology

Self-adjusting Genetic Algorithm for Optimization of Magnetic Field Value in Close Proximity of a Power Line

***Abstract**. Adjusting the parameters of the genetic algorithm to the objective function of unknown shape has always been an issue and as yet there is no reliable method for solving this problem. This paper presents possible solution and at the same time proposes a method to automate optimization process in general when using genetic algorithms. Presented results relate to the optimization of the value of magnetic field in the vicinity of overhead power line.*

Keywords: power line, magnetic field, genetic algorithm, optimization.

Introduction

The increased interest in the influence of electromagnetic fields generated by electrical equipment on living organisms, in particular human, has led to increased research in this area. They concern mainly the methods of calculation of electromagnetic field generated by electrical appliances and ways to reduce their value. Directly associated with it are problems of optimizing the parameters of screening equipment in order to maximize their effectiveness and reduce costs of such solutions.

In this paper parameters of shielding loop are subjected to optimization with the means of using two linked genetic algorithms. Results of solving this problem with the use of a single genetic algorithm using binary representation are given in [1].

Direct problem

The main purpose is to find set of parameters of a shielding loop (position, number of turns, compensation factor) that results in the greatest reduction of the value of magnetic field in area of interest placed in close proximity of a power line. The geometry of the exemplary configuration is shown in Figure 1. The model to calculate the magnetic field was taken from [1, 2].

Optimization method

Optimization was done by means of genetic algorithm. The objective function has possible multiple extremes and little is known about its shape. The other reason for choosing genetic algorithm for this task is to test if self-adjusting with use of another GA would give better results than relying on blind experiments and intuition.

Genetic algorithm

The optimization algorithm is composed of two linked genetic algorithms. Population of the first one (outer layer - OL) consist of independent genetic algorithms (inner layer - IL) working on solving the direct problem (reduction of magnetic field). One generation of the OL GA means running a number of IL GAs which run many generations till they individually reach the termination condition. Only one parameter is taken into account when evaluating an individual in IL GA – the reduction factor (RF). To assess the quality of an individual in OL GA two values are considered: RF of the best solution of the direct problem given by the last generation of IL GA and the computation time of all the generations.

This approach allows to automate optimization process including the setup of the parameters of genetic algorithm and also running multiple courses of the GA to ascertain that the given result is the global optima of the objective function.

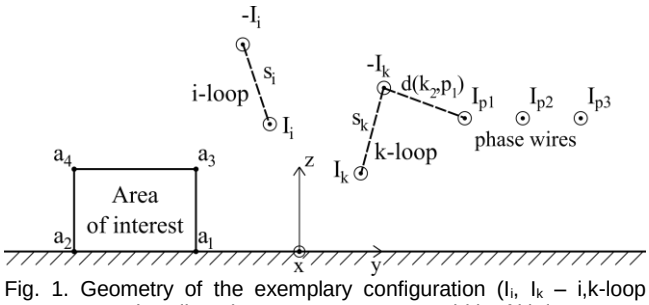

Fig. 1. Geometry of the exemplary configuration (I_i, I_k – i,k-loop currents; I_{p1}…I_{p3} – line phase currents; s_i, s_k – width of i,k-loop;

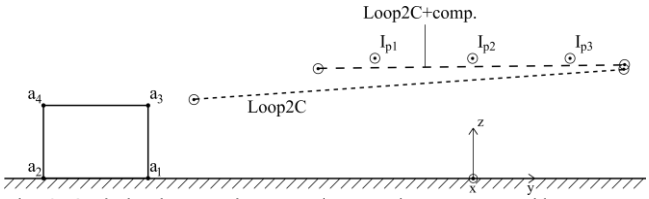

Fig. 2. Optimization results – one loop and compensated loop

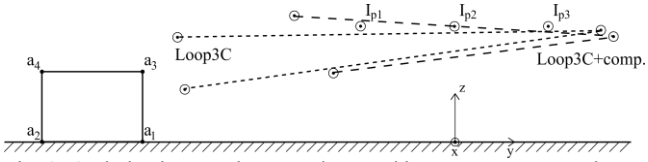

Fig. 3. Optimization results – two loops with one common conductor and compensated version

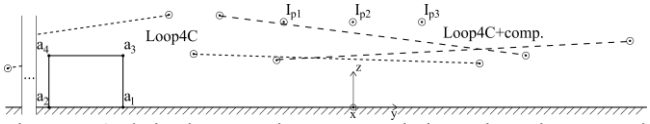

Fig. 4. Optimization results – two independent loops and compensated version

REFERENCES

[1] Cruz P., Riquelme J.M., de la Villa A., Martinez J.L., Ga-based passive loop optimization for magnetic field mitigation of transmission lines, Neurocomputing, Vol. 70, Issues 16–18, October 2007, pages 2679–2686.

[2] Budnik K., Machczyński W., Reduction of magnetic field from a power line using a passive loop conductor, *Computer Application in Electrical Engineering*, Vol. 11, Poznań 2013.

***Authors**: Mikołaj Książkiewicz, Poznań University of Technology, Szarotkowa 80, 60-175 Poznan, Poland, mikolaj.ksiazkiewicz@put.poznan.pl*

Hua LI, Wolfgang M. RUCKER

University of Stuttgart

A Hybrid Method for the Calculation of the Inductances of Coils with and without deformed Turns

Abstract*. In this paper we present an efficient hybrid method for the calculation of the inductances of coils with and without deformed turns by using the finite element method coupled with the analytical approach (FCA) and the partial element equivalent circuit (PEEC) method. To accurately calculate the inductance of a coil, the FCA is to be used. To improve the efficiency, an approximation is used to obtain the inductance's change between coils with and without deformed turns by using the PEEC method. Finally, the presented method is successfully validated by the numerical results.*

Keywords: Inductance, finite element method, partial element equivalent circuit.

Introduction

The finite element method (FEM) is commonly used to calculate the inductance of an arbitrary shaped coil, but with a high computing effort. Accordingly, the FEM coupled with the analytical approach (FCA) by using the surface current model (SCM) and the geometry factors is presented in [1]. Another numerical method is the partial element equivalent circuit (PEEC) analysis, which is based on an integral equation description of the geometry that is interpreted in terms of circuit elements [2]. To calculate the inductances of coils with and without deformed turns, it must be treated two times by using the FCA. However, it is more efficient to use the PEEC to find the influence of the deformed turns [3]. Therefore, an efficient hybrid method (HM) is presented to obtain the inductances of coils with and without deformed turns by using the FCA combined with the PEEC.

Formulations

To obtain the inductance of a coil by using FEM, the partial differential equation of the magnetostatic formulation is required, which can be derived by using the magnetic vector potential $\boldsymbol{A}$ in conjunction with Maxwell's equations and the Coulomb's gauge. Through the geometry factors with the SCM the computing effort of the FEM can be reduced significantly. The integral equation of the PEEC can be deduced according to the ideal conductor constitutive relation ($\boldsymbol{J} = \sigma \boldsymbol{E}$) combining with the Faraday's law and the definition of $\boldsymbol{A}$ in the frequency domain. The basic equations of the both methods will be given in the full paper.

By means of discretizing the considered conductor into n identical rectangular segments and using the mesh current analysis, the system equation can be solved by an iterative method. The solutions are the average electrical potential on the segment end face and the average current inside each segment. Thereby, the partial inductance matrix (PIM) of the considered coil can be obtained according to the Ohm's law.

As the PIM describes the magnetic coupling between the segments, the PIMs of the coils with and without deformed turns can be calculated. Moreover, each turn can be considered as two parts a and b, one of which is discretized into certain segments and has its own PIM. As the PIM is symmetric and the mutual inductances (MI) between parts maintained the same relative position are also the same, only the first row of the whole PIM are needed to be considered. Then, the first row of the PIM's change of x deformed turns ΔL_{1x} is given by

$$(1)\ \Delta L_{1x} = \left[\left[L_{b1b1} \quad L_{b1a1}\right] \quad \left[L_{b1b2} \quad L_{b1a2}\right] \quad \cdots \quad \left[L_{b1bx} \quad L_{b1ax}\right]\right],$$

where: L_{b1bi} or L_{b1ai} – the change of the MI between the first and the i-th deformed or normal part, respectively. Then, an approximation can be used to determine the inductance change ΔL_{xx} of coils with and without x deformed turns by just calculating the ΔL_{12} and the ratio k between L_{b1a2} and L_{b1a1} (Fig. 1). The L_{b1ai} can be approximated as follows:

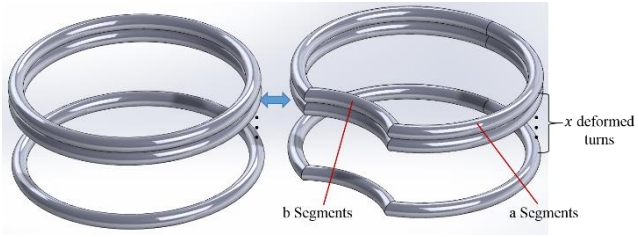

Fig. 1. Coil with and without deformed turns

$$(2)\qquad L_{b1ai} = k^{i-1} L_{b1a1}\ .$$

Thus, the inductance's change of a deformed coil can be obtained according to the inductance of a normal coil calculated by the FCA and the percentage change obtained by the PEEC. The advantage of the presented method is that the necessary computing time is significantly reduced by just calculating two deformed turns instead of the deformed coil. Furthermore, this method can also be used for a coil with normal and deformed mixed turns, as shown in the full paper.

Numerical result

Two cylindrical coils with and without five deformed turns shown in Fig. 1 are simulated. The reference results are calculated by using the FEM. The computing time τ and the percentage error η of the HM compared to the FEM and the FCA are evaluated in Table 1.

Table 1. The computing time and the accuracy of the hybrid method

	FEM	FCA	HM
$\boldsymbol{\tau}$ (s)	1497.08	320.76	165.39
$\boldsymbol{\eta}$ (%)	–	–1.47	–1.89

REFERENCES

[1] Li H., Banucu R, Rucker W.M., "Accurate and efficient calculation of the inductance of an arbitrary shaped coil using surface current model", *accepted for publication in IEEE Trans. Magn.* 2015.

[2] Ruehli A. E., "Equivalent circuit models for three-dimensional multiconductor systems", *IEEE Trans. Microw. Theory Techn.,* 22 (1974), No. 3, 216-221.

[3] Kamon M., Tsuk M. J. and White J. K.,"Fasthenry: A Multipole-accelerated 3-D inductance extraction program", *IEEE Trans. Microw. Theory Techn.,* 42 (1994), No. 9, 1750-1758

Authors*: Hua Li, University of Stuttgart, Pfaffenwaldring 47, 70569, hua.li@ite.uni-stuttgart.de*

Stanislaw GRATKOWSKI, Krzysztof STAWICKI, Marcin ZIOLKOWSKI

West Pomeranian University of Technology, Szczecin, Poland

General Closed-Form Asymptotic Boundary Conditions for Finite Element Analysis of Exterior Electrical Field Problems

Abstract*. This paper presents general closed-form asymptotic boundary conditions (ABCs) on circular, elliptical and spherical boundaries suitable for the finite element modeling of 2D and 3D electrical field problem with open boundaries. To the best knowledge of the authors of this paper, the ABCs (in such forms) have not yet been reported in the literature. The 1st and 2nd order ABCs, which can be easily implemented into existing finite element codes, are discussed in details, also for an arbitrary shape of the finite element region in 2D and for box-shaped boundaries in 3D.*

Keywords: Asymptotic boundary conditions, finite element method, open boundary problems, static fields.

Introduction

Many of the electrical field problems are not confined to finite domain, but can be considered as being of the exterior form, that is the problem domain is unbounded. Since the finite element method is a finite domain method, special techniques must be employed when the solution domain is infinite. Over the last three decades various methods of analysis for the open boundary static and quasistatic electromagnetic field problems have been investigated [1]. Among the methods, asymptotic boundary conditions (ABCs) seem to be very attractive from the numerical point of view [2], [3]. In the present paper we discuss different aspects of the ABCs for the finite element analysis of 2D and 3D electrical field problems. General expressions for the Nth order ABCs on circular, elliptical and spherical boundaries and numerical examples are given.

Asymptotic boundary conditions on circular, elliptical and spherical boundaries

To solve elliptic boundary value problems in an infinite domain by the finite element method, it is normal to divide the unbounded domain by an artificial boundary Γ into an interior region R_i and a residual, uniform region R_e. When using the finite element method in R_i, some boundary conditions must be imposed on the artificial boundary Γ. The boundary conditions (called the ABCs) should mimic the behavior of the unknown potential V at infinity and give reasonably accurate results in the interior region R_i. The potential V in the exterior region R_e (and in the outermost part of R_i) satisfies the Laplace equation:

$$\nabla^2 V = 0, \tag{1}$$

The general solutions to (1), if the potential tends to zero at infinity, can be expressed as:

2D, polar coordinates (r, φ)

$$V(r,\varphi) = \sum_{n=1}^{\infty} r^{-n} F_{1n}(\varphi), \tag{2}$$

2D, elliptical coordinates (η, ψ)

$$V(\eta,\psi) = \sum_{n=1}^{\infty} \exp(-n\eta)\, F_{2n}(\psi), \tag{3}$$

3D, spherical coordinates (R, θ, φ)

$$V(R,\theta,\varphi) = \sum_{n=1}^{\infty} R^{-n} F_{3n}(\theta,\varphi), \tag{4}$$

where $F_{1n}(\varphi)$, $F_{2n}(\xi)$ and $F_{3n}(\theta, \varphi)$ are functions of angles measured in a standard way in polar (2D), elliptical (2D) and spherical (3D) coordinates, respectively.

The solutions (2), (3) and (4) can be used to obtain ABCs on the artificial boundary Γ. After some algebra, we have found general expressions for the Nth order ABCs on circular, elliptical and spherical boundaries. They are as follows:

2D, circular boundary $r = d$

$$\frac{\partial^N V(d,\varphi)}{\partial r^N} + \sum_{m=1}^{N} \frac{\alpha_m^{(N)}}{d^{N-m+1}} \frac{\partial^{m-1} V(d,\varphi)}{\partial r^{m-1}} = O\left(d^{-2N-1}\right), \tag{5}$$

2D, elliptical boundary $\eta = \eta_0$

$$\frac{\partial^N V(\eta_0,\psi)}{\partial \eta^N} + \sum_{m=1}^{N} \beta_m^{(N)} \frac{\partial^{m-1} V(\eta_0,\psi)}{\partial \eta^{m-1}} = O\left\{\mathrm{e}^{-(N+1)\eta_0}\right\}, \tag{6}$$

3D, spherical boundary $R = d$

$$\frac{\partial^N V(d,\theta,\phi)}{\partial R^N} + \sum_{m=1}^{N} \frac{\alpha_m^{(N)}}{d^{N-m+1}} \frac{\partial^{m-1} V(d,\theta,\phi)}{\partial R^{m-1}} = O\left(d^{-2N-1}\right), \tag{7}$$

where: $\alpha_m^{(N)} = \begin{pmatrix} N \\ m-1 \end{pmatrix} \frac{N!}{(m-1)!}$, $\beta_m^{(N)} = \begin{bmatrix} N+1 \\ m \end{bmatrix}$, $\frac{\partial^0 V}{\partial \tau^0} = V$.

The coefficients $\alpha_m^{(N)}$ are known as coefficients of the Laguerre polynomials, whereas the coefficients $\beta_m^{(N)}$ are the unsigned Stirling numbers of the first kind.

Implementation of the ABCs into commercial finite element software COMSOL Multiphysics will be shown in a full version of the paper.

REFERENCES

[1] Q. Chen and A. Konrad, "A review of finite-element open boundary techniques for static and quasistatic electromagnetic field problems," IEEE Trans. Magn., Vol. 33, no. 1, pp. 663–676, 1997.

[2] S. Gratkowski, T. Todaka, M. Enokizono and R. Sikora, "Asymptotic boundary conditions for the finite element modeling of axisymmetric electrical field problems," IEEE Trans. on Magn., Vol. 36, no. 4, pp. 717–721, 2000.

[3] Y. Chu, Y. Cao, X. He and M. Luo, "Asymptotic boundary conditions with immersed finite elements for interface magnetostatic/electrostatic field problems with open boundary," Comput. Phys. Commun., Vol. 182, no. 11, pp. 2331–2338, 2011.

Authors*: Stanisław Gratkowski, stanislaw.gratkowski@zut.edu.pl, Krzysztof Stawicki, krzysztof.stawicki@zut.edu.pl, Marcin Ziółkowski, marcin.ziolkowski@zut.edu.pl, West Pomeranian University of Technology, ul. Sikorskiego 37, 70-313 Szczecin, Poland*

Daniel MARCSA, Miklós KUCZMANN

Széchenyi István University

Closed Loop Voltage Control of a Solenoid Using Parallel Finite Element Method

Abstract. *This paper presents an axisymmetric formulation of the circuit-coupled parallel finite element method (FEM) embedded in closed loop control system. The controller checks the current of the coil of the magnetic system after each time step and control the applied voltage to reach the steady state faster. The results of the voltage drive sequential and parallel finite element model are compared with the results from the analytical model. The control parameters for the PID controller were estimated using the step response of the system.*

Keywords: Field-circuit coupling, closed loop control, parallel finite element method.

Introduction

To set up the state space representation [1] of a physical system some academic cases are easy, however it is impossible for complex systems without any simplifications or neglects. These simplifications, especially the field of the air-gap assumed to be sinusoidal, the inductance of the core is neglected, or inaccurate for electromechanical actuator. Thus, the design of the controller is not so accurate by these simplified model. The behaviour of closed loop control [1, 2] is hardly depend from the controller. Ergo, the appropriate model of the system is very important task of the controller design.

To the appropriate model, the wide range of electromagnetic device, the finite element method (FEM) [2, 3] is very useful technique, when the complex geometries cannot be solved by analytical methods. But, the finite element model of the physical system is not enough to replace the state space model of the system. Modelling of physical behaviour of the electromechanical devices is a very complex task, because electromagnetic field has strong interaction with other physical fields and external circuits. These interactions need to be given a coupled-field treatment for realistic and accurate analysis. Further, most of the electromechanical systems are voltage fed, so to take into account the circuit equation is necessary for the accurate analysis, and for take into a control loop.

The above mentioned coupled numerical field simulation tool is an important technique for the solution of a wide range of problems in engineering practice. However, the solution of a large sparse system of equations is very time consuming. Thus, the solution of a large system of equations must be parallelized in order to speedup the numerical computations by domain decomposition methods (DDM) [3].

Formulation

Using the FEM [2, 3] to discretize the axisymmetric solenoid, which is based on the weak formulation of the partial differential equations. The matrix system of the field equations is the following:

$$\begin{bmatrix} \mathbf{S}+\frac{\mathbf{N}}{\Delta t} & -\mathbf{P} \\ \frac{\mathbf{Q}}{\Delta t} & \mathbf{R} \end{bmatrix} \begin{bmatrix} \mathbf{A}(t) \\ \mathbf{I}(t) \end{bmatrix} = \begin{bmatrix} \frac{\mathbf{N}}{\Delta t} & 0 \\ \frac{\mathbf{Q}}{\Delta t} & 0 \end{bmatrix} \begin{bmatrix} \mathbf{A}(t-\Delta t) \\ \mathbf{I}(t-\Delta t) \end{bmatrix} + \begin{bmatrix} 0 \\ \mathbf{U}(t) \end{bmatrix}, \quad (1)$$

where $\mathbf{A}$ is the vector of magnetic vector potential, $\mathbf{I}$ is the vector of currents in the windings, $\mathbf{U}$ is the vector of voltages at the terminal of the winding, S is the matrix related to permeability, $\mathbf{N}$ is the matrix related to electric conductivity, $\mathbf{P}$ is the matrix associated with constant coil current, $\mathbf{Q}$ is the matrix associated with flux linkage, $\mathbf{R}$ is the matrix of d.c. resistance of winding.

For the parallelization using a non-overlapping DDM [3], when the (1) is to divide into several sub-problems in which the unknown magnetic vector potentials and currents can be calculated simultaneously, i.e. in a parallel way.

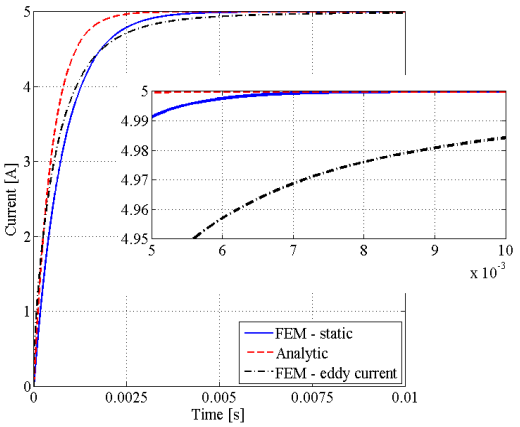

Fig. 1. Step response of the magnetic system.

The full paper will present the coupling techniques of voltage equation of the winding, and comparing them. An axisymmetric test problems has been used to compare the closed loop control with classical state space model, and with sequential and parallel finite element model. Fig. 1 shows the step response of the magnetic system.

This work was supported by the TÁMOP-4.1.1.C-12/1/KONV-2012-0017 - "Green Energy – Cooperation of the Higher Education Sector for the Development of Green Economy in the Area of Energetics".

REFERENCES

[1] Äström K.J., Murray R.M., Feedback Systems: An Introduction for Scientist and Engineers, Princeton University Press, 2008

[2] Tahmasebi R., Alizadeh H. V., Rahimi S., Boulet B., Robust H∞ Force Control of a Solenoid Actuator Using Experimental Data and Finite Element Method, *2014 IEEE Conference on Control Applications (CCA)*, 2014, pp. 1172–1177.

[3] Kruis J., Domain Decomposition Methods for Distributed Computing, Saxe-Coburg Publications, 2007.

***Authors**: Daniel Marcsa, Széchenyi István University, Hungary, H-9027, Győr, Egyetem tér 1., marcsad@sze.hu, Miklós Kuczmann, Széchenyi István University, Hungary, H-9027, Győr, Egyetem tér 1., e-mail: kuczmann@sze.hu*

Michael POPP, Patrick LAZA, Wolfgang MATHIS

Leibniz Universität Hannover, Institute of Theoretical Electrical Engineering

Modelling and Simulation Aspects of Electrical AC Machines

Abstract. *In the field of power and drive systems, electrical AC machines are mostly modelled using a set of explicit ordinary differential equations in a state space representation. It is shown, that by using other equation types for simulation, algebraic constraints arising from aggregating several machines to a more complex system can directly be considered. The effects of different model variants on numerical ODE/DAE solvers are investigated in the focus of this work in order perform efficient simulations of larger systems possessing electrical AC machines.*

Keywords: State Space Modelling, Electrical AC Machines, ODE and DAE Solvers

State space models of electrical single- and multiphase machines are widely used in the analysis and design of power and drive systems. Those models can be derived from the general machine equations [1]

$$\text{(1, 2)} \qquad \mathbf{u} = \mathbf{R}\mathbf{i} + \frac{\mathrm{d}\boldsymbol{\Psi}}{\mathrm{d}t}, \qquad \boldsymbol{\Psi} = \mathbf{L}(\theta)\mathbf{i}$$

$$\text{(3)} \qquad J\frac{\mathrm{d}^2\theta}{\mathrm{d}t^2} = -D\frac{\mathrm{d}\theta}{\mathrm{d}t} + m_i(\boldsymbol{\Psi}, \mathbf{i}, \theta) + m_e.$$

Therein the components of the vectors $\mathbf{u}$, $\mathbf{i}$ and $\boldsymbol{\psi}$ represent the voltage, current and flux linkage per phase, respectively. The self- and mutual magnetic coupling of the phase windings is expressed by the inductance matrix $\mathbf{L}(\theta)$, which is in general dependent from the rotor position angle θ. The mechanical subsystem of the rotor is described by (3), in which J is the moment of inertia, D is the mechanical damping constant, m_e is the external driving torque and m_i is the torque developed by the machines' electromagnetic subsystem.

For simulation purposes (1), (2) and (3) have to be rearranged to form a system of ordinary differential equations (ODE). This can be done for different system representations and for different state variables.

$$\text{(4)} \qquad \frac{\mathrm{d}\mathbf{i}}{\mathrm{d}t} = -\mathbf{L}^{-1}(\theta)\left(\mathbf{R} + \frac{\mathrm{d}\theta}{\mathrm{d}t}\frac{\mathrm{d}\mathbf{L}(\theta)}{\mathrm{d}\theta}\right)\mathbf{i} + \mathbf{L}^{-1}(\theta)\mathbf{u}$$

$$\text{(5)} \qquad \frac{\mathrm{d}\boldsymbol{\Psi}}{\mathrm{d}t} = -\mathbf{R}\mathbf{L}^{-1}(\theta)\boldsymbol{\Psi} + \mathbf{u}$$

Besides the explicit model representations given in (4) and (5) for the state variables $\mathbf{i}$ and $\boldsymbol{\Psi}$, respectively, both equations can be rewritten in implicit form $0 = \mathbf{F}(\mathbf{x}, \dot{\mathbf{x}}, t)$ and in explicit form with mass matrix $\mathbf{M}(t)\dot{\mathbf{x}} = \mathbf{F}(\mathbf{x}, t)$. The latter ones are relevant, when the machine model is embedded in larger systems, e. g. for power system studies. Thereby, additional algebraic constraints to the state variables have to be considered which lead to semi-explicit differential algebraic equations (DAE).

While the explicit model variants are extensively described, analyzed and used for different purposes; cf. [1, 2, 3], the latter two variants haven't been treated in this extent. Furthermore, it is obvious that the structural differences in the equations of the different model variants may influence the behavior of numerical ODE and DAE solvers used for simulation. A comparison and analysis of these different model variants with respect to numerical simulation aspects is missing so far to the author's knowledge. As a first example, Fig. 1 shows the comparative simulation results gained by computing the start-up of an asynchronous motor.

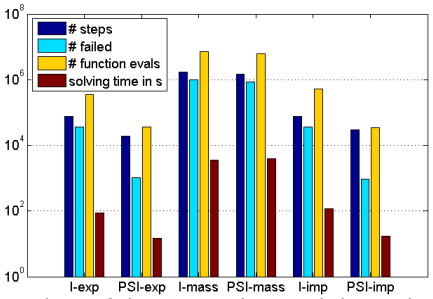

Fig. 1. Comparison of the ODE solver statistics and computation times for model variants with $\mathbf{i}$ or $\boldsymbol{\psi}$ as state variable in explicit, mass matrix or implicit model representation

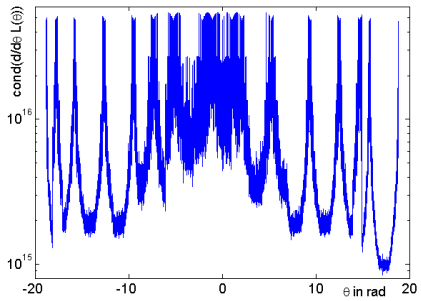

Fig. 2. Condition number of $\mathrm{d}\mathbf{L}(\theta)/\mathrm{d}\theta$ over the rotor angle θ

The numerical solver, its error tolerances and the system parameters remained unchanged. One structural reason for these significant differences in computation time can be found in the properties of the term $\mathrm{d}\mathbf{L}(\theta)/\mathrm{d}\theta$. In Fig. 2 the condition number is plotted over the rotor angle. Quite large values in combination with a strong dependency on θ result in difficulties by numerically solving such equations.

In the full paper, the modelling of different specific machine types and the derivation of model variants will be presented first. Based on the structural properties of these models numerical simulation aspects will be discussed in detail aiming towards an optimized combination of model and numerical solver.

REFERENCES

[1] Müller, G., Ponick, B., Theory of Electrical Machines (in German), *Wiley-VCH* 2009.

[2] Ong, C.-M., Dynamic Simulation of Electric Machinery, *Prentice Hall* 1998.

[3] Rothenhagen, K., Fuchs, F.W., Current Sensor Fault Detection by Bilinear Observer for a Doubly Fed Induction Generator, *IEEE Trans. Ind. Electr.* 56 (2009), No. 10, 4239–4245.

***Authors**: M. Popp, P. Laza and W. Mathis, Institute of Theoretical Electrical Engineering, Leibniz Universität Hannover, Appelstraße 9A, 30167 Hannover, Germany, popp@tet.uni-hannover.de*

Marco REIT, Michael BERENS, Wolfgang MATHIS

Institute of Theoretical Electrical Engineering, Leibniz Universität Hannover

Ambiguities in Input-Output Behavior of Driven Nonlinear Systems Close to Bifurcation

Abstract. *The Hopf amplifier based on the normal form of the Andronov-Hopf bifurcation is a peculiar exception of nonlinear amplifiers due to its sinus-to-sinus input-output behavior. We investigate ambiguities, especially the separation of solution sets, and double hysteresis behavior of an extension of the Hopf system close to the bifurcation point where a limit cycle arises. Its applicability is validated by a DSP implementation.*

Keywords: Andronov-Hopf, bifurcation, nonlinear amplifier, ambiguities.

Introduction

Calculating and analyzing the input-output behavior is a common task in control system engineering for linear time-invariant systems by means of amplitude-frequency and phase-frequency characteristics. Since nonlinear systems show harmonic distortions for single tone excitations, it is in general not possible to describe the input-output behavior with an algebraic equation. Nevertheless, there are models of nonlinear systems with focus on the single-tone behavior. Apart from their specific amplification characteristics, these Hopf-type amplifiers act on single-tone excitations like linear systems concerning their spectral behavior [1]. This is a peculiar exception of nonlinear amplifiers.

Such systems based on the normal form equation of the Andronov-Hopf bifurcation [2, 3] are described by

$$\dot{z} = (\mu + \mathrm{i})\omega_0 z + \sigma\omega_0 |z|^2 z - \omega_0 f, \qquad z(t), f(t) \in C. \tag{1}$$

Here $\mu \in \Re$ denotes the bifurcation parameter, i is the imaginary unit and ω_0 is the natural frequency of the oscillation. The coefficient σ is in general a complex quantity defined by $\sigma = \sigma_R + \mathrm{i}\sigma_I$. In order to describe the input-output characteristic, we consider the systems short below the onset of self-sustaining limit cycle oscillation. Assuming a complex sinusoidal solution in (1) with $z(t) = z_0 \mathrm{e}^{\mathrm{i}(\omega t + \varphi)}$, that results from the harmonic forcing $f(t) = f_0 \mathrm{e}^{\mathrm{i}\omega t}$, the nonlinear input-output behavior can be described for $\sigma = -1$ by the algebraic equation

$$f_0^2 = z_0^6 - 2\mu z_0^4 + \left[\mu^2 + \left(1 - \omega/\omega_0\right)^2\right] z_0^2. \tag{2}$$

The input-output characteristic of the supercritical system described by (2) is shown in Fig. 1 (a) for the input amplitude $f_0 = 0.1$. The green line marks the bifurcation point and the blue line an exemplary cross section. It becomes clear that there are no ambiguities, especially no separations of solution sets, in the only valid range of $\mu < 0$.

Further investigations on subcritical systems with $\sigma = 1$ show ambiguities and separation of solution sets in the range of $\mu < 0$ (see Fig. 1 (b)). Anyway, these solutions are not applicable due to the occurrence of an unstable limit cycle. By adding an imaginary part to σ, ambiguities and hysteresis behavior without any separation of solution sets can be shown for supercritical systems [1, 4].

However, as shown in Fig. 1 (c) we investigate an exten-sion of (1), which shows double hysteresis behavior and separation of solution sets in a valid region of μ where the unforced system has only a stable fixed point. The red line marks a second bifurcation point. Due to the sinus-to-sinus input-output behavior the response characteristic can be precisely predicted by an algebraic equation. For the verification of our results the nonlinear input-output systems are implemented and measured on a DSP.

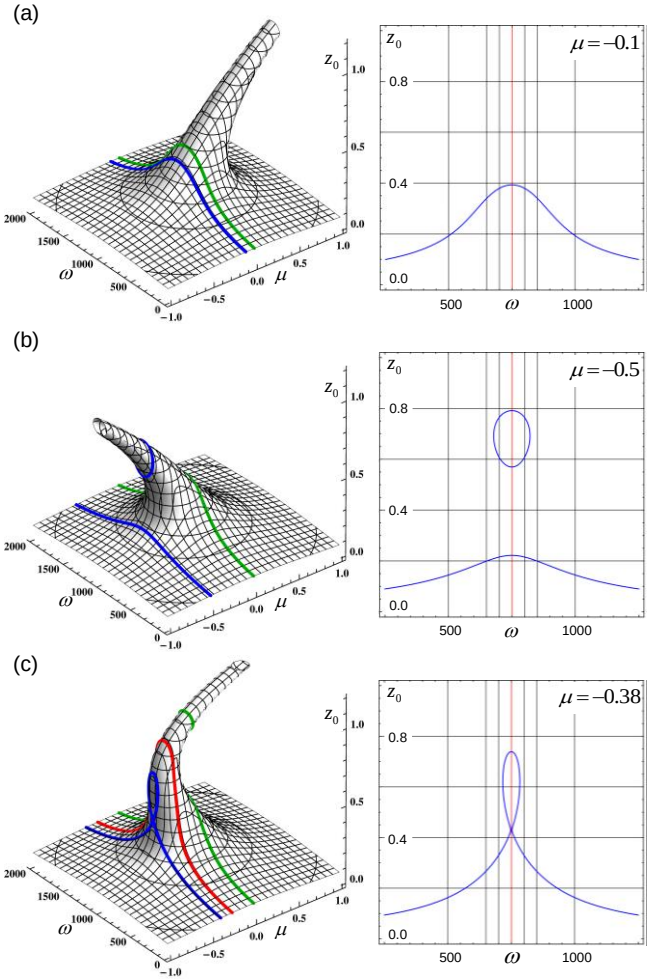

Fig.1. System response showing $\mu - \omega -$ relation (left) and exemplary cross section (right)

REFERENCES

[1] Reit M., Mathis W., A Class of Sinusoidal Driven Nonlinear Input-Output Systems with Sinusoidal Response, *International Symposium on Nonlinear Theory and its Applications*, 2014

[2] Eguíluz V. M., Ospeck M., Choe Y., Hudspeth A. J., Magnasco M. O., Essential nonlinearities in hearing, *Phys. Rev. Lett.*, 84 (2000), 5232-5235

[3] Stoop R., Jasa T., Uwate Y., Martignoli S., From Hearing to Listening: Design and Properties of an Actively Tunable Electric Hearing Sensor, *Sensors*, 7 (2007), 3287-3298

[4] Zhang Y., Golubitsky M., Periodically Forced Hopf Bifurcation, *SIAM j. Appl. Syn. Syst.*, 10 (2011), No. 4, 1272-1306

***Authors**: M. Reit, M. Berens and W. Mathis, Institute of Theoretical Electrical Engineering, Leibniz Universität Hannover, Appelstraße 9A, 30167 Hannover, Germany, reit@tet.uni-hannover.de*

Thomas VENNEMANN, Florian MEHRINGER, Victor VU, Esther DIETRICH, Wolfgang MATHIS

Institute of Theoretical Electrical Engineering (TET), Leibniz Universität Hannover (LUH)

Self-Adjusting Feed Forward Path to Compensate the Switching Noise in a ZePoC AC Voltage Standard

Abstract. *An AC voltage normal based on class-D topologies needs a low pass filter to process the output signal. To reduce the order of this filter a self-adjusting feed forward path is implemented. A compensation signal is subtracted from the binary output signal of a class-D power stage. Depending on the current differential output signal the compensation signal is optimized by an algorithm implemented on a digital signal processor.*

Keywords: ZePoC, AC voltage normal, switching noise, feed forward

Introduction

Zero Position Coding (ZePoC) was invented and initially implemented for audio coding by the TET-Institute. The main advantages of ZePoC are the low switching rate and the separated baseband [1]. ZePoC is also ideal for an AC voltage standard based on class-D topologies which is able to provide a highly accurate sinusoidal voltage.

Fig.1 shows the block diagram of the AC voltage standard. The ZePoC encoder is implemented on a digital signal processor (DSP) [2]. Depending on some encoding parameters the duty cycles of a pulse width modulated (PWM) signal are computed. A pulse shaper converts the duty cycles into a binary signal with a very high time resolution. To amplify the binary PWM signal a class-D power stage is used. If the supply voltages +1 and –1 are derived from a natural constant using a physical effect (e.g. Josephson effect), the amplitude of the amplified PWM signal is highly accurate. Fig.2a displays ten switching periods T of the binary signal $b(t)$.

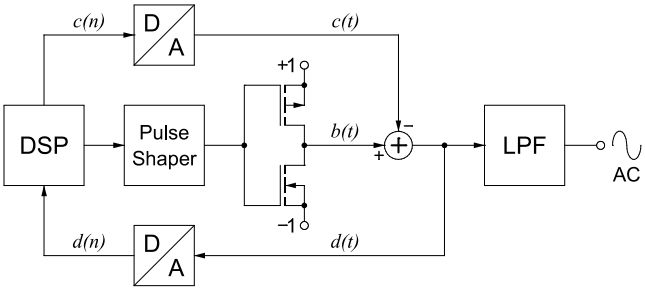

Fig. 1. Block Diagram of the AC Voltage Normal

The spectrum of $b(t)$ is shown in Fig.2b. To suppress the disturbances caused by the switching an 8th order low pass filter (LPF) must be used. Filtering is only possible because of the separated baseband which ensures a spectral gap between the AC signal and the switching noise.

To enlarge the spectral gap, the AC voltage normal is expanded by a feed forward path. The DSP outputs the time-discrete compensation signal $c(n)$. A digital-to-analog converter generates the time-continuous signal $c(t)$ which is displayed in Fig. 2c. To get $c(n)$ an inverse discrete Fourier transform (IDFT) is computed. The input of the IDFT are the spectral components of $b(t)$ which are to be compensated. For enlarging the spectral gap $c(t)$ is subtracted from $b(t)$.

The spectrum of the differential signal $d(t)=b(t)-c(t)$ is shown in Fig. 2d. For an optimal compensation of the switching noise, $d(t)$ is converted into $d(n)$ and analyzed by the DSP. An algorithm is optimizing the signal $c(t)$ until all amplitudes of the undesired frequency components are minimized. With the compensation of the switching noise a 4th order LPF is sufficient.

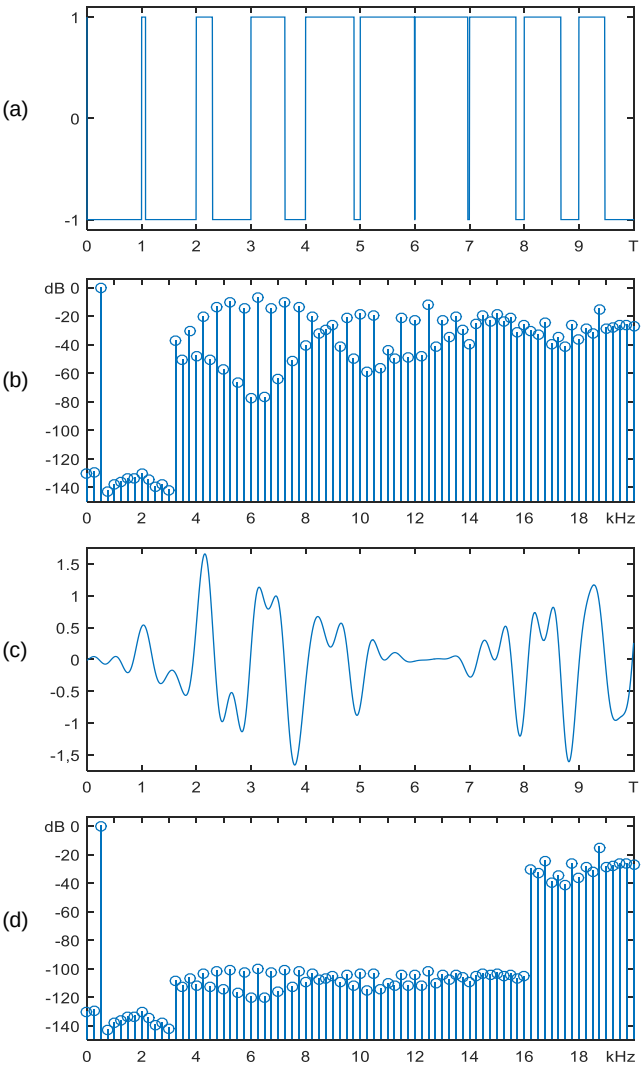

Fig. 2. Time Functions and Spectra of Signals $b(t)$, $c(t)$ and $d(t)$

REFERENCES

[1] Streitenberger, M., Zur Theorie digitaler Klasse-D Audioleistungsverstärker und deren Implementierung. VDE-Verlag 2005

[2] Vennemann, T. et al., A Novel ZePoC Encoder for Sinusoidal Signals with a Determined Accuracy for an AC Power Standard, Kleinheubacher Berichte 2014, Volume 13, 2015

***Authors**: Thomas Vennemann, Florian Mehringer, Victor Vu, Esther Dietrich and Wolfgang Mathis, Institute of Theoretical Electrical Engineering, Leibniz Universität Hannover, Appelstr. 9A, 30167 Hannover, Germany, vennemann@tet.uni-hannover.de*

Daniel STAHL, Wolfgang MATHIS

Institute of Theoretical Electrical Engineering, Leibniz Universität Hannover

Energy Transitions in Electrical Oscillators studied by the Generalized Liouville Equation

Abstract. *Noise in electrical circuits is normally treated by the Langevin approach respectively the equivalent Fokker-Planck equation. But many phenomena are attributed to the Fokker-Planck formalism while the exceedingly complex deterministic behavior is neglected. In this paper it will be shown by using the generalized Liouville equation that electrical oscillators are subject to perpetual change of energy and thus are more susceptible to phase noise the harder these energy transitions are.*

Keywords: generalized Liouville equation, deterministic behavior, oscillators.

Introduction

Langevin's paper on Brownian motion [1] adds a noise term to a deterministic equation with linear stoke damping which is rapidly fluctuating in relation to the macroscopic time scale. Alkemade, van Kampen and MacDonald extended this phenomenological approach to nonlinear damping and showed that "in non-linear systems the behavior in time of an ensemble average is no longer independent of the magnitude of the fluctuations around the average" [2].

Let $(M, \mathcal{B}, P)$ be a probability space, $(M, \mathcal{B})$ the associated measure space, M the manifold on which the dynamic system is running and $\mathcal{B}$ the Borel measure. Gerlich [3] showed in his work on the generalization of the Liouville equation that a set of mapping, i.e. a solution of the equations of motion

$$\mathbf{X}(\omega, t) = \mathbf{h}(\mathbf{X}_0(\omega), t), \tag{1}$$

can be regarded as a stochastic process. This means that the function $t \mapsto \mathbf{X}(\omega, t)$ not only depends on the initial value, but also on the random parameter $\omega \in \mathcal{B}$. However, in this paper we free ourselves from this stochastic point of view and use the available tools of probability theory. Let $\rho(\mathbf{x}_0)$ be the probability density given by the theorem of Radon-Nikodým and let $\mathrm{d}\mathbf{x}_0$ be the Lebesque measure with respect to the initial values $\mathbf{x}_0$. Note, that the variables are now written in small letters and are therefore part of a deterministic dynamical System (T, M, Φ) with T as time domain and Φ as flow. An inverse transformation $\mathbf{x}_0 = \mathbf{h}^{-1}(\mathbf{x}, t)$ of (1) is possible, if the associated Jacobian $J(\mathbf{x}_0, t) = \det(\partial \mathbf{h}/\partial \mathbf{x}_0)$ is regular for all points $\mathbf{x}_0 \in M$. Let $\tilde{\rho}(\mathbf{x}, t) = \rho(\mathbf{h}^{-1}(\mathbf{x}, t))$ be the probability density of the inverse transformation and $\tilde{J}(\mathbf{x}, t) = J(\mathbf{h}^{-1}(\mathbf{x}, t), t)$, then the transformation of $\mathrm{d}\mathbf{x}_0$ in $\mathrm{d}\mathbf{x}$ obeys $\rho(\mathbf{x}_0)\mathrm{d}\mathbf{x}_0 = \tilde{J}^{-1}(\mathbf{x}, t)\tilde{\rho}(\mathbf{x}, t)\mathrm{d}\mathbf{x}$. The r.h.s. of this equation corresponds to a function $p: \mathcal{B} \to [0,1]$ which gives for every tuple $(\mathbf{x}, t)$ in the extended phase space $M \times T$ the ensemble probability such that

$$p(\mathbf{x}, t) = \tilde{J}^{-1}(\mathbf{x}, t)\tilde{\rho}(\mathbf{x}, t). \tag{2}$$

For Hamiltonian systems the transport of a volume in phase space is conserved and therefore $\tilde{J} = J = 1$. The partial differential equation of motion for an initial density $p_0(\mathbf{x}) = p(\mathbf{x}, t_0)$ is thus the known Liouville equation. However, for dissipative non-linear systems this equation can be generalized to

$$\frac{\partial}{\partial t} p + \mathrm{div}(\mathbf{f})\, p + \mathbf{f}\, \mathrm{grad}(p) = 0 \tag{3}$$

where $\mathbf{f}: M \to TM$ is the vector field.

An oscillator is an electronic circuit with periodic alternating currents respectively voltages and few properties: (i) there exists a prescribed frequency, (ii) there exists a prescribed amplitude, (iii) the amplitude is independent of the initial conditions and (iv) the qualitative behavior does not change for sufficiently small parasitic elements [4]. The last two properties distinguish a linear time-invariant system (LTI), e.g. a harmonic oscillator, by an electrical oscillator.

Energy Transitions

The Van der Pol system

$$\dot{x} = y, \qquad \dot{y} = y(1 - x^2) - x \tag{4}$$

differs from the harmonic oscillator only by a non-linear term. This term is synonymous with the necessary feedback of an electrical oscillator, which ensures a stable limit cycle and fulfills all of the above properties. Due to its formal simplicity, the transition between dissipation (if $|x| > 1$) and focusing (if $|x| < 1$) of energy can be distinguished. These energy transitions lead to a pumping mechanism, which changes the variance of an ensemble along the limit cycle and therefore the phase shift. In particular, the physical meaning of dissipation and focusing is a geometrical consequence in phase space, not only in relation to the Latin word origin and it is not a consequence of diffusion due to a voluntary noise term in Langevin's approach. It is a divergence respectively convergence of an ensemble around an averaged value.

The Liouville formalism gives a direct way to measure energy transitions even the differential equations are high-dimensional and formal complicated, because the Jacobian $\tilde{J}$ provides time-dependent information about the volume as can be easily shown by

$$\tilde{J}\big|_{\mathbf{x}=\mathbf{h}(\mathbf{x}_0,t)} = \det\left(\frac{\partial \mathbf{h}}{\partial \mathbf{x}_0}\right) = \exp\left(\int \mathrm{div}\big(\mathbf{f}(\mathbf{h}(\mathbf{x}_0, t), t)\big)\, \mathrm{d}t\right). \tag{5}$$

By using (5) the energy transitions should be shown for a 3-dimensional system.

REFERENCES

[1] Langevin P., On the Theory of Brownian Motion, *C. R. Acad. Sci.*, 146 (1908), 530–533.

[2] Alkemade C.T.J., van Kampen N.G., MacDonald D.K.C., Non-linear Brownian movement of a generalized Rayleigh model, *Proc. R. Soc. Lond. A*, 271 (1963) 1347, 449–471.

[3] Gerlich G., Die verallgemeinerte Liouville-Gleichung, *Physica*, 69 (1973), 458–466.

[4] Mandelstam L., Papalexi N., Expose Des Recherches Recentes Sur Les Oscillations Non Lineaires, Technical Physics of the U.S.S.R., 2 (1935) 2–3, 81–134.

***Authors**: D. Stahl and W. Mathis, Institute of Theoretical Electrical Engineering, Leibniz Universität Hannover, Appelstraße 9A, 30167 Hannover, Germany, e-mail: stahl@tet.uni-hannover.de*

Mirosław WOŁOSZYN, Kazimierz JAKUBIUK, Mateusz FLIS

Gdansk University of Technology

Analysis of Resistive and Inductive Heating of Railway Turnouts

***Abstract**. Electric heating of railway turnouts is a significant technical and economic problem. For these reasons, research is needed to optimise the heating system of railway turnouts. The paper presents a comparative analysis of energy loss during heating of railway turnouts performed using two different methods. The analysis of the heating of railway was-carried out using ANSYS computer simulation software.*

Keywords: railway turnouts, resistive heating, inductive heating.

Introduction

Railway turnouts in winter conditions must be heated to maintain operability during snowfall, wind and trains blowing snow on to the rails as well as during freezing rain [1, 2, 3, 4]. The space between the rail and the needle must be free of ice and snow in order to facilitate the change of the turnout position. Railway turnouts are most frequently heated using electric resistance heaters whereas induction heaters are used less often [1, 2]. Due to considerable energy intensity of the heating process optimisation of the heating system of railway turnouts has become a significant issue. This paper presents the results of comparative analysis of energy loss during electric heating of railway turnouts using a traditional method and a using an induction heater. The heating process was analysed by performing computer simulations in the ANSYS programme.

Models of heating of railway turnouts

For the purpose of analysis a long rail with the resistance (Fig.1) and the induction heater (Fig.2) was chosen. The differential form of Fourier's Law of thermal conduction is:

$$q = -k\left(\frac{\partial T}{\partial x} + \frac{\partial T}{\partial y} + \frac{\partial T}{\partial z}\right), \tag{1}$$

where: q - heat flux density, k - the material's conductivity, T - the temperature.

It was assumed that in the first case the heater is directly adjacent to the rail whereas in the second case the heater heats a hotplate by electromagnetic induction.

The solution with the heater adjacent to the rail is characterised by considerable energy loss. The rail has large thermal heat capacity and absorbs a considerable amount of energy. Therefore, this solution requires a relatively large amount of electric energy to heat the area close to the rail. In the case of the second solution the heater is separated from the rail thus decreasing the thermal conductivity between the heater and the rail. This solution is characterised by smaller energy loss during heating when compared with the solution with a traditional heater. The area above the hotplate is heat by convection and radiation phenomena.

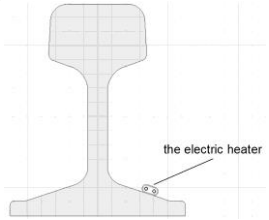

Fig. 1. The model of a rail with the electric resistance heater

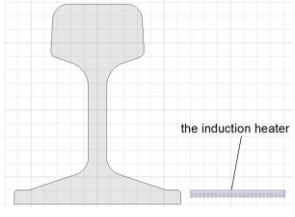

Fig. 2. The model of a rail with the induction heater

For the same electric power in both solutions (320W/m) the temperature in a second system is greater about 60°C in comparison with traditional method.

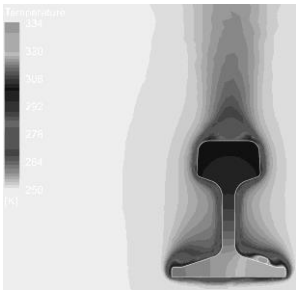

Fig. 3. The distribution of the temperature of the rail with the electric heater (Fig.1)

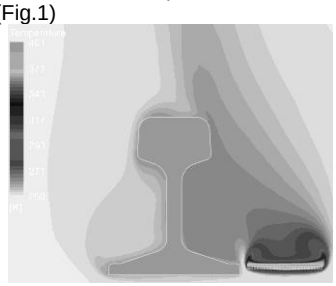

Fig. 4. The distribution of the temperature of the rail with the induction heater (Fig.2)

CONLUSIONS

The comparative analysis of energy loss during heating of the two models of a railway turnout, showed that considerable energy intensity of the traditional heating of railway turnouts. Heating the area close to the rail and the needle requires a relatively large amount of electric energy. Using the induction heater facilitates heating the area close the rail while incurring smaller energy loss.

REFERENCES

[1] Szychta E., Szychta L., Luft M., Kiraga K., Application of 3D Simulation Methods to the Process of Induction Heating of Rail Turnouts, *Infrastruct. Des. Signal. Secur*. Railw. InTech Croat., 2012.

[2] Waller C.A., Berry W.B., Kleinman R.I., Transit system third rail deicing by radio frequency induction, *Railroad Conference*, *Proceedings of the 1991 IEEE/ASME Joint*, 1991, pp. 97–101.

[3] Wolff C.A., Mounting guidelines for electric point-heating-systems, *Wolff Weichenheizungen & Oberbau GmbH*, 2006.

[4] Brodowski J., Contactless heaters designed for accelerated snow melting in rail turnouts, *Polish Railway Institute.*

***Authors**: Mirosław Wołoszyn, Gdansk University of Technology, 80-233 Gdansk Narutowicza 11/12, e-mail: miroslaw.woloszyn@pg.gda.pl, Kazimierz Jakubiuk, e-mail: kazimierz.jakubiuk@pg.gda.pl, Mateusz Flis, e-mail: mateusz.flis@pg.gda.pl*

Zuzanna KRAWCZYK, Jacek STARZYŃSKI

Warsaw University of Technology

Bone Structure Segmentation with Bio-inspired Methods

Abstract*. The article presents and compares two different segmentation methods: artificial ant colony algorithm and a method based on a human brightness perception model by a simplified retina structure. The methods were applied to medical CT images of a human pelvis in order to distinguish bone structure from the rest of the body.*

Keywords: image segmentation, artificial ant colony, human brightness perception, CT.

Introduction

Image segmentation is an important step in visualization and recognition of the anatomical structures in medical image data. Classical methods such as thresholding, region-based or edge-based segmentation algorithms [1] are often insufficient in case of medical images. The thresholding carries a risk of an easy over or under-segmentation of the structure while region-based algorithms need manually placed seeds to start to work.

To overcome this difficulty, in this paper we compare the use of two unconventional bio-inspired algorithms: one of the swarm intelligence type — called *Artificial Ant Colony (AAC)* [2], [3] method, and the other, based on the human brightness perception and foveal adaptation [4] (FA). The use of the AAC algorithm for the segmentation follows [5].

Both algorithms were applied to the CT data of the human pelvis with the grey values normalized to the interval from 0 to 255. The ultimate goal was to detect the bone structures. For the purpose of our application, we implemented the algorithms with the use of *Python* programming language. To speed up the execution of the algorithms, the efficient matrix multiplications of the *numpy* library was employed for a maximal number of suitable operations**.**

Experiments

Several initial experiments on the part of CT image with the femur head were performed in order to estimate the usefulness of the algorithms.

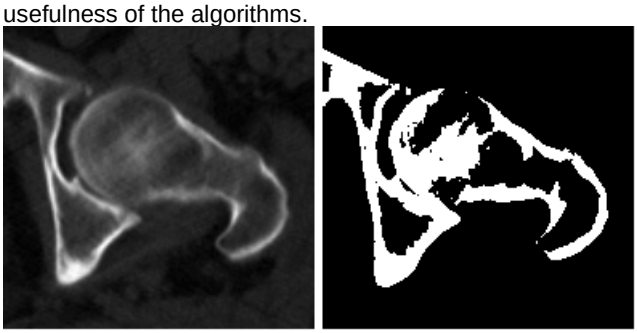

Fig. 1. Original image and the result of classical thresholding Otsu method

Fig. 2. Segmentation with the use of FA algorithm. Size of the fovea mask set to 9 pixels, cw = 3 (left image) or cw = 4 (right image)

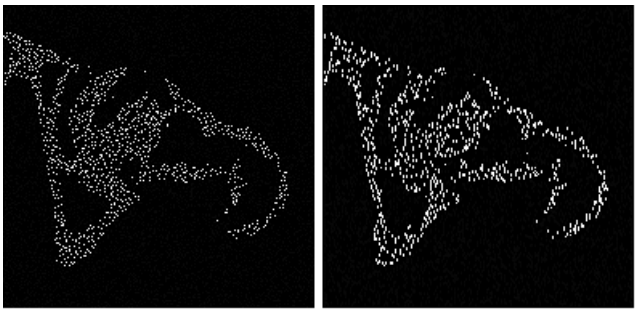

Fig. 1. Artificial ant colony after 100 (left image) and 300 (iterations). Number of ants is set to 30% of pixel number

Summary

The initial simulations are encouraging and show the potential of both methods. In the full version of the article the sensitivity of the algorithms to their defining parameters will be further analyzed. Also, a 3D version of the FA algorithm will be implemented. In order to fully benefit from the AAC method, the way to connect the ant trails should be investigated.

Acknowledgment: The CT data obtained due to courtesy of Maria Skłodowska-Curie Memorial Cancer Center.

REFERENCES

[1] Stolojescu-Crisan C., Holban S., A Comparison of X-Ray Image Segmentation Techniques, *Advances in Electrical and Computer Ingeenering*, 13 (2013), No. 3, 85-91.

[2] Alvarenga A. V., Artificial Ant Colony: Features and Applications on Medical Image Segmentation, *Pan American Health Care Exchanges PAHCE Conference, Rio de Janeiro 2011.*

[3] A. Colorni, M. Dorigo et V. Maniezzo, Distributed Optimization by Ant Colonies, actes de la première conférence européenne sur la vie artificielle, Paris, France, Elsevier Publishing, 134–142, 1991.

[4] Heucke L., Knaak M., A New Image Segmentation Method Based on Human Brightness Perception and Foveal Adaptation, IEEE Signal Processing Letters, vol. 7(2000), No. 6,129-131.

[5] V Ramos, F. Almeida, Artificial Ant Colonies in Digital Imag Habitats – A Mass Behavior Study on Pattern Recognition", Proceedings of ANTS 2000, International Workshop on Ant Algorithms.

Authors*: Zuzanna Krawczyk, Jacek Starzyński, Warsaw University of Technology, ul Koszykowa 75, 00-662 Warszawa, Poland, e-mail: krawczyz@ee.pw.edu.pl, jstar@ee.pw.edu.pl*

Tomasz CHADY, Paweł Karol FRANKOWSKI

Department of Electrical and Computer Engineering, West Pomeranian University of Technology, Szczecin

Massive Multi-Frequency Eddy Current Method for Clad Material Inspection

Abstract. *The aim of this paper is to present a massive multi-frequency method for detection of artificial defects in clad materials. A system excited by a voltage waveform created as a sum of many sinusoidal signals is proposed for this purpose. Studies show that, the multi-frequency method can be successfully used for assessment of the defects depth. The experimental verification is done and selected results are presented.*

Keywords: non-destructive testing, clad material, fatigue cracks, eddy current inspection

Introduction

Clad metals are manufactured by roll bonding a backing with a specialty metal to produce a metallurgically bonded clad. The advantage of these materials is that the end product combines the superior properties of each component metal e.g.: strength, corrosion resistance, lightweight, lower cost, thermal and electric conductivity, etc. However, even such universal materials have some limitations and during the exploitation can be damaged. Therefore, periodical inspections are required. Ideally, such testing should be done without damaging of structures and stopping exploitation. The purpose of this paper is to present multi-frequency eddy current method for periodical nondestructive inspections of such materials.

Sample

A tested sample is presented in Fig. 1. The flat clad sample was manufactured with a three sub-superficial notch 0.8, 1.5 and 3 millimeter depth in the CRA layer (Inconel 625 in this case, the base material is a carbon steel). The inspection was carried out from the Inconel side.

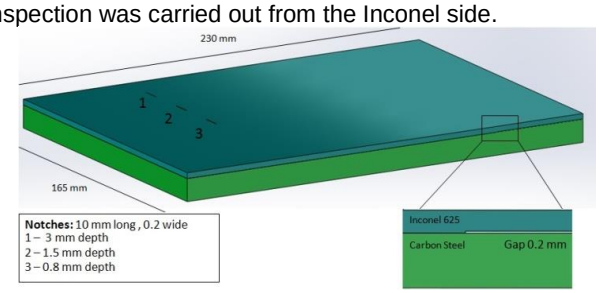

Fig. 1. Cross section of the sample, clad metal used to the produce of petrol pipeline

Method

One of the most important advantage of the multi-frequency measurement is that eddy current depth of penetration varies as a function of frequency. Lower frequencies have a larger skin depth and hence give clear signals from discontinuities located away from the coil. Tests prove that the multi-frequency excitation and spectrogram system (MFES) allows to observe changes in the structure through changes of the spectrogram parameters [1].

Results

The transducer was moved above the specimen and measurements were taken with a 1 mm step. Presented in Fig. 2 results shows dependence of the signal amplitude on depth of the notches. However, more informative plots of spectrograms were received in case of a phase shift signals. Tests prove, that the frequency for which a phase shift is achieving maximum is highly correlated with the depth of defects (Fig. 3).

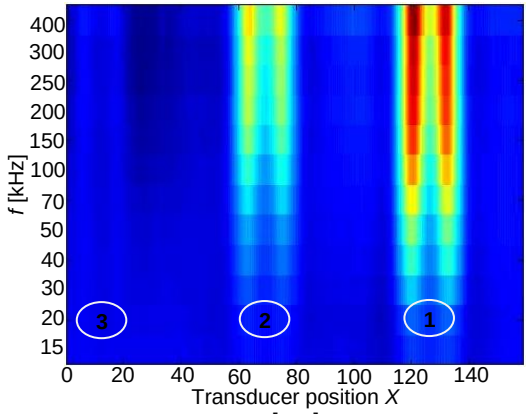

Fig. 2. Spectrogram: magnitude vs transducer position; notches: 1. depth–3mm, 2. depth–1.5mm, 3. depth–0.8mm

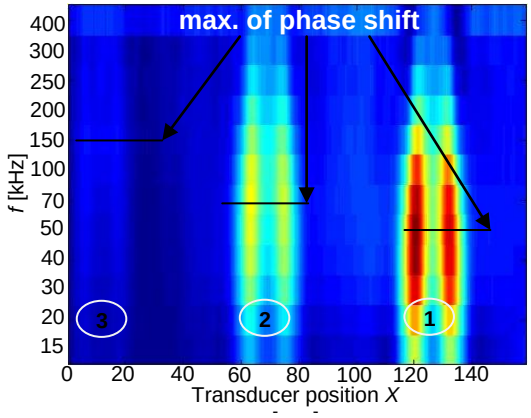

Fig. 3. Spectrogram: phase shift vs transducer position; notches: 1. depth–3mm, 2. depth–1.5mm, 3. depth–0.8mm

Acknowledgments

This work is supported in part by Foundation for Polish Science and cosponsored by UE under grant VENTURES/ 2013-11/5.

The authors would like to thank Professor J. M. A. Rebello and C.G. Camerinii from Federal University of Rio de Janerio for their effort in caring out a common research and preparation of the samples.

REFERENCES

[1] T. Chady, M. Enokizono, „Multi-frequency exciting and spectrogram-based ECT method", *Journal of Magnetism and Magnetic Materials*, t. 215, pp. 700–703, June 2000.

Authors: *Tomasz Chady, Paweł Frankowski West Pomeranian University of Technology, Department of Electrical and Computer Engineering, ul. Sikorskiego 37, 70-313 Szczecin, Poland, e-mail: {Tomasz.Chady, pfrank}@zut.edu.pl*

Diana OLEJNIK, Tomasz CHADY, Paweł Karol FRANKOWSKI

Department of Electrical and Computer Engineering, West Pomeranian University of Technology, Szczecin

Climbing Quadruped Robot for Nondestructive Testing

Abstract. *This paper presents design, construction and control of quadruped robot, capable to maneuver on vertical surfaces. A nondestructive system integrated with the robot enables location, tracking and evaluation of rebars in concrete structures. The paper illustrates robot manipulation in the kinematic approach and practical application of the platform dedicated for nondestructive testing.*

Keywords: non-destructive testing, reinforced concrete structures, quadruped robot, vacuum technology.

Introduction

The purpose of this paper is to present: design, construction and control of the quadruped robot, capable to maneuver even on vertical surfaces of reinforced concrete structures. The nondestructive system integrated with the robot enables location and tracking of the rebars in concrete structures. The robot ability of climbing is assured by the high quality vacuum system. The prototype of the measurement platform is equipped with the ejector pumps and suction cups, which make robot adhesion dependent on the surface roughness.

Structure and Control

The project of quadruped robot was prepared using the Autodesk Inventor Professional, 3D design software. Every executive element can be mapped in a CAD project, thereby the precise designing of the mounting parts and printing them using a 3D printer is possible (Fig. 1). Printed parts are made of thermoplastic polymer Acrylonitrile Butadiene Styrene (ABS) with the print temperature in the range of 210–240°

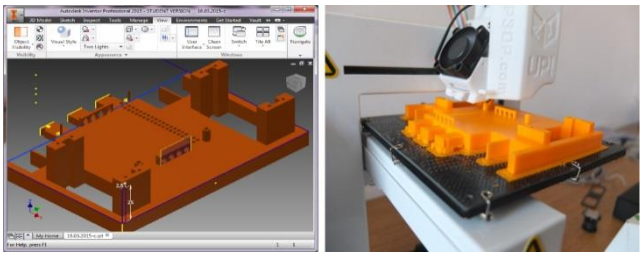

Fig.1. Autodesk Inventor - design software (left), 3D printing using UP Plus 2 (right)

To make climbing possible it is necessary to use light and strong actuators. Due to this aspect, the vacuum technique is used. The decentralized system assumed application of four ejectors pumps (one per leg) equipped with the suction cups. High friction of the rubber material allows the suction cups to withstand high forces, even at rapid accelerations in horizontal directions. Compressed air flow is controlled by the pneumatic electrovalves [1]. The robot is driven by a Raspberry PI - single-board computer. Motions of the robot legs are carried out by eight digital servos. The servos are connected to relay board and servo driver. The electrovalves and servomechanisms are controlled by the Raspberry board. An implemented software allows to both manual or automatic robot control through wireless communication. An operating system is based on the Debian/GNU Linux optimized for the Raspberry Pi hardware.

Fig. 2. Photography of the Quadruped Climbing Robot

Robotic Manipulation

The fundamental concept of robotic manipulation is based on the following equation:

$$g_{st}(\theta) = e^{\xi_1\theta_1} e^{\xi_2\theta_2} \cdots e^{\xi_n\theta_n} g_{st}(0) \quad (1)$$

where: $g_{st}(\theta)$ – current configuration, ξ – twist, θ – angle.

Product of the exponential formulas describes end-effector configuration as a function of the robot joint variables [1]. The motion program uses (1) and returns the configuration and position of the robot's legs. In this way, accuracy of the movement was increased.

Non-Destructive Testing

For preliminary tests, a low-power digital 3-D magnetic sensor MAG3110 was utilized. This magnetometer enables to measure a magnetic field in three dimensions. In the next stage it is planned to use more accurate magneto-optical sensors for precious analysis of the magnetic field and structures assessment.

Acknowledgments

This work is supported in part by Foundation for Polish Science and cosponsored by UE under grant VENTURES/ 2013-11/5 .

REFERENCES

[1] Sarkar J., Ejector enhanced vapor compression refrigeration and heat pump systems - A review, Renewable and Sustainable Energy Reviews 2012.

[2] Murray R. M., Li Z., Shankar Sastry S., A Mathematical Introduction to Robotic Manipulation, CRC Press 1994.

***Authors**: Diana Olejnik, diana_olejnik@wp.pl, Tomasz Chady, Tomasz.Chady@zut.edu.pl, Paweł Frankowski, pfrank@zut.edu.pl, West Pomeranian University of Technology, Department of Electrical and Computer Engineering, ul. Sikorskiego 37, 70-313 Szczecin, Poland*

ORAL SESSION 2 (Monday 8.06.2015, 16:40 – 18:00)			
Chairman: Masato Enokizono Chairman: Stanisław Gratkowski		enoki@oita-u.ac.jp stanislaw.gratkowski@zut.edu.pl	
	Time	**Authors**	**Title**
Invited lecture	**16:40–17:10**	**Ludger Klinkenbusch, Hendrik Brüns**	**Multipole Analysis and Complex-Source Beams in Scalar and Electromagnetic Fields**
Invited lecture	**17:10–17:40**	**Tomasz Krupicz, Ad Van Der Linden**	**COMSOL Multiphysics® for Electromagnetic Simulations**
1	17:40–18:00	Tomasz Chady, Ryszard Sikora, Przemyslaw Lopato, Grzegorz Psuj, Barbara Szymanik, Krishnan Balasubramaniam, Prabhu Rajagopal	Wind Turbine Blades Inspection Techniques

Ludger Klinkenbusch, Hendrik Brüns

Kiel University, Germany

Multipole Analysis and Complex-source Beams in Scalar and Electromagnetic Fields

Abstract. *The paper describes the combination of the spherical-multipole technique in sphero-conal coordinates with a complex-source beam as an incident field to come to a convergent series solution for the scattering of a local plane wave by the tip of an acoustically soft or hard or by a perfectly conducting semi-infinite elliptic cone. Numerical results are shown for the scattering by a quarter plane. The technique has been used to deduce exact diffraction coefficients for the corner of that structure.*

Keywords: canonical structures, complex-source beam, geometrical theory of diffraction.

Introduction

Multipole analysis counts to the classical methods in solving acoustic and electromagnetic problems [1]. It has been widely used for theoretical purposes and employed for various applications using analytical as well as numerical methods. One area of application concerns the exact solution of canonical problems the geometry of which are usually given in terms of coordinate surfaces in one of those coordinate systems where the Helmholtz equation is completely separable [2]. Of particular interest is the semi-infinite elliptic cone. First, this geometry has a tip, and the corresponding field radiated from that geometrical singularity is of interest for asymptotic methods for analyzing scattering and diffraction by electrically large complex structures. Second, the wide variety of different elliptic cone includes the circular cone, the wedge, the half plane, and the plane angular sector, that is, geometries which also show certain geometrical singularities with interesting scattering features. The paper will give a brief survey on the theoretical background and numerical results for the acoustic as well as the electromagnetic case.

Spherical-multipole expansion

In sphero-conal coordinates r, ϑ, φ the coordinate surface $\vartheta = \vartheta_0$ describes for $\vartheta_0 > \pi/2$ a semi-infinite elliptic cone symmetrically lying around the negative z-axis. For a point-source of amplitude A located at $\vec{r}_P$, the solution of the Helmholtz equation in a homogeneous domain is given by the spherical-multipole expansion [3]

$$\Phi_\tau(\vec{r}) = \mathrm{j}\kappa A \sum_{\sigma_\tau} j_{\sigma_\tau}(\kappa r_<) h^{(2)}_{\sigma_\tau}(\kappa r_>) Y_{\sigma_\tau}(\vartheta,\varphi) Y_{\sigma_\tau}(\vartheta_P,\varphi_P) \quad (1)$$

In (1), j_σ is a spherical Bessel function of order σ, $h^{(2)}_\sigma$ is a spherical Hankel function of the second kind of order σ, while Y_σ represents a Lamé product [3].

$r_< = r, r_> = r_P$ if $|r| < |r_P|$ and $r_> = r, r_< = r_P$ if $|r| > |r_P|$, j is the imaginary unit, κ the intrinsic wavenumber of the embedding medium, and σ_τ with $\tau \in \{s, h\}$ is defined by the eigenvalue equation $(\vec{r}\times\nabla)^2 Y_{\sigma_\tau} - \sigma_\tau(\sigma_\tau+1) Y_{\sigma_\tau} = 0$ subject to the conditions $Y_{\sigma_s}(\vartheta_0) = 0$ for an acoustically soft elliptic cone and $\partial Y_{\sigma_h}/\partial\vartheta\big|_{\vartheta=\vartheta_0} = 0$ for an acoustically hard elliptic cone. Similar results can be obtained for an electrically perfectly conducting cone [4].

Complex-source beam (CSB)

It can be shown [5] that by assigning a complex value $\vec{r}_P = \vec{r}_r + \mathrm{j}\vec{b}$ as the source coordinate in the free space Green's function, the original spherical wave turns into Gaussian-beam like field with its waist at $\vec{r}_r$ and the direction and focus length defined by $\vec{b}$. Using this complex source coordinate in (1) leads to the desired case of an elliptic cone illuminated by a Gaussian-like beam.

Numerical result

The Figure below shows a snapshot of the electric field for a quarter plane illuminated by a CSB incident from the right side and polarized parallel to the quarter plane.

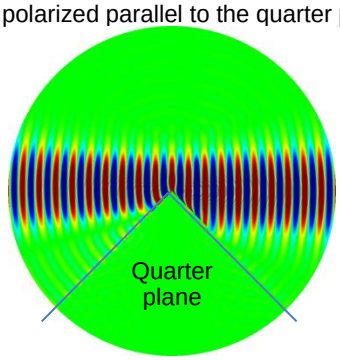

REFERENCES

[1] Bowman J.J., Senior T.B.A., Uslenghi P.L.E., Electromagnetic and acoustic scattering by simple shapes (revised printing), New York: *Hemisphere Publishing Corp*. 1987.

[2] Moon, P., Spencer, D.E., Field theory handbook (2nd ed.), Berlin, Heidelberg, New York: *Springer Verlag* 1971.

[3] Brüns, H., Klinkenbusch, L., Acoustic Scattering of a Complex-Source Beam by the Edge of a Plane Angular Sector, *Adv. Radio Sci*., 12 (2014), 179–186.

[4] Brüns, H., Klinkenbusch, L., Electromagnetic diffraction and scattering of a complex-source beam by a semi-infinite circular cone, *Adv. Radio Sci*., 11 (2013) 31–36.

[5] Felsen, L.B., Complex source point solutions of the field equations and their relation to the propagation and scattering of Gaussian beams, in *Symposia Mathematica, Instito Nazionale di Alta Matematica (Academic, London)* 18 (1976), 40–56.

***Authors**: Ludger Klinkenbusch (lbk@tf.uni-kiel.de), Hendrik Brüns (heb@tf.uni-kiel.de), Kiel University, Faculty of Engineering, Kaiserstr. 2, D-24143 Kiel (Germany)*

***Acknowledgment:** This work was supported by the Deutsche Forschungsgemeinschaft (DFG), Grant No.: KL 815/10-1&2.*

Tomasz KRUPICZ, Ad VAN DER LINDEN

Comsol Multiphysics GmbH

COMSOL Multiphysics® for Electromagnetic Simulations

Abstract. *COMSOL Multiphysics® is a numerical FEM-tool which is specialized in the simulation of the detailed interaction between many different fields of physics and engineering. For electromagnetic applications COMSOL Multiphysics® includes dedicated modules for direct current, low and high frequency as well as for wave optics and ray optics simulations. These electromagnetic modules can be easily combined with multiphysics applications. In addition, the new Application Builder allows sharing models with colleagues, peers and customers through the COMSOL Server™.*

Keywords: simulation software, multiphysics, electromagnetic simulations.

Introduction

The COMSOL Multiphysics® simulation software is a numerical tool based on the finite element method. With COMSOL the realistic interaction between electromagnetic, mechanical, thermal, chemical and fluid flow aspects in design and engineering applications can be simulated in a user-friendly and intuitive software environment without the need for in-depth programming.

COMSOL's core package includes all finite element functionality for creating geometries, defining materials and basic physical properties, meshing, setting up studies and optimizing solver settings, solving the models and post-processing. Add-on modules allow using predefined physics definitions and multiphysics couplings.

Introduced in the recent Version 5, the new Application Builder allows creating specialized applications from COMSOL models for use by others, from colleagues to customers, using the new COMSOL Server™ as platform for sharing apps.

COMSOL Modules for electromagnetic simulations

In COMSOL's electromagnetic product range many applications in direct and alternating current, radio frequency and optics are covered by the AC/DC Module, the RF Module, Wave Optics Module and the Ray Optics Module. Examples of modeling applications for these modules are: resistors, capacitors, inductors, cables, coils, electromagnets, permanent magnets, motors, generators and actuators (AC/DC), antennas, waveguides, filters, transmission lines and microwave heating (RF), fibers, optical media, plasmonics, photonics (Wave Optics) and optical ray tracing (Ray Optics).

Within the electromagnetic spectrum Figure 1 shows, as a function of object size and wavelength, when the specific electromagnetic modules are best suitable.

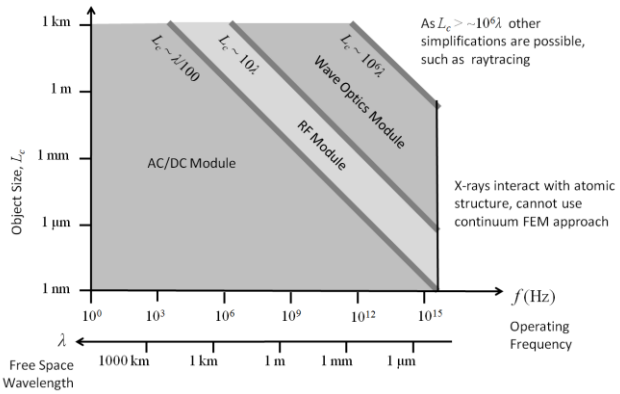

Fig.1. COMSOL Modules in the electromagnetic spectrum

In addition, COMSOL [1] offers specific electromagnetic multiphysics applications in the MEMS Module, the Plasma Module and the Semiconductor Module.

The AC/DC Module

Being the largest electromagnetic COMSOL module, the AC/DC Module includes specific interfaces for electrostatics (es), electric currents (ec), magnetic fields (mf) and magnetic and electric fields (mef). The electric circuit (cir) interface allows for the coupling of these interfaces with discrete circuit simulation.

Additional interfaces allow for the specific modeling of permanent magnets and magnetization (mfnc), rotating machinery (rmm) and superconducting materials (mfh).
For electric currents simulations of shell objects the specific (ecs) interface is available. In addition, all interfaces allow thin layer objects to be approximated by means of shell boundary conditions.

Material properties in the AC/DC Module include both conductivity, permittivity and permeability, and polarization, magnetization, remanent flux density and BH-curves.

The functionality of COMSOL Multiphysics®, in particular that of the AC/DC Module and the Application Builder can be demonstrated in more detail as shown in the example of Figure 2 [2].

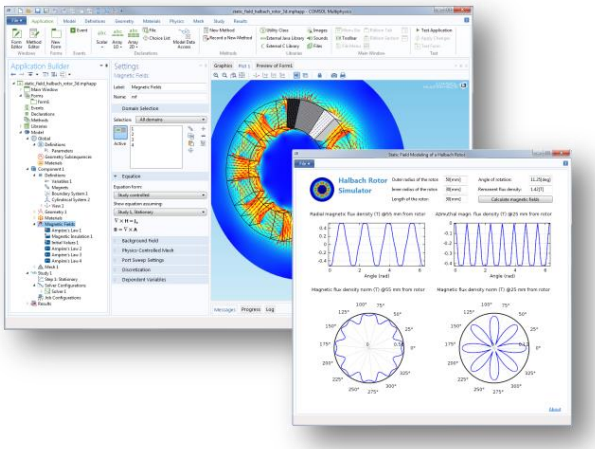

Fig. 2. COMSOL Model and COMSOL App of a generator

REFERENCES

[1] https://www.comsol.com/products
[2] http://www.comsol.com/models

Authors: *Tomasz Krupicz, Ad van der Linden, Comsol Multiphysics GmbH, Kurfürstenstrasse 84, 10787 Berlin, Germany, e-mail: info@comsol.de*

Tomasz CHADY[1], Ryszard SIKORA[1], Przemyslaw LOPATO[1], Grzegorz PSUJ[1], Barbara SZYMANIK[1], Krishnan BALASUBRAMANIAM[2], Prabhu RAJAGOPAL[2]

West Pomeranian University of Technology, Szczecin (1), Indian Institute of Technology, Madras (2)

Wind Turbine Blades Inspection Techniques

Abstract. *Wind turbines are complex composite structures, which condition should be constantly tested. In this paper the techniques which are already used or are implementable for non-destructive examination of wind turbine blades will be presented. All the techniques will be described in terms of inspection during production process and in service. New techniques like air coupled ultrasonic testing, active IR testing or terahertz imaging will be more widely presented and some exemplary results of inspections will be shown.*

Keywords: wind turbine blades, infrared testing, ultrasonic testing, terahertz testing.

Introduction

Because of higher environmental awareness of world society, share of wind energy in the total produced energy is steadily increasing. Thus more wind turbine installations will be deployed in the future, both on the land and offshore. Because of the size and exposure to weather conditions wind turbine blades (WTB) can be considered as the most critical part of wind turbine. That is the reason for development of accurate and easy to implement monitoring and testing techniques. Some of inspection methods can be utilized during production process, but their application in service would be much more difficult.

NDT techniques for wind turbine blades inspection

The wind turbine blade is a complex structure mostly made of glass-fiber, balsa wood (or plastic foam) and polymer adhesive. Thus material is nonhomogeneous and isotropic in case of both mechanical and electrical parameters. The photo of wind turbine blade cross section is presented in Fig. 1. Additionally, the surface is curved, there are big differences in wall thickness and there is no access to interior part of WTB. Accurate inspection of such structures cause many problems. There are several techniques that can be considered as applicable for non-destructive testing wind turbine blades [1-3]:

- visual inspection,
- infra-red thermography,
- ultrasonic testing,
- digital radiography,
- acoustic emission,
- tap testing,
- vibration analysis,
- microwave and terahertz techniques.

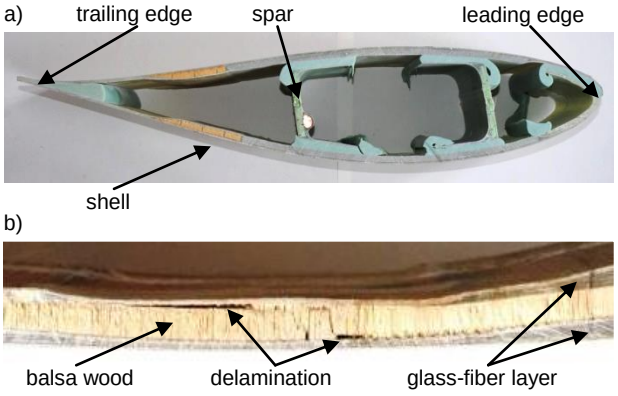

Fig.1. Wind turbine blade: a) view of cross section, b) typical defect – delamination between balsa wood core and glass-fiber laminates

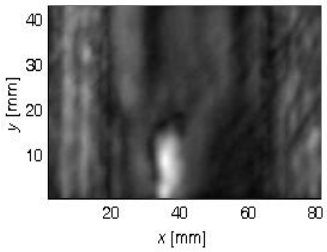

Fig. 2. Result of terahertz imaging of wind turbine blade (registered C-scan) - white area is an indication of delamination.

All of them are utilized for polymer laminates and sandwich composites inspection, thus their application in case of WTB production process is possible. The sensitivity and inspection time are the factors which determine the selection of suitable examination technique. Since blades are large-scale and on-tower, in service inspection needs much more effort. A new approach is to use a climbing robot to scan the blades. All mentioned techniques will be considered for application is such systems.

Exemplary result of terahertz inspection is presented in Fig. 2. More detailed description of this and all other techniques, results of inspections and analysis of the applicability of new methods in production phase and in service will be provided in full paper.

This work was supported in part by European Commission project HEMOW: Health Monitoring of Offshore Wind Farms (reference: FP7-PEOPLE-2010-IRSES-GA-269202)..

REFERENCES

[1] Raišutis R., Jasiūnienė E., Šliteris R., Vladišauska A., The review of non-destructive testing techniques suitable for inspection of the wind turbine blades, *ULTRAGARSAS Journal,* 63 (2008), No. 1, 26–30.

[2] Drewry M.A., Georgiou G.A., A review of NDT techniques for wind turbines, *Insight,* 49 (2007), No. 3, 137–141.

[3] Zhang H., Jackman J., A feasibility study of wind turbine blade surface crack detection using an optical inspection method, *Proceedings of International Conference on Renewable Energy Research and Applications ICRERA 2013,* Madrid, Spain, 20–23 October 2013, 847–852.

***Authors**: Tomasz Chady tchady@zut.edu.pl, Ryszard Sikora rs@zut.edu.pl, Przemyslaw Lopato plopato@zut.edu.pl, Grzegorz Psuj gpsuj@zut.edu.pl}, Barbara Szymanik szymanik@zut.edu.pl}, West Pomeranian University of Technology, Szczecin, al. Piastow 17, Szczecin, Poland*

Krishnan Balasubramaniam balas@iitm.ac.in, Prabhu Rajagopal prajagopal@iitm.ac.in, Indian Institute of Technology, Madras, IIT-Madras, Chennai – 600036, India

ORAL SESSION 3 - SEEM Session (Tuesday 9.06.2015, 8:40 – 10:30)			
Chairman: Ivo Doležel dolezel@fel.cvut.cz Chairman: Tomasz Chady tomasz.chady@zut.edu.pl			
	Time	**Authors**	**Title**
Invited lecture	**8:40–9:10**	**João Marcos Rebello, Cesar Camerini, Gabriela Pereira**	**Materials Characterization Using Electromagnetic Nondestructive Techniques**
1	9:10–9:30	Cesar Camerini, João Marcos Rebello, Tomasz Chady	Clad Material Inspection Using Non-Conventional Eddy Current Techniques
2	9:30–9:50	Hartmut Brauer, Hannes Toepfer	Interdisciplinary Research Project "Lorentz Force Velocimetry and Lorentz Force Eddy Current Testing": a Five-Years Field Report
3	9:50–10:10	Kota Sasaki, Noritaka Yusa, Hidetoshi Hashizume	Analysis on Propagation Losses inside a Metal Pipe in Nondestructive Testing Using Microwave for Wall Thinning
4	10:10–10:30	Justyna Szlagowska-Spychalska, Krzysztof Dragan, Michał Dziendzikowski	Numerically Enhanced Eddy Current Inspection of Corrosion Losses of Aircraft Structures

João Marcos REBELLO[1,2], Cesar CAMERINI[2] and Gabriela PEREIRA[1,2]

Federal University of Rio de Janeiro (1), Laboratory of Non Destructive Testing, Corrosion and Welding (2)

Materials Characterization Using Electromagnetic Nondestructive Techniques

Abstract*. Materials degradation are normally associated to microstructural changes. Cracks, corrosion problems, premature failure and others types of damage may appear during "in service" operation of equipment and are generally consequence of phases transformation, precipitation of undesirable and deleterious phases or even any change in the original material microstructure. The current paper discloses the use of electromagnetic nondestructive techniques for materials characterization, with the goal of anticipating diagnostics even with no apparent defect.*

Keywords: Electromagnetic characterization, materials properties, microstructural changes.

Introduction

In metallic materials, the atoms are arranged in compact and orderly patterns, and may own different crystallography structure configuration (body and face-centered cubic, hexagonal close packing). The alloying elements combined with the processing temperature define the crystalline structure and consequently the phases presented in the material microstructure. All materials properties are directly associated with the microstructure characteristics and for engineering aspects can be highlighted three relevant properties: mechanical resistance, corrosion resistance and toughness. These properties combined with the application environment and conditions will define materials lifetime. However, any unexpected variation during fabrication process or "in service" operations can trigger or accelerate the degradation process, decreasing the material working life. Materials degradation can manifest itself in two different ways, as defects or/and microstructural changes.

Nondestructive testing (NDT) are intensively employed for materials evaluation, but mainly focused for defects detection. Nevertheless, many types of defects are consequence of advanced stage of microstructural changes. The current paper discloses the use of electromagnetic nondestructive techniques for materials characterization with the goal of anticipating diagnostics even with no apparent defect.

Materials characterization using electromagnetic NDT

Depending on the degradation process, i.e., cracks, corrosion or microstructure variations, can be detected using conventional electromagnetic NDT techniques, such as, eddy current testing, magnetic flux leakage, however, these techniques may not give enough information about the degradation stage. As an example, an equipment with a crack may operate for several years after its first detection or even the crack may not affect the working life at all, while a material with no crack but significant changes in the original crystallographic structure can ruin very fast. These complex situations can be solved by a deep knowledge of the microstructure evolution and a detailed analysis of the corresponding degradation levels.

For an accurate characterization using electromagnetic NDT it is necessary to have a precise correlation between the inspections results and the material microstructure features, which is only obtained using advanced microstructure evaluation techniques as EBSD Scanning Electron Microscopy, Magnetic Force Microscopy, Magneto Optic Kerr Microscopy, Vibrating Sample Magnetometer. This means, there is a condition to be filled in order to successfully apply electromagnetic NDT for materials characterization. The microstructure changes which are at the origin of the observed equipment degradation may necessarily also change the materials magnetic properties.

To illustrate the scenario, different crystallography structure configuration results in different phases and consequently different materials properties. Thereby slight variations in the corrosion properties, for example, can be consequence of some crystallographic modification, which presents not only difference in corrosion properties, but also difference in many others properties from the original structure, including electromagnetic ones. These small variations in the electromagnetic properties can be analyzed by Magnetic Force Microscopy or Vibrating Sample Magnetometer and later correlated with the conventional electromagnetic NDT [1, 2].

Conclusions

The present paper explains how electromagnetic NDT can be used in material characterization. In the extended version of the current paper some examples are given in different situations: during "in service" operation and as an effective tool for quality control in the product fabrication.

Acknowledgements

National Council for Scientific and Technological Development Board (CNPq, Brazil) and Coordination for Improvement of Higher Education (CAPES, Brazil).

REFERENCES

[1] N. Sathirachinda, R. Petterson and Jinshan Pan. "Depletion effects at phase boundaries in 2205 duplex stainless steel characterized with SKPFM and TEM/EDS", Corrosion Science, 51, 2009.

[2] J.M. Rebello, C. Camerini, J.V Rocha and M.C. Areiza. "Saturated low frequency eddy current technique applied to microstructure phase quantification in duplex stainless steel", Nondestructive Evaluation/Testing: New Technology & Application (FENDT), 2013 Far East Forum on. IEEE, 2013.

Authors*: João Marcos Rebello, Federal University of Rio de Janeiro, jmarcos@metalmat.ufrj.br*

Cesar Camerini, Laboratory of Non Destructive Testing, Corrosion and Welding, cgcamerini@metalmat.ufrj.br

Gabriela Pereira, Federal University of Rio de Janeiro, gpereira@metalmat.ufrj.br

Cesar CAMERINI[1], João Marcos REBELLO[1] and Tomasz CHADY[2]

Federal University of Rio de Janeiro (1), West Pomeranian University of Technology, Szczecin (2)

Clad Material Inspection Using non Conventional Eddy Current Techniques

Abstract. *Clad steels are being used in critical equipment for deep-water oil and gas exploration. They are composed of a base material and a coating of a corrosion resistant alloy, and therefore have the mechanical properties of the base material and the corrosion resistance of the coating material. During operation fatigue cracks may arise in the welded parts. The present work uses non-conventional eddy current (EC) transducer to inspect the Clad welded regions. In the results some advantages was achieved when compared with traditional absolute EC transducers.*

Keywords: Clad material, fatigue cracks, eddy current inspection.

Introduction

The deep offshore is supposed to contain more than 5% of the world's oil, representing some 300 billion barrels of oil equivalent. Nearly 40% of these resources has not been discovered yet [1]. However, to extract this oil in a sustainably way numerous of technical and environmental challenges must be overcome, requiring new technologies to be developed. Along with the challenges of offshore exploitation came the need to look for materials with increasingly specific properties to be used in submarine structures and equipment, primarily due to the severity of the environments in which these materials are operating. In this context the steel industry has improved the development of special steel, such as clad steel. Structures and equipment made of clad steel support higher stresses during operation, keeping the same level of corrosion resistance as a steel with a single special alloy, with the advantage of being more economically attractive. Due to their characteristics, these materials are becoming more relevant in offshore projects. Clad steels are composed of a base material and a coating of a corrosion resistant alloy (CRA), and therefore they have the mechanical properties of the base material and the corrosion resistance of the coating material.

For pipelines construction in which the pipes are interconnected, it is necessary to perform circumferential welds. This type of weld in Clad steel pipes are the region that require most attention during operation, firstly because they are points of structure embrittlement and also because they will be expose to the natural process of fatigue which offshore pipelines are subjected during launch and service, such as: dynamic action of waves, ocean currents. If the crack exceeds the CRA layer and reaches the base material, the structure of the pipe will be severely impaired, due to the low corrosion resistance of the base material. Due to the possible emergence of fatigue cracks and the relevance of the structures manufactured by clad steel, it is important to perform periodic inspections of such equipment, and the implementation of nondestructive testing is indicated. The present work discloses about the use of deep penetrating eddy current (EC) testing for fatigue cracks detection in clad material.

Results

A flat Clad sample was manufactured with a sub-superficial notch one millimeter depth of the CRA layer, Inconel 625 in this case. The base material, low carbon steel, is 12 mm thick while the Inconel layer 3 mm. The inspection was performed from the Inconel side. Figure 1 presents a computed tomography of the sample, highlighted the sub-superficial notch.

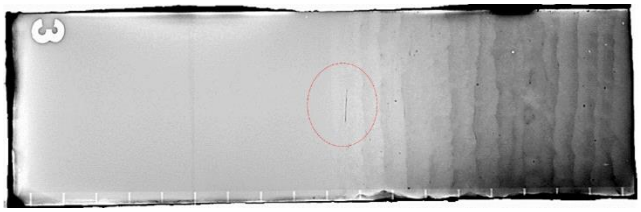

Fig. 1. Computed tomography of the Clad sample with the sub-superficial notch

The EC transducer used for inspection consists of a cylindrical ferrite core with five symmetrically placed columns. A pickup coil is wounded on the central column and four excitation coils are placed on remaining columns in pairs on two perpendicular axes [2]. Figure 2 presents the EC inspection signal of a single scan over the notch.

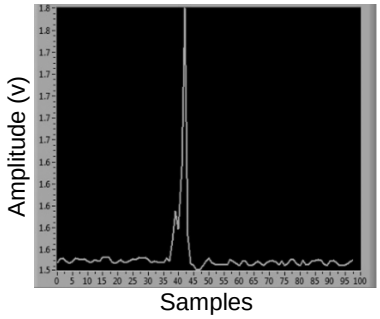

Fig. 2. Crack indication using the EC sensor operating in 5 kHz

Conclusions

The present paper applied non conventional EC technique for clad material inspection. In the extended version of the current paper a detailed presentation of the transducer will be performed and the advantages of using such transducer in comparison with conventional absolute EC probes will be also listed.

REFERENCES

[1] Retrieved May 27, 2015, from http://www.total.com/en/energies-expertise/oil-gas/

[2] T. Chady, M. Enokizono, "Multi-frequency exciting and spectrogram-based ECT method", J. Magn. Magn. Mater., t. 215, ss. 700–703, cze. 2000.

***Authors**: Cesar Camerini, Federal University of Rio de Janeiro, cgcamerini@metalmat.ufrj.br*

João Marcos Rebello, Federal University of Rio de Janeiro, jmarcos@metalmat.ufrj.br

Tomasz Chady, West Pomeranian University of Technology, Szczecin, tchady@zut.edu.pl

Hartmut BRAUER, Hannes TOEPFER

Technische Universität Ilmenau

Interdisciplinary Research Project Lorentz Force Velocimetry and Lorentz Force Eddy Current Testing – A Five-Years Field Report

Abstract. *The authors present a research project related to Lorentz force velocimetry and Lorentz force eddy current testing. Since five years an interdisciplinary team of 12 doctoral candidates and two postdocs performs several basic research projects all under the roof of Lorentz forces. There are investigated different eddy current testing techniques applied to fluids (liquid metals), electrolytes or nonmagnetic solid bodies. The paper will discuss aspects of joint research as well as the challenges of an appropriate educational program in computational engineering for this team.*

Keywords: nondestructive evaluation, eddy current testing, Lorentz force.

Introduction

Nondestructive Testing (NDT) and Evaluation (NDE) of electrically conductive objects require reliable methods to detect material anomalies or deep internal defects. Besides of radiographic, ultrasonic or optical techniques, electro-magnetic methods such as eddy current testing (ECT) find a wide range of application due to low cost, easy to use equipment and low demands to the measurement environment. However, the most limiting factors in ECT are the frequency dependent skin depth or a high velocity of the objects under test. In such cases, it is very difficult to identify deep lying defects. With Lorentz force eddy current testing (LET) a novel electromagnetic nondestructive testing technique has been developed which might be able to overcome those limitations [1, 2].

Lorentz Force Eddy Current Testing

Both, Lorentz force velocimetry (LFV) and Lorentz force eddy current testing (LET), are based on setting an electrically conductive specimen into relative motion to a constant magnetic field. Due to Ohm's law for moving conductors, eddy currents are induced in the conductor under test. The magnetic field consists of two parts, the primary magnetic field (caused by a permanent magnet) and the secondary field generated by the eddy currents.

The interaction of the constant magnetic field and the induced eddy currents results in a Lorentz force $\boldsymbol{F}_L$ acting on the specimen. Due to Newton´s third law, a drag force $\boldsymbol{F}_D$ acts on the permanent magnet (in the opposite direction) and can be measured there (Figs. 1, 2).

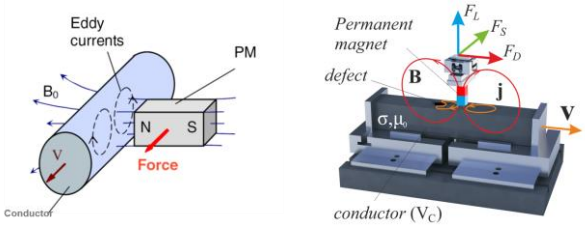

Fig.1. General working principles of LFV (left) and LET (right)

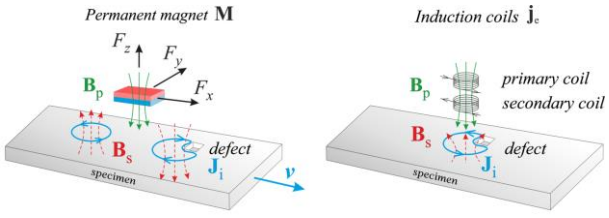

Fig. 2. Physical principle of LET (left) and ECT (right)

If a defect is present in the conductor, the distortion of the Lorentz force can be measured (Fig. 3). Based on the perturbations the defect can be identified [3].

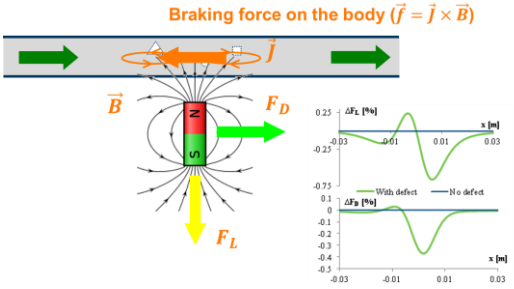

Fig. 3. Perturbation of Lorentz force exerting on permanent magnet due to defects in the conductor

Research Training Group (RTG)

Within the RTG *„LFV and LET"* 12 PhD students (from 6 countries) and actually 9 associated members (from 5 more countries) are working at faculties Mechanical Engineering, Electrical Engineering and Information Technology and Computer Science and Automation of the TU Ilmenau for their PhD. During a period of three years, they are studying together in the course "Computational Engineering" and collaborating in their research. The final presentation will address the problems in research and academic training arising from this situation.

Acknowledgment

This work has been supported by the German Research Foundation (DFG) within the Research Training Group "Lorentz force velocimetry and Lorentz force eddy current testing" (GRK 1567).

REFERENCES

[1] Thess A., Votyakov E., Kolesnikov Y., Lorentz Force Velocimetry, Physical Review Letters, 96 (2006), No. 16, 164501.

[2] Brauer H., Ziolkowski M., Eddy current testing of metallic sheets with defects using force measurements, *Serbian Journal of Elec. Eng.*, 5 (2008), No. 1, 11–20.

[3] Brauer H., Porzig K., Mengelkamp J., Carlstedt M., Ziolkowski M., Toepfer H., Lorentz force eddy current testing: a novel NDT&E testing technique, *COMPEL*, 33 (2014), No. 6, 1965–1977.

***Authors**: Hartmut Brauer, Technische Universität Ilmenau, P.O.Box 100565, 98684 Ilmenau, Germany, hartmut.brauer@tu-ilmenau.de, Hannes Toepfer,, Technische Universität Ilmenau, P.O.Box 100565, 98684 Ilmenau, Germany, e-mail:hannes.toepfer@tu-ilmenau.de*

Kota SASAKI, Noritaka YUSA, Hidetoshi HASHIZUME

Tohoku University

Analysis on Propagation Losses inside a Metal Pipe in Nondestructive Testing Using Microwave for Wall Thinning

***Abstract**. This study reports the quantitative evaluation of effects of microwave attenuation inside a metal pipe so that the microwave nondestructive testing for defects on inner pipe wall is applicable to a long-range piping system. The experiment using straight brass pipe with diameter of 19.0 mm and a length of 25.0 m is carried out in order to evaluate propagation losses and the dependence of detected signals on the propagation distance by changing a location of pipe wall thinning. The experimental result shows propagation losses and distance have a strong correlation.*

Keywords: propagation losses, microwave attenuation, nondestructive testing, pipe wall thinning.

Introduction

Nondestructive testing using microwaves has been studied as one of the efficient inspections of defects inside piping system [1, 2]. This method transmits microwaves inside pipes, thereby detecting and evaluating defects on inner pipe wall on the basis of reflected signals from the defects. Because microwaves propagate inside metal pipe with quite small attenuation, this technique is expected in rapid inspection for long-range piping systems.

Earlier studies demonstrated that artificial full-circumferential wall thinning with a depth of 1.0 mm located at approximately 25 m from a microwave excitation probe provided clear signals [3]. Furthermore, amplitude of reflected signals caused by a wall thinning correlated well with the location. However, propagation losses of microwaves that significantly affects the limitation of the inspection range in this method has not been evaluated quantitatively. To improve detectable range by this method, specifying the influential factor on attenuation and quantitative evaluation of propagation losses are essential.

Our study aims at developing a signal processing which compensates signal decay depending on the increase of the distance from the excitation probe. For this purpose, we carry out experimental evaluations of microwave signal decay using long-range pipes, and propose a new method of estimating microwave attenuation.

Experiment

This study used straight brass pipes with an inner diameter of 19.0 mm and a length of 25.0 m as shown in Fig. 1. The artificial full-circumferential wall thinning with a depth of 1.0 mm and an axial length of 50.0 mm was located L_w [m] away from the end of the excitation probe. Microwaves generated by the network analyzer were transmitted thorough the coaxial cables and propagated inside the pipe. The reflected signals are measured by the network analyzer in frequency domain, and transformed into the time domain by inverse Fourier transform to obtain signals as the reflection caused by wall thinning when the probe emitted microwave as a pulse. Frequency range in this measurement is from 12.000 to 22.000 GHz. Cut-off frequencies of microwave of TM_{01} and TM_{02} mode are 12.087 and 27.743 GHz, respectively.

Result and discussion

Fig. 2 shows maximum amplitude of reflection signals caused by wall thinning at each location with signal processing [2] which compensates dispersion of propagated microwaves. Reflected signals exponentially decrease with the increase of the distance from the excitation probe. On the basis of this results, this study proposes a compensation method of signal decay by specifying

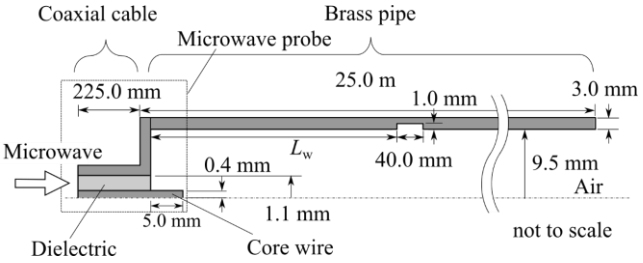

Fig. 1. Configuration of the detection test

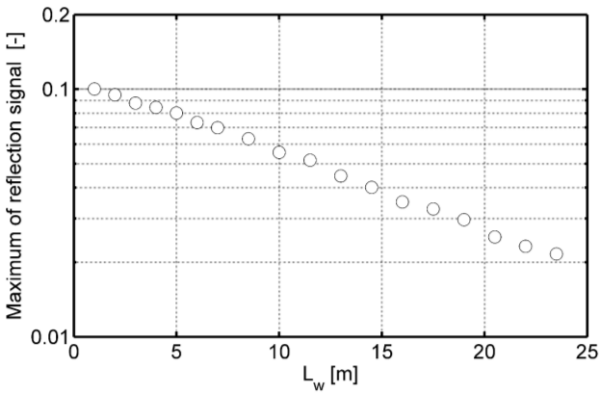

Fig. 2. Amplitude of reflected signals caused by wall thinning for the location

influential factors on microwave attenuation. The details will be presented at ISTET'15.

This work was supported by Grant-in-Aid for JSPS Fellows.

References

[1] H. Hashizume, T. Shibata, K. Yuki, Crack detection method using electromagnetic waves, *International Journal of Applied Electromagnetics and Mechanics*, 20 (2004), 171–178.

[2] Y. Sakai, N. Yusa, H. Hashizume, Nondestructive evaluation of wall thinning inside a pipe using reflection of micrwoaves with the aid of signal processing, *Nondestructive Testing and Evaluation*, 27 (2012), 171-184.

[3] K. Sasaki, N. Yusa, H. Hashizume. Evaluation of the applicability of efficient nodestructive testing using microwave for wall thinning inside a long-range metal pipe, International conference on maintenance science and technology, 2–5 November, Kobe, Japan, (2014).

***Authors**: Kota Sasaki, Tohoku University, 6-6-01-2, Aramaki Aza Aoba, Aoba-ku, Sendai, Miyagi 980-8579, Japan, e-mail: ksasa@karma.qse.tohoku.ac.jp*

Justyna SZLAGOWSKA-SPYCHALSKA[1], Krzysztof DRAGAN[2], Michał DZIENDZIKOWSKI[2]

Warsaw University of Technology (1), Air Force Institute of Technology(2)

Numerically Enhanced Eddy Current Inspection of Corrosion Losses of Aircraft Structures

Abstract. *This paper concerns applications of the Eddy Current for the corrosion detection in the aircraft structures. Additionally, the special finite element models have been developed which simulate eddy currents in materials. Numerical models have been validated by the measurements carried out on specially designed test samples. The results obtained in the study allow for building up the reference database for experimental measurements. They also provide tools for analyses of the eddy current impedance diagrams collected under variable probe parameters.*

Keywords: aircraft inspection, eddy current, finite element method (FEM), signal modeling, corrosion losses

Introduction

The possibility of combining numerical and non-destructive methods has a great importance for the industry, especially for aviation, in which the diagnosis of critical structural elements is essential [1]. In the literature a lot of works concerning the subject of modeling electromagnetic field could be found [2,3]. However, those results are scattered and concerned specific cases of geometry. In this study, a tool that improves the measurement process and could be used to analyze the electromagnetic field distributions in critical elements of aircraft was developed.

Eddy current measurement and numerical calculation

For the analysis the two-dimensional, parametric models of probe-sample relation were created. Obtained models allow for: various location of the probe relative to the sample, electromagnetic field distribution depending on the electrical properties of surface layer and around the damage (depending on location and geometry of the damage), distribution of eddy currents density etc.

It was decided to focus on two particular cases (damages that often occurred in aircraft):

a) Corrosion type: BoT (Bottom of the Top) and ToB (Top of the Bottom),
b) Corrosion damage under non-conductive layer.

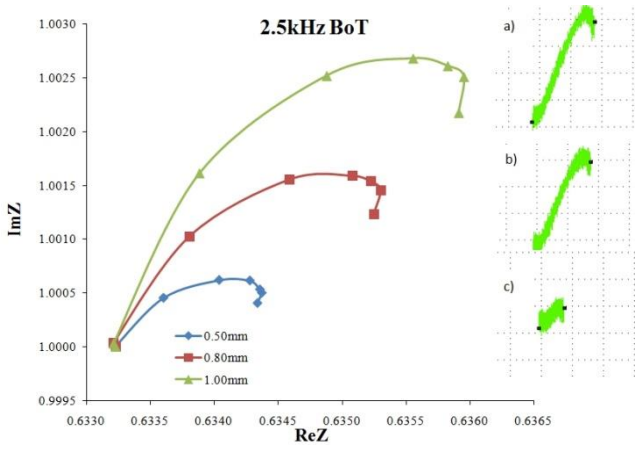

Fig. 1. Eddy current curves obtained by numerical simulation, BoT , frequency 2.5kHz

Verification of the results

Verification was based on comparison between the phase angles obtained during numerical simulation and phase angles obtained during eddy current measurements. In order to compare the numerical results with experimental results some kind of their normalization was necessary. Apart from issues of numerical modeling also statistical methods of data comparison and normalization were carried out. In the case, where C-scans were involved, analysis included also image processing. In the table below a comparison of the increases of the phase angles tangent for subsequent corrosion damages is presented as an example of the obtained results.

Table 1. Comparison of experimental and numerical normalized phase angle values for different size of damages, type BoT, frequency 2.5 kHz

	Numerical Results [%]	Experimental Results [%]
0.0–0.5	100.00	100.00
0.5–0.8	59.35	63.16
0.8–1.0	40.65	36.84
<1.0	0.00	0.00

Conclusions

To summarize research presented in this article it should be noted that the proposed method based on a combination of experimental methods (eddy current) with numerical simulations is correct and capable of industrial application. Formalism of the Finite Element Method was used to create numerical models that allowed quantitative description of the eddy current, which is the basis for determining the characteristics of the signal for selected cases of damage. The correctness of the method was confirmed by the following results which were achieved during research: •*Curves obtained by numerical simulations for the subsequent damages are consistent to curves obtained by the eddy current testing (Fig. 1).* •*Phase angles obtained by numerical simulations for the subsequent damages are consistent with phase angles obtained by the eddy current testing (Table 1).*

This work was financed by NSC Project N N507 217940.

REFERENCES

[1] Grandt A., Fundamentals of structural integrity: damage tolerant, design and nondestructive evaluation, *Wiley - Interscience*, 2004.
[2] Marlekin R., Rahman M. U., Numerical modeling and inverse profiling in non-destructive testing, *Applied Electromagnetics Conference (AEMC)*, 2009, 1–4.
[3] Thomas V., Joubert P. Y., Vourc'h E., Placko D., A novel modeling of surface breaking defects for eddy current quantitative imaging, *Sensors Applications Symposium (SAS)*, 2010, 154–157.

Authors: *Justyna Szlagowska-Spychalska, Warsaw University of Technology, szjustyna@inmat.pw.edu.pl*
Krzysztof Dragan, krzysztof.dragan@itwl.pl, Michał Dziendzikowski, michal.dziendzikowski@itwl.pl, Air Force Institute of Technology

ORAL SESSION 4 (Tuesday 9.06.2015, 11:00 – 12:20)			
Chairman: Joao M.A. Rebello jmarcos@metalmat.ufrj.br Chairman: Marcin Ziółkowski marcin.ziolkowski@zut.edu.pl			
	Time	**Authors**	**Title**
1	11:00–11:20	Antonios Lalas, Nikolaos Kantartzis, Theodoros Tsiboukis	Piezoelectrically Programmable ELC Resonators Acting as THz Modulators
2	11:20–11:40	Tomasz Rymarczyk, Przemysław Adamkiewicz, Karol Duda, Jakub Szumowski, Jan Sikora	New Tomographic Method to Determine Moisture Areas in Historical Buildings
3	11:40–12:00	Andreas Fuchs, Stefan Fuchs, Christian Reil, Hans-Peter Schmidt	Coupler Design for Contactless Power and Data Transfer
4	12:00–12:20	N. A. Akwir, J.C. Chedjou, K. Kyamakya, S.P. K. Veeranki, B.O. Mushage	Traffic Flow Simulation: Comparison Between Finite Difference Method (FDM) and Method of Lines (MOL)

Antonios LALAS, Nikolaos KANTARTZIS, Theodoros TSIBOUKIS

Aristotle University of Thessaloniki

Piezoelectrically Programmable ELC Resonators Acting as THz Modulators

Abstract. *The involvement of piezoelectric micro-electromechanical systems (MEMS) actuators to efficiently implement controllable electric field driven LC (ELC) resonators is introduced in this paper. The new device enables the modification of the structural features of an ELC-based complex medium, unveiling in this manner a significant THz modulation capability along with improved bandwidth tunability.*

Keywords: Metamaterials, microelectromechanical systems (MEMS), resonator, piezoelectric, terahertz modulator.

Introduction

Metamaterials are synthetically tailored complex media [1] with notable properties, not available in nature. Due to their unique behavior, they constitute a critical module of modern RF technology, especially in the THz regime [2]. However, their inherent lack of wide spectral bandwidths establishes various defects for real-world applications. To overcome this hindrance, radio-frequency micro-electromechanical systems (RF-MEMS) are essential to offer advanced bandwidth tunability. Split-ring resonators (SRRs) have been profitably proposed [3] for reconfigurable performance. In this work, piezoelectric MEMS actuators are proposed to alter the shape of electric-field driven LC (ELC) resonators, namely planar metamaterial components capable of sustaining epsilon-negative (ENG) resonances. A THz modulation capability is revealed by connecting/disconnecting the metal parts, allowing at the same time the desired bandwidth enhancement. Several numerical simulations verify the merits of the novel structure.

Assessment of the piezoelectric metamaterial

The featured actuator exhibits a piezoelectric expansion or contraction, and hence a displacement of the associated tip, when excited by a potential difference. Two actuators are employed, along with metal parts, to form our ELC resonator, as in Fig. 1(a). The desgn parameters are selected as: L_1 = 8 μm, L_2 = 1 μm, L_3 = 2 μm, w_1 = w_2 = 1 μm, w_3 = 0.75 μm, g_1 = 0.5 μm and g_2 = 0.1 μm. Its metal section comprises a 0.4 μm thick gold layer, while the piezoelectric components consist of lead zirconate titanate (PZT-5H). A performance evaluation is depicted in Fig. 1 in terms of deflection, whereas connection and disconnection of the associated metal parts is revealed.

The controllable ELC metamaterial is shown in Fig. 2 along

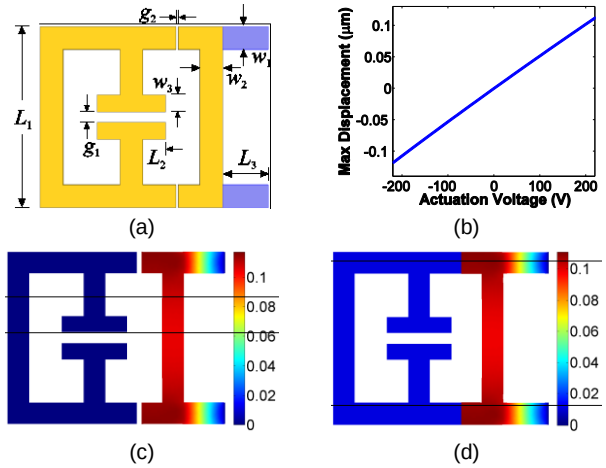

Fig.1. (a) Geometry and design parameters of the piezoelectric actuated device. (b) Behavior evaluation in terms of tip displacement for different actuation voltages, and total displacement distribution (in μm) at (c) -200 V, and (d) 200 V

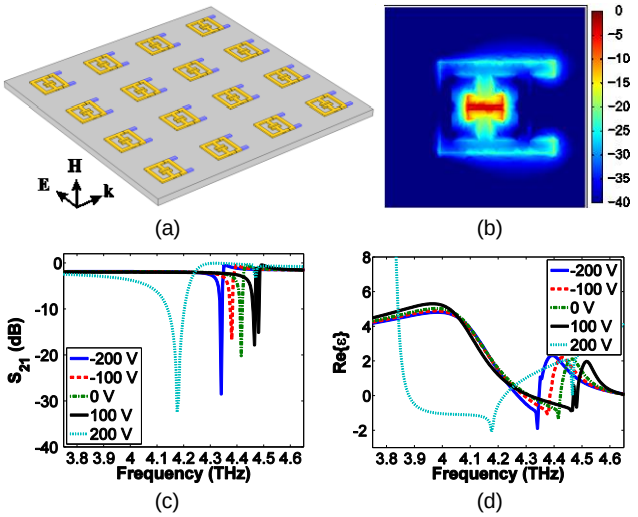

Fig.2. (a) Structure of the programmable, via piezoelectric actuators, metamaterial. Performance assessment in terms of (b) electric field intensity at the surface of the ELC resonator at 200 V and 4.175 THz, (c) S_{21}-parameter, and (d) effective electric permittivity (real part)

with a rigorous performance assessment via the finite element method (FEM). The cell period is set to 18 μm, whereas the thickness of the Si_3N_4 substrate is 2 μm. When the actuation voltage is 200 V, the metal parts touch each other, eliminating the gap. Thus, the essence of the resonator is fully modified, yielding a THz modulating activity. As observed, the nature of the material is switched between conventional attribute at 0 V and ENG behavior at 200V. Also, the transmittance of related signal is swapped between passband and stopband. This behavior is achieved for an enhanced bandwidth of about 60 GHz suitable for potential THz applications.

Acknowledgments

This research has been cofinanced by the EU and Greek national funds via the Research Funding Program: Aristeia.

REFERENCES

[1] Solymar L., Shamonina E., Waves in Metamaterials, *Oxford University Press* 2009

[2] Wang B.-X., Wang L.-L., Wang G.-Z., Huang W.-Q., Li X.-F., Zhai X., Frequency continuous tunable terahertz metamaterial absorber, *J. Lightwave Technol.*, 32 (2014), 1183–1189

[3] Lalas A., Kantartzis N., Tsiboukis T., Tunable terahertz metamaterials by means of piezoelectric MEMS actuators, *EPL*, 107 (2014), 58004

***Authors**: Antonios Lalas, lant@faraday.ee.auth.gr*

Nikolaos Kantartzis, kant@auth.gr

Theodoros Tsiboukis, tsibukis@auth.gr

Department of Electrical and Computer Engineering, Aristotle University of Thessaloniki, GR-54124, Thessaloniki, Greece

Tomasz RYMARCZYK[1,2], Przemysław ADAMKIEWICZ[1], Karol DUDA[1],

Jakub SZUMOWSKI[1], Jan SIKORA[3,4]

Net-art (1), University College of Enterprise and Administration (2), Electrotechnical Institute (3), Lublin University of Technology (4)

New Tomographic Method to Determine Moisture Areas in Historical Buildings

Abstract. *This paper presents a new nondestructive method of brick wall dampness testing in wall structures. The setup was used to determine the moisture in a specially built laboratory model. The topological methods and the gradient technique are used to optimization approach. There was construct forward model of the wall and solve inverse for visualization of moisture inside wall.*

Keywords: electrical impedance tomography, inverse problem, finite element method, level set method.

Introduction

Nondestructive methods do not require that samples be taken from the wall, which is their advantage over the destructive methods. Among nondestructive methods the most popular are electric and nuclear methods, particularly: the electric resistance method, the dielectric method, the microwave method and the neuronal method. But in the case of nondestructive methods, the dampness measuring instruments must be graduated in order to determine the correlation between their indications and the weight moisture content of the tested material. In this paper the inverse problem for the electric field is investigated. The level set method and the gradient technique are based on shape and topology optimization approach to the electrical impedance tomography. Such task can be considered as application of the electrical impedance tomography. Investigated structure is given in Fig. 1.

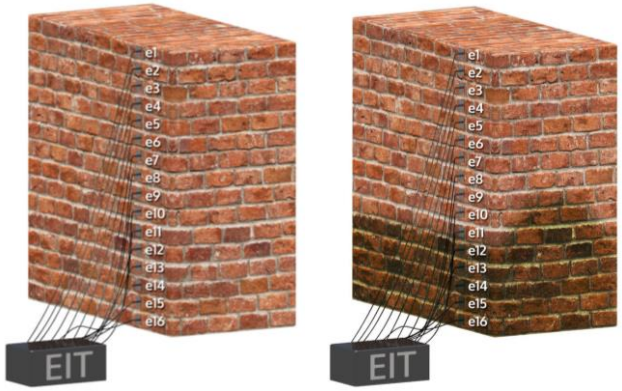

Fig. 1. Measurement EIT system with 16 electrodes on one side of the brick damp wall

Numerical methods

One step methods and topological algorithms was used to solve this problem. Numerical methods of the shape and the topology optimization were based on the level set representation and the shape differentiation and were made possible topology changes during the optimization process [2, 3, 6]. A useful concept for calculating derivatives for cost functional is the so-called material and shape derivative of states. In the application of inverse problems, these states typically are the solutions of partial differential equations which model the probing fields and which depend one way or another on the shape. Discussed technique can be applied to the solution of inverse problems in the electrical impedance tomography [1, 4, 5].

Model and results

The prototype measuring system contains a 16 electrodes for measuring damp brick wall on one side. The figure 2 shows exemplary numerical reconstruction of moisture in the damp wall by the Gauss Newton one step method.

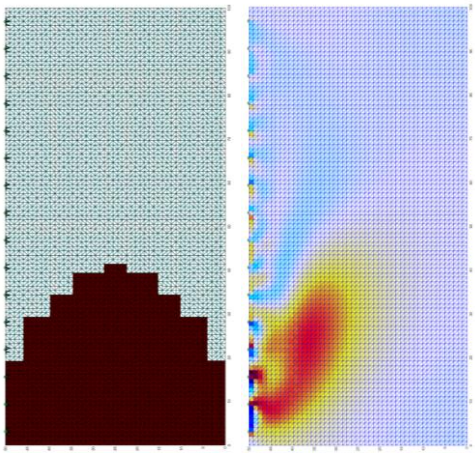

Fig. 2. The model and the numerical reconstruction of the moisture in the damp wall

REFERENCES

[1] Hoła J., Matkowski Z., Schabowicz K., Sikora J., Nita K. and Wójtowicz S., Identification of Moisture Content in Brick Walls by means of Impedance Tomography, *COMPEL*, Vol. 31, Issue 6, pp. 1774–1792, 2012.

[2] Osher S., Santosa F., Level set methods for optimization problems involving geometry and constraints. Frequencies of a two-density inhomogeneous drum, Journal of Computational Physics, vol. 171, pp. 272–288, 2001.

[3] Osher S., Fedkiw R., Level Set Methods and Dynamic Implicit Surfaces, *Springer*, 2003.

[4] Rymarczyk T.: Using electrical impedance tomography to monitoring flood banks, *International Journal of Applied Electromagnetics and Mechanics* 45, pp. 489–494, 2014.

[5] Rymarczyk T., Tchórzewski P., Sikora J.: Topological Approach to Image Reconstruction in Electrical Impedance Tomography, *ADVCOMP 2014*, ISBN: 978-1-61208-354-4, Rome, Italy, August 24–28, pp. 42–45, 2014.

[6] Sokolowski J., Zochowski A., On the topological derivative in shape optimization, *SIAM Journal on Control and Optimization*, Vol. 37, pp. 1251–1272, 1999.

***Authors**: Tomasz Rymarczyk, Przemysław Adamkiewicz, Jakub Szumowski, Karol Duda, Net-art, Związkowa 26, 20-148 Lublin, Poland, e-mail:tomasz@rymarczyk.com, Jan Sikora, Lublin University of Technology, Lublin, Poland*

Andreas Fuchs[1], **Stefan Fuchs**[1, 2], **Christian Reil**[1, 2], **Hans-Peter Schmidt**[1, 2]

[1]OTH, East Bavarian Technical University of Applied Sciences, Amberg, Germany
[2]Center for Applied ICT at OTH Regensburg and Amberg

Coupler Design for Contactless Power and Data Transfer

Abstract. *Coupler design for a combined contactless transfer of power and data is studied. The couplers feed multiple stationary loads such are contactless charging units of electric vehicles at car parks. The physical properties of the inductive couplers are modelled via 3-D FEA. The focus lies on the combined modeling of energy and data transfer. The Influence of power transfer on communication properties is studied in time and frequency domain.*

Keywords: Contactless power and data transfer, FEA coupler design

Introduction

We look into a contactless transfer of power and data for multiple loads. These loads may be charging units of electric vehicles in car parks, where data transfer has to be integrated into the supply of each charging unit [1].

The transfer system consists of power and communication electronics, a common distributing cable to supply each single load and couplers [1, 2]. These couplers consist of a ground mounted part and a counterpart fitted to the car body [3]. Power of some kW is transferred at frequencies of 20kHz up to 140kHz, according to the actual application requirements. Given the power transfer, the design of the communication system has to ensure the required bandwidth and stability despite the massive noise caused by power transfer.

Coupler and System Modelling

Couplers for such an integrated transfer have to transmit power and data simultaneously. To study various design options we carry out quasi static 3-D finite element analysis. We look into single and three-phase couplers [4] with various air gaps. Figure one and two show such couplers with magnetic field lines, that arise from power transfer.

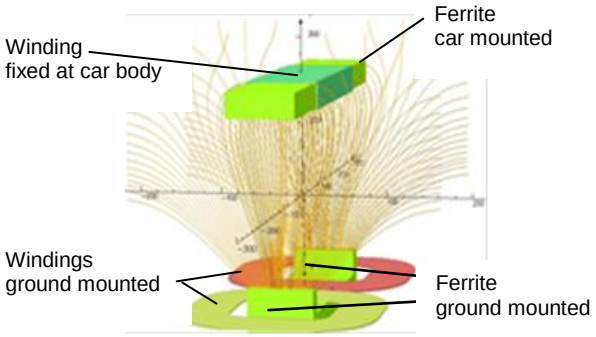

Fig. 1 Magnetic fields lines of a single phase coupler with DD-solenoid layout and large air gap

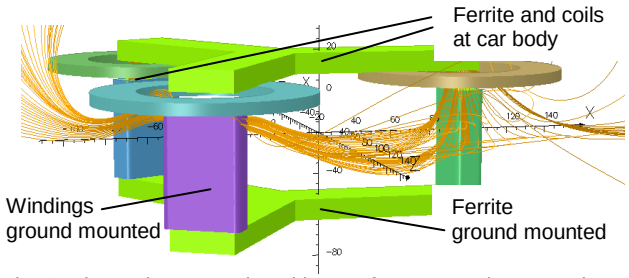

Fig. 2. Three phase coupler with transformer type layout and small air gap. On part of the coupler is shifted towards the other to yield high coupling

For the investigations we couple FEA to lumped parameter calculations. We use a controlled current source to model the power feed and a different source to model the data transfer with the equivalent circuit.

For modelling frequency shift keying (FSK), orthogonal frequency-division multiplexing (OFDM) [5] and similar modulations, we use harmonic analysis at various frequencies, if the system may be considered linear and no saturation effects have to be dealt with. For amplitude shift keying (ASK e.g. on off keying) we use time domain calculations that may also be used for saturation effects.

Design studies

In this first part of our studies we look into differences of using separate windings for data and power transfer compared to the use of a single winding for data and power. Furthermore, we look into eddy current losses and their influence on data and power transfer. We study the wanted damping of power harmonics against the unwanted damping of data signals.

Results

First results show that for a certain parameter range one might use a single coil/winding in the stationary part of the coupler for data and energy transfer without much loss in the signal to noise ratio. Further studies are needed to clarify the influence of eddy current losses, especially the influence of alumina shields that may be attached to the car body in the vicinity of the receiving coil.

REFERENCES

[1] Fuchs A., Schmidt H.-P., Contactless Power and Data Transfer for Variable Distributed Loads, IEEE WPTC 2014 JeJu., Korea Proceedings pp. 186–188.

[2] Moradewicz A.; Kazmierkowski P. “Contactless Energy Transfer System with FPGA Controlled Resonant Converter” IEEE Trans. Industrial Electronics, 57 (2010)No. 9, pp. 3181–3190.

[3] Budhia M., Boys J.T., Covic G. A., Development of a Single-Sided Flux Magnetic Coupler for Electric Vehicle IPT Charging Systems IEEE Trans. Industrial Electronics VOL. 60 (2013), No. 1.

[4] Schmidt H-.P., Fuchs A., Fuchs S. “Simultaneous Contact Less Charging of Multiple Electric Vehicles”, Proceedings IEEE E|DPC-2014, Nuremberg, Germany.

[5] Vogl U., Schmidt H.-P.,“Field Bus System with Contactless Power and Data transfer” Proceedings KommA, Lemgo, 2012. ISBN: 978-3-9814062-2-1.

***Authors**: Andreas Fuchs a.fuchs@oth-aw.de, Stefan Fuchs ste.fuchs@oth-aw.de, Christian ch.reil@oth-aw.de, Hans-Peter Schmidt h.schmidt@oth-aw.de,*
OTH East Bavarian Technical University of Applied Sciences, Kaiser-Wilhelm Ring 23, 92224 Amberg, Germany

N.A. AKWIR, J.C. CHEDJOU, K. KYAMAKYA, S.P.K. VEERANKI, B.O. MUSHAGE

Alpen-Adria Universitaet (AAU)

Traffic Flow Simulation: Comparison Between Finite Difference Method (FDM) and Method of Lines (MOL)

Abstract*. This paper considers the Lighthill and Witham model of a traffic flow scenario under realistic parameter settings. This model is expressed by a partial differential, which is further solved using FDM and MOL. A benchmarking is performed to compare the results from the two methods and, the pros and cons of each method are discussed. Finally, a recommendation is made regarding the application of these methods for complex traffic flow simulation.*

Keywords: Finite difference method, Method of lines, Partial differential equation, traffic flow.

Introduction

Mathematical models are generally used for modelling, simulation control and forecasting of transportation systems or scenarios. These models are generally expressed in the form of nonlinear partial differential equations [1],[2],. However, the numerical solution of the resulting PDEs does face some inherent challenges due to the nonlinear dynamic experienced by concrete traffic scenario. The challenges are specifically concerned with some performance metrics such as accuracy, robustness, and computing speed [3].

Our aim in this paper is to address the challenges cited above using both FDM and MOL. The benchmarking of the two methods will help to depict the advantages and drawbacks of each method. The main importance of performing the benchmarking is to demonstrate that the two methods are complementary since each can efficiently address an unsolved challenge by its counterpart. The paper is organized as follows. Section 2 provides the traffic flow model under consideration. Section 3 § 4 provide a full analytical development of the simulation concepts based on FDM and MOL, respectively. Section 5 is concerned with the presentation of simulation results and benchmarking. Section 5 is devoted to concluding remarks.

PDE Model for traffic flow

$$\frac{\partial k}{\partial t}+\frac{\partial q}{\partial x}=f(x,t) \quad (1)$$

$$q=k.u \quad (2)$$

(1) is the classical one dimensional space Lighthill and Witham for traffic flow simulation. k is the traffic density in a road segment, u is the speed, q is the traffic flow, x is the spatial coordinate and t is the temporal dimension.

FDM Method

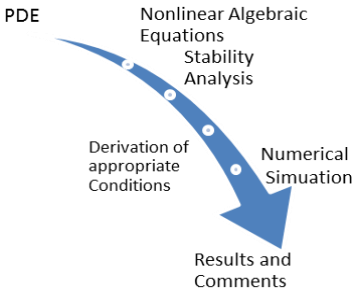

Fig. 1. Full/Complete steps of FDM

MOL Method

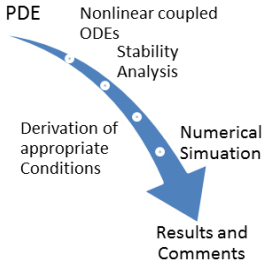

Fig. 1. Full/Complete steps of MOL

Simulation and Benchmarking

Table 1. Benchmarking w.r.t performance criteria

	Derivation of equivalent model	Stability Analysis	Simulation accuracy	Computing speed
FDM	simple	Difficult[1]	Less	High[2]
MOL	Difficult	Simpler[3]	High	Lower[4]

Conclusion

This paper has proposed an in-depth general analytical concept for solving nonlinear PDEs using both FDM and MOL. This concept has further been applied on solving the Lighthill and Witham for traffic flow simulation. The results of the two methods have been compared using specific performance criteria. It has been obtained that the two methods are complementary to each other.

REFERENCES

[1] Work, D.B. ; Bayen, A.M., „Convex Formulations of Air Traffic Flow Optimization Problems," w Proceedings of the IEEE , 2008.

[2] „Bettahar, S. ; Stambouli, A.B. ; Lambert, P. ; Benoit, A.," IEEE Transactions on Image Processing, tom 21, nr 5, pp. 2500–2512, 2012.

[3] M. L. Delle Monache; J.Reilly; S. Samaranayake; W. Krichene, P.Goatin, and A. M. Bayen, „A PDE-ODE Model for a Junction with ramp buffer," Society for Industrial and Applied Mathematics, tom 74, nr 1, pp. 22–39, 2014.

Authors*: N. A. Akwir, AAU, Klagenfurt, nkawir@edu.aau.at*
J.C. Chedjou, AAU, Klagenfurt, jean.chedjou@aau.at
K. Kyamakya, AAU, Klagenfurt, Kyandonghere.kyamakya@aau.at
S.P.K. Veeranki, AAU, klagenfurt, sai.veeranki@edu.aau.at .
B.O. Mushage,AAU, klagenfurt, bamushage@edu.aau.at

1 Only approximate analytical methods exist (e.g.: Cadran etc.)
2 Under converging parameter settings
3 Exact analytical methods exist (e.g.: Global stability, asymptotic stability)
4 Under converging parameter settings

POSTER SESSION 2 (Tuesday 09.06.2015, 14:50 – 16:40)		
Chairman: Goga Cvetkovski gogacvet@feit.ukim.edu.mk Chairman: Przemysław Łopato przemysław.lopato@zut.edu.pl		
	Authors	**Title**
1	Jacek Horiszny	Implementation of the Controlled Switching Algorithm
2	Wojciech Chlewicki, Katarzyna Cichoń-Bańkowska	Increasing the Diagnostic Capabilities of Existing Digital Radiography Systems Using Multilayer Image Reconstruction from Few Projections
3	Tomasz Giżewski, Andrzej Wac-Włodarczyk Ryszard Goleman	Application of the Virtual Identification to Ferromagnetic Materials Defects Classification
4	Arkadiusz Dobrzycki, Stanisław Mikulski	Using of Continuous Wavelet Transform for De-Noising Signals Accompanying Electrical Treeing in Epoxy Resins
5	B.O. Mushage, J.C. Chedjou, K. Kyamakya, A. Nkiediel, S. P. K. Veeranki	Dynamic Optimization and CNN-Based Solving of PDEs And ODEs
6	B.O. Mushage, J.C. Chedjou, K. Kyamakya, A. Nkiediel, S.P.K. Veeranki	Adaptive Control of Chaos Generators via RBF Neural Network and Input-Output Feedback Linearization Sliding Mode Control
7	Stanislaw Osowski, Krzysztof Siwek, Tomasz Grzywacz	Exploration of Data in Differential Electronic Noise
8	Robert Smyk, Maciej Czyżak	Pipelined Computation of Arc Tan Using CORDIC in FPGA
9	Dorota Stachowiak	Finite Element Analysis of the Active Element Displacement in the Giant Magnetostrictive Transducer
10	Wiesław Lyskawinski, Cezary Jedryczka, Dorota Stachowiak	Analysis of 6-pole IPM Synchronous Motor with Tangential Magnets Using Finite Element Method
11	Dominik Kukla, Justyna Szlagowska-Spychalska,	Identification of the Fatigue Cracking of the Aluminide Layers on the Nickel Alloy with the Application of the Optical Method ESPI
12	Ahmad Warda, Hannes Toepfer	Comparison of Figures of Merit of Information Content for Sensor Placement Optimization
13	Larisa Tretiakova	Simulation of Electrostatic Field on the Surfaces of Protective Clothing of Workers
14	Dorota Typańska, Adam Maćkowiak, Krzysztof Sieczkarek	Immunity of Intelligent Installation Model to the Pulsed Electromagnetic Disturbances
15	Rafal M. Wojciechowski, Tomasz Boczkowski, Cezary Jędryczka	Analysis of Axial Flux Permanent Magnet Coreless Motor Using 2D Edge Element Method and Superposition Principle
16	Barbara Szymanik, Mirosław Wołoszyn	Magnetic and Infrared Thermography Methods in Detection of Nonmetallic Landmines
17	Mirosław Wołoszyn, Kazimierz Jakubiuk, Mateusz Flis	Analysis of Distribution of Current Density and Temperature in Busbars
18	Michał Zeńczak	Method of Estimation of Exposure of Natural Environment on 50 Hz Electric and Magnetic Fields in Power System with Distributed and Centralized Generations
19	Kazimierz Adamiak, Maciej Włodarczyk	Electrohydrodynamics of Droplets: Direct versus Level Set Method Formulations
20	Dagmar Faktorová, Mária Pápežová	New Approach in Non-Destructive Testing of Dental Biomaterials by Using Microwaves
21	Krzysztof Budnik, Wojciech Machczyński, Jan Szymenderski	Assessment of D.C Traction Stray Currents Effects on Nearby Pipelines
22	Artur Bugała, Grażyna Frydrychowicz-Jastrzębska	Power Distribution in Photovoltaic Tracking Systems
23	A. Kuvaldin, M. Strupinskiy, N. Khrenkov, M. Fedin, B. Antonov	Parameters Analysis of Linear Inductors for the Heating of Ferromagnetic Steel Pipes
24	A. Kuvaldin, M. Fedin, R. Perov	Development of The Methods for Calculating Electromagnetic Parameters of Coreless Induction Furnaces in the Melting Process of the Lumpy Charge

Jacek HORISZNY

Gdansk University of Technology

Implementation of the Controlled Switching Algorithm

Abstract. *The peak of three-phase transformer's inrush current can reach a value that is several times greater than the rated current. The controlled switching is one of the methods of the inrush current reduction. Two concepts of the controlled switching system have been proposed in the article. Computer simulation has been used to present the functioning of both systems.*

Keywords: inrush current, controlled switching, power transformer.

Introduction

The controlled switching is recently developed method of reducing the transformer's inrush current. This method is based on an independent closing of each circuit breaker pole in the supply circuit, in the properly defined time instants [1, 2]. The information on the residual flux in each core leg is necessary to determine the time instants of the breaker's poles closing. Two general concepts of new implementation of this method have been proposed:

- energization in the case the residual magnetism is created by the last switching off of the transformer,
- energization in the case the residual magnetism is reduced to a specified level.

The first of these concepts will be further called controlled switching with the natural magnetization. The second one will be called controlled switching with the forced magnetization.

Controlled switching with the natural magnetization

In the implementation of this method, the following tasks should be performed:

1) determination of the residual flux in each leg of the transformer,
2) determination of the moments t_1 and t_2 of the breaker's poles closing,
3) generation of the signal for the breaker closing in the first phase circuit (or in two phase circuits, depending on the connection type the winding) at the time t_1,
4) generation of the signal for the breaker closing in the second and third phase circuit (or in the last phase circuit, depending on the connection type of the winding) at the time t_2.

A block diagram of the proposed system of controlled switching with the natural magnetization for a transformer with a delta connected primary winding is shown in Fig. 1.

Determination of the residual fluxes may be accomplished by integrating the voltages at the windings of the transformer during the preceding de-energization.

The moments t_1 and t_2 can be determined basing on the analytical relationship appropriate for the connection type of the transformer primary winding. In order to perform these calculations, the system should include a processor to compute the residual fluxes and the time instants t_1 and t_2.

Controlled switching with the forced magnetization

Implementation of the controlled switching is simpler if the magnetization state of the core is the same at each time when the switching on of the transformer is performed. This can be achieved by the demagnetization of the core, which is intended to bring all of the residual fluxes to zero. This process must be carried out before switching on the transformer, by a suitable demagnetization system. Implementation of this method may be as follows:

1) demagnetization of the core,
2) generation of the closing signal for the breaker in the first phase circuit (or in two phase circuits, depending on the connection type of the winding) at the time t_1,
3) generation of the closing signal for the breaker in the second and third phase circuit (or in the last phase circuit, depending on the connection type of the winding) at the time t_2.

The sequence of closing of the breaker poles is predetermined and fixed in the algorithm. Closing times of the poles are also fixed, and depend on the connection type of the primary winding of the transformer. A block diagram of the proposed system of controlled switching with the forced magnetization for a transformer with a delta connected primary winding is shown in Fig. 2. This is a modification of the system shown in Fig. 1, from which the unnecessary blocks were removed.

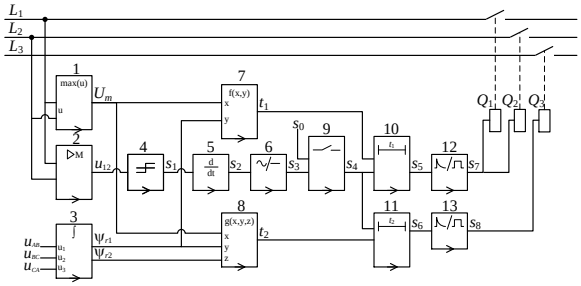

Fig. 1. A block diagram of the controlled switching system with the natural magnetization

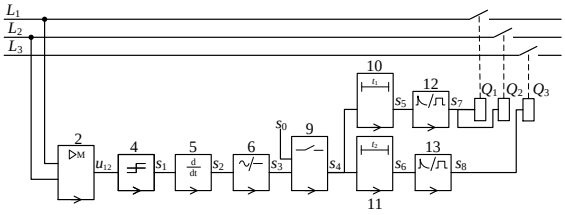

Fig. 2. A block diagram of the controlled switching system with the forced magnetization

Numerical simulations have proved that the systems shown in the drawings properly perform the controlled switching conducted in accordance with the proposed algorithms. The calculated inrush currents were reduced by this method to a level of no-load current of the transformer.

REFERENCES

[1] Brunke J.H., Frolich K.J., Elimination of transformer Inrush Currents by Controlled Switching – Part I, *IEEE Trans. on Power D.*, 16 (2001), No. 2.

[2] Brunke J.H., Frolich K.J., Elimination of transformer Inrush Currents by Controlled Switching – Part II, *IEEE Trans. on Power D.*, 16 (2001), No. 2.

Author: *Jacek Horiszny, Gdansk University of Technology, ul. Narutowicza 11/12, 80-233 Gdansk, Poland, e-mail jachoris@pg.gda.pl*

Wojciech CHLEWICKI, Katarzyna CICHOŃ-BAŃKOWSKA

West Pomeranian University of Technology, Szczecin

Increasing the Diagnostic Capabilities of Existing Digital Radiography Systems Using Multilayer Image Reconstruction from Few Projections

***Abstract**. The potential for increasing the diagnostic capabilities of digital radiography systems in terms of medical screening is described in this work. It is based on limited angle reconstruction from projections taken at different angle, which results in multilayer image. Existing digital radiography systems are supposed to be used so that the cost of upgrade is minimal. The procedure would be cost and time effective contributing to increased number of sufficiently evaluated patients.*

Keywords: digital radiography, limited angle tomography, tomosynthesis.

Introduction

Nowadays, radiological imaging is one of the most common diagnostic techniques used in medical practice. The introduction of digital radiography (DR) was the essential breakthrough. It has contributed to the cost and the radiation dose reduction, and therefore, made DR more popular in health care units.

On the other hand the technologies of three-dimensional imaging have been developed lately, including Cone-Beam Computed Tomography (CBCT) [1]. Yet cost of purchase of the CBCT imaging system, as well as the cost of daily use of such system is much higher than the cost of using DR systems. Therefore, in practice, patients have limited access to three-dimensional computerized tomography.

These factors indicate the need for research on finding middle way solution, such as extending of diagnostic possibilities of existing DR systems which are currently used in medical practice. The goal is to obtain (at least partially) the diagnostic effects comparable to fully three-dimensional computed tomography. This would allow to extend the capacity of diagnostic apparatus already in use, without significant financial cost. Similar solution dedicated to nondestructive testing has been successfully implemented [2] and therefore could be incorporated in medical imaging.

Methods

There are DR systems with motorized source detector systems already existing in the medical practice, their geometry and the projection acquisition scheme is presented in Fig. 1. The aim of that investigation is to propose the extension in the form software programs and the data acquisition procedures. In principle, the solutions is based on tomography with the limited angular range of projections or linear tomography. These two are suitable for implementation in the diagnostic systems already in use [3].

Limited angle reconstruction resulting in multilayer image

This could be achieved through modification of the projection data acquisition procedures and creating additional image reconstruction software, which is able to perform limited angle image reconstruction from projections.

Potential advantages of upgrading DR systems

The growing number of cancer disease cases and demographic change result in higher patients expectations concerning quick and precise diagnosis. The upgrade would contribute to shortening of the waiting time for examinations and reduce the overall cost.

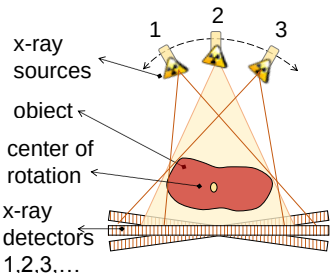

Fig. 1.The geometry of typical motorized DR system in clinical practice.

The digital tomosynthesis (DTS), a variant of the approach proposed here, is a promising tool for screening diseases and lung cancer [3] and mammography [4]. Advantages of DTS compared to one projection radiography has been confirmed clinically [3, 4].

Conclusions

The proposed solution based on the extension of existing DR systems located in health care units seems to be promising, particularly for screening of larger number of patients. It would replace costly 3D tomographic evaluation. The procedure would be cost and time effective contributing to increased number of sufficiently evaluated patients.

REFERENCES

[1] Wang J., Liang Z.R., Lu H.B., Xing L., Recent Development of Low-dose X-ray Cone-beam Computed Tomography, *Curr. Med. Imaging Rev*, 6 (2010), 72–81.

[2] Chlewicki W., Baniukiewicz P., Chady T., Brykalski A., Identification of the position of objects in three dimensions using an extended radiography system, *International Journal of Applied Electromagnetics and Mechanics*, 39 (2012), 167–173.

[3] Galea A., Durran A., Adlan T., Gayb D., Riordan R., Dubbins P. et al., Practical applications of digital tomosynthesis of the chest; *Clin Radiol* 69 (2014) No. 4, 424–430.

[4] Wu T., Stewart A., Stanton M., McCauley T., Phillipsa W, et al., Tomographic mammography using a limited number of low-dose conebeam projection images, *Med Phys* 30 (2003), 365–380.

***Authors:** Wojciech Chlewicki, West Pomeranian University of Technology, Szczecin, address: Sikorskiego 37, 70-313, Szczecin, E-mail: Wojciech.Chlewicki@zut.edu.pl*

Katarzyna Cichoń-Bańkowska, West Pomeranian University of Technology, Szczecin, address: Sikorskiego 37, 70-313, Szczecin, E-mail: Katarzyna.Cichon-Bankowska@zut.edu.pl

Tomasz GIŻEWSKI, Andrzej WAC-WŁODARCZYK Ryszard GOLEMAN

Lublin University of Technology

Application of the Virtual Identification to Ferromagnetic Materials Defects Classification

Abstract. *In the presented work the authors described individually created solution to the nondestructive testing of the materials with branched and lossy nonlinear characteristics and large values of the magnetic permeability. All of the tested details are subject to the nondestructive eddy current test. The difference lies only in the proposed data conditioning. The authors have concentrated their special attention to the selection of the classifying algorithms, the difference between the function class as well as the methods of the identification.*

Keywords: nondestructive testing, virtual instrument, classification, identification.

Introduction

The fundamental principle of the ferromagnetic material nondestructive testing is to determine the eddy currents changes inside the detail as a consequence of the magnetic field intensity as well as the frequency values [1], [2]. Essential here is the observation of the trajectory following either the impedance module or the impedance argument change. Another method belonging to the inductive way of the ferromagnetic objects testing is the one which examines the magnetic hysteresis loop. The observation of the hysteresis loop comprises the acquisition process of the induction changes or the magnetization related to the magnetic field intensity in the frequency domain. In the presented article, the authors present the method of the acquiring and conditions of the differential weigh function discrete image, analogical to the weigh function of the Preisach model, and its gradient images.

Measurement system

The methodology of the experimental research has required the measurement of two quantities: the current value in magnetizing circuit and the inductive voltage in the measuring coil. The research is conducted by the means of the circuit with the possibility of the current measuring in the magnetic circuit as well as the electromotive inductive force in the coil coupled with the magnetizing coil by the tested element (Fig.1). The basic image is the weigh function obtained by means of the unbalanced voltage. The stability conditions of the bridge imply that the unbalanced voltage up equals to zero when the parameters elements are equal in pairs with ferromagnetic elements properties among them. Nonzero value indicates that the properties of the tested detail and the pattern are different.

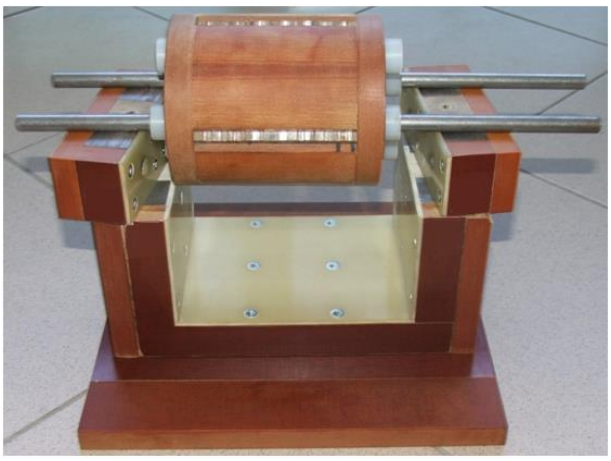

Fig. 1. Device to examination of the cylindrical samples

Experimental results

Analyzing the properties of the weigh function in the α and β domain one can observe two significant properties e.i. the values are always nonnegative and it is always symmetrical to the normal axis of α-β plane, going through the (0,0) point [1]. On the top of that the function does not possess any extremes in the case of the examined cylindrical samples. Only the maximum value can be determined. The individual properties of the density function make it difficult to analyze the data concerning their classification. The above reasons force the alternative solution. As the result of the search the idea of the application differential and the bridge measurement was came in to existence. The result of the quantity comparison alone is not as crucial as the quality comparison. In the range of increase of the input value the extremes can be determined which implies the presence in the weigh function. After the completion of the selected calculation process the Preisach surface was obtained. By means of the analysis of the selected voltage and currents from the measuring circuit, the formation mechanism of the differential surface, including more than one extreme and negative values in the class of density functions values were determined. The multifunction measuring cards and the LabView visual programming environment was applied. The program acquires data from the selected circuit and the density function surface is calculated basing on the classical algorithms. To that aim the authors made application of the density function transformation to the gradient surface. The resulting image has increased the number of differences in the details of the observed defects. The automatic algorithm calculates the extreme values or extreme values of the surface components or the gradient module (and its position) in the field of the density function.

REFERENCES

[1] Giżewski T., Goleman R., Stryczewska H.D, Wac-Włodarczyk A., Nafalski A., Numerical Pattern Identification - Application to Inductive Testing Method with Automatic Classifiers, *IEEE Trans. Magn.*, 40 (2013), No.5, 1789–1792.

[2] Wac-Włodarczyk A., Goleman R., Czerwiński D., Giżewski T., Mathematical models applied in inductive non-destructive testing, J. Magn. Magn. Mater., Elsevier, 320(2008), e1044–e1048 CD.

***Authors**: Tomasz Giżewski, Lublin University of Technology, t.gizewski@pollub.pl*

Andrzej Wac-Włodarczyk, Lublin University of Technology, e-mail: a.wac-wlodarczyk@pollub.pl

Ryszard Goleman, Lublin University of Technology, e-mail: r.goleman@pollub.pl

Arkadiusz DOBRZYCKI, Stanisław MIKULSKI

Poznan University of Technology

Using of Continuous Wavelet Transform for De-noising Signals Accompanying Electrical Treeing in Epoxy Resins

Abstract. *The following paper presents application of methods of noise reduction in acoustic emission signals, accompanying phenomenon electrical treeing of solid dielectric such as epoxy resin, based on time-frequency signal analysis. Estimation method was applied signal described by Donoho and Johnson.*

Keywords: signal filtering, wavelet transform, CWT.

Introduction

Major factor in solid dielectrics, used as insulation for high-voltage devices, are partial discharges (PD). They are present on the surfaces of dielectrics or in their structures, causing deterioration of electrical insulation properties. With PD occurring in solid dielectrics is often linked to the electrical treeing process involving the formation of a conductive or semi-conductive dielectric channels, taking the shape of a tree. Tubular discharge causes the further development of the tree, leading eventually to low-resistance short circuit.

Measurement stand and analysis

To study process of electrical treeing was used acoustic emission method (AE), involving the measurement, acquisition and analysis of acoustic signal accompanaying the process.

A characteristic feature of studied phenomenon are small,comparable to noise level, amplitudes of vibrations. Therefore, prior to submission to the recorded signals analysis it is required to reduce the noise. The complexity of the process of formation of the acoustic wave, non-deterministic nature of its parameters and the presence of strong interference mean that it becomes necessary to use modern methods of signal processing. The article presents the filtration method with the use of wavelet analysis.

Figure 1 shows a part of recorded signal and its amplitude spectrum.

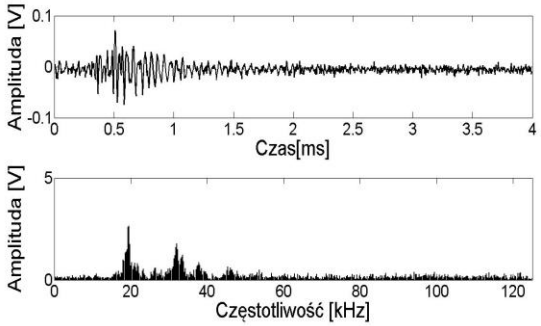

Fig. 1. a) Recorded signal, b) Signal Spectrum

EA signals de-noising by thresholding

Noise reduction can be obtained by filtration method described by D. L. Donoho and I. M. Johnstone in [3, 4]. The solution involves correction of each wavelet coefficients by means of a nonlinear function. The value of this function depends on the value of wavelet coefficients.

The authors propose two variants of the method of thresholding wavelet coefficients, so. soft estimation and hard estimation. Estimation hard is described by relationship:

$$\theta(y) = \begin{cases} y & dla \quad |y| > thr \\ 0 & dla \quad |y| \le thr \end{cases} \tag{1}$$

where : θ – estimated value of coefficient, y – value of noised signal coefficient, thr – threshold value.

Figure 2 shows signal from figure 1 after noise reduction.

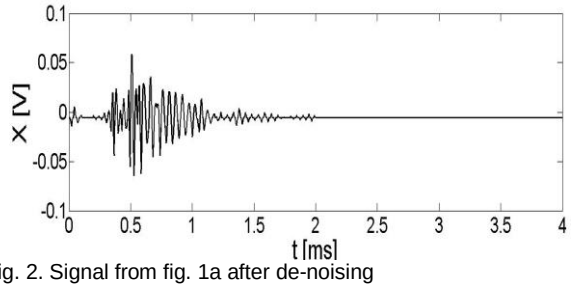

Fig. 2. Signal from fig. 1a after de-noising

Summary

This paper presents an application of wavelet transform in the reduction of noise generated during the registration of acoustic emission signals accompanying PD in solid dielectrics, especially epoxy resins. Presented charts support use of the signal de-noising method, described in the article.

REFERENCES

[1] Dobrzycki A.: Metoda emisji akustycznej w analizie i badaniu procesu drzewienia elektrycznego dielektryków stałych w silnym polu elektrycznym, *Rozprawa doktorska przedłożona Radzie Wydział Elektrycznego Politechniki Poznańskiej*, Poznań 2008

[2] Dobrzycki A., Opydo W. Stanowisko do badania sygnałów emisji akustycznej towarzyszących destrukcji polimetakrylanu metylu w silnym polu elektrycznym, *Zeszyty naukowe Politechniki Poznańskiej seria Elektryka, nr 50, Poznań 2006*, 199-208

[3] Donoho D. L., De-noising by soft-thresholding, *IEEE Transactions on information theory Vol. 41 No. 3*, May 1995

[4] Donoho D. L., Johnstone I. M., Ideal spatial adaption via wavelet shifinkage, Biometrika vol. 81, 1994, 425–455

[5] Zieliński T. P., Cyfrowe przetwarzanie sygnałów. Od teorii do zastosowań, WKŁ, 2006

[6] Mallat S. G., A theory for multiresolution signal decomposition: the wavelet representation, *IEEE Transactions on Pattern Analysis and Machnine Intelligence Vol. 11 No. 7*, July, 1989, 674-693

***Authors**: Arkadiusz Dobrzycki, Poznan Univercity of technology, Pl. Marii Skłodowskej-Curii 5 60-965 Poznań, Arkadiusz.dobrzycki@put.poznan.pl, Stanisław Mikulski, Poznan Univercity of technology, Pl. Marii Skłodowskej-Curii 5 60-965 Poznań, stanislaw.mikulski@put.poznan.pl,*

B.O. MUSHAGE, J.C. CHEDJOU, K. KYAMAKYA, A. NKIEDIEL and S. P. K. VEERANKI

Alpen-Adria Universität

Dynamic Optimization and CNN-Based Solving of PDEs And ODEs

Abstract*. In this paper, Dynamic Nonlinear Least Squares (DNLS) is applied for CNN template estimation. The CNN is designed such that it can simulate a system for which the model is unknown or uncertain but for which some experimental data is available. The Trust Region Algorithm for Nonlinear Least Square optimization problem is used for the CNN's parameters optimisation. In order to prove the effectiveness of the proposed method, illustrative examples of ODEs and PDEs models are considered.*

Keywords: State Controlled Cellular Neural Networks; Partial Differential Equations; Ordinary Differential Equations; Dynamic Nonlinear Least Squares.

Introduction

The numerical solving of nonlinear ODEs and PDEs does generally face some inherent challenges related to accuracy, robustness and computing time, just to name a few. The CNN concept is introduced in this paper in order to address the above cited challenges. The art consists of deriving for given ODEs and/or PDEs the corresponding parameter settings of the CNN model, which are called CNN-templates. The determination of the templates is the most important step of CNN's applications. In practice, it happens that parameters of a physical system (e.g. diffusivity factor of a heat transfer system, frequency of a pendulum, etc.) are completely unknowns or uncertain such that analytical derivation of the CNN template is not possible.

In this paper, we use the Dynamic Nonlinear Least Squares (DNLS) for SC-CNN template estimation of unknown system's model using some experimental data. The Trust Region Algorithm for Nonlinear Least Square optimization problem is used for the CNN's parameters optimisation. In order to illustrate the effectiveness of the method, illustrative examples of ODEs and PDEs models are considered.

Methodology

For the solution of differential equations based on CNN, the State-Controlled CNN (SC-CNN) is the most used. The dynamics of a SC-CNN is given by [1, 3]:

$$\dot{x}_i = -x_i + \sum_{j=1}^{M}\left[\hat{A}_{ij}\, x_j + \tilde{A}_{ij}\,(x_i, x_j) + A_{ij}\, y_j + B_{ij}\, u_j\right] + I_i \quad (1)$$

where the coefficient $\hat{A}_{ij}$, A_{ij} and B_{ij} are the unknown self-feedback template, feedback template and control template, respectively. $\tilde{A}_{ij}\,(x_i, x_j)$ is the unknown nonlinear template for the nonlinear terms of the ODE. The variables x_j, y_j, u_j and I_i are the state variables, the output variables, the local inputs and the bias, respectively.

Assuming all the SC-CNN templates are space and time invariant, let's rewrite the SC-CNN model with its initial condition as follows:

$$\begin{cases} \dot{x} = F(t, x(t), p) \\ x(0) = x_0 \end{cases} \quad (2)$$

where p is a $M^2 \times 1$ vector of unknown SC-CNN templates, $x \in \mathbb{R}^M$, $F(.)\colon \mathbb{R}^M \to \mathbb{R}^M$.

For the estimation of the CNN parameters, the system's states are measured with a sampling time T. Setting the initial value of the vector p randomly, we apply a numerical integration technique (e.g. fourth-order Runge Kutta) in which the step size is set equal to the sampling time of the measured experimental data. Therefore, for each integration time t_i, the solution $x^{sim}(t_i, p)$ is used along with its corresponding measured value to construct the following objective function:

$$S(p) = \sum_{i=0}^{n}\left(x^{sim}(t_i, p) - x^{meas}(t_i)\right)^2 \quad (3)$$

This objective function is then input into an optimization algorithm to update parameter p estimates. The unconstrained nonlinear objective function is used in a Nonlinear Least Squares problem. In order to solve this problem, we use the trust region algorithm, which is known to be reliable and robust, and to have strong convergence properties [2]. The output of this algorithm is the vector p of approximate templates of the SC-CNN simulating the dynamics of the system under investigation.

Results

In order to prove its effectiveness for PDEs solution, the proposed approach is applied for the estimation of the parameters of CNN simulating a heat transfer system for which the diffusivity factor is unknown. For CNN-based ODEs solution, a home heating example with five boundary surfaces is considered. For this system, we produce a corresponding CNN model despite the unknown five insulation constants for the five boundary surfaces. For the two examples, the CNNs provide a very accurate simulation of the studied systems.

REFERENCES

[1] J. Chedjou, K. Kyamakya, "A Novel General and Robust Method Based on NAOP for Solving Nonlinear Ordinary Differential Equations and Partial Differential Equations by Cellular Neural Networks," *Journal of Dynamics Systems, Measurements, and Control,* vol. 135, no. 3, p. 11, 2013.

[2] Y.-X. Yuan, "Nonlinear Optimization: Trust Region Algorithms," Chinese Academy of Sciences, 1999.

[3] J.C. Chedjou, and K. Kyamakya, "A universal concept based on cellular neural networks for ultra-fast and flexible solving of differential equations", *IEEE Transactions on Neural Networks and Learning Systems*, 2014 (In press).

Authors*: B.O. Mushage, Alpen-Adria Universität, Klagenfurt, bamushage@edu.aau.at; J.C. Chedjou, jean.chedjou@aau.at, Alpen-Adria Universität, Klagenfurt, jean.chedjou@aau.at; K. Kyamakya, Alpen-Adria Universität, Klagenfurt, kyandoghere.kyamakya@gmail.com; A. Nkiediel, Alpen-Adria Universität, Klagenfurt, alainnkie2013@yahoo.fr; S.P.K. Veeranki, Alpen-Adria Universität, Klagenfurt,* sai.veeranki@gmail.com

B.O. MUSHAGE, J.C. CHEDJOU, K. KYAMAKYA, A. NKIEDIEL and S.P.K. VEERANKI

Alpen-Adria Universität

Adaptive Control of Chaos Generators via RBF Neural Network and Input-Output Feedback Linearization Sliding Mode Control

Abstract. *This paper proposes an adaptive robust controller for chaos generators subject to external disturbances and unknown changes in the system's parameter settings. As proof of concept of the developed approach, a benchmarking is performed using a Lur'e like system, which is a classical prototype of discontinuous nonlinear system.*

Keywords: Chaos adaptive control; RBF Neural Network; Input-Output Feedback Linearization Sliding Mode Control, Lur'e like System.

Introduction

The control of a chaotic system generally consists in transforming chaotic oscillations into periodic ones and vice versa. This is an important problem, which leads to multiple potential applications, e.g. laser and chemical technologies, telecommunications, medicine, etc. In most of these physical applications, the system under control is subject to external perturbations with unknown exact values of its parameters. Therefore adaptive and disturbance rejection type-controllers are needed to guarantee their effectiveness.

This paper proposes a simple robust adaptive controller for a class of affine nonlinear chaotic systems that can be used for non-chaotic systems as well.

Methodology

We consider the class of linearizable *n*-th order uncertain nonlinear dynamic systems with external disturbance:

$$\dot{x} = \boldsymbol{f}(\boldsymbol{x}) + \boldsymbol{g}(\boldsymbol{x})u + d(t) \tag{1}$$

$$y = h(\boldsymbol{x}) \tag{2}$$

where $\boldsymbol{x} \in \mathbb{R}^n$ is the state vector, $u \in \mathbb{R}$ is the control signal, $y \in \mathbb{R}$ is the output of the system, $d(t) \leq D$ is the bounded disturbance, $g(\boldsymbol{x}) \neq 0: \mathbb{R}^n \to \mathbb{R}^n$ and $f(\boldsymbol{x}): \mathbb{R}^n \to \mathbb{R}^n$ is the unknown nonlinear function.

For the considered class of systems, the output y is connected indirectly to the input u such that it is difficult to design the controller. As $f(\boldsymbol{x})$ and $d(t)$ are assumed to be infinitely differentiable, we apply Input-Output feedback linearization to derive the equation denoting the visible relation between the output y and the input u:

$$y^{(r)} = F(\boldsymbol{x}) + G(\boldsymbol{x})u + \check{d}(t) \tag{3}$$

where $F(\boldsymbol{x})$ is an unknown nonlinear function, $\check{d}(t) \leq D$ is a summation of disturbance terms and their derivatives, $G(\boldsymbol{x}) = 1$, and r is the relative degree of the system, which is equal to n for the class of considered systems.

The control objective is to force the output y to track in finite time a desired trajectory y_d despite external perturbations and parameter changes. Therefore we apply the Sliding Mode Control strategy, which suites the best to the design of the controller that will ensure the achievement of this objective [1].

Let's denote $e = y_d - y$ the tracking error and select the sliding function as:

$$s = \left(\frac{d}{dt} + c\right)^{r-1} \cdot e \tag{4}$$

with $c > 0$.

We design the controller as:

$$u = v - \hat{F}(\boldsymbol{x}) + \eta \,\mathrm{sign}(s) \tag{5}$$

where $\eta \geq D$, $\hat{F}(\boldsymbol{x})$ is an approximation of the unknown function $F(\boldsymbol{x})$, and v is an auxiliary controller designed as:

$$v = y_d^{(r)} + k_{r-1}e^{(r-1)} + \cdots + k_2\ddot{e} + k_1\dot{e} \tag{6}$$

Based on the universal approximation theorem, a RBF Network is used to approximate $F(x)$ as follows [1]:

$$\widehat{\boldsymbol{F}}(\boldsymbol{x}) = \widehat{\boldsymbol{W}}^T \boldsymbol{h}(\boldsymbol{x}) \tag{7}$$

The network's input $\boldsymbol{x}$, applied to the Gaussian function $\boldsymbol{h(x)}$ is selected as $\boldsymbol{x} = \left[e\ \dot{e}\ \ldots\ e^{(r-1)}\right]$. Based on the Lyapunov approach, its update law is derived as:

$$\frac{d}{dt}\widehat{\boldsymbol{W}} = -\frac{1}{\gamma} s \cdot h(\boldsymbol{x}) \tag{8}$$

The corresponding Lyapunov function is defined as

$$L = \frac{1}{2}s^2 + \frac{1}{2}\gamma \widetilde{\boldsymbol{W}}^T \widetilde{\boldsymbol{W}} \tag{9}$$

where $\gamma > 0$ is a learning rate and $\widetilde{\boldsymbol{W}} = \boldsymbol{W} - \widehat{\boldsymbol{W}}$ is the error on the Network weights estimation.

In order to avoid chattering effects that maybe caused by the controller given in (5), we replace the discontinuous signum function by a saturation function.

Results

By applying the developed controller to the Lur'e like system [2], we have demonstrated through Matlab simulation that it efficiently forces the system's output to track the desired trajectory, which may be a limit cycle or a chaotic orbit. The new controller is proved to provide better results compared to the adaptive controller from [2].

REFERENCES

[1] J. Liu und X. Wang, Advanced Sliding Mode Control for Mechanical Systems, Berlin: Springer-Verlag, 2012.

[2] M. Feki, „An Adaptive feedback control of linearizable chaotic systems," *Chaos, Solitons and Fractals,* Bd. 15, pp. 883–890, 2003.

***Authors**: B.O. Mushage, Alpen-Adria Universtät, Klagenfurt, bamushage@edu.aau.at; J.C. Chedjou, Alpen-Adria Universtät, Klagenfurt, jean.chedjou@aau.at; K. Kyamakya, Alpen-Adria Universtät, Klagenfurt, kyandoghere.kyamakya@gmail.com; A. Nkiediel, Alpen-Adria Universtät, Klagenfurt, alainnkie2013@yahoo.fr; S.P.K. Veeranki, Alpen-Adria Universtät, Klagenfurt, sai.veeranki@gmail.com*

Stanislaw OSOWSKI[1,2], Krzysztof SIWEK[1], Tomasz GRZYWACZ[1]

Warsaw University of Technology (1), Military University of Technology (2)

Exploration of Data in Differential Electronic Nose

Abstract. *The paper is concerned with exploration of differential sensor signals in electronic nose. The differential electronic nose is a special type of electronic noses applying double sensor matrices and exploiting only the differential signal. The paper will study its properties in dynamic measurement of the aroma of 11 brands of cigarettes. The most important task is its sensitivity to the noise corrupting the measurement. We will compare the performance of two classifier systems applied in the nose: the support vector machine and random forest of decision trees.*

Keywords: differential nose, support vector machine, random forest, noisy measurement.

Introduction

The electronic noses applying the semiconductor sensors are very popular now in recognition of the aroma. This paper will present its differential version, which is applicable in on-line dynamic measurements of the processes. We present its application to the recognition of different brands of cigarettes using two types of classifiers: the support vector machine (SVM) of Gaussian kernel [1] and random forest (RF) of decision trees [2]. The important point in this problem is sensitivity of the solution to the noise disturbing the sensor signals and the number of used sensors.

Differential electronic nose

The differential electronic nose (D-nose) was proposed in [3] as a novel solution to the problem of on-line dynamic measurements. The system contains two identical sensor arrays: the reference array measuring the environmental conditions and the measurement array reacting on the odor produced by the investigated material. Only differential signals are stored and processed in further stages.

In the case of identical odor samples the output signal values of this differential amplifier are close to zero. Observe that at the same measuring conditions of both arrays the differential signal will greatly reduce the common distortion effects, that may arise due to the changing temperature or pressure.

The differential signal produced by both sensor arrays converted to the digital representation is next processed in computer in order to recognize the patterns represented by the sensor signals.

The D-nose in experiments applied 12 Figaro sensors installed in reference and measurement chambers. They include: 2xTGS2600-B00, 2xTGS2602-C00, TGS2610-C00, TGS2610-D00, TGS2611-C00, TGS2611-E00, 2xTGS2612-D00, 2xTGS2620-C00. Hence the dimension of the vector input **x** is also twelve.

Investigated materials

The D-nose was applied here to recognize 11 brands of cigarettes on the basis of sensor signals of D-nose measured on-line in a dynamic state. The names and producers of the cigarettes and notation of their classes, which will be used in description of results are as following: Chesterfield Blue (EU) – C1, Chesterfield Red (EU) – C2, Classic Red (Russia) – C3, Fest (Ukraine) – C4, LD Blue (EU) – C5, LD Red (EU) – C6, LD Silver (EU) – C7, Magnat (Ukraine) – C8, Viceroy Blue (EU) – C9, Viceroy Blue (Ukraine) – C10, Viceroy Red (Ukraine) – C11.

In contrast to the classical electronic nose the measurements in D-nose are made on-line in dynamic mode. It means that we do not need wait until the steady state of the sensor signal and there is no need for the baseline estimation. The recognition process of the classes will be done on the basis of transient signals of the sensors. 200 measured samples registered every half second have been acquired for each class of cigarettes. The time varying trajectory of this 12-dimensional measurement vector formed from the differential signals and mapped on 3-dimensional system using principal component analysis (PCA) is presented in Fig. 1.

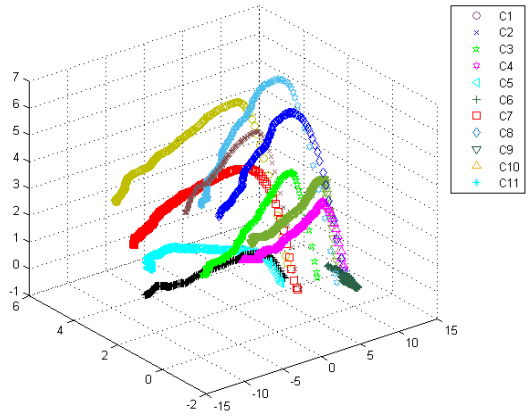

Fig. 1 Trajectory of the differential signals of D-nose mapped through PCA in 3-D coordinate system

Results of recognition

The main task of investigation is recognition of cigarette classes on the basis of the measured signals of D-nose. We have employed and compared two most efficient classifiers: support vector machine and random forest of decision trees. Using the originally measured signals both classifiers were able to recognize all classes in an excellent way (100% accuracy). Further investigations were performed in two study directions: the sensitivity of these classifiers to the noise corrupting sensor signals and the influence of the number of sensors in recognition accuracy. In this analysis we have corrupted the original signals by the random noise of normal and uniform distributions. The performed experiments have shown higher resistance of SVM to the noise. The next task was to find how many differential sensors are needed for recognition of brand cigarettes with an acceptable accuracy. This time the sensors were sequentially removed from the input vector. The results have shown that the original number of sensors can be reduced from 12 to only 5, providing acceptable accuracy of recognition for the original data. Better performance has been observed once again for SVM, used as the final recognition and classification tool.

REFERENCES

[1] Schölkopf, B., Smola, A. Learning with kernels. *MIT Press*,2002

[2] Breiman L, Random Forest, *Machine Learning*, 45 (2001), 5-32.

[3] Brudzewski K., Osowski S., Golembiecka A., Differential electronic nose and Support Vector Machine for fast recognition of tobacco, *Exp. Syst. Appl.*, 39 (2012), 9886-9891.

***Authors**: Stanislaw Osowski, Warsaw University of Technology and Military University of Technology, E-mail: sto@iem.pw.edu.pl, Krzysztof Siwek, Tomasz Grzywacz, Warsaw University of Technology, e-mail: ksiwek@iem.pw.edu.pl*

Pipelined Computation of Arc Tan Using CORDIC in FPGA

Abstract. *The paper presents the pipelined computation of the arc tan function using the modified CORDIC algorithm. The fixed point arithmetic with 17-bit length with 3-bit fractional part is used. Six CORDIC stages have been used to limit the maximum absolute error to less than 1 degree. The algorithm determines max and min values of operands and computes arc tan in the first quadrant with a final successive corrections for the remaining quadrants. Also an FPGA dedicated architecture of the circuit of the arc tan calculator is shown.*

Keywords: arc tan, CORDIC, FPGA.

Introduction

The computation of arctan function has important applications for estimation the phase angle in electrical circuits and signal processing. The computation of arc tan can be performed in software using standard mathematical library or customized hardware [1]. However, such approach can not fulfil the requirements of real-time digital signal processing with regard to the calculation speed or small pipelining rate. This class of applications imposes additional restrictions on the type of arithmetic used, word size and the kind of performed operations. The other aspect is the accuracy of the result. There exist solutions based on series expansions [2] but usually the number of required terms is too high. There are also algorithms that use the rational approximations, but they require general division that may be cumbersome in hardware. The alternative are methods based on the table look-up. This approach is viable if the delay of the look-up table is smaller than the required pipelining rate. This can be fulfilled only by small look-up table, where the address is smaller than 10-bits. The other approach represent CORDIC algorithms [3]. The arc tan is obtained in a natural manner in the CORDIC algorithm by adding rotation angles in individual iterations. When using CORDIC the crucial issues are the number of stages and the maximum error. These two factors are closely coupled.

In this paper we present a FPGA-dedicated CORDIC architecture for arc tan computation using 6 stages and the fixed point real arithmetic. The angle error does not exceed 1 degree.

Arctan computation using CORDIC

The arc tan is initially computed for the interval [0 - π/4] in the first quadrant. The coordinates x, y may have various signs. The quadrant is identified using the pair of signs. This information is used to introduce the angle correction in the final stage of the computation. In order to limit the angle to [0 - π/4] we determine $P=max(|x|,|y|)$ and, $Q=min(|x|,|y|)$. Further, x_i is identified with P and y_i with Q. The CORDIC formulas have the following form [3]:

(1a) $$x_{i+1} = x_i + y_i\delta_i$$

(1b) $$y_{i+1} = y_i - x_i\delta_i$$

(1c) $$z_{i+1} = z_i + \arctan(\delta_i)$$

and $\delta_i = \pm 0.5^i$, i=0, 1, 2, 3...,n.

The sign of δ_i depends on the sign of y. If y<0 then δ_i <0 else y>0 then δ_i >0. The sign of δ_i is selected in such a way so that the expression $-x_i\ \delta_i$ had the opposite sign with respect to y_i. This allows to reduce y_i in every step.

In the proposed architecture (Fig. 1) P and Q are determined using subtraction x-y and the sign of the sum is used to select P and Q with MUX1 and MUX2. In the second stage the operations as in (1a) and (1b) are performed. The output words of MUX1 and MUX2 are extended to 17-bit U2 form, where three LSB bits are used as fractional parts. The subsequent stages perform operations as in (1a) and (1b). The angle computation, z_i is performed by ROM1 using information on consecutive signs of y_i. The ROM2 performs the correction respectively to the current quadrant.

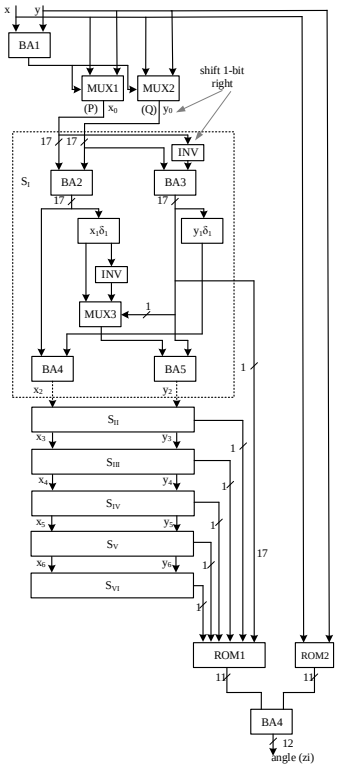

Fig. 1. CORDIC architecture for arctan computation

REFERENCES

[1] Xilinx, "LogiCORE IP CORDIC v4.0. Product specification." Xilinx, March 2011

[2] Abramowitz M., Stegun A., Handbook of mathematical functions, *Dover*, 1972

[3] Meher P., Valls J.; Juang T, Maharatna K., 50 Years of CORDIC: Algorithms, Architectures and Applications". *IEEE Trans. on Circuits & Systems-I: Regular Papers*, No. 56 , 1893–1907.

***Authors**: Maciej Czyżak[1], Robert Smyk[2], Gdansk University of Technology, G.Narutowicza 11/12, 80-233 Gdansk, e-mail: maciej.czyzak@pg.gda.pl[1], robert.smyk@pg.gda.pl[2]*

Dorota STACHOWIAK

Poznan University of Technology

Finite Element Analysis of the Active Element Displacement in the Giant Magnetostrictive Transducer

Abstract. *The paper presents a method to determine the displacement of the active element in the giant magnetostrictive transducer. In the proposed model the coupling of magnetic and mechanical field has been taken into account. To determine the distribution of the magnetic and the mechanical fields the finite element method was used. Characteristics of the displacement of the active element in the transducer as a function of the supply current were calculated and measured. The obtained results of simulations and their comparison with the measurements show that the applied method is sufficiently accurate.*

Keywords: magnetostriction, Terfenol-D rod, giant magnetostrictive transducer, finite element analysis.

Introduction

The Giant Magnetostrictive Transducers (GMT) are used in many fields such as flow control (like pumps, valves), precision positioning system, active noise and vibration control as well as sonar systems [1]. The typical GMT consists of active material such as Terfenol-D or Galfenol. Terfenol-D has the saturation magnetostriction λ_s of approximately 2000 ppm (parts per million, 10^{-6}). The magnetostriction coefficient λ is defined as the $\Delta l/l_o$, where l_o is initial length, and Δl is the resulting strain.

In this paper GMT with the active element made of Terfenol-D has been investigated. The displacement of the active element in GMT has been calculated by using the finite element method (FEM).

Magneto-mechanical coupling

In a magnetostrictive materials the strain $\boldsymbol{\varepsilon}$ and the magnetic flux density $\boldsymbol{B}$ are functions of the stress $\boldsymbol{\sigma}$ and the magnetic field intensity $\boldsymbol{H}$, i.e. $\boldsymbol{\varepsilon} = \boldsymbol{\varepsilon}(\boldsymbol{\sigma},\boldsymbol{H})$, $\boldsymbol{B}=(\boldsymbol{\sigma},\boldsymbol{H})$.The total strain $\boldsymbol{\varepsilon}$ is the sum of the mechanical strain $\boldsymbol{\varepsilon}_{mech}$ and the magnetostrictive strain (which corresponds to a relative elongation $\boldsymbol{\lambda}$). The mechanical strain can be described by the Hooke's law, i.e. $\boldsymbol{\varepsilon}_{mech} = \boldsymbol{\sigma}/\boldsymbol{E}$ where $\boldsymbol{E}$ is the matrix of elasticity of the material. Assuming that the prestress is sufficiently large, $\boldsymbol{\lambda}$ can be approximately represented as a function of the magnetization $\boldsymbol{M}$ (1a) [2]. Then the stress vector $\boldsymbol{\sigma}$ can be calculated according to the equation (1b).

$$(1)\ (a)\quad \boldsymbol{\lambda} = \frac{3}{2}\lambda_S\left(\frac{\boldsymbol{M}}{M_S}\right)^2,\quad (b)\quad \boldsymbol{\sigma} = \boldsymbol{E}\left(\boldsymbol{\varepsilon} - \frac{3}{2}\lambda_S\left(\frac{\boldsymbol{M}}{M_S}\right)^2\right)$$

where $\boldsymbol{M_s}$ is the saturation magnetization.

The relationship between the strain and the displacement $\boldsymbol{u}$ can be expressed as, $\boldsymbol{\varepsilon} = \boldsymbol{D}\boldsymbol{u}$, where $\boldsymbol{D}$ is the strain-displacement (symmetric-gradient) operator.

The nonlinear magnetostrictive model has been implemented in the commercial finite element package. More details about developed magneto-mechanical model will be given in the extended version of the paper.

Selected results and conclusions

In order to validate proposed magneto-mechanical model the prototype of GMT has been designed (Fig. 1a). The active element of the transducer (Terfenol-D rod) is placed within the solenoid coil. The important role in operation of GMT is played by the external mechanical prestress of active material [3] therefore the GMT is equipped with the preload mechanism (Fig. 2). Taking advantage of the geometrical structure of the prototype the computations are performed in an axial-symmetric domain with cylindrical coordinates (r, z, ϑ) - see Fig. 1b. In the simulations it has been assumed that GMT is supplied from DC power source.

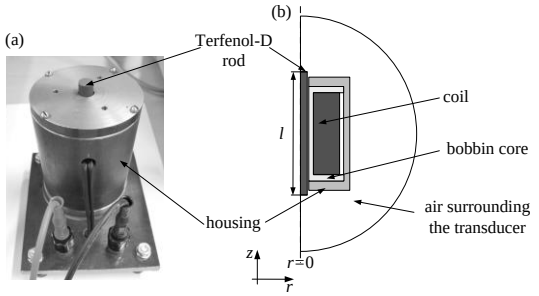

Fig. 1. (a) The prototype GMT for laboratory measurements and (b) geometry of the transducer used in this study

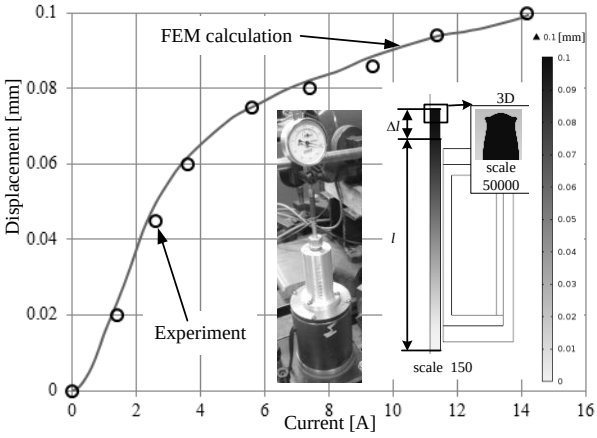

Fig. 2. The output displacement of GMT versus supply current

The displacement of the Terfenol-D rod vs. supply current under compressive prestress 8 MPa has been shown in Figure 2. Additionally the changes of diameter at end of the rod have been illustrated. The distortion have been occurred due to nonuniformity distribution of magnetic and stress fields in the end of the rod.

Displacement characteristics of the active element in GMT as a function of supply current were calculated and measured. It can be noticed that the simulation data are in a good agreement with the experimental results. More detailed results and conclusions will be given in the full version of the paper.

REFERENCES

[1] Engdahl G., Handbook of giant magnetostrictive materials. San Diego, USA: *Academic Press*; 2000.

[2] Calkins F.T., Smith R.C., Flatau A.B.; An Energy-Based Hysteresis Model for Magnetostrictive Transducers. *IEEE Trans. on Magnetic*, Vol. 36. No. 2, 2000, 429–439.

[3] Stachowiak D, The influence of magnetic bias and prestress on magnetostriction characteristics of a giant magnetostrictive actuator, *Przegląd Elektrotechniczny*, R. 89 No 4/2013, 233-236.

Author: *Dorota Stachowiak, Poznan University of Technology, Piotrowo 3a, 60-965 Poznań, Poland, E-mail: Dorota.Stachowiak@put.poznan.pl*

Wiesław LYSKAWINSKI, Cezary JEDRYCZKA, Dorota STACHOWIAK

Poznan University of Technology

Analysis of 6-pole IPM Synchronous Motor with Tangential Magnets Using Finite Element Method

Abstract*. The paper deals with the analysis of the 6 pole interior permanent magnet (IPM) synchronous motor with tangential magnets. To determine the magnetic field distribution in the considered motor the finite element method (FEM) has been applied. Simulations were performed for different positions of the magnets on the chords of the rotor package. The goal of performed studies was minimization of the magnetic flux leakage (understood as the flux between poles not crossing the air-gap) with respect to the high values of the analyzed functional parameters of the considered motor.*

Keywords: synchronous motor with tangential magnets, finite element analysis, magnetic bridge.

Introduction

Global trends in energy savings as well as the development of power electronics and manufacturing technology of the permanent magnets have led to dissemination of a permanent magnet synchronous motors (PMSM). The PMSM offers the highest power density among others types of the electrical machines. In order to achieve highest value of effective flux of PM the structures of the rotors that minimize the flux leakage are searched for. In the IPM synchronous machines the minimization of flux leakage is achieved by proper design of magnetic barriers between poles that allows for improvement of the functional parameters of the machine [1, 2].

In this paper, the authors focused on the analysis of influence of radial placement of the tangential magnets on the functional parameters of 6-pole IPM synchronous motor.

FE Model of IPM synchronous motor with tangential magnets

The field model of 6-pole IPM synchronous motor with tangential magnets has been elaborated in the professional FEM package **–** Maxwell. Due to the symmetry of the magnetic circuit of the studied motor (Fig. 2) the model was developed for the one pole pitch of the machine.

The model has been suited to determine: the magnetic field distribution, the distribution of the radial component of the magnetic flux density in the air-gap of the machine, the cogging torque characteristic, back emf waveforms at no load state, the torque vs. stator current i_{ph} and the load angle α characteristics as well as the torque ripple factor. The major dimensions of the magnetic circuit, sizes and arrangement of permanent magnets and the shape of the magnetic areas between poles (magnetic barriers) have been parameterized in order to enable optimization of the rotor structure. The large number of simulations has been performed for different values of discussed parameters. While analyzing the results it has been found that shape of magnetic areas between magnets has significant impact on various parameters of the machine. Here, to illustrate discussed impact, the results for the IPM synchronous motor with 3 different rotors have been presented. The rotors with: magnets placed close to the air-gap **–** M1 (Fig. 1a), longest magnetic barrier, marked as M2 (Fig. 1b) and magnets placed close to the shaft **–** M3 (Fig. 1c), have been investigated.

In order to enable comparative analysis between studied motors the permanent magnet size as well as the air-gap length, and stator shape have been kept unchanged. Also the winding layout and number of turns in the stator slots have been the same.

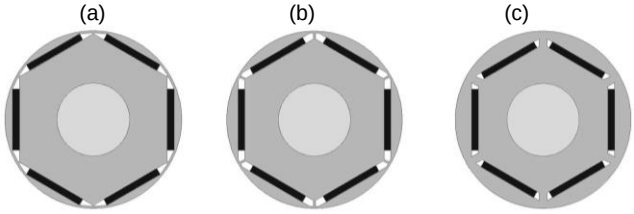

Fig.1. Structures of considered rotors: a) M1; b) M2; c) M3

The selected results and conclusions

The comparison of the magnetic flux density and flux lines distributions determined for the load condition has been shown in Fig.1. In the simulations it has been assumed that motors are supplied from the 3 phase balanced current source and the internal power angle is determined iteratively to achieve maximum average value of the electromagnetic torque waveform.

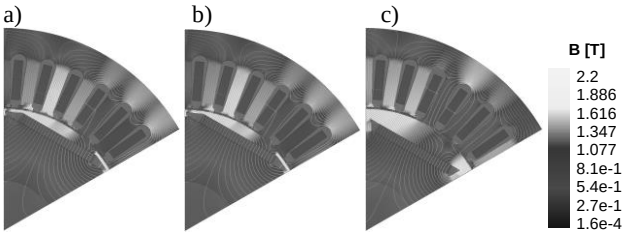

Fig. 2. Magnetic field distribution for i_{ph}= 8A and variants: a) M1; b) M2; c) M3

Obtained results shows that the highest flux leakage occurs in the structure M3. Looking on the functional parameters the torque (K_t) as well as voltage (K_v) constants are the lowest. However, the cogging torque, total harmonic distortion factor of the back emf waveforms and torque pulsations are higher for motors with the rotors M1 and M2. More detailed results and conclusions will be given in the full version of the paper.

REFERENCES

[1] Alotto P., Barcaro M., Bianchi N., Guarnieri M., Optimization of Interior PM Motors With Machaon Rotor Flux Barriers, *IEEE Trans. Magn*., 47 (2011), 958–961.

[2] Fang L., Kim S-I., Kwon S-O., Hong J-P., Novel Double-Barrier Rotor Designs in Interior-PM Motor for Reducing Torque Pulsation, *IEEE Trans. Magn*., 46 (2010), 2183–2186.

Authors*: Wieslaw Lyskawinski, Dorota Stachowiak, Cezary Jedryczka Poznan University of Technology, Piotrowo 3a, 60-965 Poznań, Poland, E-mail: Wieslaw.Lyskawinski / Dorota.Stachowiak / Cezary.Jedryczka @put.poznan.pl*

Dominik KUKLA[1], Justyna SZLAGOWSKA-SPYCHALSKA[2]

Institute of Fundamental Technological Research (1), Warsaw University of Technology (2)

Identification of the Fatigue Cracking of the Aluminide Layers on the Nickel Alloy with the Application of the Optical Method ESPI

Abstract. *The work concerns the use of eddy current method and optical method ESPI to the identification of the cracks of the diffusion aluminide layers on the nickel alloy MAR 247. Fatigue tests were performed on the samples with thicknesses of 20 and 40 μm in the tensile load condition. Eddy current and ESPI measurements were performed after predetermined sequences of load cycles and after the load was stopped at maximum tensile stress. On this basis the fatigue life of layer and its effect on durability of the samples was determined.*

Keywords: nickel alloy, fatigue testing, alumina layer, eddy current, electronic speckle pattern interferometry (ESPI)

Introduction

Research on the evaluation of the fatigue life of aluminum layers on the nickel alloys are usually limited to cracks identification through carrying out observations of the microstructure of the samples after cyclic load. This methodology is subjected to the considerable errors. The dismantling of samples from the testing machine changes the load conditions, what affect the reliability of the results. That is why there are attempts to use non-destructive methods that allow the detection of cracks during the stress test (until sample rupture) without removing the sample from the machine. Those possibilities gives us eddy current method, commonly used in flaw detection and ESPI, an optical technique which enables interferometric measurements of surface displacements. The illumination of a rough surface with coherent laser light and subsequent imaging using a CCD camera generates statistical interference patterns, the so-called speckles. When the object under test is loaded, e.g. by mechanical means, and the surface is deformed, the speckle interferogram also changes. Comparing an interferogram of the surface before and after loading will result in a fringe pattern, which reveals the displacement of the surface. This measurement allows the calculation of the three dimensional distribution of the displacement.

Results and Conclusions

Fractographic studies of the fatigue scrap showed numerous brittle fractures of the layer (Fig. 1), which were probably formed before cracking of the sample. Measurements were performed sequentially at a specified number of cycles, which allowed the identification and localization of the place where layer cracked. First, it was showed in the form of visible displacement location at the ESPI phase maps (Fig. 2.) And after a few consecutive load cycles also in eddy current measurements.

Fig.1. Brittle fracture of the layer on the fatigue scrap

Homogeneous distribution of the displacement, which characterized the initial phase of fatigue (before accumulation of the damage) was showed at the Fig 2a. At the Fig. 2b strong localization of the displacement, which in this case could be connected with deformation around the cracked layer or around the notch (stress concentrator) was showed. Further studies on the correlations of test results between both methods allow confirmation of the possibility to identify cracking of the layer. The preliminary results indicate the possibility of using non-destructive diagnostics methods to assess the fatigue life of the aluminide layers (and also other diffusion layers).

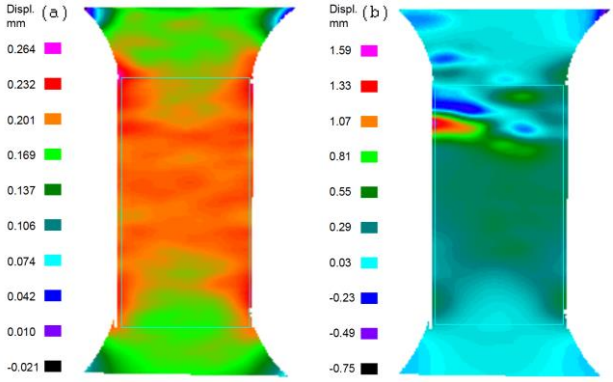

Fig. 2. Distribution of the displacement: (a) initial stage of fatigue test (b) after appearance of the localization of deformation

This work was partially financed by NCS 178781.

REFERENCES

[1] Mori T., Kuroda S., Murakami H., Katanoda H., Sakamoto Y., Newman S., Effects of initial oxidation on beta phase depletion and oxidation of CoNiCrAlY bond coatings fabricated by warm spray and HVOF processes, *Surface & Coatings Technology*, 221 (2013), 59–69.

[2] Khajavi M.R., Shariat M.H., Failure of first stage gas turbine blades, *Engineering Failure Analysis*, 11 (2004), 589–597.

[3] Szlagowska-Spychalska J., Kukla D., Dragan K., Metoda prądów wirowych do oceny konstrukcji lotniczych z uwzględnieniem metod modelowania sygnałów elektromagnetycznych, *OW PW*,1–127, 2014.

[4] Kukla D., Kowalewski Z.L., Grzywna P., Kubiak K., Assessment of fatigue damage development in power engineering steel by local strain analysis, *Metallic Materials*, 52 (2014), 269–277.

***Authors**: Dominik Kukla, Institute of Fundamental Technological Research Polish Academy of Sciences, e-mail: dkukla@ippt.pan.pl, Justyna Szlagowska-Spychalska, e-mail: szjustyna@inmat.pw.edu.pl*

Ahmad WARDA, Hannes TOEPFER

Technische Universität Ilmenau

Comparison of Figures of Merit of Information Content for Sensor Placement Optimization

Abstract. *In this paper we compare three figures of merit for estimating the information content to use it as a criterion for optimizing the placement of sensors. These figures of merit are compared for two sensor networks. In the first network, the sensors are distributed regularly, in the second one the sensors are distributed randomly. The simulation shows that small condition number with respect to the L_2-norm can relate to the sensor network which has more information or also to the ones which has less information. The comparison based on the singular value decay for the two sensor networks.*

Keywords: sensor placement optimization – information content – figures of merit.

Introduction

In inverse problems like Electrocardiography (ECG) and Magnetocardiogaphy (MCG), the accuracy of the source reconstruction depends on the information content, which mainly is influenced by the sensor placement [1]. The sensor placement optimization plays an important role in solving inverse problems by using the data collected with distributed sensors, because the error in their solutions will be determined by the sensor placement [2].

In order to find a good figure of merit for estimating the information content of a sensor configuration, we compare figures of merit, the singular value decay, the condition number (CN) with respect to the L_2–norm and RL/RL_{max} used for optimizing sensor placement (where σ are the singular values).

Simulation

We place one magnetic dipole in the ground plane at the coordinate (0.5, 0.5, 0) and the sensor network consists of 12 x 12 sensors distributed from –5.5 cm to +5.5 cm at the height 1 cm, as in Figure 1. The sensors are one-axial sensors directed in -z direction. We assume also (4x4) supposed dipoles in the ground plane, distributed regularly from –1.5 cm to 1.5 cm. One of them is placed in the same place of the true dipole to see if we can determine the right source when we solve the inverse problem. We compare figures of merit, the singular value decay (σ_i/σ_{max}), the condition number with respect to the L_2–norm ($CN = \sigma_{max}/\sigma_{min}$) and $RL = \sum_{i=1}^{r} \frac{1}{\sigma_i^2}$, for the regular network with one whose sensor position is randomized.

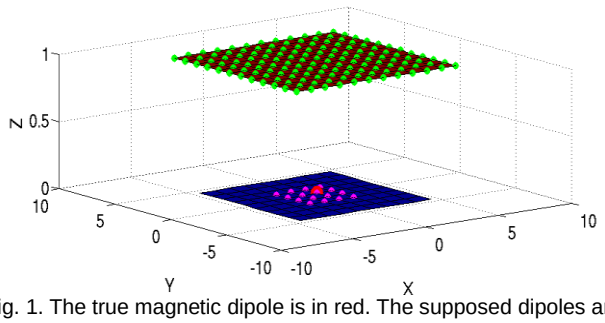

Fig. 1. The true magnetic dipole is in red. The supposed dipoles are in magenta. 12 x 12 sensors in green are located at the height 1 cm. These sensors are regularly distributed

Results

Figure 2. and 3. (left) show that the decay of the singular values for the regular network is slower than the randomized ones and it contains more information. The small condition number relates somtimes to the sensor network which contains more information but also sometimes to the ones which contains less information. RL/RL_{max} denotes more information if its increase is slower (Figure 2, 3, right). It turned out that the singular value decay proves to be a good indicator for the information content.

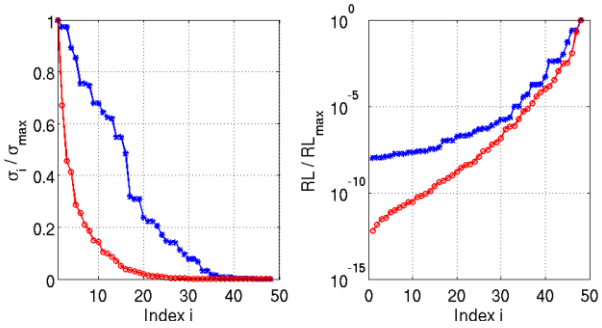

Fig. 2. Comparison of figures of merits
Left: singular value decay (σ_i/σ_{max}), Right: RL/RL_{max}.
(*): regular network with CN_{reg} = 9.9963e+03.
(o): random position sensor with CN_{rand} =1.2633e+06.

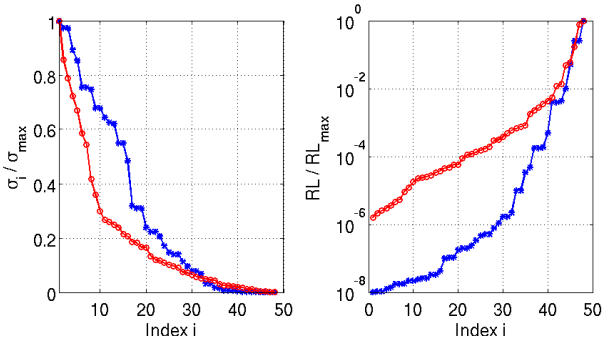

Fig. 3. Comparison of figures of merits
Left: singular value decay (σ_i/σ_{max}), Right: RL/RL_{max} .
(*): regular network with CN_{reg} = 9.9963e+03.
(o): random position sensor with CN_{rand} =794.2.

REFERENCES

[1] Nalbach M., Dössel O., comparison of sensor arrangement of MCG and ECG with respect to information content, Physica C: Superconductivity, 372-376 (2002), 254–258.

[2] Ranieri J., Chebira A., Vetterli M., Near-Optimal Sensor Placement for Linear Inverse Problems, *IEEE Trans. Signal Processing,* 62(2014), No.5, 1135–1146.

***Authors**: Ahmad Warda, Technische Universität Ilmenau, Helmholtzplatz 2, 98693 Ilmenau, ahmad.warda@tu-ilmenau.de, Hannes Toepfer, Technische Universität Ilmenau, Helmholtzplatz 2, 98693 Ilmenau, hannes.toepfer@tu-ilmenau.de*

Larisa TRETIAKOVA
National Technical University of Ukraine «Kyiv Polytechnic Institute»

Simulation of Electrostatic Field on the Surfaces of Protective Clothing of Workers

Abstract*. The issue of creating the electrostatic field and spontaneous electric discharges at the protective clothing surface was resolved in this paper. This problem is very complex since it might cause the damage of electromagnetic compatibility of electronic control systems installed in power plants, therefore the information criteria of electrostatic risks were defined as well.*

Keywords: personal protective clothing, electrostatic fields.

At industrial plants the source of electrostatic field is charged dust particles that settle on personal protective equipment – clothes, shoes, gloves, respirators. Electrostatic field violates the electromagnetic compatibility between devices of electronic control and monitoring, automated security systems and employee, as well as leads to the probability of an explosion in explosive atmospheres in case of spark discharge [1]. Experimentally it was defined that personal protective equipment has surface resistance from 10^8 to 10^{13} ohms. Surface electrostatic field are characterized by a high degree of heterogeneity and uncertainty: experimentally an uneven charge distribution in areas of kits was observed; there is a constant leakage of charges due to conductivity, moisture and pollution materials [2].

The method of computer simulation of electrostatic field on curved surfaces personal protective equipment was developed. The modelling object is an employee in the insulating protective equipment, on which surface during work electric charges are accumulated. The electrostatic field simulation on surfaces of protective clothing was carried out in three stages: a mathematical model was developed to calculate the inhomogeneous electrostatic field in the area, which surrounds the employee; the size of estimated plot and the boundary conditions on its surface were determined according to the mathematical model; the parameters of electrostatic field were calculated. For these conditions was applied the finite element method, which was implemented in the software package COMSOL.

The analysis of electrostatic field simulation results with a different distribution of surface charges gave the following results: for maximum recorded value of surface charge density σ_q = 10^{-7} C/m^2; the maximum potential is 8 kV; intensity – 1.6 · 10^4 V/m, which can lead to electromagnetic compatibility violation. Electrostatic field power lines begin on a surface of personal protective equipment and close in the airspace up to one meter from the employee (Fig. 1).

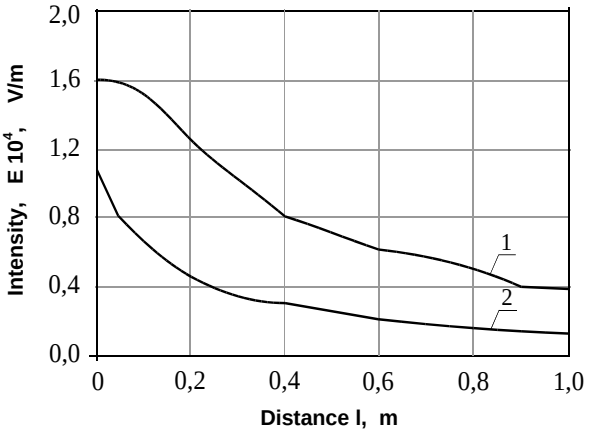

Fig. 1. The distribution of electrostatic field intensity in the surrounding area: 1 – for uneven distribution of surface charge density; 2 – for even distribution of surface charge density

The value of electrical energy, which is accumulated in the volume V = 64 m^3 by the results of numerical integration is W_e = 0,96 mJ.

Simulation results gave reason to create designs and determine modes of use personal protective equipment to minimize the risk of electrostatic (electrostatic hazards).

REFERENCES

[1] Luttgens G., Wilson N., Electrostatic hazards. *Oxford, Linacre House*, 1997.

[2] Paasi J., Fast L., Kalliohaka T. Risks of damage to electronics with reference o charged clothing. J. Electrostatics. – 2005. – No 63, 603–608.

Author*:* Larisa Tretiakova, *National Technical University of Ukraine «Kyiv Polytechnic Institute», address: 03056 Ukraine, Kiev, pr. Peremogy 37, k. 22 of. 303. E-mail lt79@ukr.net*

Dorota TYPAŃSKA[1], Adam MAĆKOWIAK[2], Krzysztof SIECZKAREK[2]

Poznan University of Technology(1), Institute of Logistics and Warehousing (2)

Immunity of Intelligent Installation Model on the Pulsed Electromagnetic Disturbances

Abstract*. The paper presents the test results of an intelligent fixed installation model for electromagnetic immunity on the pulsed disturbances. The tested model of the installation was made on the basis of intelligent building automation produced by Hager.*

Keywords: Intelligent building, KNX, electromagnetic compatibility, fixed installations

Introduction

Electromagnetic compatibility (EMC) is now a very important part of science in the field of electrical engineering. It deals studies of the effect of electromagnetic disturbances on the device. Both in terms of emissions of these disturbances and immunity on it.

Currently on the market are produced more and more devices equipped with electronic systems, which are very sensitive to electromagnetic interference. Hence it is necessary to study the whole of installation in terms of electromagnetic compatibility.

This paper presents the results of immunity test of an exemplary intelligent installation model for electromagnetic disturbances, made in laboratory environment.

Intelligent installation model

For research, the intelligent KNX installation model was performed. This model was based on building automation, manufactured by Hager. It consisted of switch on/off , illumination dimmer and blinds actuator.

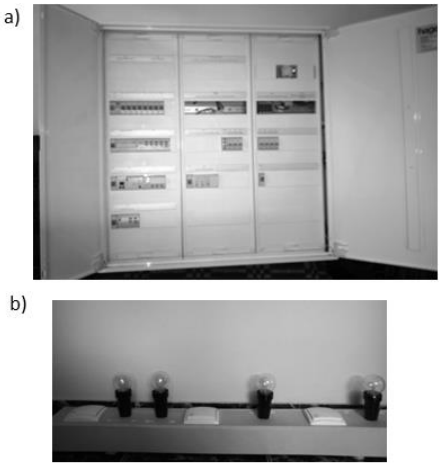

Fig. 1. a) intelligent building equipment, b) control panel

In Fig. 1 shows the view of KNX model (a) and the strip which controlled the equipment (b).

Immunity test for electromagnetic pulse disturbances

For electricity networks of low voltage (<1000 V) there are a variety of electromagnetic disturbances, for example pulse disturbances. Such disturbances are mainly voltage pulses (surge) and current (overcurrent), which overlap on the sinusoidal voltage or current network course It may have a diverse character. Can occur as a single pulse or harness, in the random or periodic method [6].

Single pulse generally characterized a short rise time and a relatively slow descent. The spectrum of such signals is a broadband. These pulses have different shapes, the most common are similar to the exponential course or oscillatory damped.

Research immunity to impulse disturbances are described by European standard system. Those tests can be divided into:

– immunity test for pulse magnetic field [2],
– immunity test to electrostatic discharge (ESD) [3],
– immunity test to fast transients EFT/Burst [4],
– immunity test on surge disturbances [5].

Presented model has been tested on all those disturbances.

Summary

Electromagnetic disturbances can be divided into disorders pulsed and continuous. This paper presents only the results of immunity test of an intelligent installation model for pulse electromagnetic disturbances. The results showed that the device is fully immune to all of those disturbances. However, was tested only a fragment of an intelligent system. So it is uncertain whether the installation made entirely in the building will also be electromagnetically compatible Each installation is working in specific terms and in such it should be studied.

REFERENCES

[1] Paul C.,Introduction to electromagnetic compatibility, *John Wiley & Sons Publishing House*, New Jersey, 2006.
[2] PN-EN 61000-4-9:1998- Electromagnetic compatibility (EMC) - Part 4–9: Testing and measurement techniques - Pulse magnetic field immunity test.
[3] PN-EN 61000-4-2:2011 - Electromagnetic compatibility (EMC) - Part 4-2: Testing and measurement techniques - Electrostatic discharge immunity test.
[4] PN-EN 61000-4-4:2013-05 - Electromagnetic compatibility (EMC) - Part 4–4: Testing and measurement techniques - Electrical fast transient/burst immunity test.
[5] PN-EN 61000-4-5:2014-10 Electromagnetic compatibility (EMC) - Part 4-5: Testing and measurement techniques - Surge immunity test.
[6] http://ww3.itr.org.pl/Projekty/Projekt1/badanie_analiza.pdf

Authors*: Dorota Typańska, Poznan University of Technology, Piotrowo 3A, 60-965 Poznań, dorota.typanska@put.poznan.pl, Adam Maćkowiak,* Institute of Logistics and Warehousing, *Estkowskiego 6, 61-755 Poznań, adam.mackowiak@ilim.poznan.pl, Krzysztof Sieczkarek,* Institute of Logistics and Warehousing, *Estkowskiego 6, 61-755 Poznań, krzysztof.sieczkarek@ilim.poznan.pl.*

Rafal M. WOJCIECHOWSKI, Tomasz BOCZKOWSKI, Cezary JĘDRYCZKA

Poznan University of Technology, Institute of Electrical Engineering and Electronics

Analysis of Axial Flux Permanent Magnet Coreless Motor Using 2D Edge Element Method and Superposition Principle

Abstract. *In the paper, the low power axial flux permanent magnet coreless motor (AFPMCM) has been analysed. To determine the electromagnetic field distributions and the electromagnetic torque in the studied AFPMCM the field model based on superimposing axial symmetric 2D solutions obtained by means of the edge element method has been proposed and tested. The authors developed the computer software for the electromagnetic field computations. The selected results of electromagnetic torque characteristics have been presented.*

Keywords: Superposition principle, edge element method, axial flux permanent magnet coreless motor.

Introduction

In the paper the low power 14 pole-pair axial flux permanent magnet coreless motor (AFPMCM) has been considered. The construction of the motor has been illustrated in Fig. 1. The stator of the motor has been made of printed circuit board (PCB) laminate on which the 3 phase winding has been placed. The winding is connected into the star and consist of 21 concentric coils. The rotor consists of disc shape polyamide plate and 28 cylindrical neodymium iron boron permanent magnets of type N38. To determine the 3D magnetic field distribution in the presented machine the authors used own developed computer code utilizing the method of superposition (SP) of distributions determined from 2D models. In the development of 2D models the edge element method (EEM) [1] has been applied. Developed software has been used to perform a number of design calculations. Finally the structure of the magnetic circuit has been chosen and the mechanical construction of the prototype elaborated. The performance of bullied prototype has been measured in order to validate proposed approach and developed computer program for analysis of the AFPMCM.

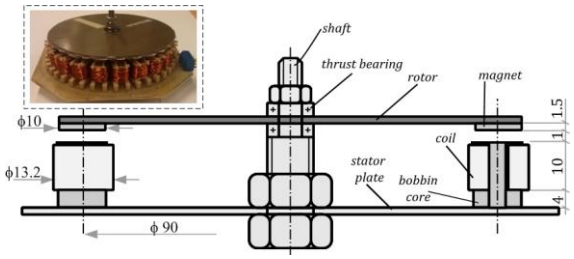

Fig. 1. View of the AFPMCM motor construction

Field model of AFPMCM motor

The distribution of the magnetic field in the considered motor has been determined using own developed software basing on the 2D edge element method and superposition principle (*2D EEM-SP*). For the studied coreless structure – i.e. when no ferromagnetic material is in the considered region, the superposition of magnetic fields excited by rotor and stator can be applied. Moreover due to axial symmetry of the coils and magnets the 3D field in the motor can be represented by the projection and superposition of 2D solutions calculated for the each coil and the each magnet. To determine the magnetic field distribution excited by the particular coils and magnets the edge element method applied for solving the 2D axial symmetry problems has been used. Next the obtained field distributions have been transformed from 2D axial symmetry local coordinate systems to the global 3D space. The advantage of proposed approach is significant reduction of computational effort. First, it should be noticed that it is not necessary to repeat the calculations of the magnetic field for every coil. To determine the field distribution of coil supplied by given value of the current I_m the values of magnetic flux density $\boldsymbol{B}$ or magnetic vector potential $\boldsymbol{A}$ calculated for the unit current (1A) are simply multiplied by I_m. In a similar way the magnetic field distribution of magnets can be detrained. Here the potentials are multiplied by (-1) for the opposite direction of the magnetization vector. Developed software, besides calculating and plotting the field distributions, allows also for determining the integral parameters of studied AFPMCM, like electromagnetic torque or normal force between rotor and stator of the motor. For the calculations of electromagnetic forces and torques in the edge element space the formulas given by [2] have been used.

Results and Conclusions

In order to proof usefulness of proposed approach for analysis of the AFPMCM the obtained results have been verified by means of measurements of the motor prototype as well as simulations performed using 3D finite element model developed in the commercial FEM package – Maxwell. As an example, the comparison of the electromagnetic torque vs. current and the rotor angular position α has been shown in Fig. 2. Presented torque characteristics have been obtained for the BLDC control mode (i.e. $i_a = -i_b = I_m$ and $i_c = 0$) and for two chosen values of current I_m equal to 0.6 and 1 A, respectively.

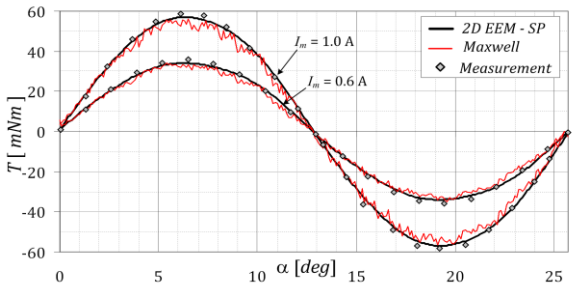

Fig. 2. The waveforms of the electromagnetic torque as a function of rotor position for the considered motor

On the basis of the obtained results it can be concluded that both, the proposed superposition method and performed 3D FEA, are very close to the results of the experiments. The relative difference between the results of simulations and measurements is less than 4.1%. The biggest advantage of the proposed method is the significant reduction of the computation time. For the proposed superposition method the magnetic field distribution is computed in less than 5s while performing on the same computer the 3D FEA takes about 30 min.

REFERENCES

[1] Demenko A., Sykulski J.K., Network equivalents of nodal and edge elements in electromagnetics, *IEEE Trans. Magn.,* 38 (2002), no. 2, 1305–1308.

[2] Demenko A., Lyskawinski W., Wojciechowski R.M., Equivalent formulas for global magnetic force calculation from finite element solution, *IEEE Trans.Magn.*, 48 (2012), no. 2, 195–198.

***Authors**: Rafal M. Wojciechowski, e-mail: rafal.wojciechowski@put.poznan.pl; Tomasz Boczkowski, e-mail: tomasz. boczkowski@onet.pl; Cezary Jędryczka, Poznan University of Technology, ul. Piotrowo 3a, e-mail: cezary.jedryczka@put.poznan.pl*

Barbara SZYMANIK[1], Mirosław WOŁOSZYN[2]

West Pomeranian University of Technology, Szczecin (1), Gdansk University of Technology (2)

Magnetic and Infrared Thermography Methods in Detection of Nonmetallic Landmines

Abstract. *Several methods are used in detection of antipersonnel mines. Especially the mines with plastic or wooden casings are difficult to detect. The magnetic and infrared thermography methods are described in this paper. Moreover some experimental results of the detection of the selected, nonmetallic mines are presented.*

Keywords: plastic mines, infrared thermograph method, magnetic method, detection.

Introduction

The history of landmines dates 1277 when the Chinese used contact fused explosive mechanism to repel invading Mongols [1]. Land mines can be divided into antitank and antipersonnel mines. The antipersonnel mines are designed to maim and kill people. Their casings can be made from metal, wood or plastic. Several methods are used for detection of mines [3], but in case of plastic mines the detection is impeded.

In this paper the two alternative methods of nonmetallic landmine detection are shown: the magnetic method and the active infrared thermography. The experimental results of the detection of selected, plastic mines using both methods are also presented.

Magnetic Method

Every object built of ferromagnetic materials, which is located in the Earth's magnetic field, disturbs the uniformity of this field. The plastic mine can consist of small parts of metal and also can be contaminated by ferromagnetic particles. The disturbance of Earth's magnetic field by mine is extremely weak. Two optically-pumped magnetometers G823A are used in detection of mines. One of them was moving above the hidden mine and other was used as reference magnetometer (Fig.1).

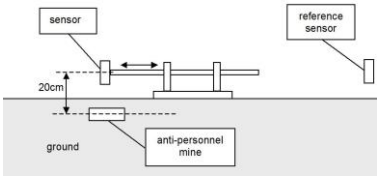

Fig. 1. The methodology of measuring of the mine's magnetic filed

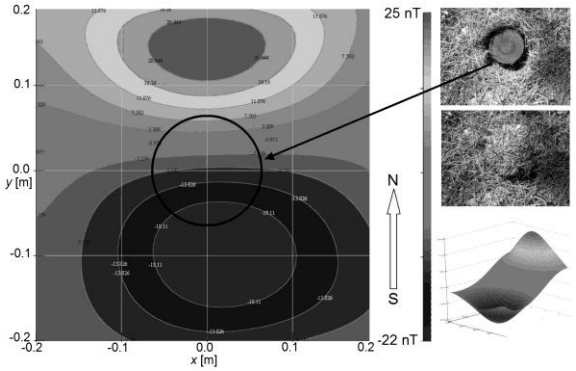

Fig. 2. The magnetic anomaly of GYATA 64 mine

The magnetometers were synchronized what allowed to achieve sensitivity about ten pT. The disturbance in the magnetic flux density caused by GYATA 64 mine was shown in Fig. 2. The magnetic signal is big in this case (maximum pp = 47 nT). The following position of the mine was obtained after calculations [4] (x_c = 4.6 cm, y_c = 1.6 cm, z_c = 25.3 cm, the real position was x_r = 0 cm, y_r = 0 cm, z_r = 20 cm). The identification of plastic mine by using the magnetic method is difficult because ferromagnetic particles and elements inside the mine are diffused.

Infrared Thermography Method

Active infrared thermography with microwave excitation is a relatively new method of the landmines detection [2] and may be considered complementary to magnetic method. Microwave enhanced infrared thermography is based mainly on two physical phenomena: the microwave heating and the heat transfer. The thermal contrast between the landmine and soil is produced by the rapid, volumetric microwave heating. The sensitive thermovision camera is afterwards used to observe the thermal patterns obtained at the ground's surface. With this method one is able to detect an object, determine its size and approximate location.

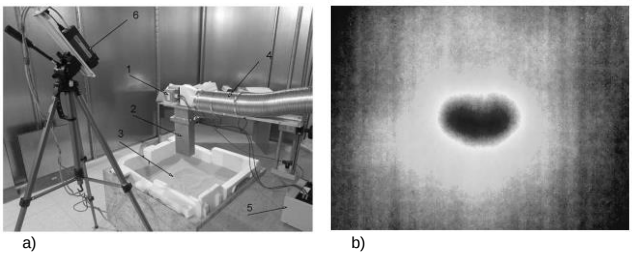

a) b)

Fig. 3. a) the experimental setup: (1) 1kW magnetron, (2) rectangular waveguide, (3) sand container, (4) cooling system, (5) power supply, (6) thermovision camera. b) The thermal signature of GYATA 64 landmine

The Fig. 3a presents the experimental laboratory setup. In the Fig. 3b the exemplary result of GYATA 64 landmine detection is shown. The landmine was buried at the depth of 3 cm. The heating time was set to 10 minutes, and the time of the natural cooling of the system (observation time) was set to 5 minutes.

This work was partially supported by the CNBiR, Poland, under the Grants No.: DOBR/0062/R/ID1/2012/03.

REFERENCES

[1] Schenk W.C., The origins of military mines, part I, *The Engineer, Bulletin*, Nov. 1998.

[2] Mende H., Dej B. Khana S., Apps R., Boyle M. Addison F., *Microwave enhanced IR detection of landmines using 915 MHz and 2450 MHz*, Defence R&D Canada - Ottawa, 2004.

[3] Woloszyn M., Locating and Identifying Ferromagnetic Objects, *International Journal of Applied Electromagnetics and Mechanics,* vol.39, no.1–4, pp.175–182, 2012.

Authors*: Barbara Szymanik,* West Pomeranian University of Technology, Szczecin, *szymanik@zut.edu.pl, Mirosław Wołoszyn, Gdansk University of Technology, Narutowicza 11/12, 80-233 Gdansk, miroslaw.woloszyn@pg.gda.pl*

Mirosław WOŁOSZYN, Kazimierz JAKUBIUK, Mateusz FLIS

Gdansk University of Technology

Analysis of Distribution of Current Density and Temperature in Busbars

Abstract*. Warming of elements of electric devices is most important problem both at constructing as exploitation of these devices. At warming, coupling of electromagnetic field and thermal field plays essential role. This is particularly essential at heterogeneous distribution of these fields. The distribution of temperature in two type of electric devices are presented in this paper. Calculations were made in the package ANSYS.*

Keywords: busbar, temperature, current.

Introduction

During the construction and exploitation of electric devices and machines a serious issue is encountered – that of their heating up according to Juole's law [3]. In the case when the heating up in some areas is not heterogeneous, the theoretical or theoretical-empirical formulas are usually not precise enough and the calculation of the amount of heat is performed using numerical methods [1, 2, 3]. This applies to both steady and transient states of the heating up process. Mathematical models of the process of heating up, due to its complex character, must be simplified accordingly. This work investigates on the basis of a chosen example mainly the problem of coupling of electromagnetic and thermal fields. The analysis of the problem of coupled fields is generally possible only by applying numerical methods. The purpose of this paper is to present on the basis of a selected example the occurring differences in temperature calculated taking into account the coupling of both tested fields or when the coupling is not considered.

Tested objects and their mathematical models

A two three-phase system of rectangular busbars with and without a nonmetallic cover were chosen as examples (Fig.1).

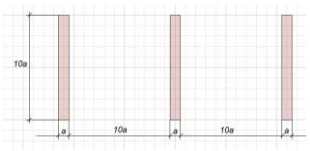

Fig. 1. The busbar model without a cover (*a* = 5 mm)

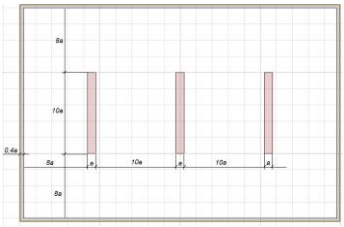

Fig. 2. The busbar model with a cover (*a* = 5 mm, b = 2 mm)

The distribution of the electromagnetic field in the quasi steady state and the temperatures in the transient state is described by the following equations:

$$\nabla^2 \underline{A} - j_z \omega \mu \sigma \underline{A} = -\mu \underline{j}_w \tag{1}$$

$$\rho c_p \frac{\partial T}{\partial t} = \lambda \nabla^2 T + \frac{j^2}{\sigma} \tag{2}$$

where: $\underline{A}$ – complex vector magnetic potential, $\underline{j}_w$ – forcing current vector, j – current density vector module, μ – magnetic permeability, σ – conductivity, ω – angular frequency, $j_z = \sqrt{-1}$, T - temperature, ρ - density, λ – thermal conductivity and, c_p – specific heat capacity.

The conductivity depends on a temperature in the following way:

$$\sigma(x,y,T) = \frac{\sigma_o}{1 + \alpha\,[T(x,y,t) - T_o\,]} \tag{3}$$

where: T_o –reference temperature, σ_o – conductivity in a reference temperature, α – factor of temperature changes.

Steady state of thermal field is definited as a transient state after properly long time. The dependence (3) couples electromagnetic with thermal field. The equations (1) and (2) were solved by MES method in the package ANSYS. Fig. 2 and Fig. 3 present the calculation results in the form of distributions of temperature for the investigated area of busbars. The calculations were made for model with and without a cover in steady state taking coupling into account.

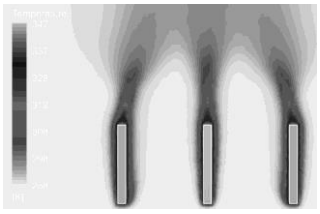

Fig. 3. The distribution of the temperature in the busbar model without a plastic cover (I_{sk} = 1000 A)

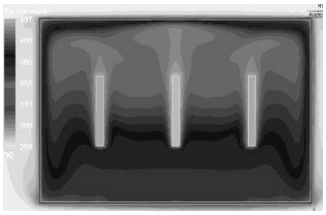

Fig. 4. The distribution of temperature in the busbar model with a plastic cover (I_{sk} = 1000 A)

CONLUSIONS

The problem of coupling of electromagnetic and thermal field is very important. The temperature in the model with a cover is greater about 100°C in comparison with the model without a cover. The analyze of the same devices without coupling of electromagnetic and thermal field, showed that the temperature of a busbar is less about 9°C (without a cover) and 43°C (with a cover). Therefore, it is very important convection cooling mechanism and taking into account the coupling between the two fields.

REFERENCES

[1] Maksymiuk J., Pochanke Z., Fundamentals of computation Power devices *(in Polish)*, *WNT Warsaw* 1976.

[2] Jakubiuk K., Aftyka W., Heating of fuse-elements in transient and steady-state. *7 International Conference of Electrical Fuses and their Applications*, Gdańsk 2003, pp.181–187.

[3] Jakubiuk K., Electrical explosion and implosion of conductors. *Gdansk University of Technology*, 2000.

Authors*: Mirosław Wołoszyn, Gdansk University of Technology, 80-233 Gdansk Narutowicza 11/12, miroslaw.woloszyn@pg.gda.pl, Kazimierz Jakubiuk, kazimierz.jakubiuk@pg.gda.pl, Mateusz Flis, mateusz.flis@pg.gda.pl*

Michał ZEŃCZAK

West Pomeranian University of Technology, Szczecin

Method of Estimation of Exposure of Natural Environment on 50 Hz Electric and Magnetic Fields in Power System with Distributed and Centralized Generations

Abstract. *Development of distributed generation will have influence on structure of power transmission and distributed network. Distributed sources have lower power and therefore the lines of lower voltage are used. Therefore electric field intensity near such the lines is lower. On the other hand magnetic field intensity may be quite essential. The main aim of paper is presentation of method of estimation of "ballast" of natural environment by 50 Hz electric and magnetic fields in power system with distributed and centralized generation in real operation conditions.*

Keywords: overhead power line, electric field, magnetic field, distributed generation.

Introduction

There are possible three scenarios of development of electric power system (EPS):

- extremely centralized EPS, with one big electric power station or generation center,
- extremely distributed EPS with sources of electrical energy directly by consumers,
- mixed structure of EPS with big power stations and distributed generation.

The third scenario is most probably in the close future, because sun and wind are main sources of energy for distributed generation and there is necessity of existence of big electric power stations. Development of distributed generation will have influence on structure of power transmission and distribution networks. Distributed sources have lower power and therefore the lines of lower voltage can be used for sending power from these sources. Therefore electric field (EF) intensity is lower by such the lines. If the currents are considered, the situation is not so synonymous, because by the lower power and lower voltage, currents may be quite essential. Methods of estimation of EF intensity (E) and magnetic field (MF) intensity (H) near power transmission lines are well known [1, 2]. The main aim of paper is estimation of "ballast" of natural environment by EF and MF 50 Hz caused by distributed and centralized generations. Figure 1 presents the structure of power system with centralized generation (CG) and distributed generation (DG).

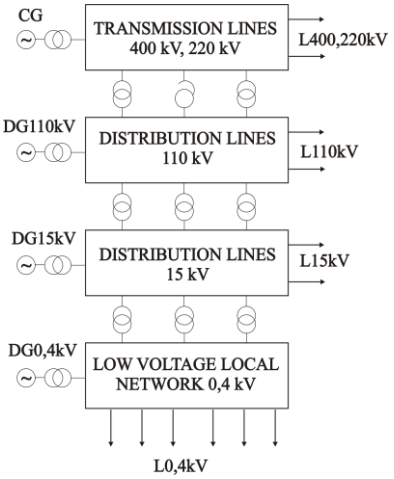

Fig.1. Power system with distributed and centralized generations

EF near power lines

EF intensity near power lines is the function of voltage and configuration of line. Generally the higher voltage, the higher EF intensity.

MF near power lines

MF intensity near power lines is the function of flowing currents and configuration of line. Value of MF intensity changes in big range, because the currents in phase wires change from $I \approx 0$ to current-carrying capacity of lines (I_{cc}).

Power system with DG and CG

The balance of generated power and load:

$$P_{CG} + P_{DG110} + P_{DG15} + P_{DG0,4} = P_L \,, \tag{1}$$

$$P_L = P_{L400,220} + P_{L110} + P_{L15} + P_{L0,4} \,, \tag{2}$$

where: P_{CG}, P_{DG110}, P_{DG15}, $P_{DG0,4}$ – value of generated power in particular level of voltage, P_L – total power of load, $P_{L400,220}$, P_{L110}, P_{L15}, $P_{L0,4}$ – power of load in particular level.

Equation (1) can be divided by P_L:

$$k_{CG} + k_{DG110} + k_{DG15} + k_{DG0,4} = 1 \,, \tag{3}$$

where: k_{CG}, k_{DG110}, k_{DG15}, $k_{DG0,4}$ – coefficients of power participation in generation by sources on particular level.

In order to compare exposure in EF and MF, the volumetric energy density of EF and MF are used and sum of them W:

$$W_H' = \frac{\mu_0 H^2}{2} \,,\; W_E' = \frac{\varepsilon_0 E^2}{2} \,,\; W = W_E' + W_H' \tag{4}$$

Analysis shows, that "ballast" of natural environment by EF may be the same for Dg and CG, but is different for MF.

REFERENCES

[1] Krajewski W., Analysis of electric and magnetic fields around a lineman during live working, *Electrical Review*, 83 (2007), No. 9, 57–59.

[2] Wróblewski Z., Habrych M., Electromagnetic field distribution under high voltage lines depending on geometrical systems of phase conductors on pillar, *Electrical Review*, 81 (2005), No. 6, 15–19.

Authors: *Michał Zeńczak, West Pomeranian University of Technology, Szczecin, E-mail: michal.zenczak@zut.edu.pl*

Kazimierz ADAMIAK[1], Maciej WŁODARCZYK[2]

University of Western Ontario (1), Kielce University of Technology (2)

Electrohydrodynamics of Droplets: Direct versus Level Set Method Formulations

Abstract. *Two different numerical approaches for simulating droplet behavior in the external electric field are compared. First one is based on a direct solving of a differential equation resulting from the balance of all forces acting on the droplet surface. The second uses the concept of the Level Set Method. The former predicts the exact droplet surface, but it leads to a slow convergent iterative process and is unable to handle the surface break-up. The latter replaces the droplet surface with a fuzzy interface, but is much more efficient and faster.*

Keywords: electrohydrodynamics, droplets, electric field.

Introduction

In numerous engineering applications and in nature liquid droplets may be exposed to an external electric field. These can be insulating or conducting, neutral or charged, droplets suspended in another fluid or deposited on a substrate. In most of these cases droplets can be distorted, broken or disintegrated. They can also oscillate, rotate or move. The electric forces can be used for droplet coalescence, mixing, deposition or spreading. Numerical simulation of this process can be very useful in optimization of practical devices or explaining some natural phenomena.

Direct simulation of droplet deformation

When a liquid droplet is suspended in another medium and exposed to an external electric field, the droplet is being distorted. The dynamics of this distortion results from the balance of all acting forces: capillary, inertial, viscous, gravity and electrical. While fluid flow and electrical effects can be easily determined, the droplet distortion must be calculated from the capillary equation [1]:

$$\sigma\left(\frac{1}{R_1}+\frac{1}{R_2}\right)+\frac{\varepsilon E_n^2}{2}+\Delta P = 0 \tag{1}$$

subject to the constant droplet volume constraint, where: ρ – the fluid density, σ – the surface tension, $1/R_1+1/R_2$ – the sum of the principal radii of curvature, ε – the permittivity of the ambient medium, E_n – the normal component of the electric field and ΔP_1 – the pressure difference between the droplet interior and the ambient medium.

Level set method

This method describes evolution of the droplet surface by tracing an isopotential curve of the level set function Φ, which is governed by the equation [2]

$$\frac{\partial \Phi}{\partial t}+u\cdot\nabla\Phi=\gamma\nabla\cdot\left(\varepsilon_{ls}\nabla\Phi-\Phi(1-\Phi)\frac{\nabla\Phi}{|\nabla\Phi|}\right) \tag{2}$$

where: ε_{ls} - the parameter controlling the interface thickness and γ - the re-initialization parameter and $\boldsymbol{u}$ – fluid velocity vector. A new version of this technique based on using the fractional partial derivatives is currently investigated.

Results

The direct method has been applied to simulate elongation a non-viscous droplet exposed to the uniform electric field in microgravity conditions. The droplet is suspended in air, is assumed to be ideally conducting and electrically neutral. Initially, it is motionless and spherical.

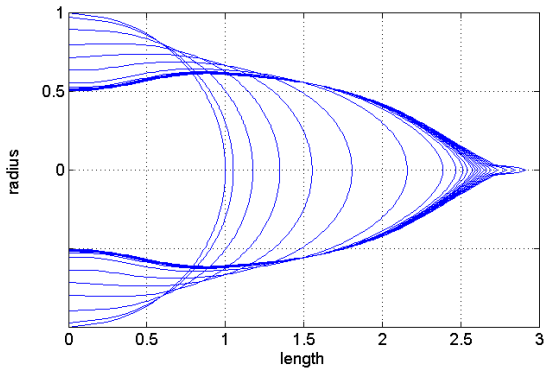

Fig. 1. History of deformation of the liquid droplet instantaneously exposed in a uniform electric field

Fig.2 shows predicted deformation of an initially spherical viscous droplet suspended in another viscous fluid and exposed to an external electric field. Both media are electrically conductive, but the droplet conductivity is smaller. The breakup mode is quite unusual: a hole is created first leading to a toroidal shape, which next disintegrates into a set of smaller pieces.

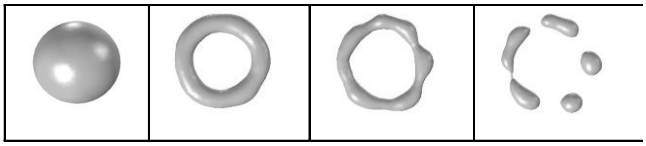

Fig. 2. Breakup of the 1.3 mm droplet suspended more conductive fluid in 7kV/cm electric field

REFERENCES

[1] Adamiak K., Floryan J.M., Dynamics of water droplet distortion and breakup in a uniform electric field, *IEEE Trans. Ind. Appl.*, 47 (2011), No. 6, 2374–2383.

[2] Ghazian O., Adamiak K., Castle G.S.P., Numerical simulation of electrically deformed droplets less conductive than ambient fluid, *Colloids and Surfaces A: Physicochemical and Engineering Aspects,* 423(2013), 27–34.

***Authors**: Kazimierz Adamiak, University of Western Ontario, Dept. of Electrical and Comp. Eng., London, Ontario, Canada N6A 5B9, kadamiak@eng.uwo.ca, Maciej Wlodarczyk, Kielce University of Technology, Fac. of Electrical Eng., Automatics and Computer Science, 25-314, Kielce, Poland, e-mail: mwlodar@tu.kielce.pl*

Dagmar FAKTOROVÁ, Mária PÁPEŽOVÁ

University of Žilna

New Approach in Non-Destructive Testing of Dental Biomaterials by Using Microwaves

Abstract*. The paper deals with new approach to the finding of various defects, material degradation in dental materials by using electromagnetic highfrequency method. Our aim is to implement microwave nondestructing methods to the finding inhomogenity in dental material and to compare our results with low frequency method such as eddy current method and methods which are directed to the approaches connected with the mechanical properties investigation..*

Keywords: non-destructive testing, dental materials, microwave frequencies, biomaterials.

Introduction

The quickly growing dental technique needs new methods which are able quickly, cheap and effectively testing of dental material without destructive approach in the finding of various inhomogeneity, materials degradation and defects, which can lead in the future to the destruction of used biomaterial or to the destruction of implant [1]. The microwave frequencies in regard to their wave length may be very important tool in the prevention of devastative processes of replaced teeth material and implants.

The microwave non-destructive methods includes the development of sensors, methods of calibration techniques to detection cracks, defects, cavities, various heterogeneities of materials etc. Monitoring dielectric properties of biomaterials, especially in the microwave frequency range, exploring new possibilities of application new materials elements is very important to improve quality of biomaterials and level of treatment. This all facts predestinate the microwave non-destructing methods to become very perspective tool in dental medicine. Almost all technique, which are used in dental medicine for defect in dental material or implant quality testing are ionizing and very expensing. On the other hand the microwave methods can became considerable alternative in both nonionizing and cheaper approach.

Numerical and Experimental Results

Two possibilities of microwave non-destructive method were considered in our research:

1. the finding of dental infilling material degree degradation by using the method for the dielectric parameters of infilling dental material measurement,
2. the finding the defect presence in the volume of dielectric dental material used in the role of infilling of repaired teeth.

The experimental measurement of dielectric constant were done for very often used dental material PMMA - Poly(methyl methacrylate) [1, 2].

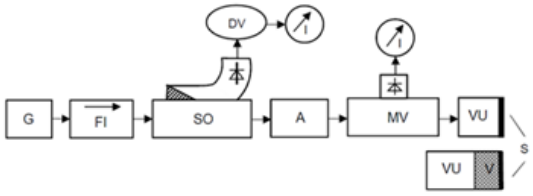

Fig.1. The experimental set-up for dielectric properties of dental biomaterial measurement, G – high – frequency generator, FI – ferrite isolator, SO – directional coupler, A – attenuator, MV – measuring line, VU – waveguide section, V – measured sample, DV – cavity wavemeter, I –zero indicator, S – short circuit, VU – waveguide section, V – measured sample, DV – cavity wavemeter, I –zero indicator, S – short circuit

The used method belongs to the reflection methods and investifgated material is placed to the volume of waveguide.

The real value of PMMA material complex permittivity was used for numerical simulation of heterogeneous structure of repared teeth: enamel – dentine – biomaterial PMMA. This model created from three various dielectric materials were modified up to real situation in dental practice and results used for examination of degradation of material in the agressive environment of human mouth cavity. The inhomogenity existence in such heterogeneous structure was finding of from the changed amplitude value of scaterring *S* parameters which are connected with the reflection S_{11} and transmission S_{21} of electromagnetic wave from and through the reconstructed teeth.

The inhomogenity presence were numerically simulated by using patch antenna in the role of source of electromagnetic wave and the detector of reflected electromagnetic wave. The example of the most basic simulation with one patch antenna and the block of homegeneous sample is in Fig. 2a.

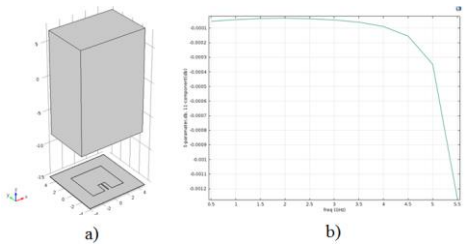

Fig. 2. a) 3D geometry of patch antenna and PMMA in the free space, b) frequency dependence of S_{11} range 0.5-5.0GHz

There are in Fig. 2b results for reflection parameter S_{11}. In the case of changed situation e.g. the presence of defect the amplitude of *S* parametr will be changed and the presence of inhomogenity can be found and in the next step evaluated.

REFERENCES

[1] Gundas S. edt., Advances in Induction and Microwave Heating of Mineral and Organic materials Microwave Engineering, The Use of Microwave Enrgy in Dental Prosthesis, InTech, 423–458, 2011.

[2] Craig R.G., Restorative Dental Materials, 7th ed. St. Louis: C.V. Mosby Co; 458–511, 1985.

Acknowledgments

This work was supported by the Slovak Scientific Agency VEGA under the grant No. 1/0846/13.

Authors*: Dagmar Faktorová, dagmar.faktorova@fel.uniza.sk, Mária Pápežová, maria.papezova@fel.uniza.sk, University of Žilina, Univerzitná 8215/1, 010 26 Žilina, Slovak Republic*

Krzysztof BUDNIK, Wojciech MACHCZYŃSKI, Jan SZYMENDERSKI

Poznan University of Technology

Assessment of D.C Traction Stray Currents Effects on Nearby Pipelines

Abstract. *D.C electrified traction systems are a potential source of stray currents. The important problem, technically, is to evaluate the harmful effects (electrolytic corrosion) that an electrified railway has on nearby earth-return circuits (e.g. pipelines). The electric circuit approach, based on the complete field method of solution of the transmission-line problem (the earth-return circuit theory), to model stray currents interference on extended structures is presented. The electrode kinetics (polarization phenomenon) is taken into account in the model developed.*

Keywords: stray currents, d.c. traction, earth return circuit, polarization.

Introduction

The electromagnetic compatibility of components of electric traction system is a criterion participating more and more in the decision of network planning and operation. D.C electrified traction systems are a potential source of stray currents. The important problem, technically, is to evaluate the harmful effects (electrolytic corrosion) that an electrified railway has on nearby earth-return circuits (e.g. pipelines). The best approach to assessing stray currents interference is to determine the change in current density/potential on the structure influenced by the stray currents. The response of the structure is a function of three factors: the location of the structure with respect to the electric flow field generated by the stray current source, the magnitude of the electric field, and the electrochemical response of the structure to the interference.

The "field approach" – e.g. the Boundary Element Method can be used to model the electrochemical polarization that occurs on the subjected structure [1]. On the other hand the "electric circuit approach", based on the earth-return circuit theory [2, 3, 4], is more suitable for modeling extended structures (pipelines, cables).

The first objective of the paper is to summarize the problems of the modeling of d.c. stray currents generated in the vicinity of the d.c. electrified railways. Two methods are presented. An exact method of calculation is based on the complete field method of solution of the transmission-line problem. The analysis given is applicable to any d.c. railway system in which tracks can be represented by a single earth return circuit (equivalent rail) with current (shunt) energization. In the approximate method, the equivalent rail with current energization is modeled as a large multinode electrical equivalent circuit with lumped parameters. The circuit is a chain of basic circuits, which are equivalents of homogenous sections of the rail [5]. It is assumed in the paper that the system considered is linear, that the earth is homogeneous with finite conductivity and that the effects of currents in nearby underground metal installations on the potential generated in the earth by track currents (primary earth potential) can be disregarded.

The second objective of the paper is to simulate the response of foreign metallic structure buried in the stray currents area. Taking into account that the driving electric field in the earth is produced by the current (shunt) energization [2] of the equivalent rail, calculations are made and formulas derived applicable to the analysis of currents and potentials along a pipeline laid in the proximity with railway tracks. The formulas in partially closed forms are presented for calculation of such parameters as the longitudinal current, potential to the remote earth and potential to the adjacent earth along the pipeline. Moreover, the attempt is undertaken, to incorporate the electrode kinetics into the simulation model in which the polarization phenomenon (Tafel equation) is modeled by a non-linear resistance being iteratively calculated [5].

The efficiency of the simulation program developed is demonstrated by illustrative calculations.

Example of calculation

The rail with parameters $R = 0.02$ Ω/km and $G = 0.76$ S/km is energized at points $x_0 = -2.5$ km (substation) and $x_L = 2.5$ km (vehicle) with an unit-current. The 3D earth potential due to stray currents of the d.c. electrified railway system has been calculated at the depth 1m in the soil with the conductivity $\gamma = 0.01$ S/km. The result of calculations based on the exact method is shown in Fig.1.

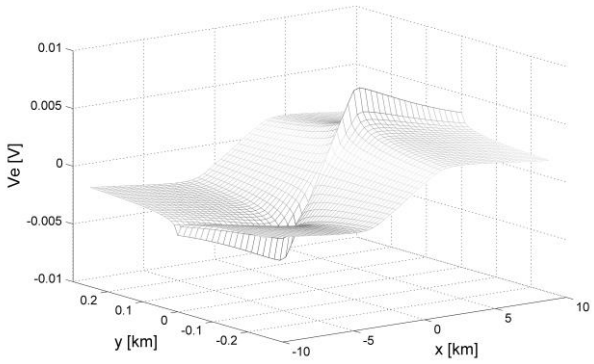

Fig.1. 3D distribution of the earth potential due to stray currents

References

[1] Bortels L., Dorochenko A., Van den Bossche B., Weyns G., Deconinck J., Three-Dimensional Boundary Element Method and Finite Element Method Simulations Applied to Stray Current Interference Problems. A Unique Coupling Mechanism That Takes the Best of Both Methods. *Corrosion*, 63 (2007), No. 6, 561–576.

[2] Sunde E. D., Earth conduction effects in transmission system, *Dover* 1968

[3] Machczyński W., Obwody ziemnopowrotne w polu elektrycznym prądów błądzących. *Przegląd Elektrotechniczny,* (2002), nr 8, 535–540.

[4] Machczyński W., Simulation model for drainage protection of earth–return circuits laid in stray currents area; *Electrical Engineering*, 84 (2002), No 3, 165–172.

[5] Czarnywojtek P., Machczyński W., Computer simulation of responses of earth-return circuits to the a.c. and d.c. external excitation. *European Transactions on Electrical Power*, 13 (2003), No. 3, 173–184.

Authors*: Wojciech Machczyński, Poznan University of Technology, ul. Piotrowo 3a, 60-965 Poznań, Poland, e-mail: Wojciech.Machczynski@put.poznan.pl*

Artur BUGAŁA, Grażyna FRYDRYCHOWICZ-JASTRZĘBSKA

Poznan University of Technology

Power Distribution in Photovoltaic Tracking Systems

Abstract. *The paper presents an analysis of DC power dynamic fluctuations in photovoltaic tracking and fixed systems for Poznań, Poland (52°24'30"N i 16°56'3"E). A measurement stand consisting of 2-axis Sun tracker and fixed unit is shown. The results of annual energy, average irradiance and insolation analysis are presented. The legitimacy of PV module positioning in local climatic conditions is described.*

Keywords: tracking system, elevation angle, photovoltaics, power distribution.

Introduction

Power generation and the amount of energy accumulated is strongly dependent on the structural and technical parameters of the PV module and it is a function of spatial orientation, latitude, declination and hour angle [1].

It is possible to increase the efficiency of solar energy systems using one - axis or two - axis tracking systems. The last allow to increase the size of power generated by the modules about 30% [2, 3], wherein recorded also 40 % - 50% energy gain [4].

The positioning of the photovoltaic receiver can be performed in an open system or in a closed system. An example of the first solution is clock positioning, in the second, the control is implemented on the basis of signals coming from external sensors.

Operation systems

The two - axis tracking system changing positions along the horizontal and vertical axis was installed at a distance of about 3 meters from the fixed system in order to ensure identical operating conditions.

In order to determine the current position of the module magnetic encoders are employed, integrated with a linear servomotor, which measure angular displacement. Electric energy transformation is realized by DC/AC microinverter with a maximum power point tracking. Power density of solar radiation was measured using two sensors based on a silicon diode as a light – sensitive element and microprocessor unit containing calibration data. The fixed system operates at a set tilt angle $\beta = 37°$ and an azimuth angle of 180° with a polycrystalline photovoltaic module of the same power as the two - axis tracking unit.

Figure 1 presents a design of a system consisting of a fixed unit and the two - axis tracking one.

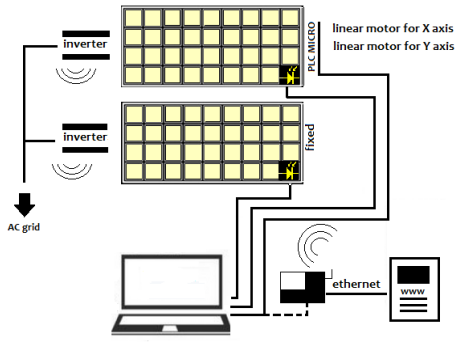

Fig. 1. A diagram of the system used for the comparative analysis of the operation of the fixed system and the two-axis tracking system

Figure 2 presents an execution of the design, including the fixed unit and the two–axis tracking.

Fig. 2. Fixed unit and two - axis tracking one with the photovoltaic module, solar radiation power density sensor and microinverter

Results of measurements

Year - long measurements of the electric energy generated by both photovoltaic systems were conducted. Cumulative energy was defined, including the energy consumed for the system's controlling and powering purposes.

Figure 3 presents monthly electric energy generation by both systems.

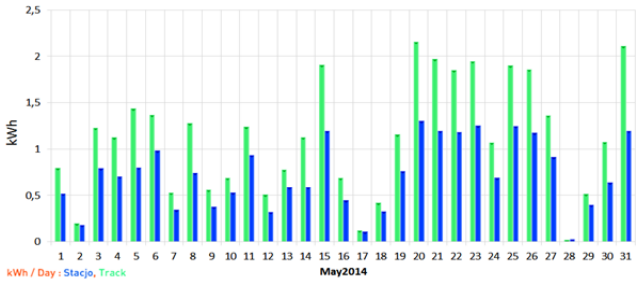

Fig. 3. Monthly electric energy generation by the two-axis tracking system and the fixed one in May, 2014

REFERENCES

[1] Teneta J., Więckowski Ł., Czasowa charakterystyka produkcji energii elektrycznej w nadążnych systemach PV, *Dissemination of the Achievements of Polish and Global Photovoltaics in the Process of Education on University Level*, Krynica Zdrój, 12–15 May 2011.

[2] Serhan M., El-Chaar L., Two axes sun tracking system: Comparsion with a fixed system, *Internetional Conference on Renewable Energies and Power Quality (ICREPQ'10)*, Granada, 2010.

[3] Frydrychowicz-Jastrzębska G., Bugała A., Sun Tracking in PV Systems Aspects, *Monograph Computer Applications in Electrical Engineering*, (2012), 333–346.

[4] German company Ingenleurbüro, Mencke & Tegtmeyer GmbH.

***Authors**: Grażyna Frydrychowicz-Jastrzębska, Poznan University of Technology, Piotrowo 3a, grazyna.jastrzebska@put.poznan.pl, Artur Bugała, Poznan University of Technology, Piotrowo 3a, artur.bugala@put.poznan.pl*

A. Kuvaldin[1], M. Strupinskiy[2], N. Khrenkov[2], M. Fedin[1], B. Antonov[1]

NRU «MPEI» (1), SST Company Group, Mytischi, Russia (2)

Parameters Analysis of Linear Inductors for the Heating of Ferromagnetic Steel Pipes

Abstract. *An analysis of electric and power parameters of linear inductors designed for pipeline heating has been performed. Modelling by using ELCUT software package made it possible to choose the optimal dimensions of the inductor and the magnetically shell. A conclusion has been made about possible application of these units for the heating of comparatively short pipelines.*

Keywords: induction heating, linear inductor, magnetically shell, electric and power parameters.

Linear inductors found an application in solving of a number of tasks of induction heating including that of long length products (tape, wire) and rotating cylindrical items. For practice, it is of interest to use linear inductors powered mainly by current of industrial frequency 50 Hz for the heating of pipelines made of ferromagnetic steel and designed for various fluids transportation. In some cases, linear inductors can compete with the units currently used for pipelines heating, such as those based on series resistance cables, induction-resistive (so called skin-systems) and others [1, 2]. To improve power parameters of the linear inductors, it is worthwhile to complete them with magnetically shell (Fig. 1).

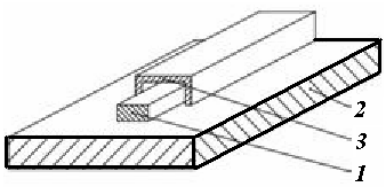

Fig. 1. System: Inductor (*1*) – magnetically shell (*2*) – ferromagnetic steel (*3*)

There are developed magnetically shell made with the use of ferromagnetic particles and bonding polymer materials which are technologically convenient for this application.

For these units' performance definition and parameters optimisation, the modelling of the system consisting of the linear inductor, magnetically shell and ferromagnetic steel has been performed by using ***ELCUT*** software package.

The input date for the modelling are: power per meter length being transferred to the ferromagnetic steel (pipe's wall) –20–70 W; pipe wall thickness b_2 = 3–5 mm; relative magnetic permeability and specific loss in the magnetically shell depending on the magnetic field strength. The data are the current frequency (50–200 Hz), the spacing between the inductor and the heated pipe b_4 = 3–5 mm and the magnetically shell dimensions.

The geometric model for the electric and power parameters calculation is shown in Fig. 2.

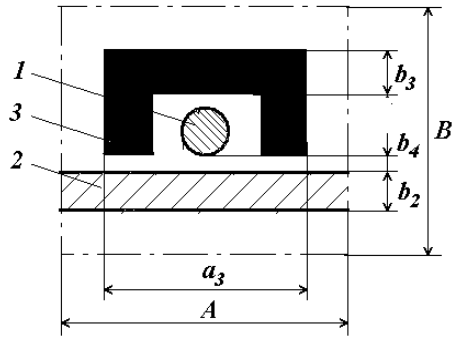

Fig. 2. Geometric model for electromagnetic calculation: *1 – inductor, 2 – magnetically shell, 3 – pipe wall*

Dependencies of the power parameters of the said inductors, including power dissipated in the inductor, magnetically shell and pipe wall, on a number of factors including the current strength, frequency, dimensions, etc. have been obtained. In particular, dependencies of electrical efficiency and cos φ obtained for definite system dimensions at the inductor currents up to 100 A are presented. The electromagnetic calculation results are used as input data for modelling of thermal modes of the inductor – magnetically shell – ferromagnetic steel system operation.

The obtained results of the researches are intended to be used (applied) in development of heating units for comparatively short (up to 30 m) pipelines.

REFERENCES

[1] Strupinskiy M., Khrenkov N., Kuvaldin A., Fedin M. Simulation of electromagnetic field in ferromagnetic steel taking into account hysteresis effect, International Symposium on Heating by Electromagnetic Sources HES-10. Padua, May 18–21, 2010, 83-89.

[2] Kuvaldin A., Strupinskiy M., Khrenkov N., Fedin M.. Development of methods for electrical and thermal calculation of induction heating systems for pipelines // The 15th International Conference on Computational Problems of Electrical Engineering, University of Zilina (Slovak Republic), 9th–12th of Sept. 2014,19.

Authors: *Kuvaldin Aleksandr, Fedin Maxim, Antonov Boris, National Research University «Moscow Power Engineering Institute», Moscow, Russia, Krasnokazarmennaya St., E-mail: kuvaldinab@mpei.ru*

Strupinskiy Mikhail, Khrenkov Nikolay, Special Systems and Technologies, Company Group, Mytischi, Moscow region, Russia, E-mail: hrenkov@sst.ru

A. KUVALDIN, M. FEDIN, R. PEROV

NRU «MPEI»

Development of The Methods for Calculating Electromagnetic Parameters of Coreless Induction Furnaces in the Melting Process of the Lumpy Charge

***Abstract**. A mathematical model for calculating of electric mode of the coreless induction furnace in the initial period of melting of the charge has been developed. Mathematical temperature dependences for heat power of a load, electrical efficiency and power factor were obtained.*

Keywords: coreless induction furnace, lumpy charge, electromagnetic calculation, mathematical model.

The initial period, when the most significant changes happen in the electrical and geometrical parameters of the charge, is the most difficult for the mathematical description of the process of melting of the charge in the coreless induction furnace (CIF).

ANSYS Maxwell package was used to solve this problem. Three-dimensional model of the "inductor-loading» (Fig. 1) was created in this package. The dimensions of the computational domain - twice overall dimensions the model. The condition of zero magnetic potential A = 0 is specified at the border of the area .

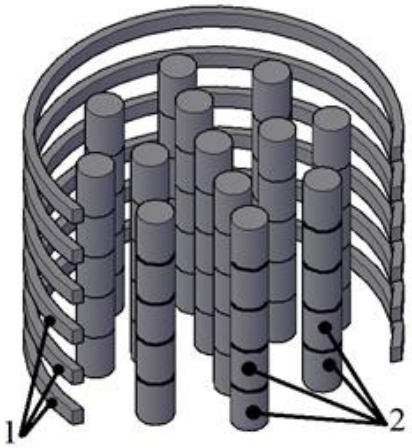

Fig. 1. Geometric model for electromagnetic calculating

The method of calculation makes it possible to break the cylinders 2 (they are located in the inductor 1) in height (Fig. 1). This allows to identify the end effects. It is possible to use cylinders of different lengths and diameters, which allows to simulate different variants of the used charge.

The selected for calculation Eddy Current enables to calculate the problem with the induced currents. In this case the grid is constructed in the load considering the depth of electromagnetic wave penetration into the material.

Heat release power in the load, the electrical efficiency and power factor depending on the temperature at various granulometric composition and properties of the charge were calculated. Fig. 2 shows the calculated power distribution of heat in the cylinders for height and radius of the "inductor – charge" system for laboratory CIF with the following parameters: power – 2 kW, the frequency – 22 KHz, the inductor internal diameter – 70 mm, the height of the inductor – 100 mm. In Fig. 2a numerals I, II, III correspond to the rows of cylinders (diameter 5 mm) of the charge (starting from the center); in Fig. 2b, the distance h is measured from the lower end of the inductor, this distance corresponds to the third, fourth and fifth cylinder in height, if you count from the bottom on Fig. 1 (for other cylinders pattern is symmetric).

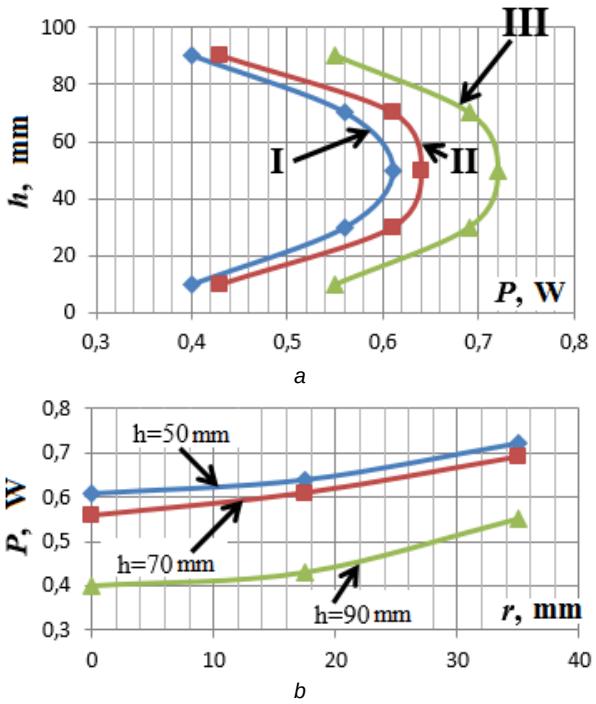

Fig. 2. Distribution of heat power in the cylinders in height (*a*) and radius (*b*)

The results are used in thermal calculation and for the development of control system of the coreless induction furnaces for melting of the lumpy charge.

REFERENCES

[1] Babat G.I. Induction heating of metals and its industrial application. M .: Energia, 1965, 552 p.

[2] Kuvaldin A.B., Fedin M.A., Alferova E.S. Mathematical modeling of the induction crucible furnace with a lump load. // Energy and Resource Saving - XXI Century / - Orel, 2014. P. 58–60.

***Authors:** Kuvaldin Aleksandr, Fedin Maxim, Perov Roman, National Research University «Moscow Power Engineering Institute», Moscow, Russia, Krasnokazarmennaya St.,14*
E-mail: kuvaldinab@mpei.ru

ORAL SESSION 5 (Tuesday 9.06.2015, 17:00 – 18:00)			
Chairman: Hartmut Brauer hartmut.brauer@tu-ilmenau.de Chairman: Dorota Stachowiak dorota.stachowiak@put.poznan.pl			
	Time	**Authors**	**Title**
1	17:00–17:20	Valeri Mladenov, Stoyan Kirilov, Georgi Tsenov	Synthesis and Analysis of a Memristor-Based Perceptron Element for Logical Function Emulation
2	17:20–17:40	Helmut Wernick, Patrick Hölzl, Bernhard Zagar	Determination of Spatial Conductivity Variations within Conductive Rubber: A Comparison of Two Methods
3	17:40–18:00	Krzysztof Lenarczyk	Work Development in Order to Reduce Losses in the Transmission System

Valeri MLADENOV, Stoyan KIRILOV

Technical University of Sofia, Bulgaria

Synthesis and Analysis of a Memristor-Based Perceptron Element for Logical Function Emulation

Abstract. *The main purpose of the present research is to propose a new memristor-based synaptic device for using in perceptron circuits and to confirm its advantages and efficiency. A serial synaptic circuit constructed by two memristors connected in opposite directions is analyzed. Voltage pulses with long duration are used for adjusting the synaptic weight. The operating binary input signals are with short duration to avoid altering the synaptic weight. A successful operation of the new memristor linear synapse is established after scaling the synaptic weights.*

Keywords: memristor; synaptic weight; perceptron; logical function.

Introduction

The artificial neural network simulates the structure, the processing methods and the system operation of biological neural system [1]. Many researches are attracted by neural networks advantages and applications – good performance, parallel processing, distributed storage, self learning, self adapting and fault tolerance. The perceptron is simplest kind of neural network, it is a nonlinear neuron and it can implement basic learning and parallel processing and also it can emulate simple logical functions. In the last few years, many scientists pay attention to memristor-based neural networks because memristor elements and circuits are capable of emulating the biological synapses by changing and retention of their state [1, 2]. The lack of analysis of a linear memristor-based synapse with two serial-biased memristors which is a new circuit and it has a novel behavior as an integrator is a precondition for the present investigations. In Section 2 a simple perceptron circuit for emulating the logical functions *OR* and *AND* is analyzed. The memristor-based serial synapse model is validated in Section 3. In Section 4 the concluding remarks are given.

A Simple Perceptron Circuit Investigation

The perceptron for emulating the logical functions OR and AND is presented in Fig. 1 [1, 2]. The current time steps number is denoted with *t*. The input signals $x_1(t)$ and $x_2(t)$ are multiplied by the initial synaptic weights $w_1(t)$ and $w_2(t)$. The weight coefficients are based on memristors, and a possibility for updating the weights exists.

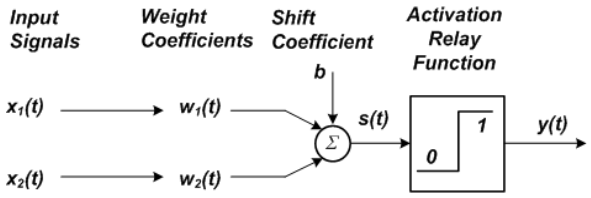

Fig. 1. Schematic of a simple classical two-input perceptron circuit

The error signal *e(t)* is obtained using the current value of the output signal *y(t)* and the desired output signal *d(t)* is evaluated with respect to the logical function *OR*. The difference between the signals *d(t)* and *y(t)* is *e(t)* [1, 2]. The error signal e(t) is then multiplied by the input signals $x_1(t)$ and $x_2(t)$, respectively and after that we obtain the correcting adjustments [1, 2]:

$$\Delta w_1(t) = e(t)x_1(t);\ \ \Delta w_2(t) = e(t)x_2(t);\ \ \Delta b(t) = e(t) \tag{1}$$

The new values of the synaptic weights and the shift coefficient are: [1, 2]:

$$w_{1new}(t+1) = w_1(t) + \Delta w_1(t);\ \ w_{2new}(t+1) = w_2(t) + \Delta w_2(t);\quad b_{new} = b_{old}(t) + \Delta b(t) \tag{2}$$

The results for the memristor perceptron are given in Fig. 2.

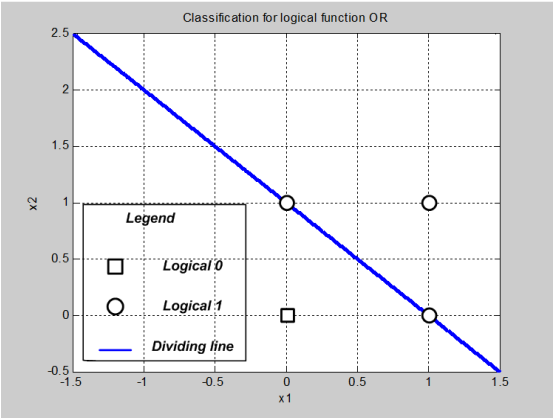

Fig. 2. The classification result of the adjusted perceptron for emulation the logical function OR

A Simple Memristor-Based Synaptic Circuit

The schematic of the new memristor-based synapse device is presented in Fig. 3. It consists of two serial-connected memristors in opposite directions.

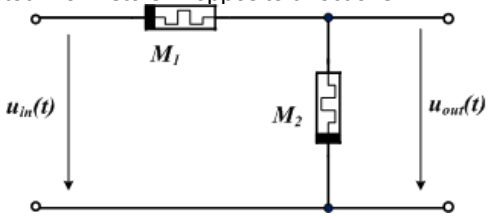

Fig. 3. Memristor-based serial synapse circuit

The synaptic weight of the memristor-based synapse is:

$$w = \frac{M_2}{M_1 + M_2} = \frac{\mu R_{ON}}{D^2}\int_{t_0}^{t} idt' = k\int_{t_0}^{t} idt' = \frac{k}{R_{ON} + R_{OFF}}\int_{t_0}^{t} udt' \tag{3}$$

Conclusion

The new memristor series circuit acts as integrator and successfully emulates the synaptic bonds in the neural networks, the synaptic weight is adjusted easy by rectangular voltage pulses.

REFERENCES

[1] Fausett, L. Fundamentals of Neural Networks. Prentice Hall, 1994, ISBN 0130422509.

[2] M.Sah, C. Yang, H. Kim, T. Roska, L. Chua. Memristor Bridge Circuit for Neural Synaptic Weighting. (CNNA), IEEE, pp. 1 – 5, DOI: 10.1109/CNNA.2012.6331434, 2012.

***Authors**: Valeri Mladenov, Stoyan Kirilov, Technical University of Sofia, 1000 Sofia 8 St. Kl. Ohridski Blvd, Department. of Theoretical Electrical Engineering, E-mails: valerim@tu-sofia.bg, s_kirilov@tu-sofia.bg*

Helmut WERNICK, Patrick HÖLZL, Bernhard ZAGAR

Johannes Kepler University Linz

Determination of Spatial Conductivity Variations within Conductive Rubber: A Comparison of Two Methods

***Abstract**. In this contribution, two different measurement methods to analyze the spatial distribution of the conductivity of a conductive rubber specimen are presented. More precisely, one indirect method, namely magnetic field tomography combined with thermography, and one direct measurement method are examined.*

Keywords: magnetic field tomography, inverse problems, electrical conductivity measurement.

Introduction

Elastomer composites are filled with carbon black particles in order to enhance the mechanical properties like stiffness, flexibility, wear resistance, UV resistance and more. By also adding highly conductive carbon black particles (CCB), rubber also gains significant electrical conductivity. The homogeneity of the spatial distribution of the conductivity within the rubber is vital for the fabrication of sensors, actuators or flexible heating pads from this type of rubber. In this study, the spatial conductivity distribution of a vulcanized natural rubber specimen with 31 phr (parts per hundred rubber) CCB content is analyzed. Two different methods are utilized and compared for their results and effectiveness.

Sample preparation

For an initial analysis, a specimen consisting of natural rubber and highly conductive carbon black of the type Ketjenblack EC – 300J (KB300) from AkzoNobel Chemicals, Netherlands, was manufactured. The specimen has a total size of 200 x 450 x 1.7 mm³ and was vulcanized in a hot molding press. In order to establish an electrical contact, on both small sides of the specimen a bare steel wire was inserted before the vulcanization process. The homogeneity of the material is mainly influenced by parameters of the production process. The spatial conductivity distribution correlates to the homogeneity of the material and the CCB particle distribution within.

Measurement setup

For both methods, a three axis translation stage is used to scan over the specimen. An NI-6221 data acquisition card, which samples synchronized with the movement of the translation stage, is used for conditioning and digitizing the sensors signals. The first method utilizes a magnetic field image combined with a thermal image to determine the local value of the conductivity. The second method directly measures the local resistance of the specimen. An approximate isotropic behavior in z – direction is assumed in both cases.

Method 1

The first method is based on magnetic field measurements in a plane above the current carrying specimen, utilizing a giant magneto resistance (GMR) sensor NVE AA005-02. The sensor scans above the specimen in a known distance z to measure the magnetic field components $H_x(x,y)$ and $H_y(x,y)$. The underlying current density vector $\vec{J}(x,y)$ can be derived by solving the inverse problem from the law of Biot – Savart by a deconvolution approach utilizing the Lucy – Richardson algorithm [1]. Due to the small thickness of the specimen, the z – component of the current density is considered in contrast to the other dimensions negligible and therefore $J_z(x,y)\approx 0$.

The stationary temperature $T(x,y)$ on the specimens surface measured via its thermal radiation signature is a measure for the spatial convective loss density per unit area $q(x,y)=h\ (T(x,y)-T_\infty)$, which equals the local power dissipation density per unit area $p_v=\int \vec{J}\vec{E}dz$ produced in the depth of the specimen, when driven by a current density $\vec{J}$. The spatial distribution of conductivity $\sigma(x,y)$ is then given, after applying the results for the local current density $\vec{J}(x,y)$ from the deconvolution algorithm described before, by:

$$\sigma(x,y) = \int \frac{\left|\vec{J}(x,y)\right|^2}{h(T(x,y)-T_\infty)} dz \qquad (1)$$

where: h – heat transfer coefficient calculated from the Nusselt number [2], $T(x,y)$ – measured temperature rise, dz – integration path along the deepth – direction, T_∞ – ambient temperature.

Method 2

The second method is designed to measure via a four – terminal sensor tip, equipped with a guard ring to electrically isolate the surrounding surface elements, directly the local resistance $R_z(x,y)$ along the z – direction on a grid with a 4 mm spacing. With these series of measurements the local conductivity is calculated from:

$$\sigma_Z(x,y) = \frac{l}{R_Z(x,y)A}\ , \qquad (2)$$

where $R_z(x,y)$ – measured resistance, A – active area of the sensor tip, l – (local) thickness of the specimen.

Results

The Fig. 1a, b show the measurement results. Both methods give approximately the same conductivity reading. Better spatially resolved results are obtained by method 1, but requiring more computational power and higher mechanical accuracy than method 2. Method 2 has lower spatial resolution, which is principally limited by the tip size.

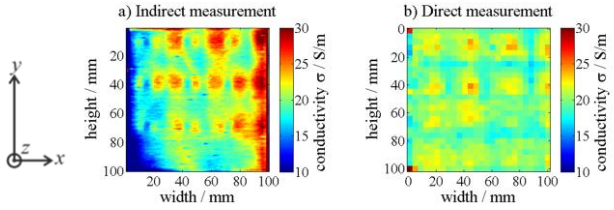

Fig.1. Computed conductivity of the specimen by (a): magnetic field deconvolution combined with thermal imaging; (b) direct measurement

REFERENCES

[1] Hölzl P., Deconvolution of High-Resolution Magnetic Field Scans for Improved Current Density Imaging, *IEEE Trans. Magn*., 50 (2014), No. 2, 101–104.

[2] Holmann J. P., Heat Transfer, 7th Ed., *McGraw-Hill 1992.*

***Authors**: Helmut Wernick, helmut.wernick@jku.at, Patrick Hölzl, patrick.hoelzl@jku.at, Bernhard Zagar, bernhard.zagar@jku.at, Johannes Kepler University, Altenbergerstr. 69, AT-4040 Linz*

POSTER SESSION 3
(Wednesday 10.06.2015, 8:40 – 10:10)

Chairman: Eugenio Costamagna eugenio.costamagna@unipv.it
Chairman: Michał Zeńczak michal.zenczak@zut.edu.pl

	Authors	Title
1	Luo Hanwu, Cheng Peng, Liu Haibo, Kang Kai, Yang Fan, Yang Qi	Investigation of Contact Resistance Influence on Power Cable Joint Temperature Based on 3-D Coupling Model
2	Luo Hanwu, Fan Lingqiang, Liu Haibo, Kang Kai, Yang Fan	Investigation on the Electromagnetic Transient of Parallel Transmission Lines Considering the Interference from Magnetic Storm
3	Degui Yao, Jiajia Hu, Xiaokuo Kou, Manling Dong, Fan Yang	A Novel Potential Measurement Method Based on 16-channel Automatic Circularly Switching Control Principle
4	Yuelong Jia, Li Hao, Zhengjun Shi, Haojun Zhu, Jiansheng Yuan	Simplified Method for Computing Reactance in the Design of Saturated-Core Superconducting Fault Current Limiter
5	Przemyslaw Lopato	Automatic Defect Recognition for Pulsed Terahertz Inspection of Dielectric Composite Materials
6	Maciej Włodarczyk, Andrzej Zawadzki, Sebastian Różowicz	Fractional Models of Selected Combustion Engine Ignition Systems
7	Sebastian Różowicz, Szymon Tofil	The Influence of Impurities on the Operation of Selected Fuel Ignition Systems in Combustion Engines
8	Paolo Di Barba, Fabrizio Dughiero, Michele Forzan, Elisabetta Sieni	A Novel NSGA-Inspired Optimization Algorithm for the Design of Electromagnetic Devices and Application in MFH
9	Mykhaylo Zagirnyak, Viktoriya Kovalchuk, Tetyana Korenkova	Identification of Parameters of Electrohydraulic Complex with Periodic Nonlinear Processes in the Pipeline Network
10	Nikolai Khrenkov, Mikhail Strupinskiy	Electric Field Strength in a Skin-Effect Based Heater
11	Milena Kurzawa, Wiesław Łyskawiński, Rafał M. Wojciechowski	Measurement Verification of a Field-Circuit Model of the Wireless Energy Transmission System
12	Grzegorz Psuj, Barbara Szymanik	Fatigue Monitoring of Steel Structures Using Electromagnetic and Infrared Thermography Inspection Methods
13	Dong Manling, Hu Jiajia, Yao Degui, Kou Xiaokuo, Yang Fan	The Sensitivity Fault Diagnosis Method of Grounding Grid Based on LSQR Regularization Algorithm
14	Marcin Ziolkowski, Stanislaw Gratkowski	Genetic Algorithm Coupled with Bézier Curves Applied to the Magnetic Field on a Solenoid Axis Synthesis
15	Tomasz Chady, Ryszard Sikora,, Piotr Baniukiewicz, Leszek Misztal, Paweł Waszczuk	Multi-sensor System for NDT of Welded Elements Exploited in Aircraft Industry
16	David Panek, Vaclav Kotlan, Roman Hamar And Ivo Dolezel	Optimization of Inductor for Pre-Heating Material Before its Laser Welding
17	Krzysztof Stawicki, Beata Szuflitowska, Marcin Ziółkowski	Recent Simulation Results of the Magnetic Induction Tomography Forward Problem
18	Damian Mazur, Piotr Maciąg	Current Adjuster for Frequency Converter

Hanwu LUO[1], Peng CHENG[2], Haibo LIU[1], Kai KANG[1], Fan YANG[2], Qi YANG[2]

East Inner Mongolia Electric Power Company Limited (1), Chongqing University (2)

Investigation of Contact Resistance Influence on Power Cable Joint Temperature Based on 3-D Coupling Model

Abstract. *Aiming at the overheating problem of cable joint, a 3-D finite element model of a single-core cable joint considering the coupling of electromagnetic field and temperature field has been built. In order to consider the heat losses generated by contact resistance of cable joint, the equivalent conductivity is calculated. The validity of the model and calculation method is verified by the comparison with analytical values.*

Keywords: cable joint, electromagnetic field, temperature field, contact resistance.

Introduction

As the weakest link of power cable, overheat of cable joint can lead to open circuit, short circuit, even fire and explosion of power cable [1]. Therefore, temperature is an important indicator to reflect that the operation state of cable joint is good or not.

In previous studies, many scholars focus on the temperature field and ampacity using 2-D model of cable body [2]. However, the 2-D model is not suitable to analyze the temperature property of cable joint, due to the heat transfer in radial direction and in axial direction should be taken into consideration.

In this paper, a 3-D electromagnetic-thermal coupling analysis model of cable joint is investigated and validated.

Methodology

The magnetic vector potential equation can be described as

$$(\nabla\cdot\frac{1}{\mu}\nabla)\boldsymbol{A}=-\boldsymbol{J}_s+j\omega\sigma\boldsymbol{A} \tag{1}$$

where: μ – permeability, $\boldsymbol{A}$ – magnetic vector potential, σ – electrical conductivity, $\boldsymbol{J}_s$ – current density, ω – angular frequency.

σ can be expressed by the following equation.

$$\sigma=\frac{\sigma_{20}}{1+\alpha(T-20)} \tag{2}$$

where: σ_{20} – electrical conductivity at 293.15 K, α – temperature coefficient, T – temperature.

The associated steady-state heat conduction equation can be described by the following equation.

$$\nabla\cdot(\lambda\nabla T)+Q_v=0 \tag{3}$$

where: λ – thermal conductivity, Q_v – heat source per unit volume.

The equivalent conductivity can be expressed as:

$$\sigma_2=\frac{\sigma_1}{k}\cdot\left(\frac{r_1}{r_2}\right)^2 \tag{4}$$

where: σ_1 – electrical conductivity of cable conductor, σ_2 – equivalent electrical conductivity, r_1 – radius of cable conductor, σ_2 – equivalent electrical conductivity; r_2 – outer radius of the connection tube, k – ratio.

The Q_v can be calculated as follows:

$$Q_v=\frac{1}{\sigma}|\boldsymbol{J}|^2 \tag{5}$$

Example Calculation and Validation

When $\boldsymbol{J}_s$ is 645A and k is 5, the temperature distribution is calculated, as shown in Fig.1.

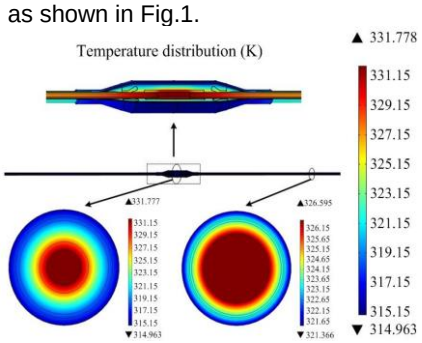

Fig. 1. 3-D temperature distributions of cable joint

The calculated results are compared with the analytical results.

Discussion

The influence of contact resistance on the thermal property of cable joint is shown in Fig. 2.

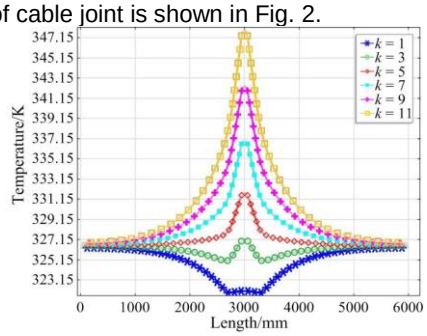

Fig. 2. Axial temperature field distribution curves with k

Conclusion

The results show that the existence of the contact resistance can result in increasing the electromagnetic loss and temperature rise of cable joint.

REFERENCES

[1] Yomna O, et al., Thermal modeling of medium voltage cable terminations under square pulses, IEEE Trans. Dielectr. Electr. Insul., Vol. 21, no. 3, pp. 932–939, Jun. 2014.

[2] George J, et al, Ampacity calculation for cables in shallow troughs, IEEE Trans. Power Del., Vol. 25, no. 4, pp. 2064–2072, Oct. 2010.

***Authors**: Cheng Peng, the State Key Laboratory of Power Transmission Equipment & System Security and New Technology, School of Electrical Engineering, Chongqing University, Chongqing 400044 China, e-mail: chengpeng19870825@163.com*

Hanwu LUO[1], Lingqiang FAN[2], Haibo LIU[1], Kai KANG[1], Fan YANG[2]

East Inner Mongolia Electric Power Company Limited (1), Chongqing University (2)

Investigation on the Electromagnetic Transient of Parallel Transmission Lines Considering the Interference from Magnetic Storm

Abstract. *Tremendous change of earth's magnetic field caused by the solar activity is called magnetic storms. When storms occur, the electric field, which is produced by time-varying magnetic field on the ground, produces the geomagnetic induced current (GIC) by the circuit which is made up of the power lines, transformers and the ground. In general, the frequency of GIC is 0.0001-0.01 Hz. If the quasi-DC current flows AC/DC parallel lines on the same tower, it will have some adverse impact on the over-voltage of system, secondary arc current and other electromagnetic transient problems*

Keywords: magnetic storms, AC/DC parallel lines, GIC, electromagnetic transient introduction.

Introduction

Geomagnetic storm disturbance can cause earth space irregular changes in the magnetic field strength and direction. The time-varying magnetic field produce frequency of 0.0001Hz~0.01Hz induction electromotive force in transmission line, which is harmful to the safety of the operation of power grids [1].

In this paper, firstly, the coupled interference relationship of magnetic storms and power lines are analyzed; secondly, based on AC/DC parallel transmission line model which considers the coupling interference, the influence rule of magnetic storms on electromagnetic transient characteristics of AC/DC parallel transmission line is researched.

Methodology

When the change rate of geomagnetic field level component (d$\boldsymbol{H}$/dt) is known, the excitation current $\boldsymbol{J}_c$ in the model can be calculated by the following equation.

(1) $$\oint_l \frac{\partial \boldsymbol{H}}{\partial t} \cdot dl = \frac{\partial}{\partial t} \int_s \boldsymbol{J}_c \cdot dS$$

Thus, according to D'Alembert equation and induction control equations [2], the induced current density $\boldsymbol{J}_0$ in the conductor can be calculated as followings.

(2) $$\begin{cases} \nabla^2 \boldsymbol{A} - \mu\varepsilon \dfrac{\partial^2 \boldsymbol{A}}{\partial t^2} = -\mu \boldsymbol{J}_c \\ \nabla^2 \phi - \mu\varepsilon \dfrac{\partial^2 \phi}{\partial t^2} = -\dfrac{\rho}{\varepsilon} \end{cases}$$

(3) $$\begin{cases} \nabla \times (\mu_0^{-1} \mu_r^{-1} \boldsymbol{B}) + \boldsymbol{J}_0 = \boldsymbol{J}_e \\ \sigma \dfrac{\partial \boldsymbol{A}}{\partial t} - \sigma \boldsymbol{V} \times \boldsymbol{B} = \boldsymbol{J}_0 \\ \boldsymbol{B} = \nabla \times \boldsymbol{A} \end{cases}$$

Results

Table 1. The coupling relationship of space time-varying magnetic field with a single loop overhead lines

Magnetic field gradient （nT/s）	Excitation source (A/(m^2.s))	The coupling current （A）
1.6	0.00255	2.41
0.8	0.00127	1.25
0.4	0.000637	0.68
0.2	0.000318	0.35

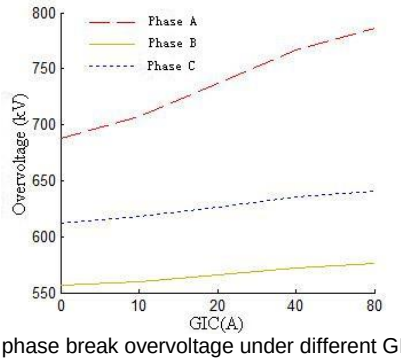

Fig. 1. Three phase break overvoltage under different GIC

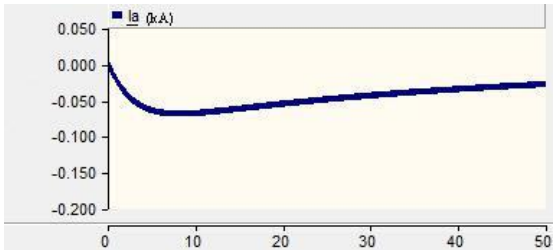

Fig. 2. Secondary arc current of transmission line under the geomagnetic storm disturbance GIC 80 (A)

Conclusion

First, as the increase of the GIC caused by the geomagnetic storm, the change of the three-phase break overvoltage is acute. When the geomagnetic storm GIC is 80A, three-phase break overvoltage increases above 10%. Second, when geomagnetic storm occurs, the biggest offset value increases and the time to reply balance is long, which may lead to the failure of circuit reclosing.

REFERENCES

[1] Boteler D. H., et al., The effeets of geomagnetic distuthances on electrical systems at the Earth's surface, Advances Space Research, vol.2, no.2, pp.17–27, 1998.

[2] S.W. Kim, et al. Coupled Finite-element-Analytic Technique for Prediction of Temperature Rise in Power Apparatus, IEEE Transactions on Magnetics, vol.38, no.2, pp.921–924, 2002.

***Authors**: Fan Lingqiang, the State Key Laboratory of Power Transmission Equipment & System Security and New Technology, School of Electrical Engineering, Chongqing University, Chongqing 400044 China, e-mail: flq372390822@163.com*

Degui YAO[1], Jiajia HU[2], Xiaokuo KOU[1], Manling DONG[1], Fan YANG[2]

State Grid Henan Electric Power Corporation Research Institute, China (1), Chongqing University (2)

A Novel Potential Measurement Method Based on 16-channel Automatic Circularly Switching Control Principle

Abstract. *This paper proposes a novel potential cycle measurement method based on 16-channel automatic circularly switching control principle of the resistance network. 1,680 valid potential data and 1,560 effective branch voltage data can be collected by this method through only 16 accessible node downleads on the grounding grid, which can maximize the use of limited accessible node downleads. A much more accurate result of grounding grid corrosion diagnosis can be obtained by using these plenty of valid voltage data.*

Keywords: potential, 16-channel, cycle measurement, grounding grids.

Introduction

Grounding grid has a pivotal role in power systems, and the research on its corrosion diagnosis has always been a research topic. In order to diagnose the corrosion of the grounding gird, the electromagnetic field theory and the electric circuit theory are widely used in this area[1]. When using electric circuit theory, an underdetermined equation that describes the nonlinear relationship between branch resistance and node voltage will be established and solved[2]. In order to obtain an accurate solution for this underdetermined equation, plenty of data is necessary. However, there is still no a good solution so far.

In this paper, a potential measurement method based on 16-channel automatic circularly switching control is proposed. Through this method, enough valid potential data can be attained, and it can be used for the corrision diagnosis of the grounding grid, both the laboratory test and field test proved that a much more accurate solution can be obtained from adequately large data.

Measurement methodology

Randomly choose 16 accessible node downleads of the grounding grid, circularly make two of the nodes as the channel that the excitation current inflow and outflow of the grounding grid according to P_1-P_2, P_1-P_3, P_1-P_4 ... P_1-P_{16}; P_2-P_3, P_2-P_4 ... P_2-P_{16}; P_3-P_4 … P_3-P_{16}; ...; P_{15}-P_{16} (where Px represents node x, as shown in Fig.1), and the remaining 14 nodes as the potential measurement nodes, thus according to the mathematical combination principle, $C_{16}^{2}=120$ groups of potential voltages will be obtained by only 16 nodes through only one measurement. In addition, there are 14 effective node potentials in each group of data; so the total number of effective node potential data is 120 × 14 = 1,680. When choosing the node whose node number is 16 as the common zero potential reference node for all potential data, there will be 13 effective branch voltage data in each group; That is to say, 120 × 13 = 1,560 branch voltage data can be obtained through a single measurement just by using only 16 accessible node downleads.

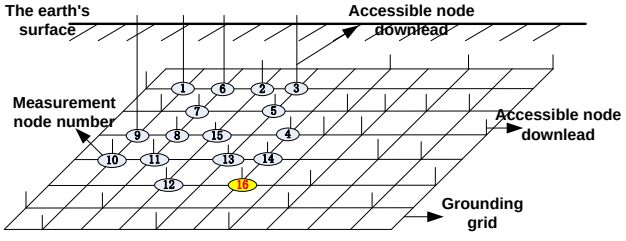

Fig. 1. The measurement schematic

Measurement system setup and test

The design, implementation and testing of the system are explained in this part. The system mainly includes the excitation current source module and the current switching module. The excitation current source module has an output current of 1A, with error less than ±0.15%; the current switching module consists of multi-channel analog switches, triodes and relays, and it is used to adjust the node's location of current injected and outflow. In order to confirm the accuracy of the measured data, a contrast was performed between the measured and simulated experiments. Part of the contrast results are shown in Table 1.

Table 1. Part of the contrast results

Device measured data/mV	Computer simulated data/mV	The measurement error/mV	The percentage error
237.80	237.76	0.04	0.0168%
246.67	245.10	1.57	0.641%
252.83	252.20	0.63	0.250%
251.11	250.13	0.98	0.392%
258.61	257.92	0.69	0.268%
258.99	256.23	2.66	1.04%
245.94	245.13	0.81	0.330%
251.38	250.63	0.75	0.300%
251.16	251.06	0.10	0.040%
...	…	…	…

Conclusion

From the results presented in part III we can see that, the error of measured data and simulation data is about 1%, which can meet the minimum permissible error of general algorithm requirements to data error. To prove the necessity of plenty of data when solving the underdetermined equations, the laboratory test and field test was performed, and accurate diagnosis results can be obtained when using large amount of data while not when using little data.

This work is supported by State Grid Henan Electric Power Corporation Research Institute, China.

REFERENCES

[1] Colominas, et al., Computer Analysis of Earthing Systems in Horizontally or Vertically Layered Soils, *Electric Power Systems Research*, 59 (2001), No. 3, 149–156.

[2] Lawson V.R., Problems and Detection of Line Anchor and Substation Ground Grid Corrosion, *Industry Applications, IEEE Transactions on*, 24 (1988), No. 1, 25–32.

***Authors**: Degui Yao, State Grid Henan Electric Power Corporation Research Institute, Zhengzhou, Henan Province, China, E-mail: yaodegui@263.net*

Jiajia Hu, Chongqing University, Chongqing, China, E-mail: huji_fish@qq.com

Yuelong JIA[1], Li HAO[1], Zhengjun SHI[2], Haojun ZHU[2], and Jiansheng YUAN[1]

Department of Electrical Engineering, Tsinghua University (1), Grid Planning & Research Centre, Guangdong Power Grid Corporation (2)

Simplified Method for Computing Reactance in the Design of Saturated-Core Superconducting Fault Current Limiter

Abstract. *The saturated-core superconducting fault current limiter (SCSFCL) can limit current when short-circuit fault occurs. But in steady state of power grid, it should have low reactance. So its core maintains deeply saturated by large bias DC excitation. Generally, the computation process of its steady-state reactance consume much time and may lead to large error due to nonlinear solution. Noting that the deep saturation region of B-H curve is nearly a straight line, a simplified method is presented in this paper. The nonlinear problem is converted to a linear one by using the concept of equivalent permeability. Furthermore, the computation method can even be simplified as static-magnetic-field computation, when the eddy current effect in the cores and structure parts is ignored. The computation result shows this simplified method meets the engineering design requirements.*

Keywords: dynamic permeability, reactance design, saturated core, superconducting fault current limiter.

Introduction

The saturated-core superconducting fault current limiter (SCSFCL) is an effective means of limiting the short-circuit fault current. The principle structure is shown in Fig. 1. In steady state of the power grid, its core maintains deeply saturated by large bias current in the superconducting DC coil and the reactance of the AC coils is low, so that the grid is not affected. When short-circuit fault occurs, high voltage pulses will be induced on the SCSFCL to limit fault current.

Among these two working states, only the steady-state reactance is the basic indicator for structure design. This is because the structure requirements for two working states are opposite to each other and the limiting-state reactance is closely related to the particular installation location.

Generally, nonlinear model with both DC and AC excitation is used for computing steady-state reactance and is solved in time domain [1]. However, such method consumes a lot of time and may lead to large error due to the nonlinear solution. A simplified computation method based on equivalent linear permeability is presented.

Simplified method to compute steady-state reactance

The deep saturation region of B-H curve, like P_1-P_2 part in Fig. 2, can be regarded as a straight line with constant slope [2]. Based on this, the computation can be simplified.

Magnetic field in AC coils can be divided into two parts:

(1) $$H(t) = H_{DC} + H_{AC}(t),$$

(2) $$B(t) = B_{DC} + B_{AC}(t),$$

where H_{DC} and B_{DC} are magnetic field excited only by DC coil when current in AC coils is 0, and $H_{AC}(t)$ and $B_{AC}(t)$ are the changing part when AC current in AC coils is added. Obviously, $H_{AC}(t)$ and $B_{AC}(t)$ are key to computing reactance.

As the B-H curve can be expressed as $B(t)=f[H(t)]$, combine (1)-(2) and apply Taylor expansion to the right part:

(3) $$B_{DC} + B_{AC}(t) = f[H_{DC}] + f'[H_{DC}]H_{AC}(t) + \frac{f''[H_{DC}]}{2}H_{AC}^2(t) + \ldots.$$

Considering $B_{DC}=f[H_{DC}]$ and $f''[H_{DC}]=f'''[H_{DC}]=\ldots=0$, so:

(4) $$B_{AC}(t) = f'[H_{DC}]H_{AC}(t),$$

which means $H_{AC}(t)$ and $B_{AC}(t)$ are in linear relationship. An AC B-H curve can be defined as B_{AC}-H_{AC} in the new coordinate system $B_{AC}0'H_{AC}$ shown in Fig. 2, where P_1-P_2 part is a straight line passing origin 0'. So the computation of $H_{AC}(t)$ and $B_{AC}(t)$ becomes a linear problem with an equivalent permeability $f'[H_{DC}]$ for cores, which is the slope of P_1-P_2 part and also the dynamic permeability. Certainly, in the computation of $H_{AC}(t)$ and $B_{AC}(t)$, DC coil is removed.

In fact, $H_{AC}(t)$ is not strictly sinusoidal due to variation of static permeability of cores when AC excitation waves. But, as the static permeability of cores maintains much higher than that of the air, the leakage flux changes little with the variation of AC excitation. So $H_{AC}(t)$ is almost in linear relation with AC excitation current, meaning that $H_{AC}(t)$ is nearly sinusoidal. Based on the above analysis, $B_{AC}(t)$ is also nearly sinusoidal. So the problem becomes a sinusoidal steady one and can be solved by phasor method.

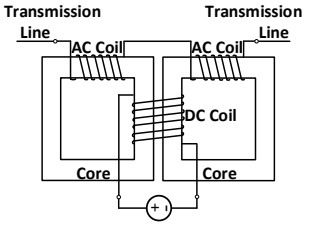

Fig.1. Structure of SCSFCL

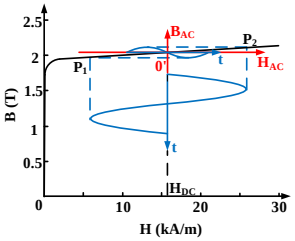

Fig.2. B-H curve and waveforms

Considering that the eddy current in laminated cores and structure parts is small enough to be ignored, the method can be further simplified as a static-magnetic-field linear-model solution. For a linear model without eddy current, its inductance is constant and unchanging with frequency. So a DC current with arbitrary value can be added to AC coils and the inductance can be obtained from magnetic energy, and the reactance can be got directly.

Computation example

An SCSFCL is simulated with ANSYS Maxwell by the three methods. The parameters are omitted here. The reactance computed by the time-domain nonlinear model, the frequency-domain linear model and the static-magnetic-field linear model are 0.380Ω，0.363Ω and 0.363Ω .

Conclusions

1) It is not necessary to employ nonlinear model or to compute in time domain for the design computation of steady-state reactance of the SCSFCL.

2) Considering the deep saturation region of B-H curve is nearly a straight line, computation of the reactance can be simplified as a static-magnetic-field linear-model solution.

REFERENCES

[1] Y. Nikulshin et al., Dynamic core length in saturated core fault current limiters, *Superconductor Science and Technology*, 26 (2013), No. 9, 095013.

[2] C. Zhao et al., Transient Simulation and Analysis for Saturated Core High Temperature Superconducting Fault Current Limiter, *IEEE Trans. Magn.*, 43 (2002), No. 4, 1813-1816.

***Authors**: Yuelong Jia, Dept. of Electrical Engineering, Tsinghua University, Beijing 100084, P.R. China, rhinestone@163.com*

Przemyslaw LOPATO

West Pomeranian University of Technology, Szczecin

Automatic Defect Recognition for Pulsed Terahertz Inspection of Dielectric Composite Materials

Abstract. *Condition of polymer composite materials can be evaluated using time domain terahertz technique. This method provides spectroscopic information about measured object, thus opposite to radiographic techniques, it is possible to recognize a type of defect only based on single point measurement, without any information about its vicinity. Automatic defect recognition scheme (using this principle) will be presented in this paper. New features based on measured signals will be also proposed.*

Keywords: nondestructive testing, automatic defect recognition (ADR), terahertz testing.

Introduction

Application of polymer composites in aerospace and renewable energy industries is constantly growing. That is the reason for development of accurate and easy to automate nondestructive evaluation methods. Terahertz technique using electromagnetic waves in 0.3–10 THz frequency range seems to be a good candidate for this task [1–4]. This method provides spectroscopic information about measured object, thus it is possible to recognize a type of defect only based on single point measurement, without any information about its vicinity (opposite to radiographic techniques). Terahertz inspection with pulsed excitation is reported as a source of many useful information about the internal structure of the dielectric material [1–5].

Automatic defects recognition algorithm

The block scheme of automatic defects recognition algorithm for terahertz inspection of composite materials is presented in Fig. 1. The task of preprocessing stage is to enhance the signal and reduce the noise without destroying the important features for diagnosis. In the proposed scheme, signal preprocessing consists of time domain median filtering and registration of B-scan signals using algorithm presented in [6]. The profile of curved surfaces is approximated in order to preserve information about its local variations caused by surface defects (e.g. impacts of high energy). Next step is features calculation. Based on enhanced signals – time, frequency and joint time-frequency domain features are calculated. As an example, an influence of defect on frequency response is presented in Fig. 2.

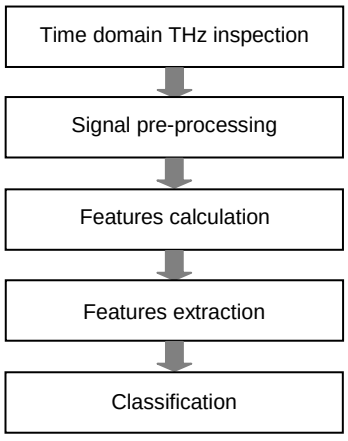

Fig. 1. Block scheme of automatic defects recognition algorithm for terahertz inspection of composite materials

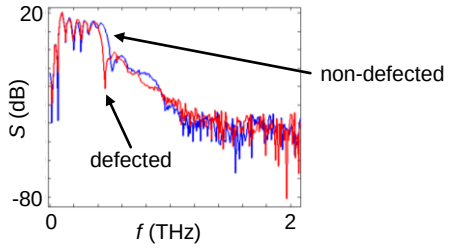

Fig. 2. Comparison of frequency response in case of defected and healthy area.

Principal component analysis is utilized as features extraction algorithm. This operation noticeably reduces feature space dimension. Because of their high accuracy [7], multilayered artificial neural networks are utilized as supervised classifiers.

More detailed ADR algorithm description and exemplary results of terahertz inspection and defects identification will be provided in full paper.

This work was supported in part by European Commission project HEMOW: Health Monitoring of Offshore Wind Farms (reference: FP7-PEOPLE-2010-IRSES-GA-269202)..

REFERENCES

[1] Mittelman D. (Ed.), Sensing with terahertz radiation, Berlin, 2010.

[2] Stoik C., Bohn M., Blackshire J., Nondestructive evaluation of aircraft composites using reflective terahertz time domain spectroscopy, *NDT&E International*, 43 (2010), 106–115.

[3] Lopato P., Chady T., Terahertz detection and identification of defects in layered polymer composites and composite coatings, *Nondestructive Testing and Evaluation*, Vol. 28, Iss. 1, (2013).

[4] Jin Y.S., Kim G.J., Jeon S.G., Terahertz dielectric properties of polymers, *Journal of the Korean Physical Society*, Vol. 49, no. 2, August 2006, 513–517.

[5] Yin X., Ng B. W.-H., Fischer B. M., Ferguson B., Abbott D., Support Vector Machine Applications in Terahertz Pulsed Signals Feature Sets, IEEE Sensors Journal, Vol. 7, no. 12, (2007).

[6] Lopato P., Chady T., Gorący K.: Image and signal processing algorithms for THz imaging of composite materials, *Review of Progress in Quantitative Nondestructive Evaluation,* Vol. 29a–29b, Vol. 1211, 2010, pp. 766–773.

[7] Kotsiantis S. B., Supervised Machine Learning: A Review of Classification Techniques, *Informatica*, no. 31, 2007, pp. 249–268.

***Author**: Przemyslaw Lopato e-mail: plopato@zut.edu.pl, West Pomeranian University of Technology, Szczecin, al. Piastow 17, Szczecin, Poland*

Maciej WŁODARCZYK, Andrzej ZAWADZKI, Sebastian RÓŻOWICZ

Kielce University of Technology

Fractional Models of Selected Combustion Engine Ignition Systems

Abstract*. This paper attempts to introduce a quasi-inductive element into ignition system and describe it by fractional order equation. Two typical systems have been studied and numerical analysis has been conducted.*

Keywords: ignition system, fractional order derivatives, transient states.

Introduction

Ignition systems of modern vehicles are modeled by electrical circuits whose mathematical description is given by nonlinear equations. Studies on the dynamics of ignition systems are hard and results of analysis and digital simulation differ from the experimental ones. In our paper an attempt has been made to introduce quasi-inductive element L^{α} into a model of the ignition system and describe it by fractional order equation.

Fractional models of ignition systems

Generally, ignition systems can be represented as systems with energy storage in inductance and the ones with energy storage in capacitance [1]. Replacing the inductive element (ignition coil) with L^{α} element we obtain two models shown in Figure 1.

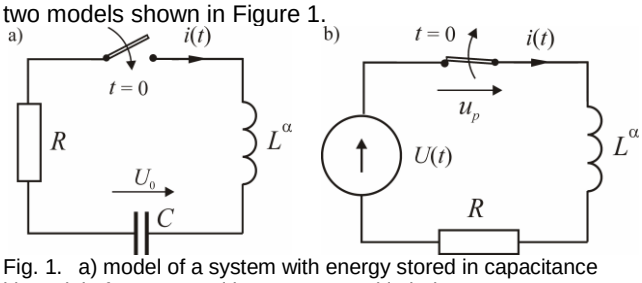

Fig. 1. a) model of a system with energy stored in capacitance b) model of a system with energy stored in inductance

Analysis of transient state and digital simulations

Two systems presented in Fig.1 are analyzed. System 1a can be written as:

$$u(t) + Ri(t) + L\,{}_0^C D_t^{\alpha} i(t) = 0; \quad u(t) = \frac{1}{C}\int i(t)dt + U_0, \tag{1}$$

where: $u(t)$ capacitor voltage, ${}_0^C D_t^{\alpha} f(t)$ - derivative of non-integer order α, according to Caputo definition [2, 3].
Reducing the set into one equation with respect to i(t) and using Laplace transformation [4] we obtained current transform

$$I(s) = -CU_0 / [Cs(Ls^{\alpha} + R) + 1]. \tag{2}$$

To determine inverse transform a continued fraction expansion (CFE) metod [4] was applied. Accordlingly, for fifth-order approximationl (5A) we obtained current series for $\alpha = 0.9, 0.8, 0.5$ and compared them to the ones in classical circuit *RLC*.

The system presented in Fig. 1b models transient state for a switch-off state of RL^{a} circuit. As it is well known there is no classical solution in this case as commutation laws are not satisfied. For an ideal open switch and time t > 0 we got the equation:

$$L\,{}_0^C D_t^{\alpha} i(t) + u_p(t) = U, \tag{3}$$

where $u_p(t)$ is a voltage on an open switch.
Current equals $i(t) = -\delta(t)$ so voltage transform on switch contact is:

$$U_p(s) = \frac{U}{s} + \left(\frac{U - sRL}{sR}\right)s^{\alpha} \tag{4}$$

By determining the inverse transform as described above voltage series shown in Fig. 3 were obtained.

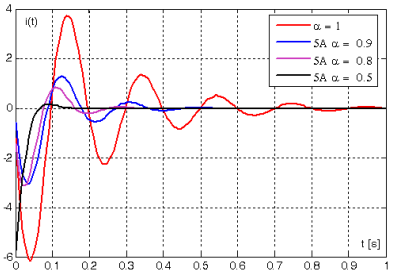

Fig. 2. Current series for RCL^{α} for a switch-on state of a circuit

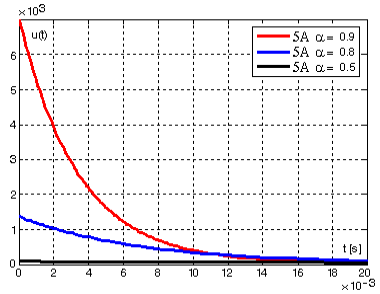

Fig. 3. Voltage series for derivatives $\alpha = 0.9\,,\ 0.8\,,\ 0.5$

Conclusion

As it can be seen digital solutions confirm that modeling of a nonlinear coil by an element of fractional order is useful.

REFERENCES

[1] Ezekoye D., Hall M., Matthews R., Railplug Ignition System for Enhanced Engine Performance and Reduced Maintenance, USA, 2005.
[2] Kaczorek T., Selected problems of fractional systems theory,. Springer-Verlag, Berlin-Heidelberg, (2011).
[3] Włodarczyk M., Zawadzki A., Connecting a Capacitor to Direct Voltage in Aspect of Fractional Degree Derivatives. Przegląd Elektrotechniczny, R. 85 NR 10/2009, str.: 120–122
[4] Krishna B.T., Studies on fractional order differentiators and integrators: A survey, Signal Processing 91, 2011, pp. 386–426.

Authors*: Maciej Włodarczyk, Andrzej Zawadzki and Sebastian Różowicz are with the Kielce University of Technology, 25-314 Kielce, al. Tysiąclecia Państwa Polskiego 7, Poland, e-mails: {m.wlodarczyk, a.zawadzki, s.rozowicz} @tu.kielce.pl).*

Sebastian RÓŻOWICZ, Szymon TOFIL

Kielce University of Technology

The Influence of Impurities on the Operation of Selected Fuel Ignition Systems in Combustion Engines

Abstract*. The paper attempts to determine the impact of fuel impurities on the value of fuel energy spark discharge and the wear of spark plug electrode. Spark plugs were analyzed in two typical configurations of the ignition system. For the analyzed systems, a number of tests to determine the wear of spark plug electrode subjected to different types of impurities were conducted. The value of spark discharge energy for new and worn spark plugs was calculated.*

Keywords: ignition system, spark plugs, fuel mixture impurities, electrode burning

Introduction

The study of ignition system dynamics in modern vehicles is a hard issue. The results of the analysis and digital simulation differ from experimental ones. The present paper attempts to determine the impact of fuel impurities on spark discharge energy and the wear of spark plug electrode.

Model of the ignition system

On the whole, ignition systems can be represented as systems accumulating energy in the inductance and capacitance [1,2]. Figure 1 presents a general diagram of mathematical model where R_{ls} element functions as a spark plug with capacitance and resistance denoted as C_{45} and R_{45}.

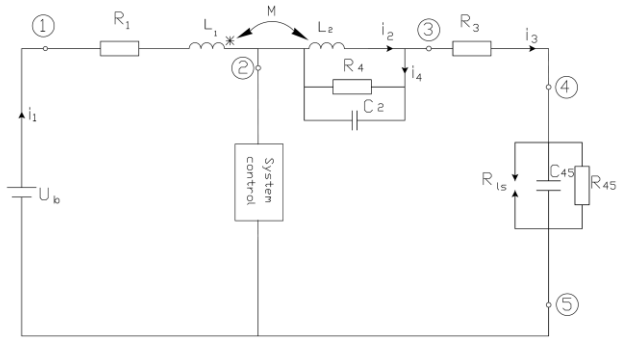

Fig. 1. Model of ignition system for simulation studies

The effect of fuel impurities on the wear of spark plug electrodes

Analysis and observation of spark plug wear was conducted by means of a digital microscope HIROX KH-8700. The image of the gap between electrodes for the spark plugs ISKRA after an 800-hour operation is shown in Figure 2a (operation in the capacitive system) and 2b (operation in the induction system), and the wear of spark plug electrodes after a 1400-hour operation is shown in Figures 2c and 2d.

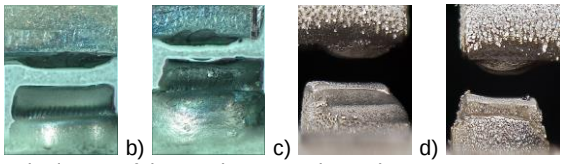

a) b) c) d)

Fig. 2. The image of the gap between electrodes

a) spark plug Iskra after an 800- hour of operation – capacitave system,
b) spark plug Iskra after an 800- hour operation – induction system,
c) spark plug Iskra after a 1400 hour-operation – capacitave system ,
d) spark plug Iskra after a 1400 hour- operation – induction system

Determination of spark discharge energy for different types of electrodes

For spark plugs ISKRA discharge energy for capacitor discharge system calculated on the basis of the results presented in Fig.3 amounts to 32,6mJ.

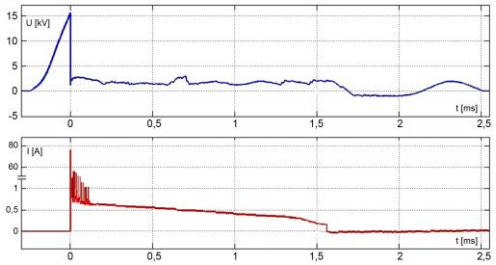

Fig. 3. Current and voltage for a new spark plug E=32,6mJ.

For an 800-hour operation of spark plugs E=26,25mJ was obtained for capacitor discharge system. (Fig.4.).

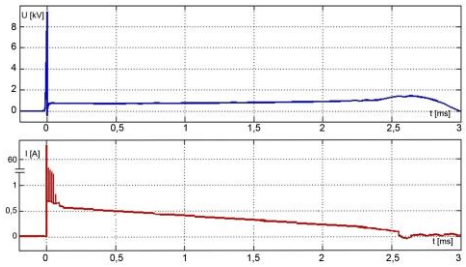

Fig. 4. Current and voltage for an 800-hour operation of spark plugs E=26,25mJ

Conclusion

As it can be seen the wear of spark plug electrode significantly influences the value of spark discharge energy.

Acknowledgements

The research was supported by the National Centre for Research and Development (NCBiR), project No. PBS1/B5/13/2012.

REFERENCES

[1] Ezekoye D., Hall M., Matthews R., Railplug Ignition System for Enhanced Engine Performance and Reduced Maintenance, USA, 2005.
[2] Hunicz J., Wac E., Kabała J., Badania porównawcze nowych konstrukcji świec zapłonowych, Eksploatacja i niezawodność 3/2006

Authors*: Sebastian Różowicz and Szymon Tofil are with the Kielce University of Technology, 25-314 Kielce, al. Tysiąclecia Państwa Polskiego 7, Poland, E-mails: {s.rozowicz, tofil} @tu.kielce.pl).*

Paolo DI BARBA[1], Fabrizio DUGHIERO[2], Michele FORZAN[2], Elisabetta SIENI[2]

University of Pavia (1), University of Padova (2)

A Novel NSGA-Inspired Optimization Algorithm for the Design of Electromagnetic Devices and application in MFH

Abstract. *Magnetic Fluid Hyperthermia, a clinical treatment of cancer that uses of magnetic nanoparticles fluid heated by time varying magnetic field. The design of an experimental device to evaluate the heating rate of magnetic nanoparticles inside cells cultured in a Petri dish has been carried out by resorting to a variant of the algorithm NSGA to induce a uniform magnetic field inside the Petri. Population-Adapting Migration Non-dominated Sorting Algorithm is proposed for the automatic design of the device.*

Keywords: Magnetic fluid hyperthermia, multi-objective optimization, genetic algorithm, finite-element analysis.

Introduction

Magnetic fluid hyperthermia is a cancer therapy that uses magnetic fluid to heat locally cancer cells [1, 2]. In fact it is well known that a magnetic nanoparticle fluid heats when a time varying magnetic field at few hundred of kHz is applied [3]. In order to assess the heating capability of the magnetic fluid in biological systems, the nanoparticle fluids must be subject to a highly homogeneous magnetic field.

In the paper the optimal design of the inductor coil used to heat a magnetic nanoparticle fluid, which has previously injected inside cells cultured in a Petri dish, is presented. The inductor design is guided by means of multi-objective optimization considering as goal functions the uniformity of the magnetic field intensity in the Petri dish and maximum strength of the magnetic field [3]. In the proposed case study a modification of NSGA algorithm is presented, i.e.: Population-Adapting Migration Non-dominated Sorting Algorithm (PA-MNSGA).

Direct and inverse problem

The inductor has to generate a uniform magnetic field on the Petri dish bottom where cells, cultured in monolayer, have been treated with a magnetic nanofluid. Fig. 1 shows the 2D cross section of the device, that exhibits axial-symmetry [4]. The magnetic field source is a two-turn inductor with internal radius of 85 mm equipped with ferrite blocks placed as in Fig. 1 in order to properly distribute the magnetic flux lines. The axy-symmetric model is solved in time harmonic conditions using Finite Element method [5]. The supply voltage has been fixed to 600 V, a typical maximum value to avoid the use of an impedance adapter.

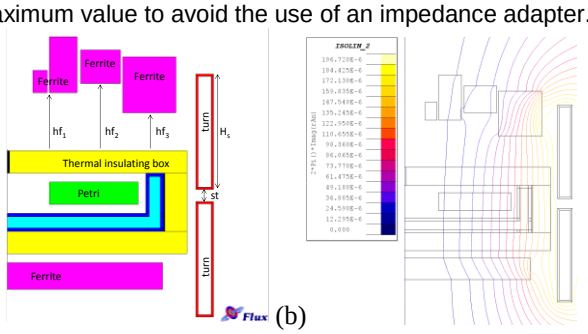

(a) (b)

Fig.1. (a) Geometry of the designed device and (b) magnetic flux lines

The optimization problem aims at minimizing the inhomogeneity of the magnetic field in the Petri dish bottom (f_1), computed using the "proximity criterion" [4], and maximize the magnetic field strength in the Petri dish bottom (f_2). In the PA-MNSGA algorithm the updating of the design variables is managed by means of a modified NSGA algorithm. The algorithm considers an initial population of N_p (e.g. N_p = 20) individuals, that are subsequently modified because of migration of new individuals. Each migration event adds a new population with N_m ($N_m \leq N_p$) individuals, and different genetic characteristic, inside the current population. Moreover, Population-Adapting is a technique that increases the size of the population. A criterion for modifying N_p is applied after the Non-Dominate Sorting: if the number N_1 of individuals belonging to the first Pareto front is greater than the population size N_p, the new population grows to $N_p' = N_1$ individuals. At each evolution step the population size is modified with reference to the number of individuals in the first Pareto front, N_1. In case $N_1 < N_p$ the new population size is reduced to the initial one, N_p, by applying the Non-Dominate Sorting. The convergence of the whole evolution is governed by a 'front mobility' parameter.

In the case study, five design variables (Fig. 1) are considered: the vertical positions of the upper ferrites ('hf_1', 'hf_2', 'hf_3'), the gap between the two turns ('st') and the turn height (H_s).

Results

Fig. 2 shows an approximation of the Pareto front; a solution belonging to Pareto front is also shown.

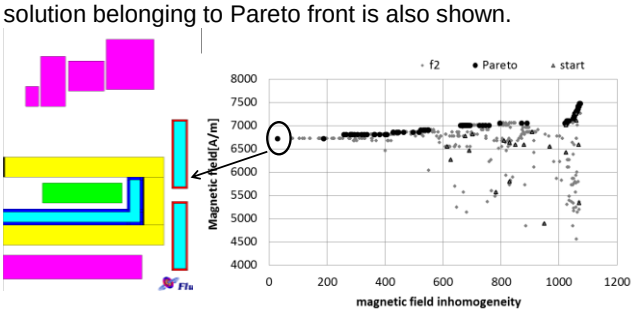

Fig. 2. Individual generated, Pareto front and optimized geometry

REFERENCES

[1] Goya G.F., Asín L., Ibarra MR. Cell death induced by AC magnetic fields and magnetic nanoparticles: Current state and perspectives. Int J Hyperthermia 2013;29:810–8.

[2] Hildebrandt B., Wust P., Ahlers O., Dieing A., Sreenivasa G., Kerner T., et al. The cellular and molecular basis of hyperthermia. Crit Rev Oncol Hematol 2002;43:33–56.

[3] Rosensweig R. E. Heating magnetic fluid with alternating magnetic field. J Magn Magn Mater 2002;252:370.

[4] P. Di Barba, F. Dughiero, M. Forzan, E. Sieni. Sensitivity-based optimal shape design of induction-heating devices. IET Sci Meas Technol in press. doi:10.1049/iet-smt.2014.0227.

[5] FLUX. (CEDRAT): www.cedrat.com/software/flux/flux.html n.d.

***Authors**: Paolo Di Barba, University of Pavia, via Ferrata, 5 27100 Pavia, Italy, paolo.dibarba@unipv.it, Fabrizio Dughiero, Michele Forzan, Elisabetta Sieni, University of Padova, via Gradenigo, 6/a 35131 Padova, Italy, fabrizio.dughiero@unipd.it, michele.forzan@unipd.it, elisabetta.sieni@unipd.it.*

Mykhaylo ZAGIRNYAK, Viktoriya KOVALCHUK, Tetyana KORENKOVA

Kremenchuk Mykhailo Ostrohradskyi National University

Identification of Parameters of Electrohydraulic Complex with Periodic Nonlinear Processes in the Pipeline Network

Abstract. *An electrohydraulic complex equivalent circuit taking into account cavitational processes in the pipeline network is proposed. It is shown that equations of energy balance of hydraulic power harmonic components between the power supply and hydraulic system elements may underlie identification of electrohydraulic complex parameters.*

Keywords: electrohydraulic complex, hydraulic power, cavitational self-oscillations, harmonic analysis

Introduction

During operation of electrohydraulic complexes (EHC), conditions resulting in development of cavitational processes characterized by occurrence of self-oscillations of pressure and discharge in the hydraulic network, decrease of efficiency, vibration, noise, erosive destruction of the material of the pump unit (PU) impeller blades and pipeline walls, appear rather often.

The analysis revealed that the problem of occurrence and development of cavitation is most completely considered in PU [1]. At the same time, there is practically no account of problems connected with appearance of cavitational processes in pipeline networks, which results in the increase of hydraulic resistance, hydraulic power losses at the pipeline elements and the whole hydraulic system.

Taking the above said into consideration, the purpose of the paper consists in determination of the parameters of EHC equivalent circuit at periodic nonlinear processes in the pipeline network. It will allow elimination of the condition when PU cavitational stoppage or pipeline network choking due to growth of the volume of cavitational cavities are possible.

Method and research results

An equivalent electric circuit including a rotation-frequency controlled PU, a pipeline network and a consumer is offered for description of transition processes in EHC (Fig. 1). The following designations are used in the circuit: $H_0\nu^2$ – source of hydraulic supply, m; $\nu = \omega_i / \omega_n$ – PU relative rotation frequency; ω_i ,ω_n – current and nominal value of motor rotation frequency, respectively, s^{-1}; H_{st} – source of static back pressure, m; R_p , $R_{net\ i}$,R_{con} – hydraulic resistances of the pump, i –th section of the pipeline and the consumer, respectively, kg/m^{4}s; $R_{kav}(t)$ – nonlinear hydraulic resistance describing periodic nonlinear cavitational processes at the pipeline network section, kg/m^{4}s; $L_{net\ i}$, $C_{net\ i}$ – inductance and capacitance of the i -th section of the pipeline, kg/m^4, m^{-1}, respectively; $Q_p(t)$, $Q_{net\ i}(t)$, $Q_{con}(t\ )$ – discharge at the pump output, at the i -th section of the pipeline and at the consumer, respectively, m^3/s; $Q'_i(t)$ – discharge losses at the i -th section of the pipeline, m^3/s.

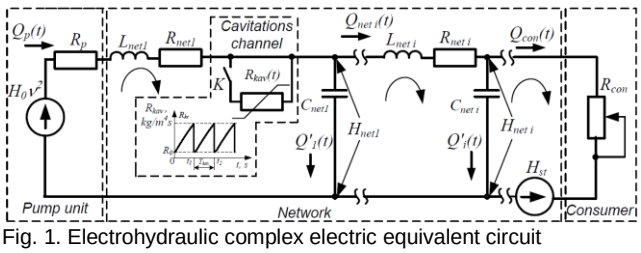

Fig. 1. Electrohydraulic complex electric equivalent circuit

Change of load condition in the hydraulic system caused by cavitational processes is directly connected with power parameters of EHC operation.

Taking into account the distribution of power losses at the elements of EHC power channel the energy balance equation of the following form is true:

$$p_s(t) = \Delta p_p(t) + \sum \Delta p_{neti}(t) + \Delta p_{kav}(t) + \Delta p_{st}(t) + p_{con}(t)$$

where $p_s(t)$ – power at the output of the hydraulic source, W; $\Delta p_p(t)$ – power losses at PU output; $\Delta p_{kav}(t)$ – cavitation losses of hydraulic power, W; $\sum \Delta p_{neti}(t)$ – total power losses at the i -th sections of the pipeline, W; $\Delta p_{st}(t)$ – hydraulic power losses for overcoming static back pressure, W; $\Delta p_{con}(t)$ – hydraulic power at the consumer, W.

To research the processes of energy conversion in EHC at periodic variation of head and discharge the method of power signals harmonic analysis [2] is used. This method makes it possible to present hydraulic power as a sum of a constant and harmonic (cosine and sine) components.

The energy balance equations for hydraulic power harmonic components between the power supply and EHC elements have been considered as a system of identification equations. Its solution allowed determination of the unknown parameters of EHC equivalent circuit, calculation of power losses, real values of efficiency at the elements of EHC power channel.

Conclusion

It has been shown that representation of an electrohydraulic complex by an electric equivalent circuit makes it possible to determine hydraulic power and power losses at any section of the hydraulic system when periodic nonlinear processes develop in the pipeline network.

It has been established that identification of the parameters of electrohydraulic complex is to be based on the equations of power balance of hydraulic power harmonic components between the power supply and the hydraulic system elements.

REFERENCES

[1] Marcelo Martins Stopa, Cardoso Filho and Carlos B. Martinez Incipient Detection of Cavitation Phenomenon in Centrifugal Pumps, IEEE Transactions On Industry Applications (2014), Iss. 50(1), 120–126.

[2] Zagirnyak M., Rod'kin D., Korenkova T. Enhancement of instantaneous power method in the problems of estimation of electromechanical complexes power controllability, Przeglad Elektrotechniczny (Electrical review), 2011, № 12b, 208–212.

***Author**: Mykhaylo Zagirnyak, E-mail mzagirn@kdu.edu.ua, Viktoriya Kovalchuk, e-mail: viktoria_kovalc@mail.ru, Tetyana Korenkova, e-mail: tanya74kor@gmail.com, Kremenchuk Mykhailo Ostrohradskyi National University, Kremenchuk, Ukraine*

Nikolai KHRENKOV, Mikhail STRUPINSKIY

Special Systems and Technologies, LLC, Russia

Electric Field Strength in a Skin-effect Based Heater

Abstract. *Results of electric field research in skin-effect based heaters of long pipelines are presented. The research has been performed using computer models and heater samples.*

Keywords: skin-heater, electric field strength, SECT

Introduction

At long-distance pipe transport of various liquids (oil, water, etc.) a need of their heating in cold season arises. One of the best methods of the long and extra-long pipelines heating is SECT – skin electric current thermosystem. The length of a pipeline powered from only one end is directly related to the power voltage level. The power voltage value, in its turn, is limited by corona start voltage in the SECT heater.

Subject of research

The SECT heater is a coaxial line consisting of an insulated conductor running inside a ferromagnetic tube acting as a return lead. The power voltage is applied at the near end of the heater; at the far end the conductors are short-circuited. The inner conductor insulation diameter is much less than the inner diameter of the tube, for convenience of the heater installation on a pipeline. By this reason the inner conductor is located eccentrically to the outer conductor (tube) (Fig. 1).

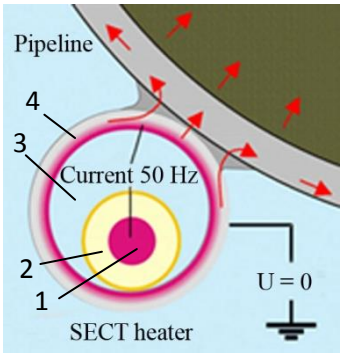

Fig. 1. Cross section of the SECT heater
1 – inner conductor; 2 – electrical insulation; 3 – air; 4 – outer conductor.

The presence of significant air space inside the SECT heater is limiting the power voltage value due to corona discharge appearance which can start already at E = 2000 V/m. The goal of this work was to determine the areas of highest electrical field strength depending of the SECT heater design.

Methods and results of the investigation

The investigation has been performed digital models of SECT heaters and their experimental samples. The software package ELCUT that uses the finite element method was applied to electric fields modeling in the heater.

The following techniques are used to prevent corona discharge in high-voltage electrical cables: smoothing of the conductors surface, application of semi-conductive layers between the conductors and the insulation, exclusion of air bubbles inside the cable insulation.

The design versions of the SECT heater considered in this paper are presented in Table 1 where the results obtained on the models are also shown.

Table 1. Electric field strength (V/m) in SECT heaters of various designs.

Heater's design	Ewire	Eair
Cable in the center of the tube	823	550
Cable touches the tube's wall	1850	1800
Air bubble inside the insulation	2700	1500
The conductor is made compressed	1540	2300
The conductor is covered by semi-conductive layer	1520	2180
The insulation if wound by insulating cord	1170	1400

Ewire – the maximum field strength in the insulation;
Eair – the maximum field strength in the air.

A typical electric field pattern in the insulation and in the air is shown in Figure 2.

Experimental research carried out on samples of skin heaters, confirmed the possibility of increasing the voltage corona discharge. In the case where the isolation of the inner conductor of the heater was wrapped cord, corona starting voltage increased by 55%. Estimated increase (Table 1) defined on the model will be 58%.

Conclusion

1. The best electric field distribution occurs when the conductor is located in the center of the return lead.
2. It is highly important to exclude air bubbles appearance inside the insulation.
3. The methods normally used for high-voltage cable conductor smoothing and application of semi-conductive layers don't give the expected result.
4. Application of an insulating cord above the insulation to exclude its contract with the outer conductor results in a good effect that is experimentally confirmed.

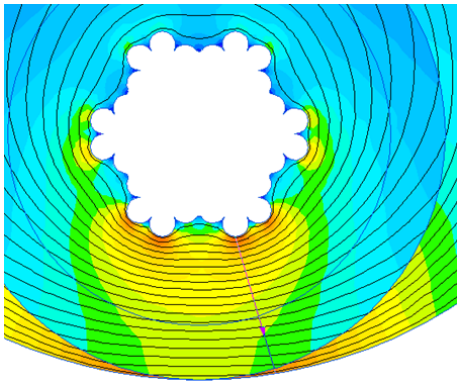

Fig. 2. Electric field strength in the SECT heater in case when the insulation of the inner conductor touches the outer conductor.
Ewire = 1850 V/m, Eair = 1800 V/m

Milena KURZAWA, Wiesław ŁYSKAWIŃSKI, Rafał M. WOJCIECHOWSKI

Poznan University of Technology

Measurement Verification of a Field-circuit Model of the Wireless Energy Transmission System

Abstract. *In the paper, the wireless transmission energy system (WTES) using the high-frequency air-transformer has been discussed and investigated. The considered system consists of two magnetically coupled coils, which have been connected to the elements of external circuits. To analyze the electromagnetic filed and to define the parameters of the considered system the field-circuit model has been elaborated in the Maxwell environment. In order to verify the calculation results obtained in the field-circuit model the experimental setup has been developed. The results of simulation calculations have been compared with the measurements obtained in the experimental setup.*

Keywords: air-transformer, field-circuit model, wireless energy transmission.

Introduction

High-frequency coreless transformers are commonly used in the wireless charging systems of electronic devices, in the battery charging systems for the electric cars [1], and in the medicine for battery charging of cardiac assist devices [2]. In the Authors' opinion for the design of such systems it is advantageous to use the 2D or 3D field models of air-transformers coupled with the external circuits containing both the active and passive elements and their interconnections, i.e. field–circuit model. The reliability and accuracy of such models are best to verify by the measurement. Therefore, to confirm the correctness of the proposed approach a simple wireless energy transmission system has been considered and investigated Obtained results of simulations have been compared with the measurements performed in the experiment setup.

Structure of the considered WTES system

The considered wireless transmission energy system consists of two magnetically coupled coils, i.e. the transmitter and receiver coil. The transmitter coil is connected in parallel with the capacitor C_1 and the high-frequency voltage source, while the receiver coil is connected in series with capacitor C_2 and resistor R_o, which represents the load of the system. In the considered WTES, it has been assumed that the transmitter coil has 10 turns and its radius and height are equal to 22.6 mm and 3 mm. The radius and height of the receiver coil are equal to 19.7 mm and 4.4 mm, respectively; and coil has 20 turns. The capacitances C_1 and C_2 have been selected to eliminate the influence of the self-inductance of coils, thereby increasing the efficiency of the energy transmission system The view of the considered system on the elaborated experimental setup have been shown in Fig. 1.

To analyze of electromagnetic field and to calculate the lumped parameters of considered WTES the field-circuit model has been elaborated. The professional finite element method (FEM) package *Maxwell* has been employed. The model has been developed as 3D using the Ω-$\boldsymbol{T}$ formulation. The applied model allows not only to calculate the magnetic field distributions and the parameters of WTES but also to analyze the influence of dielectric displacement currents in air on those parameters and field distributions. The detailed description of the developed model will be presented in the extended version of the paper.

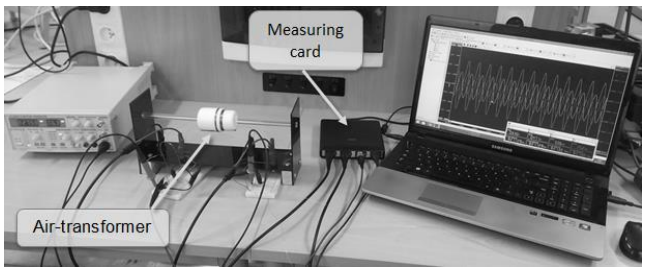

Fig. 1. View of the experimental setup

Selected results

The comparative analysis between the simulations and the measurements results obtained in the experimental setup has been performed. Here, the dependences of voltage on system load as a function of the distance between the coils for the simulation and the measurement are illustrated in Fig. 2. The starting point (d = 0 mm) means the distance between the coils equals zero. The study was performed for the resonance frequency equal to 840 kHz.

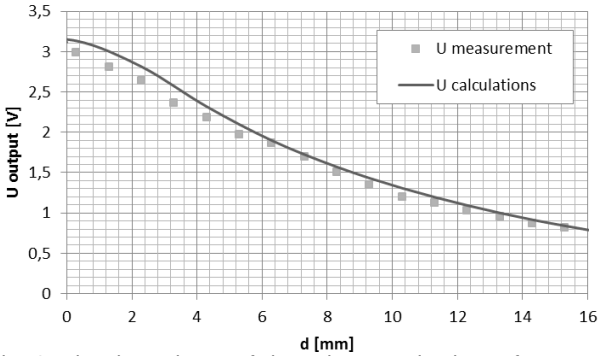

Fig. 2. The dependence of the voltage on load R_o of system as a function of the distance d between the coils

On the base of performed investigations it can be stated that the results of measurements are sufficiently close to the results of simulation. The small differences between results – especially when the receiver and transmitter coils close to each other may be caused by many factors, for example the inaccurate representation of the geometry of the real system in the numerical model.

Conclusion

In the paper the comparison between the simulations and measurements results obtained for the simple system with the coreless transformer has been performed. Authors carried out the large number of tests checking the accuracy of the developed model by comparison to measurements. In this short digest only the selected results have been presented. Nevertheless the performed researches allowed for the positive verification of the proposed field-circuit model of the wireless power transmission system.

REFERENCES

[1] Ahn S., Lee J. Y., Cho D. H., Kim J., Magnetic field design for low EMF and high efficiency wireless power transfer system in on-line electric vehicles, CIRP Design Conference 2011, pp. 233–239.

[2] Maradewicz A, Kaźmierkowski M.P., Resonant converter based contactless power supply for robots and manipulators, Journal of Automation Mobile Robotics and Intelligent Systems, Vol. 2, No. 3, 2008, pp. 20–25.

Authors: *Milena Kurzawa, milena.r.kurzawa@doctorate.put.poznan.pl, Wiesław Łyskawiński, wieslaw.lyskawinski@put.poznan.pl, Rafał M. Wojciechowski, rafal.wojciechowski@put.poznan.pl, Poznan University of Technology, Piotrowo Street 3, 60-965 Poznań,*

Grzegorz PSUJ, Barbara SZYMANIK

West Pomeranian University of Technology, Szczecin

Fatigue Monitoring of Steel Structures using Electromagnetic and Infrared Thermography Inspection Methods

Abstract*. Two nondestructive methods are used for evaluation of fatigue stage in steel samples under load: the infrared thermography (IRT) and electromagnetic (EM). The IRT allows to observe the general global condition of the material while the EM to carry out local, detail examination of the fatigue stage in critical region. Both methods have different physical basics what allows to obtain a wider range of information about the state of the structure. The presented inspection results are compared and discussed.*

Keywords: fatigue evaluation, electromagnetic nondestructive evaluation, infrared inspection.

Introduction

Assessment of a structure fatigue life depends on many factors such as stress history, environmental conditions and initial material characteristics i.e. fracture toughness, critical load or tensile strength. The estimation of fatigue failure risk requires to carry out the analysis and prediction algorithms taking into consideration initial strength capacity, production technology and types of possible flaws introduced during production or operation period [1]. The process requires also determination of local condition of the material, which involves evaluation of its microstructure, applied and residual stress values in accordance to strain state as well as crack grow area within the examined region. Therefore, the need for application of nondestructive testing and evaluation methods contributing the process of determining the state of stress and damage in the material emerges [1, 2]. Some of the most commonly used techniques are: visual, penetrant, ultrasonic, acoustic, radiographic and electromagnetic.

Inspection methodology

During the selection of nondestructive testing methods contributing the process of assessing the degradation state of the material several factors must be taken into account. It is important to analyze what type of defects may occur in examined construction together with the capacity of the NDT technique to distinguish between the areas having the flaws and without them. Furthermore, the possibility of carrying out a rapid assessment of the overall condition of the structure as well as obtaining detail information for the selected critical areas has to be also considered. Therefore in this paper two nondestructive testing methods are used to monitor the progress of fatigue process in steel samples: electromagnetic for local and detail examination of crucial region and infrared allowing estimation of the general condition state of tested material.

Due to the electromagnetic properties of steels utilized for the constructions, the use of electromagnetic testing methods becomes a natural solution for evaluation of theirs damage stage. Material properties are influenced by the stress and fatigue loading conditions. It is known that microstructure features affect the magnetic one [2]. Therefore, by monitoring changes of magnetic properties, the damage state of the material can be evaluated. Various magnetic properties can be considered in the process of damage state evaluation [2, 3]. Hysteresis loop parameters such as remanence or coercivity as well as Barkhausen noise characteristic values such as signal's energy shows good correlation with the damage state of the material.

In the recent times the increased importance of thermographic method may be also observed. Active infrared thermography is one of the methods that are widely used in the nondestructive testing of materials. Internal structure of the tested material, in particular defects (such as cracks or weakening of the structure caused by the mechanical stress) affect the free flow of heat. Sensitive infrared camera is used to observe the temperature distribution on the sample's surface. The high temperature resolution allows to observe even small internal inhomogeneities in the form of the overheated or colder places, showing the location, size and type of defects. In the global assessment the most important is that the infrared camera with a high resolution allows the simultaneous observation of relatively large areas. The observation allows the initial location of the areas where the material is subjected to higher loads. Another advantage of this method is the ability to quickly inspect the materials due to the fact that the ferromagnetic materials have generally a high thermal conductivity coefficient. After preliminary location of the areas susceptible to damage, the thermal camera with the micro lens can be used for the final, local assessment of the steel structure.

Conclusions

This paper presents in detail the experimental methodologies and the results of the electromagnetic and infrared investigation of the steel samples under load. The selected methods allows to observe the fatigue process by means of different physical aspects (e.g. changes of magnetic and thermal properties during fatigue). Thereby making it possible to obtain a wider range of information about the state of the structure. The details of the experiment, results comparison and discussion will be presented in the full version.

REFERENCES

[1] Dobmann G., Ciclov D. C., Kurz J. H., NDT and fracture mechanics. How can we improve failure assessment by NDT? Where we are – where we go?, Insight, Vol. 53, No. 12, 2011.

[2] Palit Sagar S., et al., "Magnetic Barkhausen emission to evaluate fatigue damage in low carbon structural steel", International Journal of Fatigue, Vol. 27, 2005, pp. 317–322.

[3] Psuj G., Chady T., Enokizono M., Observation of material degradation under fatigue and static loading condition using selected electromagnetic NDT methods, *Material Science Forum*, 721, 120, 2012, 120-126.

[4] Maladegue X.. Theory and practice of infrared technology for nondestructive testing. JohnWiley and Sons, 2001.

Authors*: Grzegorz Psuj, West Pomeranian University of Technology, Szczecin, al. Piastów 17, 70-310 Szczecin, Poland, e-mail: gpsuj@zut.edu.pl , Barbara Szymanik,* West Pomeranian University of Technology, Szczecin*, al. Piastów 17, 70-310 Szczecin, e-mail: szymanik@zut.edu.pl*

Manling DONG[1], Jiajia HU[2], Degui YAO[1], Xiaokuo KOU[1], Fan YANG[2]

State Grid Henan Electric Power Corporation Research Institute, China (1), Chongqing University (2)

The Sensitivity Fault Diagnosis Method of Grounding Grid Based on LSQR Regularization Algorithm

Abstract. *This paper first presents the fault diagnosis sensitivity methods of grounding network, and then put forward the use of regularization LSQR algorithm for fault diagnosis of grounding grid. This method can obtain the potential and current data of outgoing line, with reducing the iteration times without lower the accuracy. Finally, laboratory test is performed to verify the feasibility and the results showed that grounding network fault diagnosis system makes an accurate judgment about the experimental ground grid.*

Keywords: regularization, sensitivity method, grounding grid, fault diagnosis

Introduction

Grounding grid plays an important role in power systems, and the research on its corrosion diagnosis has always been a notable topic [1]. The diagnosis method based on the circuit theory regards grounding grid as a pure resistance network, by injecting a current into grounding grid and measure the node voltage. And then grounding network fault diagnosis equation for the inverse problem.is established. In actual power systems, the grounding grid is covered with larger area, so a comprehensive measurement for the whole grounding grid is unrealistic [2].

In this paper, we put forward the sensitivity method based on LSQR regularization algorithm. In order to make the diagnosis equations for grounding network have the characteristics of linear, we combine regularization algorithm and LSQR algorithm to solve the sensitivity equation and it can improve the efficiency of the fault diagnosis of substation grounding network.

Grounding network fault diagnosis method of sensitivity

The diagnosis model is based on circuit theory which regards the grounding grid as a pure resistance grid with N nodes and B branches. Through electric network theory, we can set up a goal function shown as (1):

$$\min f(\boldsymbol{R}) = \frac{1}{2}\left\|\boldsymbol{U}_n(\boldsymbol{R}) - \boldsymbol{U}_{n0}\right\|^2, \boldsymbol{R} = \left[R_1, R_2, \cdots, R_B\right]^T \quad (1)$$

where: $\boldsymbol{U}_{n0}$ – node voltage measurements, $\boldsymbol{U}_n(\boldsymbol{R})$ –the calculated node voltage value , $\boldsymbol{R}$ – unknown resistance value.

By minimizing the f ($\boldsymbol{R}$) we can obtain the branch resistance and its variation in accordance with measured value. When two nodes selected for incentive of grounding network, for the i^{th} time of incentive, $\boldsymbol{I}_S^i$ is the excitation current source vector, $\boldsymbol{Y}_n$ is the node admittance matrix, thus, there is $\boldsymbol{Y}_n\boldsymbol{U}_n^i = \boldsymbol{I}_S^i$ and do the total differential at node voltage $\boldsymbol{U}_n^i$, we can get function (2):

$$d\boldsymbol{U}_n^i = \sum_{k=1}^{B}\frac{\partial(\boldsymbol{Y}_n^{-1}\boldsymbol{I}_S^i)}{\partial R_k}dR_k = \sum_{k=1}^{B}\left[\frac{\partial(\boldsymbol{Y}_n^{-1})}{\partial R_k}\boldsymbol{I}_S^i + \boldsymbol{Y}_n^{-1}\frac{\partial(\boldsymbol{I}_S^i)}{\partial R_k}\right]dR_k \quad (2)$$

Due to $\boldsymbol{I}_S^i$ being a constant, its differential to $\boldsymbol{R}_k$ is 0, and then we can attain the sensitivity equation (3):

$$d\boldsymbol{U}_n = \boldsymbol{P}d\boldsymbol{R} \quad (3)$$

Where $d\boldsymbol{U}_n$ is a column vector with $T\times N$ columns, $\boldsymbol{P}$ is the sensitivity matrix with $T\times N$ rows and B columns.

Solve diagnosis equation based on the regularization LSQR method

LSQR method is a very effective algorithm to solve the large and sparse linear equations $\boldsymbol{Ax} = \boldsymbol{b}$ and least square problem $\min\left\|\boldsymbol{Ax}-\boldsymbol{b}\right\|_2$. When the matrix is ill-posed, LSQR method can obtain a much more accurate solution by fewer iteration steps. We transferred the least square problem to formula (4) through LSQR algorithm，

$$\min\left\|\boldsymbol{r}_k\right\|_2 = \min\left\|\boldsymbol{U}_{k+1}\boldsymbol{t}_{k+1}\right\|_2 = \min\left\|\boldsymbol{t}_{k+1}\right\|_2 \quad (4)$$

It could reduce the condition number of sensitivity matrix, improved equation of state and sped up the iterative convergence by using LSQR regularization algorithm to solve the sensitivity equation of fault diagnosis on grounding grid.

Laboratory test

An experimental verification was performed on the 5 x 5 resistance network whose branch resistance value was 1Ω. And the branch 6 and 31 of the network were designed bigger than others to simulate the corrosion. Then the result (shown in Fig. 1) obtained through the method proposed in this paper matched with the designed status, which indicated a high accuracy of this method.

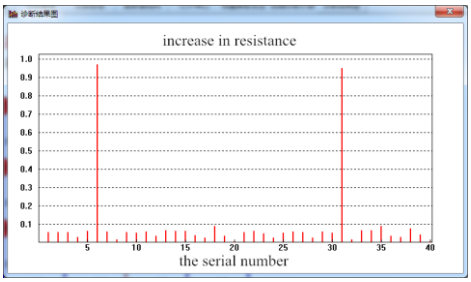

Fig. 1. The result of diagnosis

REFERENCES

[1] J.Yuan, H.Yang, L. Zhang, X. Cui, and X. Ma, Simulation of Substation Grounding Grids with Unequal-potential, *IEEE Trans. Magn*., 36 (2000), No. 41, 1468–1471.

[2] Bo Zhang, et al., Diagnosis of Breaks in Substation's Grounding Grid by Using the Electromagnetic Method, *IEEE Trans. Magn.,* 38 (2002), No. 21, 473–476.

Authors*: Manling Dong, State Grid Henan Electric Power Corporation Research Institute, Zhengzhou, Henan Province, China, E-mail: dongmanling0211@163.com.*

Jiajia Hu, Chongqing University, Chongqing, China, E-mail: hujj_fish@qq.com

Marcin ZIOLKOWSKI, Stanislaw GRATKOWSKI

West Pomeranian University of Technology, Szczecin

Genetic Algorithm Coupled with Bézier Curves Applied to the Magnetic Field on a Solenoid Axis Synthesis

Abstract. *Electromagnetic arrangements which create a magnetic field of required distribution and magnitude are widely used in electrical engineering. Development of new accurate designing methods is still a valid topic of technical investigations. From the theoretical point of view the problem belongs to magnetic fields synthesis theory. This paper discusses a problem of designing a shape of a solenoid which produces a uniform magnetic field on its axis. The method of finding an optimal shape is based on a genetic algorithm (GA) coupled with Bézier curves.*

Keywords: Bézier curves, genetic algorithms, magnetic field synthesis; nonlinear inverse problems.

Introduction

Magnetic fields generation of a specified distribution has been discussed in numerous papers but it remains as an important problem of contemporary research and applications. Usually, a source of a magnetic field are set of coils and various types of solenoids. This paper is a continuation of [1, 2] and discusses a problem of designing a shape of a solenoid which produces a uniform magnetic field on its axis. The applied method is based on a genetic algorithm (GA) coupled with Bézier curves [3].

Problem Description

Assume it is required to generate a uniform magnetic field in a certain region which lies very close to the solenoid's axis symmetry (z-axis in cylindrical coordinate system). The task is to find the optimal shape of a solenoid represented by unknown $f(z)$ curve, so that the magnetic field is uniform on the axis z ($\boldsymbol{H} = -H_0\ \mathbf{1}_z$). The inner and outer surfaces of the solenoid are created by the rotation of curves $r = f(z)$ and $r = f(z) + t$ around the z-axis, respectively. The solenoid is of height $2l$ and contains a large number N of tightly wound turns of wire with current, then there is an effective current density J within the solenoid, where $J = NI/2lt$. In such a case the actual solenoid can be replaced by a region carrying a constant current density J (Fig. 1).

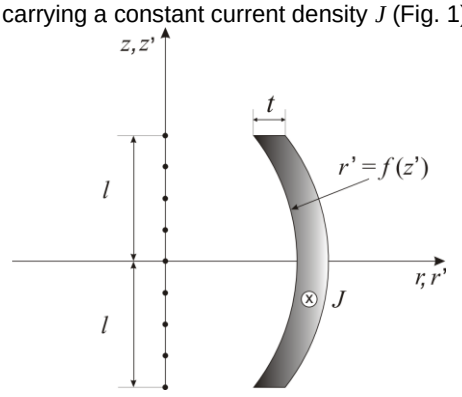

Fig. 1. A definition sketch for a solenoid of unknown shape $r = f(z')$ and solenoid's thickness t

By using the formula for the magnetic field intensity on the circular loop axis, it can be shown that the relation between required magnetic field intensity H_0 on solenoid's axis and current density J can be described by following nonlinear integral equation:

$$\frac{2H_0}{J} = \int_{-l}^{l} K\left[z,\ z',\ f\left(z'\right)\right]\ dz' , \tag{1}$$

where: K – kernel of the integral equation, z', r' – coordinates of the source points within the solenoid, z – field points on the z-axis.

Its solution gives the required shape of the solenoid. In order to solve equation (1) genetic algorithm coupled with Bézier curves based method has been utilized. The design parameters are coordinates of the Bézier curve control points and solenoid's thickness t.

Numerical Results

The exemplary calculations have been performed for desired magnetic field H_0 equal to 35 kA/m. Optimal shape of the solenoid has been presented in the Fig. 2.

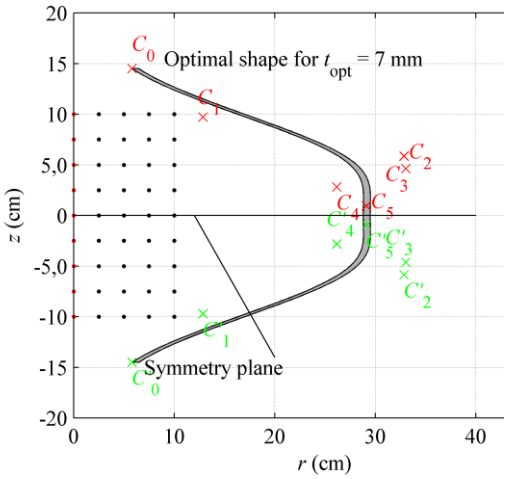

Fig. 2. Optimal shape of the solenoid for desired H_0 = 35 kA/m

REFERENCES

[1] K. Adamiak. Tichonov's regularization method applied to the magnetic field on a solenoid axis synthesis. Archiv fur Elektrotechnik, 59, 1977, pp. 19–22.

[2] M. Ziolkowski and S. Gratkowski. Genetic algorithm and Bezier curves based shape optimization of conducting shields for low frequency magnetic fields. IEEE Transactions on Magnetics, Vol. 44, No. 6, 2008, pp. 1086–1089.

[3] M. Ziolkowski: "Topology Optimization of Magnetic Field in Three-dimensional Finite Region", Engineering Optimization, Vol. 44, No. 6, 2012, pp. 673–684.

Authors: *Marcin Ziolkowski, West Pomeranian University of Technology, Szczecin, Sikorskiego 37, 70-313 Szczecin, Poland, e-mail: marcin.ziolkowski@zut.edu.pl, Stanislaw Gratkowski, West Pomeranian University of Technology, Szczecin, Sikorskiego 37, 70-313 Szczecin, Poland, e-mai:l stanislaw.gratkowski@zut.edu.pl*

Tomasz CHADY, Ryszard SIKORA, Piotr BANIUKIEWICZ, Leszek MISZTAL, Paweł WASZCZUK

West Pomeranian University of Technology, Szczecin

Multisource system for NDT of welded elements exploited in the aircraft industry

Abstract. *This article describes a multisource system for nondestructive testing of welded elements exploited in the aircraft industry developed in West Pomeranian University of Technology, Szczecin in the frame of CASELOT project. The system is designated to support the operator in flaws identification of welded aircraft elements using data obtained from X-ray inspection and 3D triangulation laser scanners. For proper defects detection set of special processing algorithms were developed. For easier system exploitation and integration of all components user friendly interface in LabVIEW environment was designed. In this paper all aspects of the system development were presented.*

Keywords: nondestructive testing, radiography, 3D triangulation laser scanner, artificial intelligence.

Radiography is frequently used in aircraft industry as the nondestructive testing method. The time and cost of the X-ray inspection can be significantly reduced by using artificial intelligence systems. In this paper we propose a computer system, which supports the operator in the decision process. The elements can be inspected in a fully automatic manner. Additionally, in order to improve quality of the assessment, information about a 3D weld profile is utilized.

The multisource system for NDT of welded elements contains highly specialized measuring and control devices. It consist of digital X-ray inspection system, two 3D triangulation laser scanners and dedicated motorized platform for precise rotating of the aircraft parts. The whole system is controlled by a PC computer via a user interface developed in LabVIEW programming environment.

The user interface is used for enabling communication between an operator and devices, which are parts of the system. The main task of the interface is to support the operator in decision making and informing about the results of detection and identification algorithms that are used for testing. Moreover, the software provides necessary tools to maintain flow of data essential for algorithms execution. Every aspect related with the system can be controlled via the interface.

Radiograms are processed in several steps [1]. In the first step, the radiogram is acquired into the computerized ADR system. Next, during the pre-processing stage, the position of the weld line is found in the radiogram.

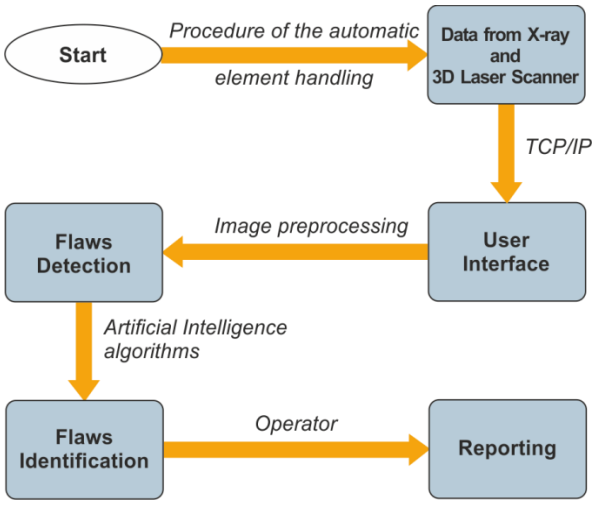

Fig. 1. Scheme of the multisource system for inspection of welded elements exploited in aircraft industry

Because of low contrast of imperfections in the weld area, it is important to process only this part of radiogram. An extraction of the weld line from the radiogram allows the defects' search area to be reduced and as a result improves the total score of detecting suspicious segments and minimizes the probability of false alarms. Next, the weld line is thresholded with the use of local and adaptive methods and then the output binary image is processed by morphological operators to remove possible noises. Finally, several numerical features that describe the shape of revealed objects in the radiogram are evaluated. Based on these features, the classification of defects is performed. The last mentioned step was implemented using artificial intelligence methods. For resolving the problem of identification, different algorithms from supervised methods family are used i.e. rough sets which have well-established theory, based on the extensions of sets theory. Due to those extensions the lower and upper approximation of sets is defined. This allows to create information system in the form of decision table composed of the collected data, decision-making attributes and defined approximations, which assigns each object to a particular class with the determination of the strength of its membership. This table is converted into easily interpretable rules. Evaluation results are applied as the result of analysis of confusion matrix and their parameters. On the basis of mentioned matrix accuracy measure coefficients are calculated, as well as other parameters i.e.: sensitivity and specificity, which are the fractions of correctly classified positive and negative observations, also applying cross validation brings the most in terms of confirmation of accuracy estimation. The results of detection and identification of the defects are presented to the operator in a clear graphical form for verification.

Acknowledgements

This work is supported by the National Centre for Research and Development, Poland (NCBiR) and EC under cosponsored research project CASELOT. Grant No. INNOLOT/I/9/NCBR/2013 (2013-2018).

REFERENCES

[1] Sikora R., Chady T., Baniukiewicz P., Lopato P., Napierala L., Pietrusewicz T., Psuj G.: Intelligent System for Radiogram Analysis for Welds' Defects Inspection – Results of Chosen Algorithms' Work, Proceedings of 18th World Conference on Nondestructive Testing, (WCNDT), 16–20 April 2012, Durban, South Africa.

Contact author: *Tomasz Chady, West Pomeranian University of Technology, Szczecin, al. Piastów 17, 70-310 Szczecin, e-mail: tchady@zut.edu.pl*

David PANEK[1], Vaclav KOTLAN[1], Roman HAMAR[1] and Ivo DOLEZEL[2]

University of West Bohemia, Pilsen, Czech Republic (1), Czech Technical University, Prague, Czech Republic (2)

Optimization of Inductor for Pre-Heating Material before its Laser Welding

Abstract*. The shape of an inductor for pre-heating metal parts is optimized with the aim to reach the prescribed distribution of temperature along the place to be consequently welded by laser beam. The task represents a nonlinear inverse multi-parametric problem that is solved for a given range of field current frequencies. While the direct part of the problem is solved by a fully adaptive higher-order finite element method, the inverse part is solved using selected genetic algorithms. Tested is also the influence of frequency of the field current. The methodology is illustrated by a typical example.*

Keywords: laser welding, induction pre-heating, coupled problem, inverse problem, genetic algorithm.

Introduction

Induction pre-heating of metals before their laser welding (and also their post-heating) is of great importance for reducing residual mechanical stresses of thermoelastic origin [1]. The aim of this process is to reach the prescribed temperature pattern in the heated material, which requires an appropriate shape of the inductor.

Formulation of the technical problem

The process of edge welding is depicted in Fig. 1. The inductor and laser head are fixed and move at a small velocity ***v*** above the trace of the weld. The inductor preheats the trace to 200–300°C and after some time it is welded by laser beam.

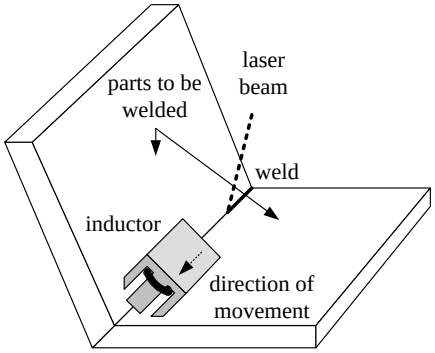

Fig. 1. Schematic view of system for edge welding

Mathematical model and its numerical solution

From the physical viewpoint, the process of pre-heating is a coupled problem characterized by a nonlinear interaction of electromagnetic and temperature fields. The first one is described by a modified Helmholtz equation [2] for the magnetic vector potential (including also the influence of velocity ***v***) the second one by the heat transfer equation [3] that also respects this velocity.

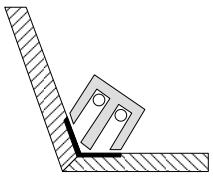

Fig. 2. Transversal cut through the system: the black area indicates the place with expected highest power

Two functionals were defined for the solution of the inverse problem: the highest possible power delivered to the material in the domains indicated in Fig. 2 and lowest possible power delivered elsewhere. As the inductor is sufficiently long in the direction of the weld trace, the solution was performed in 2D using our own code Agros2D. The code is based on a fully adaptive higher-order finite element method and also contains module OptiLab that allows solving inverse multiparametric and multicriteria problems by both gradient and evolutionary algorithms.

Illustrative example

The parts to be welded are made of steel S355. The angle between them is right. The temperature-dependent physical properties of this material, its saturation curve and other important quantities are known. The inductor made of ferrite is wound by one massive copper turn of a rectangular cross section. The velocity of motion v = 2 mm/s. The computations were carried out for frequencies of the field current frequency ranging from 10 to 25 kHz.

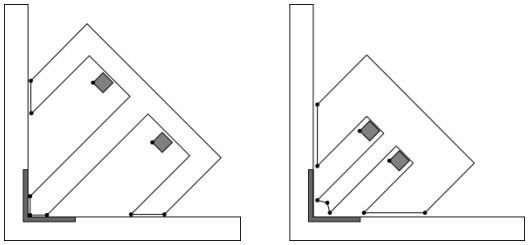

Fig. 3. Two shapes of the inductor: before optimization – left, and after optimization – right (black points indicate variable parameters)

Figure 3 shows the shape of the inductor before optimization (left) and after optimization (right). The field current amplitude is 300 A and its frequency is 25 kHz. The power delivered to the required area (indicated in black) before optimization is 140 W/m, after it 1272 W/m, which is about nine times higher. The power delivered to other parts dropped from 2900 W/m to 2052 W/m.

Financial support of the Grant project TACR TA03010354 and Grant project GACR P102/11/049 is gratefully acknowledged.

REFERENCES

[1] Mackwood A.P., Crafer R.C., Thermal modelling of laser welding and related processes: a literature review. *Optics & Laser Technology*, Vol. 37 (2005), No. 2, pp. 99–115.

[2] Kuczmann M., Iványi A., The finite element method in magnetics. *Akadémiai Kiadó*, Budapest, 2008.

[3] Holman J.P., Heat transfer. *McGraw-Hill*, New York, 2002.

Authors*: David Panek, Vaclav Kotlan, Roman Hamar, University of West Bohemia, FEL, Univerzitni 26, 306 14 Plzen, Czech Republic, E-mail {vkotlan, hamar, panek50}@kte.zcu.cz*

Ivo Dolezel, Czech Technical University, FEL, Technická 2, 166 27 Praha 6, Czech Republic, E-mail dolezel@fel.cvut.cz

Krzysztof STAWICKI, Beata SZUFLITOWSKA, Marcin ZIOLKOWSKI

West Pomeranian University of Technology, Szczecin, Poland

Recent Simulation Results of the Magnetic Induction Tomography Forward Problem

***Abstract**. In this paper we present results of simulations of the Magnetic Induction Tomography (MIT) forward problem. Two complementary calculation techniques have been implemented and coupled, namely: the finite element method (applied in a commercial software Comsol Multiphysics) and the second, algebraic manipulations on basic relationships of electromagnetism in Matlab. The developed combination can save a lot of time and make a better use of the available computer resources.*

Keywords: magnetic induction tomography, eddy current testing, finite element method, boundary conditions.

Introduction

Magnetic Induction Tomography (MIT) system has been developed and constructed at the West Pomeranian University of Technology, Szczecin for inspection of low conductivity objects. Such objects can usually contain inclusions of different electromagnetic properties, i.e.: electrical conductivity σ (usually a few S/m), electrical permittivity ε [F/m] and magnetic permeability μ [H/m].

One of the highly promising MIT application is a biomedical diagnosis, because electrical properties of biological tissues are known to be sensitive to their physiological and pathological conditions. For example, it has been reported in the literature [1, 2] that cancerous tissue has a meaningfully higher electrical conductivity than the surrounding tissues. Differences in electromagnetic properties values between various types of tissues (e.g. healthy and cancerous cells) are much more significant in comparison to other parameters, such as, for example density.

The principle of the measuring system

The measurement MIT system consists of two main elements, which are usually placed coaxially to each other, i.e.: magnetic field exciter (ferrite core coil with an aluminium screen [4]) and a receiver (two differentially connected air core coils). The object under test is situated between them and during the measurements either rotates (in case of a cylindrical structure) or moves along the selected direction. The remaining components of the system (signal generator with a high speed amplifier, control unit, data acquisition unit and a positioning system), though important, are not considered in the simulations. The exciter's coil is supplied by a low frequency (of the order of tens of kilohertz) sinusoidal current with an amplitude of tens of milliamperes and generates a time varying magnetic field, of the same frequency. This field, called the primary magnetic field, excites eddy currents in the conducting object. Amplitudes and spatial distribution of eddy currents vary depending on conductivities and shapes of the object and inclusions. Eddy currents create their own magnetic field, called the secondary field. The main aim of the measuring MIT system is to acquire the secondary magnetic field changes (through the sensing coils) resulting from non-uniform electrical conductivity distribution in the object. The results of the secondary field measurements have been presented in previous papers [3, 4]. The numerical modelling of such a process is commonly called the "forward problem". Next, the so called "inverse problem" takes places, i.e. reconstruction of the conductivity distribution basing on the secondary magnetic field measurements.

The method for solving the forward problem

The whole measuring system can be simulated as one unified model in any finite element method (FEM) software taking into account equation formulation for the magnetic vector potential $\boldsymbol{A}$, however, in case of complex 3D geometry such an approach requires huge computer resources (memory and time). In this paper we propose the alternative method which is based on dividing the above complex computation process into smaller consecutive parts. First, the magnetic field of the exciter is computed in the axisymmetric FEM model. Asymptotic boundary conditions [5] adopted at the outer boundary of the model enable to use extremely fine mesh and obtain accurate values of the field in a limited space. Then, from the values of the primary magnetic field and parameters of the object and inclusions (conductivities and shapes), boundary conditions at the edges of the object and inclusions are calculated. In the next step these boundary conditions are applied in the 3D FEM model (electric scalar potential Φ formulation). The model contains only the object with inclusions inside. Reduced number of algebraic equations allows to use the extra fine mesh and compute accurately induced eddy currents. Finally, the secondary magnetic field and the electromotive force induced in receiver coils is calculated.

In the full version of the paper the governing equations, calculation procedure explained in detail, and numerical results obtained for exemplary parameters will be provided.

REFERENCES

[1] Li X., Mariappan L., He B., Three-Dimensional Multiexcitation Magnetoacoustic Tomography with Magnetic Induction, *Journal of Applied Physics*, vol. 108 (2010), 124702.

[2] Surowiec A.J., Stuchly S.S., Barr J.R., Swarup A., Dielectric properties of breast carcinoma and the surrounding tissues, *IEEE Transactions on Biomedical Engineering*, 35 (1988), No. 4, 257–263.

[3] Stawicki K., Gratkowski S., Komorowski M., Pietrusewicz T., Numerical simulations and experimental results for magnetic induction tomography system, *Przegląd Elektrotechniczny*, 85 (2009), nr 4, 44–46.

[4] Stawicki K., Gratkowski S., Komorowski M., Pietrusewicz T., A New Transducer for Magnetic Induction Tomography, *IEEE Transactions on Magnetics*, 45 (2009), No. 3, 1832–1835.

[5] Gratkowski S., Pichon L., Gajan H., Asymptotic Boundary Conditions for Open Boundaries of Axisymmetric Magnetostatic Finite-Element Models, *IEEE Transactions on Magnetics*, 38 (2002) No. 2, 469–472.

***Authors**: Krzysztof Stawicki, krzysztof.stawicki@zut.edu.pl, Beata Szuflitowska beata.szuflitowska@zut.edu.pl, Marcin Ziółkowski, marcin.ziolkowski@zut.edu.pl, West Pomeranian University of Technology, ul. Sikorskiego 37, 70-313 Szczecin, Poland*

Damian MAZUR, Piotr MACIĄG

Rzeszow University of Technology, Poland

Current adjuster for frequency converter

Abstract. *Potentiometer current adjuster are widely used in several automation controllers. One example is speed control in inverters or adjusting some regulation parameters as location or angle. It is important to not only control actual current but also display this current on the electronic display or interrupt circuit when current is higher than fixed level. This paper presents current adjuster based on Atmega8 microcontroller and seven-segment display.*

Keywords: ATmega8, current adjuster, embedded systems, seven-segment display, potentiometer.

Introduction

Current adjusters operating at 4-20mA are widely used in several areas of industrial automation. Adjustment of the angle of rotation or speed control of conveyor are only two from many examples. Fig. 1 presents typical problem in which can be used current adjuster 4-20mA.

Conveyor drops off a certain, predetermined amount of the mixture on the scales. Appropriate speed of conveyor is set by microcontrollers which in input take actual measurement of weight of the mixture, and in the output serve current in the range of 4-20mA. This current is then passed to the power inverter. Unfortunately experience shows that feedback loop between scale and conveyor does not work reliably. It happens that, inappropriate current level is serve to inverter, or current level is higher than 20mA and whole system freezes. There is need to provide additional controller (current adjuster), by which operator can manually set speed of conveyor [1].

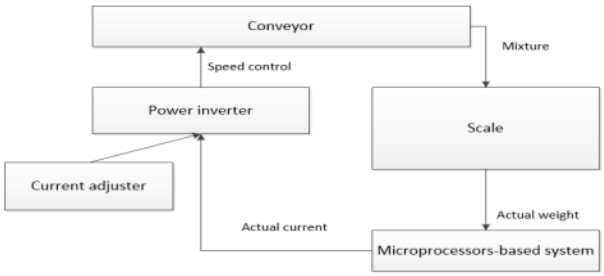

Fig. 1. Mixture weight measurement.

Current measurement with using ATmega A/D converter

This chapter briefly presents algorithm and program used to measure actual current level. The main part of program is based on features provided by ATmega A/D converter. Initialization of program include setting appropriate configuration bits. In this system internal 2.56V reference voltage is used.

```
1  void ADC_init()
2  {
3      setADC_DDR();
4      setADC_out();
5      ADMUX = _BV(REFS0) | _BV(REFS1) | 0x05;
6      ADCSRA = _BV(ADEN) | _BV(ADPS2) | _BV(ADPS1) | _BV(ADPS0);
7      ADCSRA |= (_BV(ADFR) | _BV(ADSC));
8  }
```

Listing 1. Analog to Digital Converter initialization.

In lines 3 and 4 appropriate voltage measurement pin is selected and set as input (pin PC5), next internal pull up is disabled. In lines from 5 to 7 appropriate ADC channel is selected, and conversion type is set to Free Running, which means that ADC samples input and updates internal registry continuously.

```
1  uint32_t ADCmeasure()
2  {
3      saveMeasure = ADC;
4      saveMeasure = saveMeasure*256UL/1024UL;
5      for(licznik; licznik < WAIT; licznik++){
6          asm("nop");
7      }
8      return saveMeasure;
9  }
```

Listing 2. Voltage measurement procedure.

Actual voltage level can be read from ADC register. In Listing above actual measurement is putted to saveMeasure variable. It is important to remember that value stored in ADC register is in range from 0 to 1023. To achieve actual voltage level, this value should be multiplied by reference voltage, and divided by 1024.

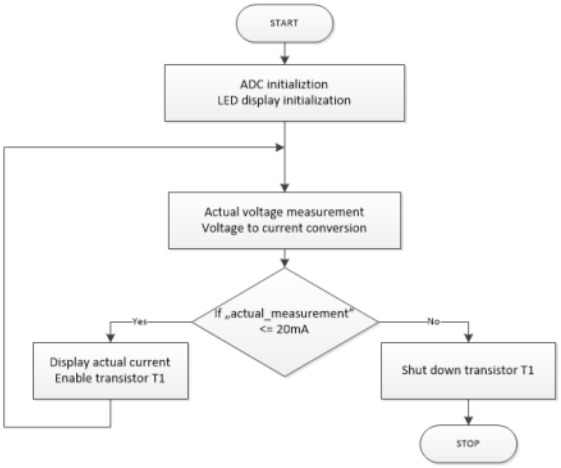

Fig. 2. Program main loop.

Conclusions

This paper briefly presents project of current adjuster which is designed based on ATmega8 microprocessor. The main part of program uses Analog to Digital Converter functionality. Adjusters similar to those presented in this paper are widely used to control many automation processes.

REFERENCES

[1] Lenk J,. Simplified design of voltage-frequency converters, Newnes, 2007.
[2] Morton J., AVR: An Introductory Course, Newnes, 2007.
[3] Garde D., Programming and Customizing the AVR Microcontroller, McGraw-Hill, 2007.
[4] Kuhnel C., AVR RISC Microcontroller Handbook, Newnes, 1998.

***Authors**: Damian MAZUR, mazur@prz.edu.pl, Piotr MACIĄG, piotr.maciag32@gmail.com, Rzeszow University of Technology, Poland*

ORAL SESSION 6 (Wednesday 10.06.2015, 10:10 – 11:30)			
Chairman: Kazimierz Adamiak kadamiak@eng.uwo.ca Chairman: Jerzy Barglik jerzy.barglik@polsl.pl			
	Time	**Authors**	**Title**
1	10:10–10:30	Krzysztof Gajowniczek, Tomasz Ząbkowski	Clustering Approach for Short Term Electricity Forecasting
2	10:30–10:50	A. Jaworek, A. Marchewicz, A.T. Sobczyk, A. Krupa, T. Czech	Spectral Emission Characteristics of Corona Discharge
3	10:50–11:10	Sławomir Grzyb, Przemysław Orłowski	Feedback Control System with PWA Load Dependent Reference Buffer Occupancy for Congestion Control in Packet Networks.
4	11:10–11:30	Tomasz Chady, Yijin Li, Sreedhar Unnikrishnakurup	Evaluation of THz Systems for Composite Structures Inspection
11:30 –11:50		**CLOSING CEREMONY**	

Krzysztof Gajowniczek[1,2], Tomasz Ząbkowski[1]

Department of Informatics, Warsaw University of Life Sciences (1), Systems Research Institute, Polish Academy of Sciences (2)

Clustering Approach for Short Term Electricity Forecasting

***Abstract**. Smart meters open new possibilities for short-term electricity load forecasting at different scales. In this paper, our contribution is twofold: (1) we deal with short term electricity load forecasting for 24 hours ahead on the individual household level, (2) we investigated different time series similarity measures for the purpose of clustering and further increase the electricity load forecasting.*

Keywords: artificial neural networks, hierarchical clustering, smart metering system, time series clustering, time series similarity measures.

Introduction

Installation of smart meters opens new possibilities for advanced analytics of electricity consumption at the individual household level. One of the most important tasks in various Smart Grid applications is the short-term electricity load forecasting at different scales, from an individual customer to a whole group of customers.

In this paper, based on various similarity measures and clustering algorithms, we will study an approach to forecast the hourly electricity loads for individual consumers for 24 hours ahead, taking into account the one neural network model for all the households in each group and comparing the results with the base model built for all the consumers.

Time series similarity

The time series distance measures are usually divided into four categories [1, 2]: (1) shape based – Euclidean, Short Time Series, Dynamic Time Warping, (2) edit based - Real Sequences, Longest Common Subsequence, (3) features based – Autocorrelation, Crosscorrelation, Fourier coefficients, TQuest, Integrated Periodogram, Wavelet Feature Extraction and (4) structure based. This article focuses on the first three categories because they are applicable to all cases.

Clustering method

Ward's minimum variance method [3] can be defined and implemented recursively by a Lance–Williams algorithm. The Lance–Williams algorithms are the infinite family of agglomerative hierarchical clustering algorithms which are represented by a recursive formula for updating cluster distances in terms of squared similarities at each step (each time a pair of clusters is merged).

To choose optimal number of clusters the Calinski and Harabasz index [4] was used.

Numerical experiment

The data have been obtained from Pecan Street Inc. via the WikiEnergy project [5]. The data set contains data from 61 homes, in which the household aggregate power demand are monitored at 1 hour intervals over 6 months from December 2012 until June 2013.

To assess the model performance for forecasting by 10-fold cross validation, we used Mean Absolute Percentage Error and resistant Mean Absolute Percentage Error [6].

For training neural networks we used the BFGS (Broyden – Fletcher – Goldfarb – Shanno) algorithm, which belongs to the broad family of quasi-Newton optimization methods. Input layer consisted of 52 perceptrons, hidden layer consisted of 20 perceptrons and finally, the output layer consisted one perceptron. All the perceptrons were activated by logistic function and as loss function we chose the least squares estimator.

In all cases the optimum number of clusters based on Calinski-Harabasz was set to 2. Number of households in each clusters was not constant and is ranged from 30 and 31 for Real Sequences, up to 53 and 8 for Crosscorrelation. The greatest increase in accuracy was obtained for Dynamic Time Warping. Please, see Tab. 1 for details.

Table 1. Obtained results

	MAPE		r-MAPE	
Cluster number	1	2	1	2
Base model	1.670		0.462	
Euclidean	0.714	1.360	0.427	0.480
Short Time Series	2.220	0.593	0.500	0.420
Dynamic Time Warping	0.695	0.701	0.417	0.452
Real Sequences	0.588	1.870	0.404	0.524
Longest Common Subsequence	1.870	4.820	0.524	0.468
Autocorrelation	2.230	0.835	0.427	0.531
Crosscorrelation	0.831	1.360	0.471	0.480
Fourier coefficients	0.714	1.360	0.427	0.480
TQuest	0.677	1.810	0.440	0.487
Integrated Periodogram	3.300	0.701	0.517	0.452
Wavelet Feature Extraction	0.714	1.360	0.427	0.480

Conclusion

In this paper, we presented an approach to forecast electricity load on individual level data for a group of customers. The result of MLP network model used for 24 hours ahead short term load forecast shows that models' performance differs substantially and it is dependent of the time series similarity measures.

The study is cofounded by the European Union from resources of the European Social Fund. Project PO KL „Information technologies: Research and their interdisciplinary applications", Agreement UDA-POKL.04.01.01-00-051/10-00.

REFERENCES

[1] Mori U., Mendiburu A., Lozano J.A. TSdist: Distance Measures for Time Series data, (2014), R package version 1.2, http://CRAN.R-project.org/package=TSdist
[2] Montero P., Vilar J.A. TSclust: An R Package for Time Series Clustering, Journal of Statistical Software, 62(1), (2014), 1-43
[3] Ward J.H. Hierarchical Grouping to Optimize an Objective Function, Journal of the American Statistical Association, 58(301), (1963), 236–244.
[4] Calinski T., Harabasz J. A Dendrite Method for Cluster Analysis, Communications in Statistics – Theory and Methods, 3(1), (1974), 1–27.
[5] https://dataport.pecanstreet.org/
[6] Moreno J.J.M., Pol A. P., Abad A.S., Blasco B.C. Using the R-MAPE index as a resistant measure of forecast accuracy, Psicothema 25(4), (2013), 500-506.

***Authors**: Krzysztof Gajowniczek, Warsaw University of Life Sciences, Nowoursynowska 159, 02-787 Warsaw, Poland, krzysztof_gajowniczek@sggw.pl and Systems Research Institute, Polish Academy of Sciences, Newelska 6, 01-447 Warsaw, Poland Tomasz Ząbkowski, Warsaw University of Life Sciences, Nowoursynowska 159, 02-787 Warsaw, Poland, tomasz_zabkowski@sggw.pl*

A. Jaworek, A. Marchewicz, A.T. Sobczyk, A. Krupa, T. Czech

Institute of Fluid Flow Machinery, Polish Academy of Sciences, Gdańsk, Poland

Spectral Emission Characteristics of Corona Discharge

Abstract. *The paper presents results of experimental investigations of emission intensity of selected spectral lines, emitted by corona discharge from tip of sharp electrode at high voltage in air. From the measurements and theoretical considerations it was determined that the emission intensity for silent corona discharge is a third-order polynomial function of voltage between the electrodes.*

Keywords: electrical discharge, corona discharge, emission spectroscopy

Corona discharges are applied in many fields of industry (for example, electrostatic precipitators, powder guns, xero) or appear as negative phenomenon (HV lines). Usually, corona discharge is characterized by the relation between voltage between the electrodes and current flowing between them, known as current-voltage characteristics. Another method of electric discharge characterization is spectroscopic measurement of selected spectral lines emitted by the discharge. The emission intensity of spectral lines depends both on discharge current and electric field in corona active region, which is usually close to sharp electrode, for example, the tip of needle.

The paper presents investigations of current voltage and spectral emission characteristics of corona discharge between a needle electrode and plate in the air. The spectral characteristics were determined as intensity of optical emission of selected spectral lines in the vicinity of sharp electrode versus voltage applied between electrodes. It has been shown that the emission intensity in selected spectral lines depends on the type of discharge and the discharge power. In the specific experimental conditions in air, mainly the N_2 second positive system (SPS), which is visible as faint violet light, has been recorded for glow or onset streamer discharges investigated. The emission intensity of other gaseous species (oxygen, carbon dioxide, argon), which are normally contained in air, was at very low level, at the voltage ranges applied, or was outside the spectral range of the spectrometer used. From the measured light emission spectra of discharges from the needle, the dependence of the amplitude of selected spectral lines can be approximated by a third-degree polynomial. This approximation has been supported by theoretical considerations, which assumed that the emission intensity Φ of a specific spectral line is proportional to the number of molecules n_{ex} in excited or ionized states characteristic of this line, which spontaneously return to the ground state:

$$\Phi = \alpha n_{ex}, \tag{1}$$

where α is a proportionality coefficient. Additional it was assumed that in weakly ionized gases, the total number of molecules excited to specific energy state or ionized in a unit time is a function of the total number n_e of free electrons colliding with gaseous molecules, of appropriate kinetic energy within the range of E_T (threshold kinetic energy for a specific ionization/excitation process) and E_M (maximum kinetic energy gained by electrons in the discharge), and the ionization/excitation cross section $\sigma(E_e)$ for these molecules:

$$n_{ex} = n_e \int_{E_T}^{E_M} f_e(E_e)\sigma(E_e)\mathrm{d}E_e, \tag{2}$$

where $f_e(E_e)$ is the electron energy distribution function, described by the Maxwell-Boltzmann statistics.

Further simplification assumes that the cross section for ionization or excitation, close above the threshold energy E_T, can be linearized. For example, Go et al. [1] have shown that for nitrogen the cross section for ionization can be approximated by a linear function of electron energy up to about 50 eV.

Combining the integral (2) with Townsend law, the emission intensity law for each spectral line in corona discharge can be written as:

$$\Phi = CU(U - U_T)^2, \tag{3}$$

where C is a constant. The emission intensity is a third-degree polynomial function of the voltage between electrodes. The regression lines based on Equation (3) are drawn in Fig. 1. It should be noted that the measuring results departure from equation (3) for the breakdown streamers discharge, and that for this type of discharge also other spectral lines can occur.

By numerical simulation of electric field in the vicinity of needle electrode using COMSOL Multiphysics software, the zone of SPS excitation has been determined and was compared qualitatively with discharge photographs (Fig. 2), assuming SPS excitation energy of 10 eV.

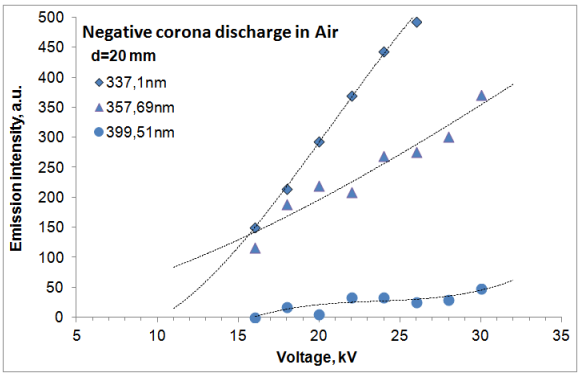

Fig. 1. Emission intensity of spectral lines of corona discharge (continuous lines - third degree polynomial)

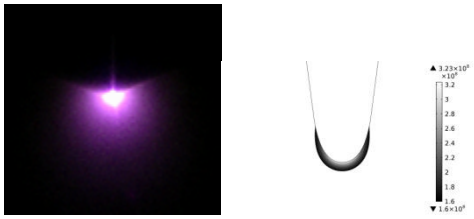

Fig. 2. Photograph of corona discharge near needle electrode (a), ionization/excitation zone of corona discharge near needle electrode determined from threshold electric field (voltage -30 kV)

References

[1] Go D.B., Fisher T.S., Garimella S.V., (2009), Direct simulation of ionization and ion transport for planar microscale ion generation devices. J. Phys. D: Appl. Phys. 42, paper No. 055203 (11pp).

Sławomir GRZYB, Przemysław ORLOWSKI

West Pomeranian University of Technology, Szczecin, Poland

Feedback Control System with PWA Load Dependent Reference Buffer Occupancy for Congestion Control in Packet Networks

***Abstract**. In the environment of multiply concurrent data exchange flows, congestion avoidance plays the significant role in increasing network reliability and efficiency. A method of active egress queue length control in use not to over on underutilize buffer occupancy in non-stationary, discrete, dynamical model of communication channel is described in this paper. This approach allows to optimize available network nodes resources to avoid congestions effects or to minimize or alleviate negative impact of these congestion on network throughput.*

Keywords: congestion control, discrete-time systems, particle swarm optimization, dynamical model.

Introduction

Optimizing utilization of available network resources leads to improve the efficiency of different sorts of transmission grids [1]. Many approaches can be taken in alleviation the result of network congestion. Remarkable attention is recently paid to modelling and methods for piece-wise affine (PWA) systems. The main aim of the paper is to introduce an algorithm controlling egress queue length in the congested node. This can be accomplished by tuning the number of packets requested from the source to assumed egress buffer utilization level in the congested node. This assumed buffer occupancy level should depend on available egress throughput, which is varying in time. This approach helps to minimize buffer overflow issue. The piecewise affine function is used to adopt requested number of packets in non-stationary, discrete dynamical system. In order to tune coordinates in piecewise affine function, modified Newton's method is applied [2].

Model of network section

The network model is like in [3] and consist of source S, some specified number of network nodes, congested node CN and destination D, like in Fig. 1.

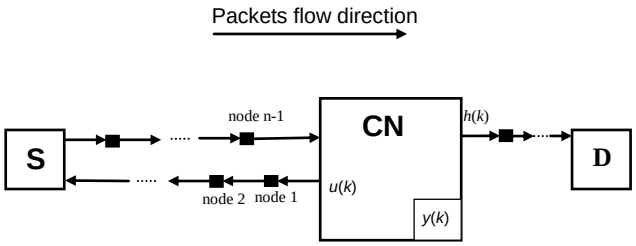

Fig. 1. Block diagram of network sector with time varying delay

CN can be in a state, when some portion of accumulated data is transferred towards D, due to available egress bandwidth, while the rest is kept in egress buffer. In that manner the difference between packets coming into the congested node and packets outgoing to the destination increases the buffer occupancy in CN when it is positive or decreases when it is negative. The amount of accumulated packet in CN buffer y is controlled by the controller. Congested node sends the control signal $u(k)$ backwards to the source. This is done to adjust the number of packets sent from source to destination through the congested node to network conditions, which vary in time.

Strategy of congestion control

CN buffer should be in such utilization level, which allows to accumulate packets in case of congestion appearance. This lays the foundation for a conception to depend expected buffer occupancy y_{ref} of CN to available throughput, which varies in time. PWA method is applied to design this dependency. The piecewise affine method can be presented in the following way:

$$y_{ref}\left(d\left(k\right)\right)=\begin{cases} z_3 & d\left(k\right)\le z_1 \\ \dfrac{\left(z_4-z_3\right)\left(d\left(k\right)-z_1\right)}{\left(z_2-z_1\right)}+z_3, & z_1<d\left(k\right)<z_2 \\ z_4 & d\left(k\right)\ge z_2 \end{cases} \tag{1}$$

where: y_{ref} – expected buffer occupancy of congested node, z_1-z_4 – coordinates of the PWA function.

Appling the controller with proportional gain z_5 and PWA method like in (1), optimal variables set z_1-z_5 is determined by numerical optimization. Fig. 2. illustrates the queue length of congested node obtained during numerical simulation .

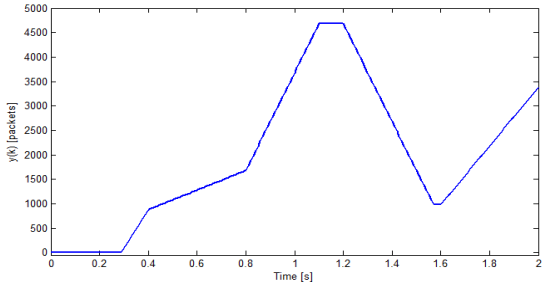

Fig. 2. Queue length $y(k)$ of congested node CN

Conclusion

Proposed method rely on active control of egress queue length as a function of available output bandwidth. Modified Newton's method combined with piecewise affine algorithm are used to designate optimal egress buffer level.

REFERENCES

[1] Hazra J., Sinha A.K., Congestion management using multiobjective particle swarm optimization, IEEE Trans. Power Syst., vol. 22 (2007), No.4, 1726–1734.

[2] Coleman T.,F., Li Y., On the Convergence of Reflective Newton Methods for Large-Scale Nonlinear Minimization Subject to Bounds, Mathematical Programming, Vol. 67 (1994), No 2, 189-224.

[3] Grzyb S., Orłowski P., Mathematical model of the congested communication channel in networks with time-varying parameters, Pomiary Automatyka Kontrola, vol. 59 (2013), No. 11, 1151-1154.

***Authors**: Sławomir Grzyb, West Pomeranian University of Technology, Szczecin, Poland, slawomir.grzyb@zut.edu.pl, Przemysław Orłowski, West Pomeranian University of Technology, Szczecin, Poland, przemyslaw.orlowski@zut.edu.pl*

Tomasz CHADY[1], Yijin LII[2], Sreedhar UNNIKRISHNAKURUP[3]

West Pomeranian University of Technology, Szczecin (1)
Nanjing University of Aeronautical and Astronautics, Nanjing, China (2)
CNDE, Mechanical Engineering Department, Indian Institute of Technology Madras, Chennai 600036 (3)

Evaluation of THz Systems for NDT of Composite Structures

Abstract. *These paper presents results achieved with a terahertz time domain system used for inspection of a designated phantom and composite samples. The phantom enables to verify effective resolution and sensitivity of the system. Two setups of the THz system were evaluated. Results of experiments are presented and discussed.*

Keywords: *nondestructive testing, terahertz inspection, THz time domain system,* composites inspection.

Introduction

Electromagnetic waves of terahertz frequency range (0.5–10 THz) are increasingly used in various fields of science and industry. Properties of THz radiation are creating unique possibility to utilize it for inspection of plastics and composites. Especially, the terahertz time domain systems provide signals containing information about the internal structure of plastics and composite materials. These materials are replacing traditionally used metal components and will become a core of modern constructions.

Evaluation of Terahertz Inspection Systems

The block schemes of the THz time domain systems are shown in Fig. 1. Two basic configurations may be used. The first type of configuration with a receiver and transmitter mounted separately at a right angle and a second configuration, which includes an additional THz beam splitter. Both arrangements have some advantages and disadvantages. In order to evaluate them, a special phantom made of PMMA having artificial defects has been designed and manufactured using a CNC machine.

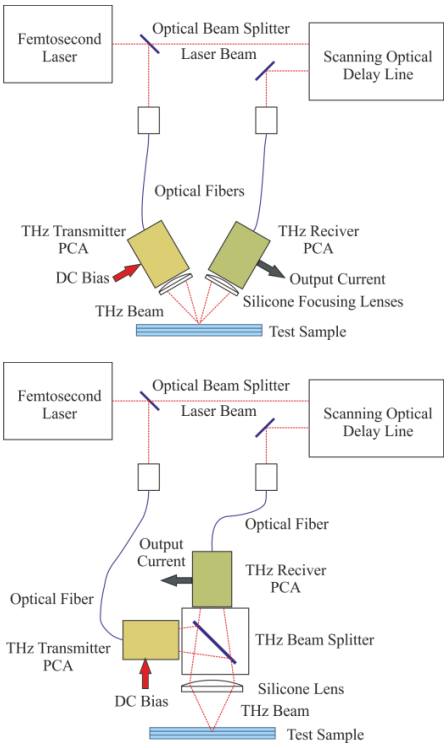

Fig. 1. Block schemes of the terahertz time domain inspection systems equipped with two separate heads (upper scheme) and the heads connected through the beam splitter (lower scheme)

One of utilized notch patterns set comprises of two parallel slits manufactured with different distances between each other. Such arrangement of the notches can be used to evaluate spatial resolution of the system. All measurements were carried out using both configurations presented in Fig. 1 and for different distances between the heads and surface of the sample. Figure 2 shows only a few selected results. The upper plot represents a B-scan measured for the whole set of double-notches. The lower plots shows results achieved for the notches manufactured with the smallest distances (0.5 and 1 mm). Other results, their quantitative evaluations and conclusions will be given in the full version of the paper. Additionally, in Fig. 3 a C-scan of the engraved inscription ISTET'15 is presented.

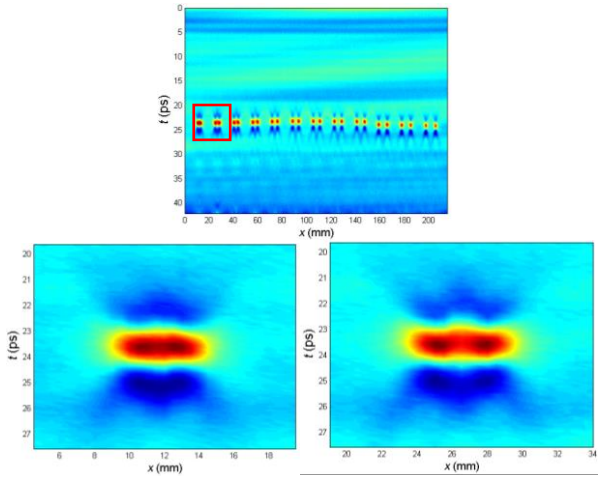

Fig. 2. B-scans for the double-notches pattern (measured using the THz system with the beam splitter)

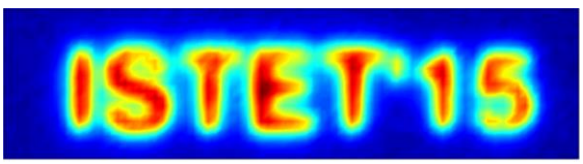

Fig. 3. C-scan of the engraved inscription ISTET'15

Acknowledgements

This work was supported in part by European Commission project HEMOW: Health Monitoring of Offshore Wind Farms
(reference: FP7-PEOPLE-2010-IRSES-GA-269202).

Contact author: *Tomasz Chady, West Pomeranian University of Technology, Szczecin, al. Piastów 17, 70-310 Szczecin, e-mail: tchady@zut.edu.pl*

Polskie Sieci Elektroenergetyczne

Energia
w dobrych rękach

Jesteśmy operatorem elektroenergetycznego systemu przesyłowego w Polsce. Naszym nadrzędnym celem jest zapewnienie ciągłości funkcjonowania i niezawodnej pracy polskiego systemu przesyłowego, co gwarantuje utrzymanie bezpieczeństwa energetycznego kraju. Jesteśmy właścicielem ponad 13 500 kilometrów linii oraz 103 stacji elektroenergetycznych najwyższych napięć.

www.pse.pl